ISSN 0918-4597

NRIM

Research Activities

1995

National Research Institute for Metals

Japan

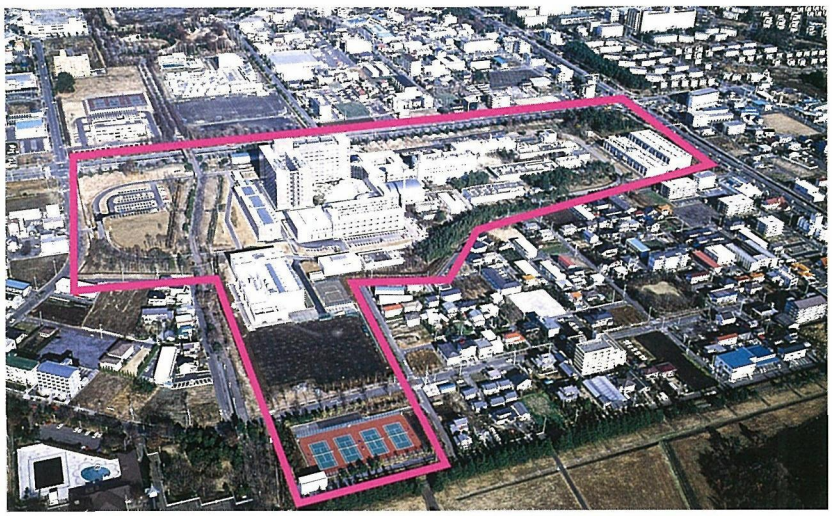

Sengen Site

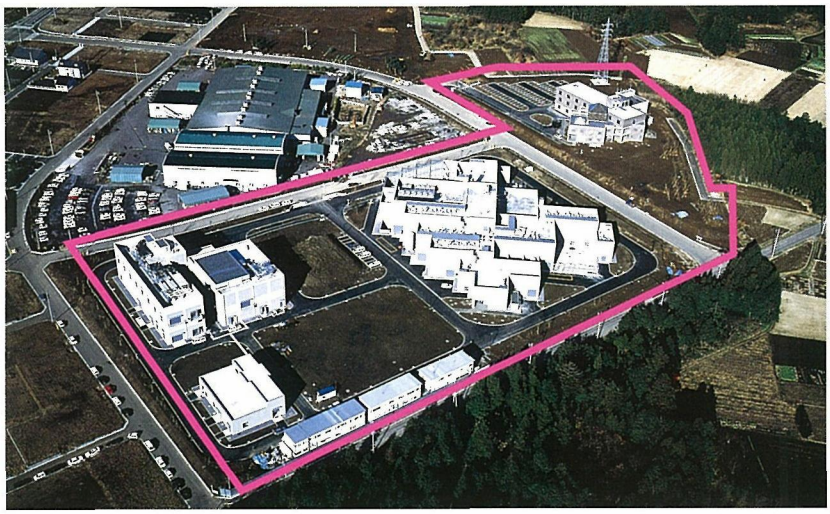

Sakura Site

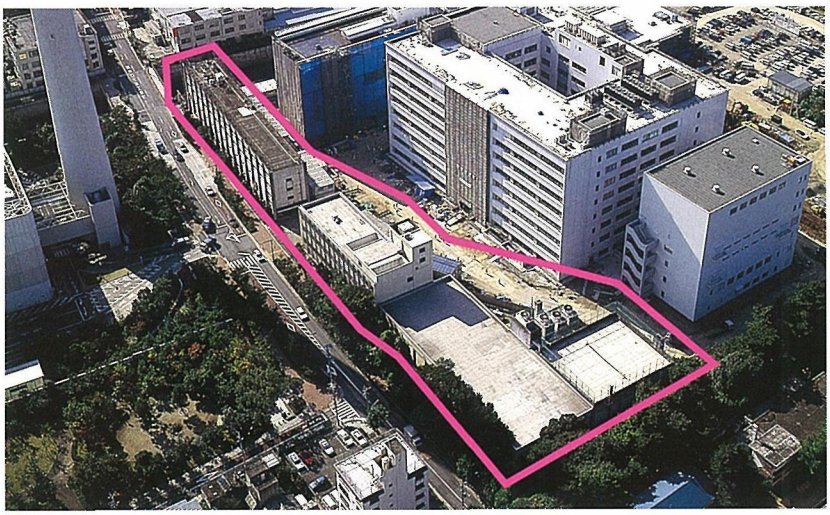

Meguro Site

Preface

FY 1994 is the midpoint for the 4th Long-Term Program of the National Research Institute of Metals (NRIM), which began in FY 1992. This Program focuses on materials research based on fundamental science. Within this framework, we are proceeding in our research activities to develop new materials and to enhance the reliability of existing materials. We hope you find the projects and related work described in NRIM Research Activities to be of interest.

On July 1 of last year NRIM moved its headquarters to Tsukuba, where it has established world-class facilities with the support and dedicated efforts of its sponsors, staff, and the community. Now it is time for NRIM to fully function as a center of excellence (COE) open to the world. At our Extreme Field Research Center, international collaborations in forefront research areas, such as the development of nanostructured materials, are already in progress. At the Sengen area site, we are accelerating our computational materials science research with the installation of a supercomputer and are engaging in a materials research initiative to help protect and conserve the global environment.

The 14th report of the Science and Technology Congress in FY 1987 (Basic Project for R&D on the Science and Technology of Matter and Materials) is now being put into practice with the enactment of the "Science and Technology Basic Act" last November. Responding to the societal needs for materials technology research, we are going to make our best effort, coupled with the high ideals of the National Institutes, to achieve these goals.

To all of you who have supported NRIM, we greatly appreciate your continued understanding and encouragement.

Masatoshi Okada

Dr. Masatoshi Okada
Director-General

NRIM Research Activities 1995

Contents

Research Topics 1

Theory of Adsorption of Cl on GaAs(001) Surfaces 1
Porosity Plays a Key Role in the Microstructure of Plasma Sprayed Coatings 3
Effect of Ultrasonic Vibration on Solidification Structures of Cast Irons 5
Direct Observation of the Lattice Defects with Transmission Electron Microscope 7
Self-controlling in Elevated-temperature Fatigue Crack Growth for Structural Materials 9
Fatigue Life Prediction of Huge Welded Structures Division 11
Improvement of High Temperature Strength in TiAl with Sb Addition 13
Fermi Surface of the New Three Dimensional Organic Conductor $(DMe\text{-}DCNQI)_2Cu$ 15
Field-induced Transition of f Electron Nature from Itinerant to Localized 17
Development of Powder Particle Assembly Technology 19
Cavitation Mechanisms in Superplastic Ceramics 21
Extreme High Vacuum Integrated Process Using Magnetic Levitation Transports for Creation of Nano-structure Materials 23
Studies on the New Intermetallic Compound Superconductors of Borocarbide System 25
Generation of the Highest Field, 21.8 T, of Superconducting Magnet by the Hybridization of Metallic and Oxide Superconducting Coils 27
Silicon Isotope Enrichment by Infrared Laser Irradiation 29
Developments of High Strength and High Conductivity Cu-Ag Alloy Wires and Sheets 31
New High Field Magnets and Facilities 33
Cytotoxity Evaluation of Metal Salts and Its Compound Effects — Toxicity Decreasing Due to Titanium and Iron Salts — 35

Research in Progress 1994–1995 37

List of Research Subjects 37
Research Programme 42

Publications 115

Papers Published in 1994 115
NRIM Publications (Apr. 1994 to Mar. 1995) 126

International Exchange 127

International Collaboration Research 127
List of Guest Researchers 128
Brief Introduction of STA Fellowship 131

Organization of NRIM 132

Organization 132
Budget and Personnel in Fiscal Year of 1994 132

How to get to NRIM 133

List of Keywords 135

Research Topics

❐ Theory of Adsorption of Cl on GaAs(001) Surfaces

T. Ohno, Materials Physics Division

Keywords: GaAs(001) surface, chlorine, adsorption, first-principles theory

Introduction

The interaction of adsorbates with semiconductor surfaces has been one of the main subjects in surface science for many years. Halogens are the most electronegative and reactive atoms. How halogens react with semiconductor surfaces is of great interest from a scientific point of view. The reaction also plays an essential role in such technologically important processes as reactive ion etching. Despite its scientific and technological importance, the reaction of halogens on semiconductor surfaces is not very well understood.

In this study we theoretically investigate the interaction of chlorines with the reconstructed GaAs(001) surfaces, employing first-principles pseudopotential techniques. Chlorine is the most important halogen used in GaAs etching. The GaAs(001) surface is known to exhibit a large number of reconstructions depending on processing conditions. Among them, the Ga-rich (4 × 2) surface and the As-rich (2 × 4) surface are considered, both of which have three dimers and one dimer vacancy within the surface unit cell.[1] The energetics of dissociative adsorption of Cl_2 molecules on these surfaces is investigated and the geometries of the chlorinated surfaces are determined. The presence of dimer vacancies is shown to remarkably alter the interaction of chlorines with the GaAs(001) surfaces, compared with the chlorination of simple dimerized surfaces with no vacancy.[2]

Methodology

The total energy are calculated within the local density functional (LDF) approach. The total energy functional are minimized with respect to both the plane-wave coefficients of the occupied orbitals and the ionic degrees of freedom by using the conjugate-gradient technique. In computing the total energy, we employ the Wigner form of the exchange-correlation energy and ab initio norm-conserving pseudopotentials. Separable pseudopotentials are used for the Ga and As atoms and non-separable BHS-type pseudopotential is used for the Cl atom. The pseudo wave functions are expanded in terms of a plane-wave basis set corresponding to a kinetic-energy cutoff of 7.29 Ry. Four special k points are employed to sample the primitive surface Brillouin zone. The surface is modeled using supercells containing six layers of GaAs and one layer of hypothetical hydrogen used for the surface termination. The atoms are assumed to be in their fully relaxed positions when the forces on the ions are smaller than 0.15 eV/A.

Results and Discussions

Now we consider the chlorination of the GaAs(001) Ga-rich (4 × 2) surface. The Ga-rich (4 × 2) surface where every fourth Ga dimer is missing [Fig. 1(a)] obeys the electron counting model; all Ga dangling bonds are empty and all As dangling bonds are filled. When a Cl_2 molecule is deposited on the Ga (4 × 2) surface [Fig. 1(b)], the Cl_2 molecule is found to dissociate and adsorb at the Ga-Ga dimer in onefold-coordinated sites [Fig. 1(c)]. Figure 2 presents the calculated total energy and Cl-Cl bond length as a function of the height of the Cl_2 molecule above the Ga (4 × 2) surface. It is clearly shown from this figure that the total energy decreases and the Cl-Cl bond length increases as the Cl_2 molecule approaches from above the middle of the Ga dimer [Fig. 1(b)]. Consequently, the Cl_2 dissociative adsorption is a barrierless and exothermic reaction.

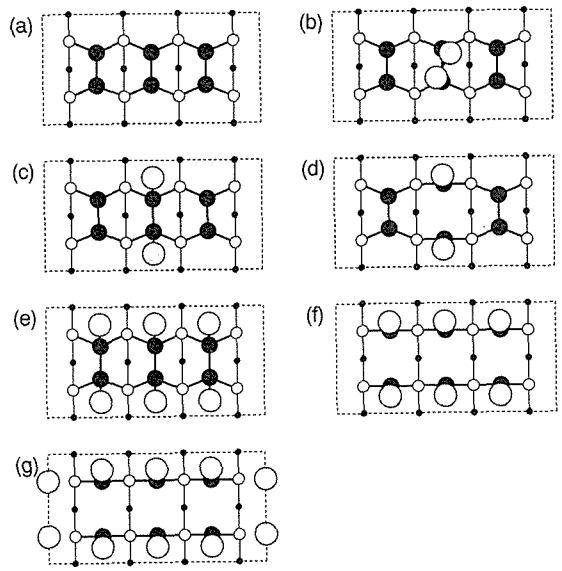

Fig. 1 Schematic atomic structures of the chlorinated GaAs(001) Ga-rich (4 × 2) surfaces. The large solid circles describe the Ga atoms in the first layer and the small solid ones are in the third layer. The open and dotted circles denote the As atoms in the second layer and the adsorbed Cl atoms, respectively.

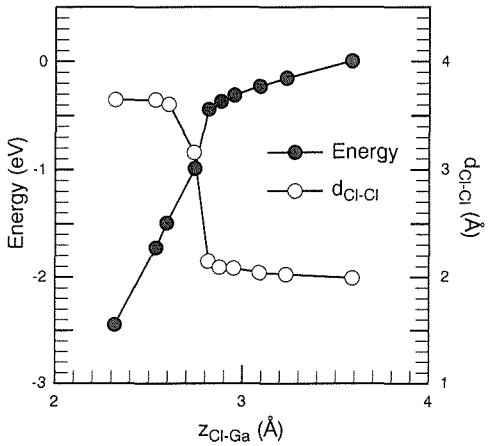

Fig. 2 Calculated total energy and Cl-Cl bond length as a function of the height of Cl_2 molecule above the Ga-rich (4 × 2) surface. The Cl_2 molecule approaches from above the middle of the center Ga dimer of the Ga-rich (4 × 2) surface.

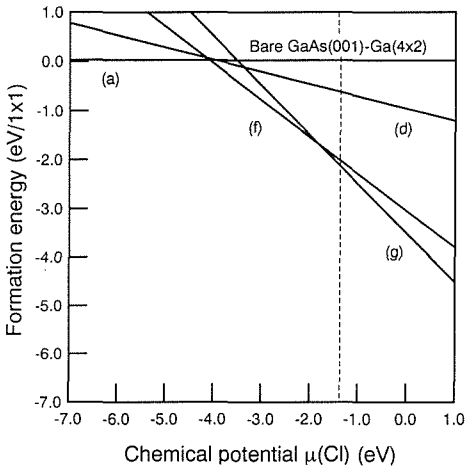

Fig. 3 Calculated surface formation energy for the chlorinated GaAs(001)-Ga (4 × 2) surfaces including (a), (d), (f), and (g) in Fig. 1. The vertical dashed line is the chemical potential at which Cl_2 molecules can be formed with no cost in energy.

The chlorinated Ga-Ga dimer [Fig. 1(c)] does not obey the electron counting model, having unfilled As dangling bonds. Since the breaking of the chlorinated Ga-Ga dimer makes all As dangling bonds filled, the Ga-Ga dimer is easily broken, resulting in formation of GaCl with two backbonds to the As layer below [Fig. 1(d)]. When all Ga dimers are chlorinated [Fig. 1(e)], the chlorinated Ga-Ga dimers are broken without any potential barrier. The breaking of the Ga-Ga dimer is certainly a prerequisite for etching. The calculated surface formation energy shown in Fig. 3 indicates that the surface covered with GaCl [Fig. 1(f)] is the most stable chlorinated Ga-rich (4 × 2) surface.

On the GaAs(001) As-rich (2 × 4) surface, on the other hand, the dissociative adsorption of Cl_2 molecules is an activated process with a potential barrier and the As-As dimers cannot be broken by the adsorption of Cl atoms. The Cl atoms bond more strongly to the second-layer Ga atoms exposed by the As dimer vacancy than to the As dimer atoms. After the Cl atoms adsorb on the second-layer Ga atoms, the As dimers are chlorinated.

Recent temperature-programmed desorption (TPD) measurements show that GaCl is the only desorption product from the chlorination of the Ga-rich (4 × 2) surface by Cl_2 whereas desorption of $AsCl_3$, $GaCl_2$, and GaCl is given from the chlorination of the As-rich (2 × 4) surface. The present calculated results[3] are consistent with these TPD measurements and provide significant insights into the chlorination process of semiconductor surfaces, although the details of the desorption processes are still an open question.

References

1. *Energetics of As Dimers on GaAs(001) As-Rich Surfaces*, T. Ohno, Phys. Rev. Lett., 70 (1993): 631–634.
2. *Barrierless Dimer Breaking at Semiconductor Surfaces by Chlorine Atoms*, T. Ohno, Phys. Rev. Lett. 70 (1993): 962–965.
3. *Chlorination of Ga-rich and As-Rich Reconstructed GaAs(001) Surfaces*, T. Ohno, *in Proc. 22nd International Conference on the Physics of Semiconductors*, ed. by D.J. Lockwood (World Scientific Publishing, (1995): 545–548.

❒ Porosity Plays a Key Role in the Microstructure of Plasma Sprayed Coatings

S. Kuroda, Advanced Materials Processing Division

Keywords: mercury intrusion porosimeter, high pressure infiltration, interlamellar contact, microcracking, rapid solidification

Plasma spray technology has found a wide range of applications in industries owing to its capability to form thick coatings of a wide range of materials at a high deposition rate. As compared to the progress in the application, however, understandings of the structure-property relationship of sprayed coatings seem to be lagging behind. One of the reasons may be the microstructure of the sprayed deposits, which is very different from more conventionally fabricated materials made by casting or powder metallurgy. Sprayed deposits consist of layers of a large number of rapidly solidified splats and porosity can often affect the property dramatically.

Visualization of Porosity in Sprayed Deposits

We have applied a high-pressure infiltration technique to fill the porosity in sprayed deposits with a low melting-point Bi alloy. Figure 1 shows the back scattered electron images of (a) polished cross section and (b) fractured surface of a Ni-20wt%Cr alloy plasma sprayed in air. The substrate temperature during deposition was around 500 K. The bright areas correspond to the impregnated Bi alloy in the deposit, the black areas to oxides, and the gray areas to the alloy matrix. Here two types of pores can be clearly recognized, i.e., chamber-type pores and thin interlamellar gaps. It is interesting that the wavy interlamellar gaps tend to be concave toward the spraying direction, indicating that the trapping of gas at the impact of molten particles was the cause of such pores. The connection among the pores in the deposit is difficult to recognize in the photo and the routes for the Bi-alloy must be very winding and difficult to trace on such a plane cross section. It is noteworthy that such information on porosity can hardly be obtained without impregnation.

In Fig. 2, a polished cross section of an alumina deposit impregnated with Cr_2O_3 is shown for comparison, where porosity appears white as well. In addition to the two types of pores found in the Ni-Cr deposit, a number of vertical microcracks are evident. Hence the connection among the pores can be found easily by way of these microcracks. These photos clearly indicate the existence of porosity with high aspect ratios, such as the intermellar gaps and vertical microcracks, which may be small in terms of volume but can affect the deposits' properties remarkably.

Gas in Closed Pores

What about the closed pores, which cannot be impregnated? In Fig. 3, the mass spectrum of gas detected when a Ni-Cr specimen was fractured in a vacuum chamber is compared with that of the environment in the chamber. The result indicates that the composition of the gas in the closed pores

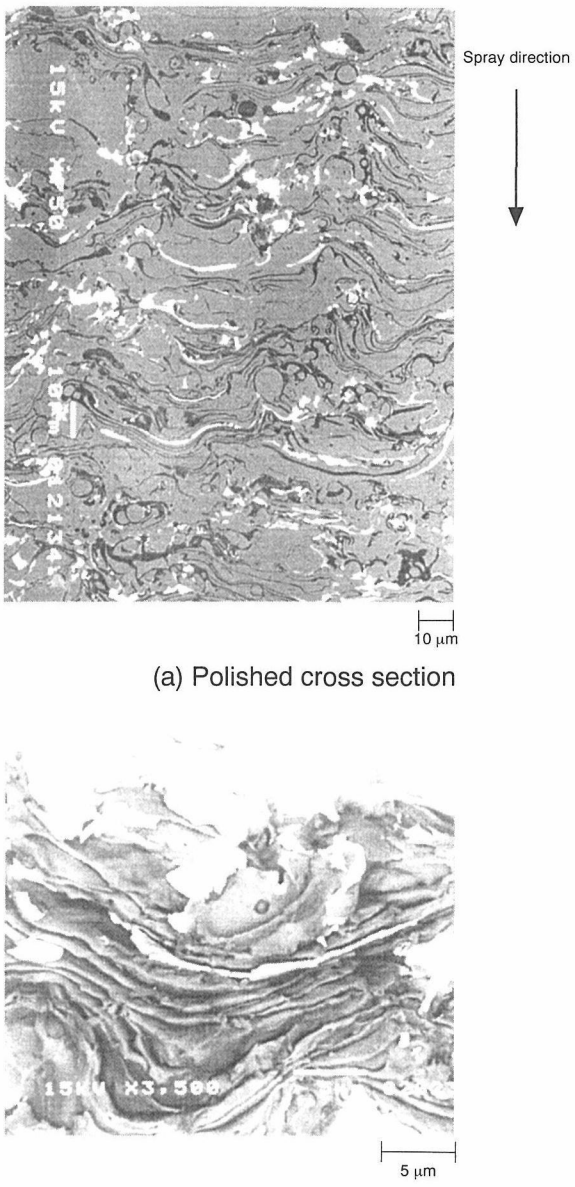

Fig. 1 Back scattered electron images of polished cross section of Ni-20Cr deposits (T_s = 500 K) infiltrated with the Bi-alloy (a) and a fractured surface of the sample (b).

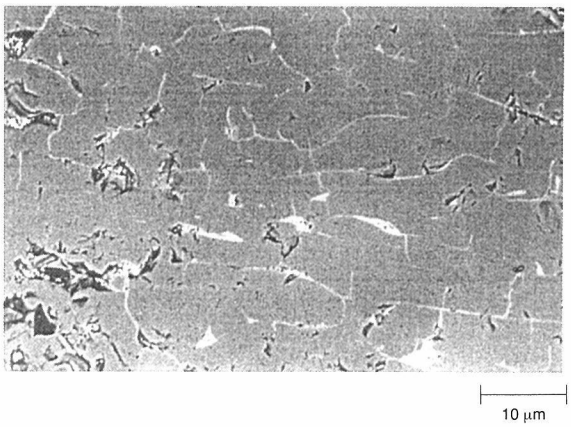

Fig. 2 Back scattered electron image of polished cross section of an alumina deposit (T_s = 480 K) treated with the chromic acid impregnation technique. White areas correspond to porosity filled with Cr_2O_3.

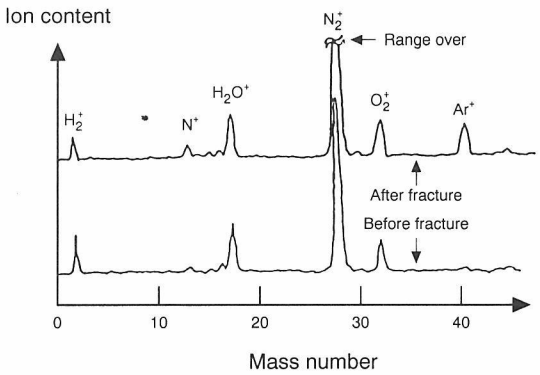

Fig. 3 Mass spectrum of the gas released from a Ni-20Cr deposit when fractured.

is mainly N_2 and a small amount of Ar. Since the composition of gas at the location of the substrate during spraying was mainly air mixed with Ar, the plasma gas, the entrapped gas should have been of the same composition. Lack of O_2 indicates that it has been consumed by oxidation of the deposit. From alumina deposits, no such release of gas could be detected, suggesting that there is almost no closed pore in the alumina deposit due to numerous microcracks.

Effects of Substrate Temperature on the Pore Structure

Mercury intrusion porosimeter was used to examine the effect of substrate temperature during deposition on the porosity of Ni-20Cr deposits. Specimens were placed in an evacuated cell, into which mercury was poured and high pressure was applied. The volume of mercury forced into the sample was measured as a function of the applied pressure. Then, the pressure P can be related to the pore radius r by the following equation,

$$r = \frac{-2\gamma\cos\theta}{P} \qquad (1)$$

where γ is the surface tension of mercury and θ the contact angle of mercury on the material. Equation

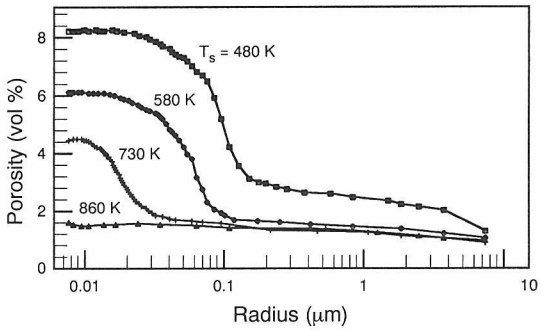

Fig. 4 Effects of substrate temperature on the cumulative pore size distribution of Ni-20Cr deposits.

1 assumes independent cylindrical pores not connected with each other. Within sprayed deposits, however, there are at least 3 types of porosity as we have seen, which form a complex 3-dimensional network[1]. When mercury porosimeter is applied to such materials, the break-through pressure at which mercury starts to penetrate into the specimen corresponds to the narrowest structural feature of the pore network, which is the intermellar gaps in the present case.

Figure 4 shows the effects of the substrate temperature T_s on the cumulative pore size distributions of the Ni-Cr deposits. At T_s = 480 K, the majority of the pores is penetrated at a pressure corresponding to r = 0.1 μm. This size roughly corresponds to the spacing at the periphery of intermellar gaps in Fig. 1. As the temperature is raised, both the size and amount of porosity decrease and finally at T_s = 860 K, the deposit seems to become almost impenetrable for mercury even at a pressure over 100 MPa. Examination of impregnated specimens revealed that the interlamellar contact significantly improves as T_s goes up. We believe that the change is due to improved wetting of molten droplets on the coating surface because heat treatment after deposition gave only a modest reduction in porosity[2].

In conclusion, porosity plays a critical role in the structure property relationship of sprayed coatings and needs to be evaluated carefully. It is time to understand better the mechanisms of porosity formation to find a way to control the coating structure and properties more effectively.

References

1. *Evaluation of the Pore Structure in Plasma-Sprayed Coatings*, S. Kuroda, Proc. 8th Cimtec, Florence, July, (1994): 373–380.
2. *Quenching Stress in Plasma Sprayed Coatings and Its Correlation with the Deposit Microstructure*, S. Kuroda, T. Dendo and S. Kitahara, J. Thermal Spray Technol., 4 (1995): 75–84.

❒ Effect of Ultrasonic Vibration on Solidification Structures of Cast Irons

Y. Ohsawa, Advanced Materials Processing Division

Keywords: ultrasonic vibration, fine structures, cast iron, sialon

The effect of ultrasonic vibration added during the solidification of metals has been studied for the purpose of getting fine structures, preventing segregation, degassing melt and removing inclusions. Previous studies were limited to the field of applying ultrasonic vibration indirectly through casting molds. Until now, few studies have been done on direct transmission of ultrasonic vibration to molten metals. Since a horn has to have following properties, such as an excellent high temperature strength, a high strength against a thermal shock, a great resistance to erosion by molten metals and a high Young's modules at high temperature.

The NRIM and Shinagawa Refractors Co., Ltd. have jointly developed a system of applying ultrasonic vibration to molten metals during solidification. The system consists of a high frequency generator (frequency 19 kHz using electric power of 1.2 kW), an oscillator, an amplitude measuring device, a two-stage water-cooled booster, a horn, a casting mold and a thermometer. The distinct characteristic of this system is that a ceramic material known as sialon (Si-Al-O-N) is used. Sialon is the compound in which some of silicon and nitrogen atoms in silicon nitride(Si_3N_4) are replaced with aluminum and oxygen atoms, and feature an excellent high temperature strength and a great resistance to erosion by molten metals. Figure 1 shows the horn and mold arrangement to apply ultrasonic vibration to molten metals. The sialon horn was preheated to prevent thermal shock before being immersed into melt.

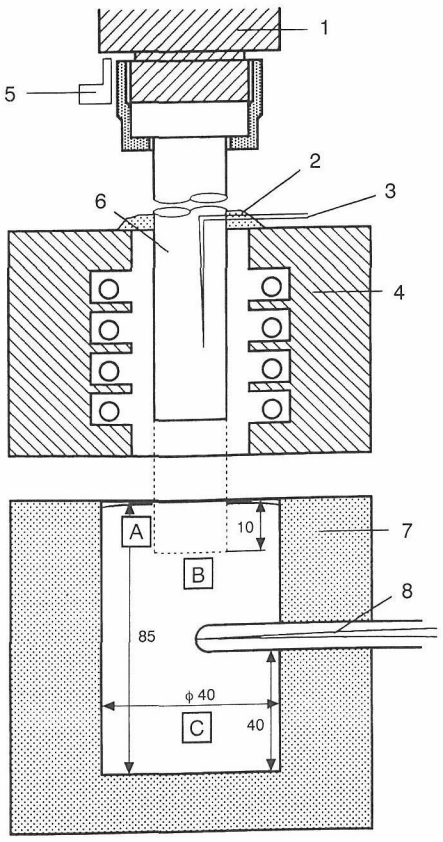

1: Booster, 2: Heat insulating material,
3: Thermo-couple, 4: Furnace,
5: Amplitude probe, 6: Sialon horn,
7: CO_2 sand mold, 8: Thermo-couple,
A, B, C: Samples of microstructures observed

Fig. 1 Horn and mold arrangement to apply ultrasonic vibration to molten metals.

An electrolytic iron, an electrode graphite and a Fe-75%Si alloy were melted to make a base cast iron with a high frequency furnace. C/V and spheroidal graphite cast irons, with hypo-eutectic and hyper-eutectic composition, were melted and poured into two CO_2 sand mold. One was applied the ultrasonic vibration and the other was not. Vibration started at 1623 K. The vibration was continued just after the eutectic solidification started. Immersion depth of horn to molten metal was 10 mm. The number and the diameter of equivalent circle of graphite nodule in C/V and spheroidal graphite cast irons were measured using an image analysis processor.

Ultrasonic vibration amplitude was approximately 15 μm. The solidification structures applied ultrasonic vibration show that graphites become finer and that the growth direction of primary austenite in hypo-eutectic cast iron is random as is shown in Al alloys[1].

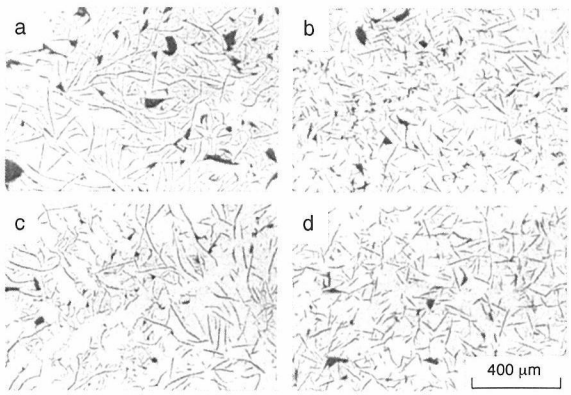

Fig. 2 Effect of ultrasonic vibration during solidification on micro-structures of flake graphite cast iron ingots. Vibration was kept down to the eutectic temperature. a,b:hyper eutectic, c,d:hypo eutectic, a,c:no vibration, b,d:vibration

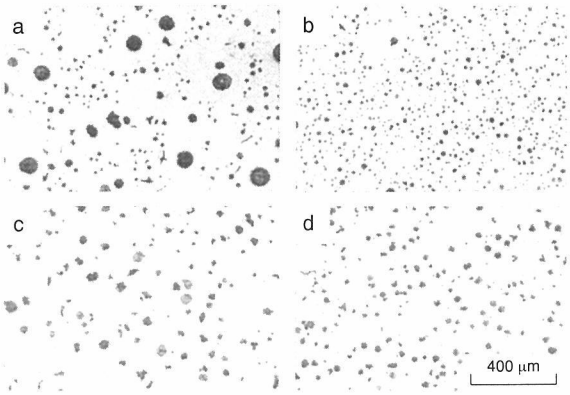

Fig. 3 Effect of ultrasonic vibration during solidification on micro-structures of spheroidal graphite cast iron ingots. Vibration was kept down to the eutectic temperature. a,b:hyper eutectic, c,d:hypo eutectic, a,c:no vibration, b,d:vibration

Figure 2 shows microstructures in the center of flake graphite iron castings. Graphite are broken and distributes homogeneously due to the fluid flow caused by the ultrasonic vibration. The graphite structure with vibration in hyper-eutectic(b), in hypo-eutectic(d) show relatively fine and straight compared with structure without vibration(a)(c).

In the case of hyper-eutectic C/V cast irons, vermicular graphites become finer spheroidal graphites by the ultrasonic vibration. This is due to the fact that finer spheroidal graphites crushed by the ultrasonic vibration is stable in molten metal. Then, a lot of spheroidal graphites exist in hyper eutectic C/V cast irons.

Figure 3 shows microstructures in the center of spheroidal graphite iron castings. Graphite structures of hyper-(b) and hypo-eutectic(d) cast irons vibrated are finer than those of the sample(a)(c) without vibration. Especially, in hyper-eutectic samples, primary graphites are broken and become remarkably small. This can be explained according to the difference in strength between graphite and austenite.

Figure 4 shows the number and the diameter of equivalent circle of graphite nodules in C/V and spheroidal graphite iron castings obtained by the image analysis processor. The number of graphite per unit area increases approximately 3 and 2 times in C/V and spheroidal graphite cast irons, respectively, by applying ultrasonic vibration. The mean diameter of equivalent circle is approximately 13 μm in this structure.

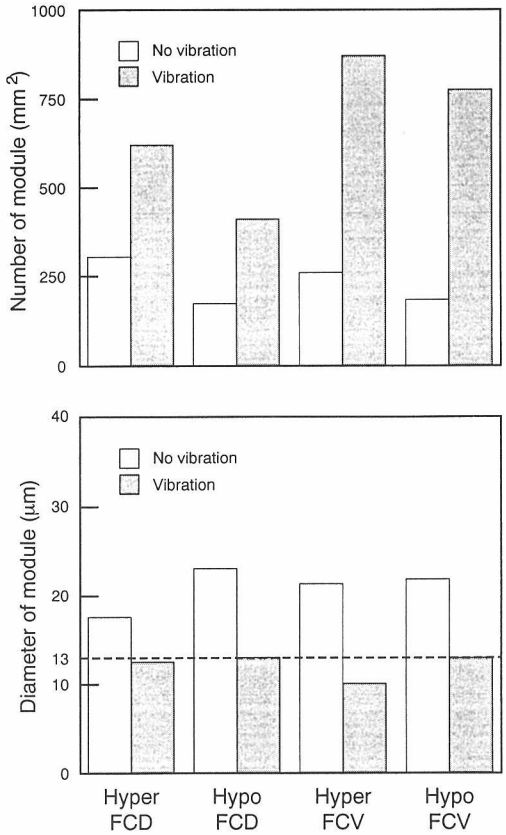

Fig. 4 Effect of ultrasonic vibration during solidification on the number and the diameter of equivalent circle of graphite nodule.

Graphite structures become finer by applying ultrasonic vibration during cooling down to the eutectic temperature in all iron castings. The effect of ultrasonic vibration on grain refinement is larger in hyper-eutectic than in hypo-eutectic composition of both of C/V and spheroidal graphite irons. The mechanical fracture by ultrasonic vibration is considered closely related to the small strength of graphite.

Reference

1. *Application Modes of Ultrasonic Vibration to Molten Metal and Their Effect on Solidification Structures*, Y. Ohsawa, A. Sato, T. Namai, G. Arakane, 65 (1993): 288 (in Japanese).

❐ Direct Observation of the Lattice Defects with Transmission Electron Microscope

K. Furuya, Materials Characterization Division

Keywords: radiation damage, *in situ* analysis, 1 MeV TEM, electron irradiation, stacking faults

Introduction

The process of radiation damage of metallic materials begins with the elastic scattering of atoms in the crystalline structure by injecting energetic electrons and ions. This atomic process produces self vacancies and interstitials which interact each other and result in many types of defects and defect clusters. Successive irradiation and thermal recovery cause the changes in defect structures which are supposed to have a wide range of relaxation time from varying from pico seconds to several hours. Therefore, the resultant microstructures generally becomes complicated with the formation of stacking faults, dislocation loops, voids, precipitates and so on. The basic understanding of the radiation damage process requires *in situ* observation of thermally unstable changes in lattice defects during the irradiation experiments.

A transmission electron microscope (TEM) with high spatial resolution about 0.1 nm is one of the apparatus to have a possibility of demonstrating the real time changes of atomic structures with electron and/or ion irradiation. Several technical problems, however, arise in the *in situ* TEM related to the degradation of resolution due to the modification of the hardware and to the continuous image drifts under the irradiation. The purpose of this research is to develop a new TEM for *in situ* analysis of the microstructural aspects of materials under electron and ion irradiation.

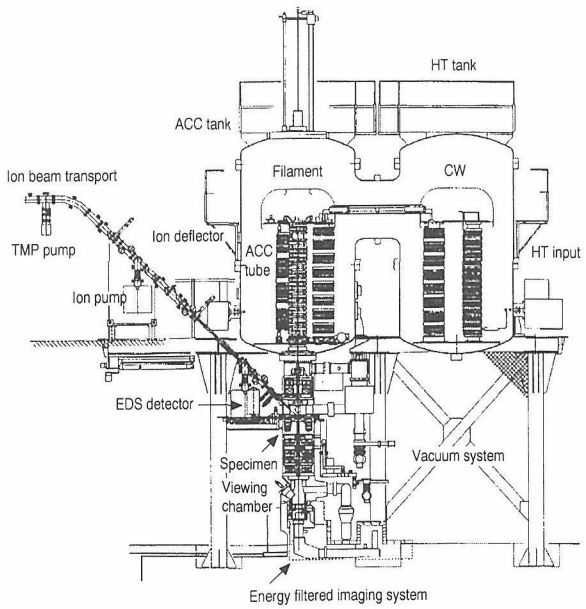

Fig. 1 Schematic drawing of the dual ion beam interfaced in situ analytical ultra high voltage electron microscope.

1000 keV *In Situ* TEM at NRIM

A new 1000 keV *in situ* TEM system with dual ion beams interface has been developed at NRIM. The schematic drawing of the system is shown in Fig. 1. The voltage of 1 MeV for electron was chosen with following three reasons. 1) The efficient production of Frenkel defects in most of metals and alloys, 2) To secure the resolution better

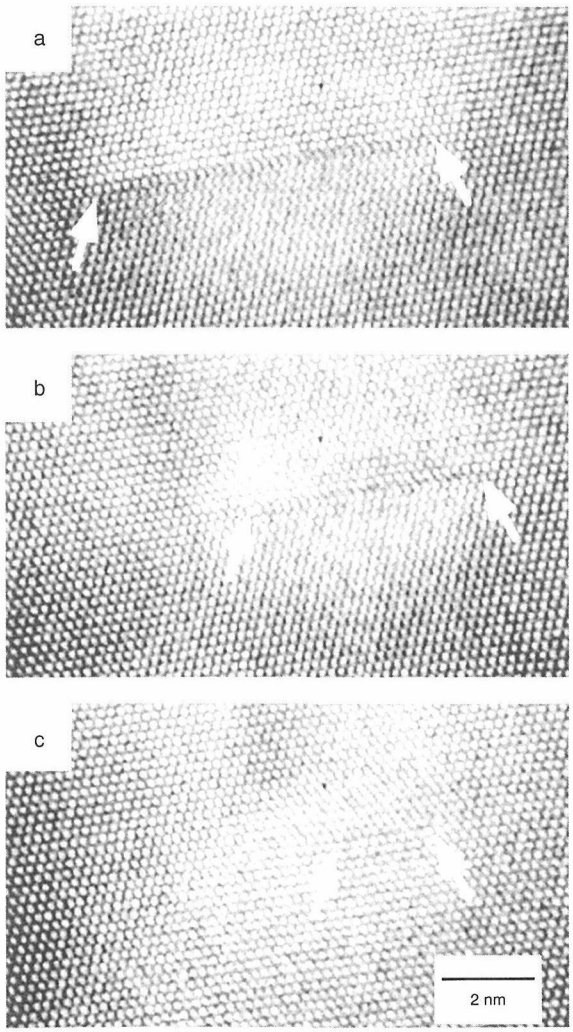

Fig. 2 The results of successive observation of a secondary defect in pure Al after irradiation with 1000 keV electrons to a dose of 6.0 × 10^{25} electrons/m^2 at room temperature. a) 0 sec, b) 20 sec and c) 40 sec.

than 0.13 nm, 3) The penetration large enough for the observation of thick foils and 4) The space at specimen position large enough for stressing, heating and cooling. The attached analytical tools such as energy dispersive X-ray spectroscopy (EDS) and energy filtered imaging system (i-PEELS) are essential to characterize the micro compositional changes of irradiated materials.

Dual ion accelerator system consist of 200 keV and 30 KeV implanters with a hollow cathode heavy ion source and a RF discharge light ion source, respectively. The high energy beam was selected through a 1.5 T analyzing magnet at an angle of 45 degrees, and then deflected vertically with an angle of 44 degrees for introducing into the TEM. The low energy beam was vertically analyzed before entering the port of the TEM. The beam lines were carefully controlled by electrostatic lenses and evacuated by ion pumps and magnetically suspended turbo pumps for keeping the resolution of the TEM. TEM images are collected and magnified directly with CCD-TV camera through a real time image processor. Analogue images were recorded directly on the VTR tapes and Digitized images were stored in computer disks.

The preliminary experiments to clarify the "dynamic" resolution of the *in situ* TEM were carried out on aluminum TEM specimens at room temperature. The specimens were irradiated with the relatively strong 1000 keV electrons of 1.0×10^{23} electrons$\cdot m^{-2} \cdot s^{-1}$, and the atomic displacements and the dynamic changes in the morphology of secondary defects were recorded with VTR tapes. The result in Fig. 2 is a set of images grabbed from the tape at which the specimen was irradiated to 6.0×10^{25} electrons$\cdot m^{-2} \cdot s^{-1}$. Since the specimen was aligned along (110) zone axis, one can observe aluminum atoms showing the interatomic distance of 0.2 nm. Especially pointed out is the plane shape atomic displacement associated with large distortion of lattice fringes in one of two series of apparent (111) planes, while no alteration in the number of lattice planes happens on both sides of lattice distortion. Further noted is the extraordinary contrast appearing below the plane which implies the atomic disorder and strain on the preferential (111) plane. Successive illumination of electrons resulted in the shrinkage of the line defect which indicated the recovery and rearrangement of atoms by the thermally activated process and by the electron irradiation. Although the physical model of the line defect could not be proposed without any image simulations of the crystalline of aluminum containing defects and clusters, it should be reminded that the faulted Frank loops are generally formed on the (111) plane for FCC metals. The present results surely demonstrate the usefulness of the *in situ* irradiation of materials in TEM followed by or with HRTEM observation for disclosing the mechanism of radiation damages in sub-nanometer scales.

❐ Self-controlling in Elevated-temperature Fatigue Crack Growth for Structural Materials

S. Matsuoka, E. Takeuchi, K. Miyahara, H. Hirukawa and N. Nagashima, Environmental Performance Division

Keywords: intelligent materials, self controlling, elevated-temperature, fatigue crack growth

Introduction

A new material concept, known as intelligent material or smart material, has been proposed and developed to establish the reliability of engineering structures such as air crafts, space structures and nuclear power plants. The intelligence of the material is defined as self detectability for environmental change and feasibility of sensing, processing and actuating.

Self-control of materials damage as well as vibration damping, noise suppression, geometric shape change and others is important for intelligent structural materials. Small cavities which do not deteriorate the mechanical properties exist in structural materials. An attempt is made to implant the sound-emitted material, phase-transformed material or surface-film-controlled material into the cavities[1, 2]. The implantation could make the structural material possible to self-sense and self-restore or self-arrest the damage during operation (see Fig. 4).

In this study, the arrest in elevated-temperature fatigue crack growth by dispersed Y_2O_3 and Pb particles is investigated. Fatigue fracture surfaces obtained are examined by an AFM/STM hybrid system to clarify the arrest mechanisms.

Experimental Procedure

Two series of materials were employed in this study[1, 2]. One is a series of Fe-20Cr alloys containing dispersed particles of Y_2O_3, Al_2O_3 and ZrO_2 in weight percents from 0.3 to 1.2. The size and spacing of oxide particles were about 30 and 200 nm. Another is a series of stainless steels containing dispersed Pb particles in weight percent of 0.2. The size and spacing of Pb particles were about 3 and 30 μm.

Fatigue crack growth tests were conducted in air at test temperatures between ~25 and 550 °C under a test frequency of 50 Hz, using compact-tension specimens with 35-mm-width and 8-mm-thickness for Fe-20Cr alloys and with 50-mm-width and 10-mm-thickness for stainless steels. A special Pmax-constant Δ K-decreasing method[1] shown in Fig. 1 was employed to obtain the fatigue threshold and crack growth properties under the closure-free condition.

Fracture surfaces obtained were examined by the AFM/STM hybrid system[3, 4]. AFM topographic images were obtained under the constant repulsive force condition, using a cantilever with a spring constant of 100 n/mm. A three-sided pyramidal diamond tip at the end of the cantilever was conductive by the boron-implantation. Contact current images were obtained through a STM electric circuit in parallel with AFM topographic images.

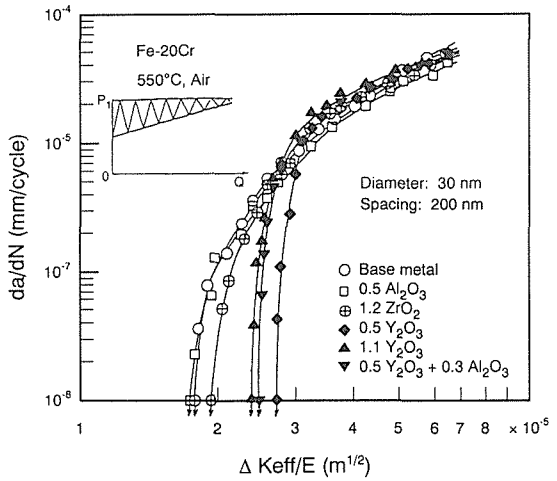

Fig. 1 Fatigue crack growth properties in air at 550 °C for Fe-20Cr alloys with dispersed oxide particles.

Experimental Results

The relationships between the fatigue crack growth rate, da/dN, and effective stress intensity factor range, ΔKeff, are shown in Fig. 1 in Fe-20Cr alloys[1]. The fatigue crack growth properties including the fatigue threshold were coincident each other at 25 °C. On the other hand, the fatigue threshold was about 50% higher for the alloys containing Y_2O_3 particles than for the host material and alloys containing Al_2O_3 and ZrO_2 at 550 °C, as shown in Fig. 1.

Similar results were obtained for two stainless steels, SUS304 (Fe-18Cr-8Ni) and SUS403

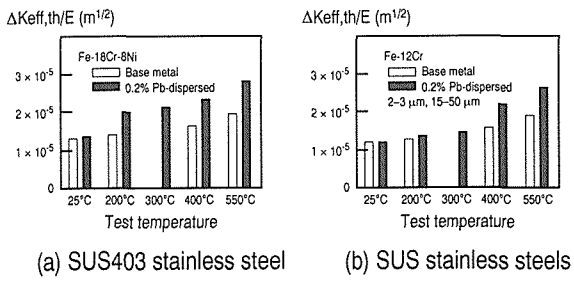

(a) SUS403 stainless steel (b) SUS stainless steels

Fig. 2 Fatigue threshold versus test temperature for two stainless steels.

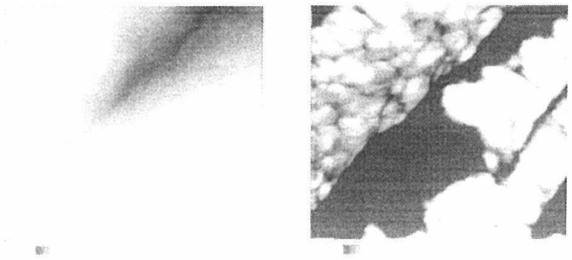

(a) Topographic image (b) Contact current image

Fig. 3 AFM topographic and contact current images of fatigue surface in air at 200 °C for SUS303 stainless steel with dispersed Pb particles.

(Fe-12Cr)[2]. Figure 2 shows the relationships between the fatigue threshold and test temperature. Dispersed Pb particles resulted in the 50% increase in fatigue threshold at elevated temperatures.

Figure 3 shows AMF topographic and contact current images of the fatigue surface obtained at 200 °C for SUS304 steel with Pb particles[4]. The topographic image was smooth, while the current image was consisted of bright and dark portions. The less current flows in the darker portion.

Discussion

Figure 4 shows the schematic illustration of the increase in fatigue threshold at elevated temperatures[1, 2]. The thick oxide film is formed at elevated temperatures such as 550 °C. The film prevents dislocations emitting from the crack tip and results in the higher fatigue threshold. For host materials (Fig. (a)), however, the spalling of the oxide film is prompted by the segregation of sulfur, S, at the interface between the oxide film and matrix. For Fe-20Cr alloys with dispersed Y_2O_3 particles (Fig. (b)), Y_2O_2 particles suppress the spalling of the oxide film by trapping S at the interface between Y_2O_3 particle and matrix. As the results, the strength properties of the oxide film are improved and the fatigue threshold is increased.

For stainless steels with dispersed Pb particles (Fig. (c)), the oxide film is spalled at the crack tip, whereas it is repaired by the molten lead at elevated temperatures. As the results, Pb particles gave rise to the increase in fatigue threshold for SUS403 (Fe-12Cr) martensitic stainless steel above the temperature of 400 °C, which is higher than the Pb melting point of 327 °C, as shown in Fig. 2. The increase in fatigue threshold occurred above 200 °C for SUS304 (Fe-18Cr-8Ni) austenitic stainless steel. This is due to the fact that the temperature at the crack tip is higher than the Pb melting point of 327 °C, even at the test temperature of 200 °C, because the heat conductivity of the austenitic stainless steel is low. In addition, the current image in Fig. 3(b) backs up the schematic explanation for repairing the oxide film by Pb particles in Fig. 4(c), if the dark portion in the current image is covered with the Pb oxide film with the lower electric conductivity and the bright portion with the Fe or Cr oxide film with the higher electric conductivity[4]. The measurement by the application of AMF nanofabrication suggested that the thickness of these oxide films were smaller than 10 nm[4, 5].

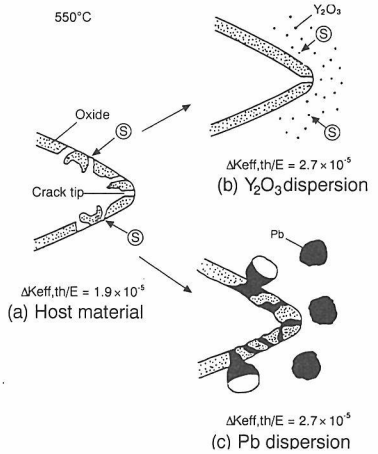

Fig. 4 Schematic illustration of oxide films at the fatigue crack tip at the elevated-temperature.

Accordingly, it is concluded that Y_2O_3 and Pb dispersion could show the arrest function of the fatigue crack growth at elevated temperatures. That is to say, the fatigue crack initiated, for example, from the notch root stops its growth, when its front encounters with Y_2O_3 or Pb Particles.

References

1. *Arrest Function in Elevated-Temperature Fatigue Crack Propagation for Y203-Dispersed Alloy,* E. Takeuchi, S. Matsuoka, K. Miyahara, H. Hirukawa and Y. Ikeda, Trans. Japan Soc. Mech. Eng. (in Japanese) 60-575 (1994): 1484–1492.
2. *Arrest Function in Elevated-Temperature Fatigue Crack Propagation for Stainless Steels with Dispersed Lead Particles,* E. Takeuchi, S. Matsuoka, K. Miyahara, H. Hirukawa and N. Nagashima, ibid. 61-581 (1995): 39–44.
3. *Observation of Oxide Particles and Thickness Measurement of Oxide Films by an AFM/STM Hybrid System,* K. Miyahara, S. Matsuoka, H. Hirukawa and N. Nagashima, ibid. 61-583 (1995): 581–588.
4. *Observation of Elevated-Temperature Fatigue Surfaces for Stainless Steels with Dispersed Lead Particles by an AFM/STM Hybride System,* H. Hirukawa, S. Matsuoka, K. Miyahara and E. Takeuchi, ibid. 61-584 (1995): 697–704.
5. *Application of Surface Fabrication to Strain Measurement in Nanometer Scale with the Scanning Tunneling Microscope,* K. Miyahara, S. Matsuoka, N. Nagashima and H. Hirukawa, J. Test. & Eval. 22-2 (1994): 121–126.

❐ Fatigue Life Prediction of Huge Welded Structures Division

A. Ohta, N. Suzuki and Y. Maeda, Environmental Performance

Keywords: fatigue, weldment, steel, residual stress

The fatigue strength of large welded beam significantly decreases from that of small welded specimen as shown in Fig. 1[1]. The reduction of fatigue strength occurs from the tensile residual stress which exists in large weldments. The fatigue strength of welded beam does not vary with the stress ratio[2] (The stress ratio, R, is the ratio between the minimum stress, σ_{min}, and the maximum stress, σ_{max}. The variation of waveform with R is shown in Fig. 2), as the tensile residual stress in welded beam reaches to the yield strength, σ_y, of material and the maximum stress becomes to be the yield strength by a shakedown in spite of the stress ratio. This fatigue strength which is not affected by the stress ratio is defined as the basic fatigue strength of welded joint.

However, the residual stress in small welded specimen is usually small and the maximum stress increases with the increase of the stress ratio. Therefore, the fatigue strength for small welded specimen decreases with the stress ratio as shown in Fig. 3[3].

It is proposed[3] to correct the S-N curve by the modified Goodman relation considering the existence of tensile residual stress of the yield strength magnitude. The correction is performed by the following equation.

$$\Delta\sigma = \Delta\sigma_0 \frac{\sigma_B - \sigma_y}{\sigma_B - \Delta\sigma_0} \qquad (1)$$

where $\Delta\sigma_0$ is the fatigue strength at R = 0, σ_B is the tensile strength. A dot-dashed curve in Fig. 4 is the corrected curve by eq. (1). The curve locates far below the experimental results for slit welded specimens which contain high tensile residual stress of the yield strength magnitude (open squares) as in welded structures.

A direct method ($\sigma_{max} = \sigma_y$ test) to obtain the basic fatigue strength of welded joints was proposed by maintaining the maximum applied stress to be the yield strength of base metal[4]. This stress condition is considered to exist in the fatigue critical area of welded joints.

The comparison of the results between $\sigma_{max} = \sigma_y$ test for small welded specimens and R = 0 test for slit welded specimen which contain high tensile residual stress of the yield strength magnitude is

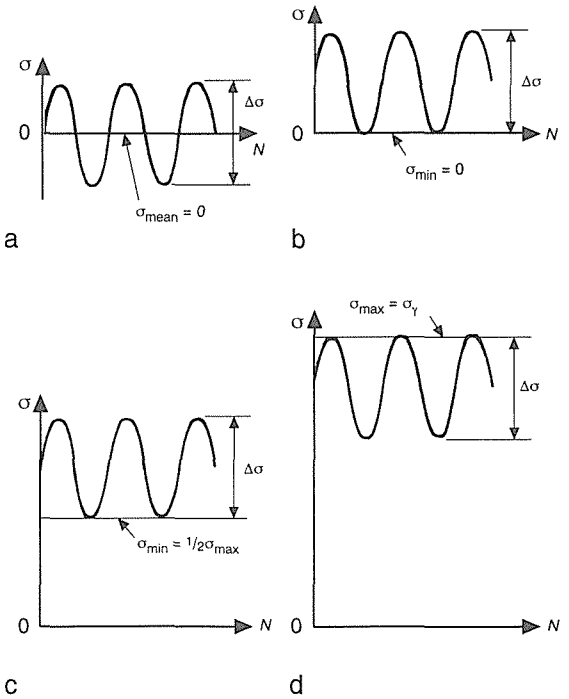

Fig. 2 Waveform of various test conditions. a: R = −1, b: R = 0, c: R = 0.5 and d: $\sigma_{max} = \sigma_y$

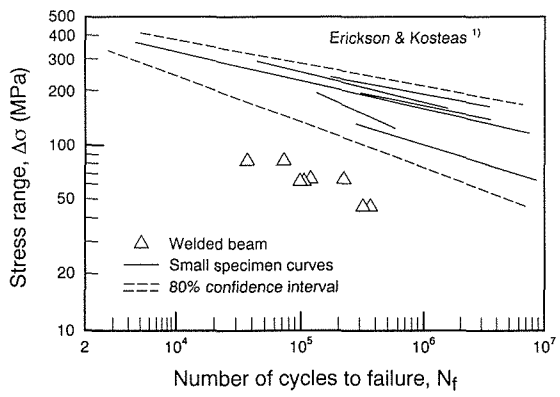

Fig. 1 Difference in fatigue strength between large welded beam and small welded specimen.

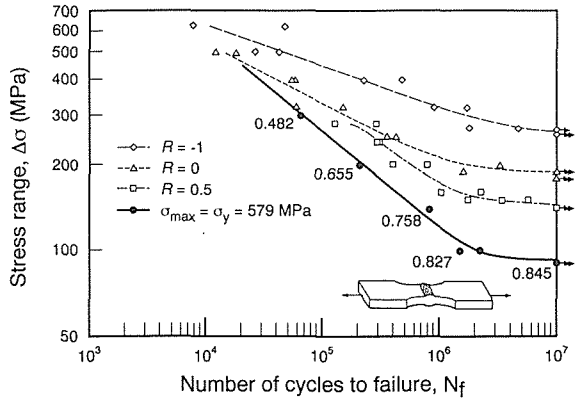

Fig. 3 Change of fatigue strength of small welded specimen with stress ratio.

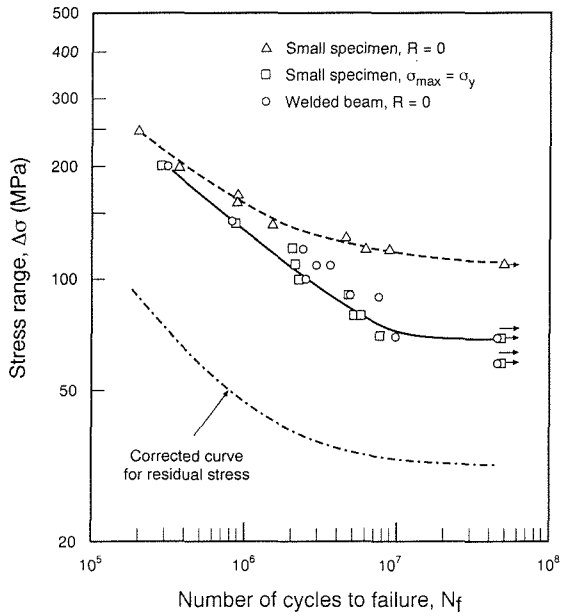

Fig. 4 Coincidence of fatigue strength between slit welded specimen which contain yield strength magnitude tensile residual stress and small welded specimen.

made in Fig. 4. It is clear that both results coincide very well with each other[5]. That is, the basic fatigue strength of welded structures can be predicted easily by the $\sigma_{max} = \sigma_y$ test for small specimens.

References

1. *Assessing Transverse Fillet Weld Fatigue in Aluminum from Full-Size and Small-Specimen Data,* D. Erickson and D. Kosteas, ASTM STP 1058 (1990): 34–46.
2. *Fatigue Strength of Welded A514 Steel Beams, Proc. Conf. Fatigue of Welded Structures,* J.W. Fisher, The Welding Institute, 1 (1971): 135–148.
3. *Design of Pressure Vessels for Low-Cycle Fatigue,* B.F. Langer, Trans. ASME Ser. C (1962): 389–402.
4. *Fatigue Strength Evaluation of Welded Joints Considering High Tensile Residual Stresses,* A. Ohta, Y. Maeda, T. Mawari, S. Nishijima and H. Nakamura, Int. J. Fatigue 8 (1986): 147–150.
5. *A Method for Obtaining Conservative S-N Data for Welded Structures,* H. Nakamura, S. Nishijima, A. Ohta, Y. Maeda, K. Uchino, T. Kohno , T. Toyomasu and I. Soya, J. Testing & Evaluation 16 (1988): 280–285.

❐ Improvement of High Temperature Strength in TiAl with Sb Addition

K. Hashimoto, M. Nobuki, E. Abe, M. Nakamura, (3rd Research Group), H. Doi, T. Kimura* and M. Isoda**

Keywords: titanium-aluminides, solid-solution hardening, particle reinforcement, high temperature strength

Introduction

Intermetallic compound TiAl base alloys exhibit good high-temperature mechanical properties that make them attractive candidates for a variety of applications in advanced turbine engines or an aero-space plane frame which is exposed to a temperature above 1273 K. Under the consideration of an aero-space plane project in Japan, however, an increase in the strength at high temperatures up to 1373 K is required for TiAl base alloys to be used for application in an aero-space plane frame[1].

High temperature strength can be improved by solid solution strengthening, precipitation strengthening and/or fiber or particle reinforcement. However, it has not been established which of three strengthening methods is the most effective in improving the strength in such a high temperature region for the TiAl base alloys. In this study, we have investigated the effect of Sb addition on high temperature strength of TiAl base alloys, particularly focusing on the solution strengthening due to solute Sb and on particle-reinforcement due to a large amount of Sb-rich phase precipitates.

Strengthening Due to Solute Atoms[2]

Nine elements, Cr, Ga, Hf, Nb, Pd, Pt, Sb, Ta and Zr were used as additive solute in 50at%Ti-(50-C)at%Al-Cat%X, and 50at%Al-(50-C)at%Ti-Cat%X alloys with C content up to 2at%. These alloys were examined in a temperature range from room temperature to 1273 K by compression test. Regression analysis was applied for the relations between the proof stress and additive elements characters such as atomic diameter, atomic weight, number of electrons per atom and melting temperature. The result indicated the additive element with a large difference in atomic size between additive element and titanium or aluminum is effective in improving high temperature strength due to solid solution. The increment of the proof stress at 1073 and 1273 K with the addition of a solute atom is shown in Fig. 1(a) and (b) as a function of the atomic size difference which is normalized by the average atomic size of Ti and Al. The effect of Sb addition was the most high in strengthening per solute atom.

Figure 2 shows the equilibrium phase diagram at 1373 K which was obtained in the present experiment and the chemical compositions of the alloys used. The main feature of the diagram is as follows: The maximum Sb solubility in a TiAl phase is less than 0.4 at%, and the TiAl phase coexists with a Sb-rich phase (D8m type) in a two-phase field of (TiAl + Sb-rich phase) and in a three-phase field of (TiAl + Sb-rich phase + Ti3Al). High temperature hardness measurement, specific thermoanalysis and transmission electron microscopic observation revealed that the D8m phase has the highest hardness of 470 Hv at 1373 K among three phases, is stable up to 1773 K, and precipitates

*Materials characterization division

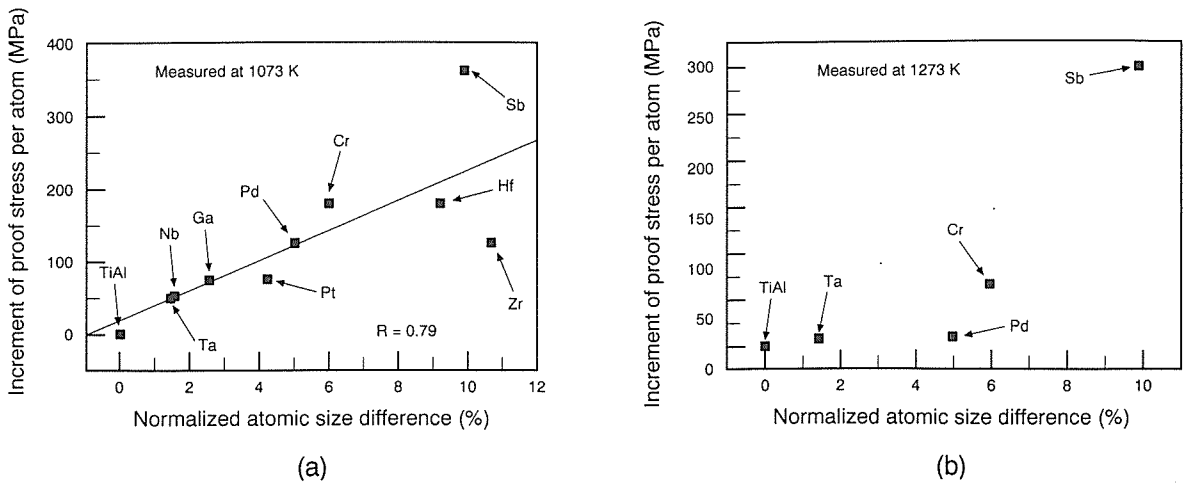

(a) (b)

Fig. 1 Increment of the proof stress by solute elements at (a) 1073 K, and (b) 1273 K. Atomic size difference is normalized by the average atomic size of titanium and aluminum.

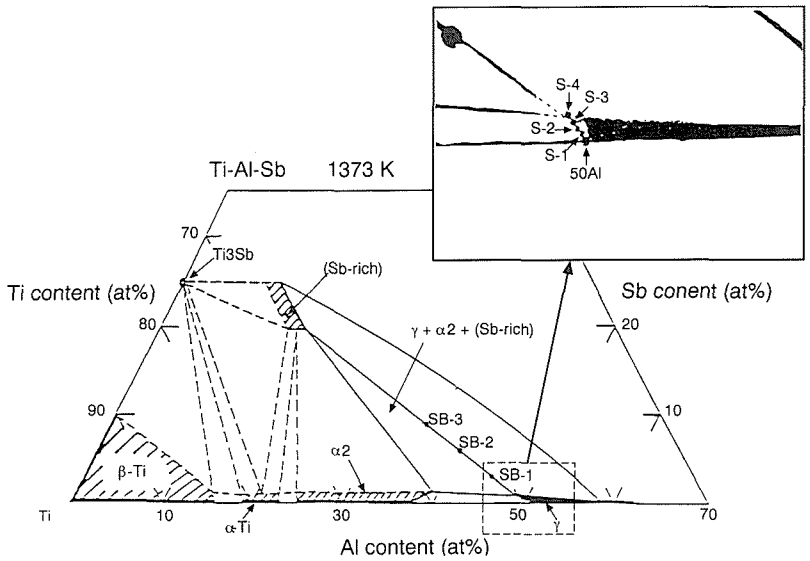

Fig. 2 Equilibrium phase diagram of Ti-Al-Sb system at 1373 K.

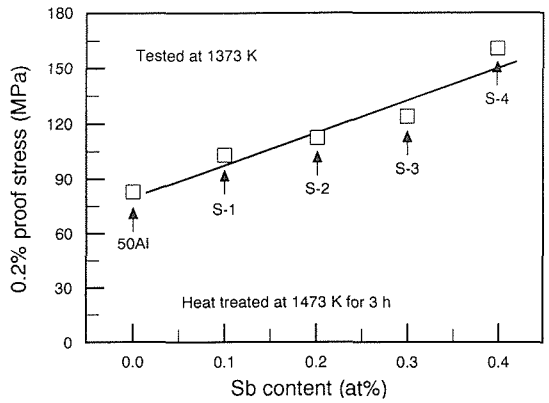

Fig. 3 Effect of Sb addition on proof stress at 1373 K.

finely in the particle size of 200nm-10μm in TiAl phase grains. These results suggest a possibility of solution strengthening due to Sb, particle-reinforcement due to a large amount of the D8m phase particles, and also a possibility of precipitation strengthening due to fine particles of the D8m phase.

Figure 3 shows the relation between the proof stress and solute Sb content in the TiAl base alloys at 1373 K. The high temperature strength increases with increasing Sb content, and the maximum proof stress of 160MPa being the twice higher than that of the binary alloy was obtained for the alloy with the addition of 0.4at%Sb.

Particle-reinforcement Due to D8m Phase[3]

Figure 4 shows the change of the proof stress at 1373 K with the volume fraction of the D8m phase particles in the alloys of Sb-1, -2, -3. The proof stress increases with the increase of the D8m phase volume fraction, and the maximum proof stress of 160 MPa was obtained for Sb-3 alloy with the D8m phase particles of 40vol%. This result indicates that the particle-reinforcement is operative even at 1373 K in the TiAl base alloys. The TiAl phase in the alloys of SB-1, -2, -3 also contained solute Sb up to 0.4at%, and then the combination of particle-

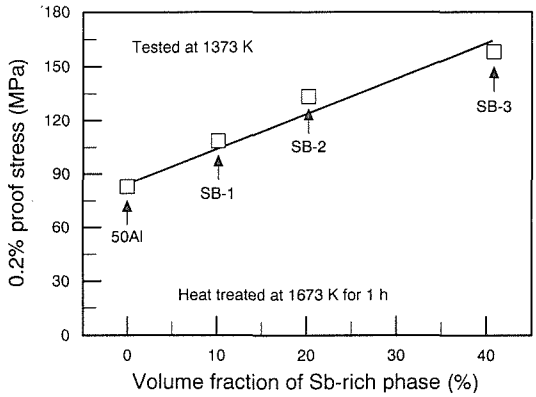

Fig. 4 Proof stress at 1373 K vs. volume fraction of Sb-rich phase.

reinforcement and solution strengthening might be anticipated. However, the maximum proof stress exhibited the same value as that in the solution strengthening alloy of S-4. Hence, we are now studying the reason why the results are inconsistent with the anticipation mentioned above for improving the high temperature strength of TiAl base alloys.

References

1. *Japanese National Project on Intermetallics*, T. Maruo and M. Tomita, Proc. Conf. on Critical Issues in the Development of High Temperature Structural Materials, TMS (1993): p. 477.
2. *Effect of Third Elements on High Temperature Strength of TiAl Base Alloys*, K. Hashimoto, M. Nobuki, H. Doi, T. Kimura, T. Tsujimoto and M. Nakamura, J. JIM, 57 (1993): 898–904 (in Japanese).
3. *High Temperature Strength and Room Temperature Ductility of TiAl Base Alloys with Antimony*, K. Hashimoto, M. Nobuki, H. Doi, E. Abe and M. Nakamura, Proc. 124th TMS Int. Sympo. on Gamma Titanium Aluminides (1995): 761–770.

❐ Fermi Surface of the New Three Dimensional Organic Conductor (DMe-DCNQI)$_2$Cu

S. Uji, The 4th Research Group

Keywords: quantum oscillation, Fermi surface, organic conductor

Introduction

The novel molecular conductor containing Cu ions, (DMe-DCNQI)$_2$Cu has attracted a great deal of interests due to the characteristic physical properties. One of the striking features in the (DMe-DCNQI)$_2$Cu system is the fact that a drastic metal-insulator (M-I) transition is induced by the substitution of the hydrogen with deuterium in the DMe-DCNQI molecules. A metal-insulator-metal (M-I-M) reentrant transition is found in the partially deuterated system, and in the alloy of the undeuterated and the fully deuterated systems. The M-I- and M-I-M transitions induced by the deuteration have been explained in terms of the chemical pressure (Fig. 1). However, the mechanism of the drastic transitions, which is closely related to the Fermi surface (FS) structure, has not been clarified yet.

In order to investigate the FS, we have carried out the de Haas-van Alphen (dHvA) measurements for the single crystals of the undeuterated and partially deuterated (DMe-DCNQI)$_2$Cu. One undeuterated sample (*h*) and two selectively deuterated samples (*d2*[1,1;0] and *d4*[1,1;2]) were measured. Both of the deuterated samples show the M-I-M transition (Fig. 1).

Results and Discussion

Typical dHvA oscillations for the *h* salt are presented in Fig. 2. The Fourier transform spectra are shown in the insets. The observed frequency is in the range from 350 T to about 15000 T for all the salts. For θ = 0°, one oscillation denoted by α is evident. For ω = 26°, the three different oscillations (δ_2, ε_5 and ε_6) are seen. Figure 3 presents the angular dependences of the low frequencies (F < 3000 T). We find seven different oscillations (α, β, γ, $\delta_1 \sim \delta_4$) with low frequencies (F < 3000 T). Many high frequency (F > 3000 T) oscillation (ε_1, ε_2,...) are observable in the (001) plane.

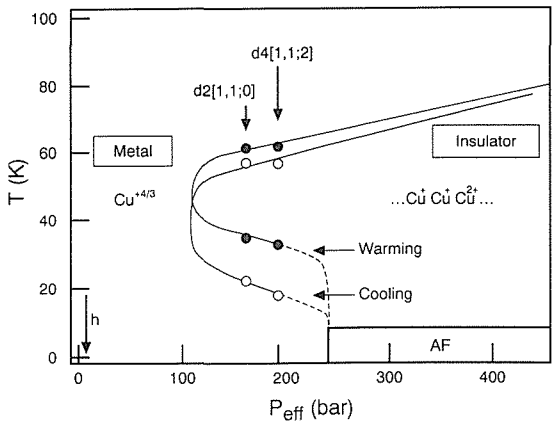

Fig. 1 P-T phase diagram of (DMe-DCNQI)$_2$Cu.

Taking into account of the contribution of the LUMO of the DCNQI molecules and the d_{xy} orbital of the Cu ions, the tight binding band calculation was carried out. The band structure consists of the two energy bands; the 1D energy bands having the p_π character, and the 3D energy band arising mainly from the d_{xy} orbital. The solid lines in Fig. 3 show the calculated frequencies corresponding to the extremal cross sectional areas of the 3D FS. The calculated results are in good agreement with the experimental results. Therefore, we conclude that the 3D FS exists, and that the seven low frequency oscillations (α, β, γ, $\delta_1 \sim \delta_4$) arise only from the 3D FS.

The high frequency oscillations (*F* > 3000 T) are observed in the (001) plane. On a basis of the calculated band structure, the high frequency oscillations are concluded to come from the large cyclo-

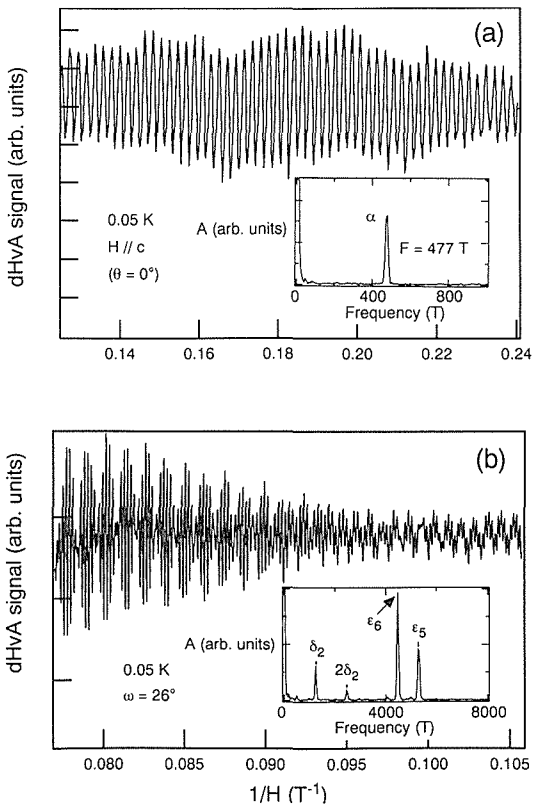

Fig. 2 The dHvA oscillations of the h salt at 0.05 K (a) for H//c axis (θ = 0°) and (b) for H in (001) plane (ω = 26°). ω is the angle from the c axis. The Fourier transform spectra are shown in the insets.

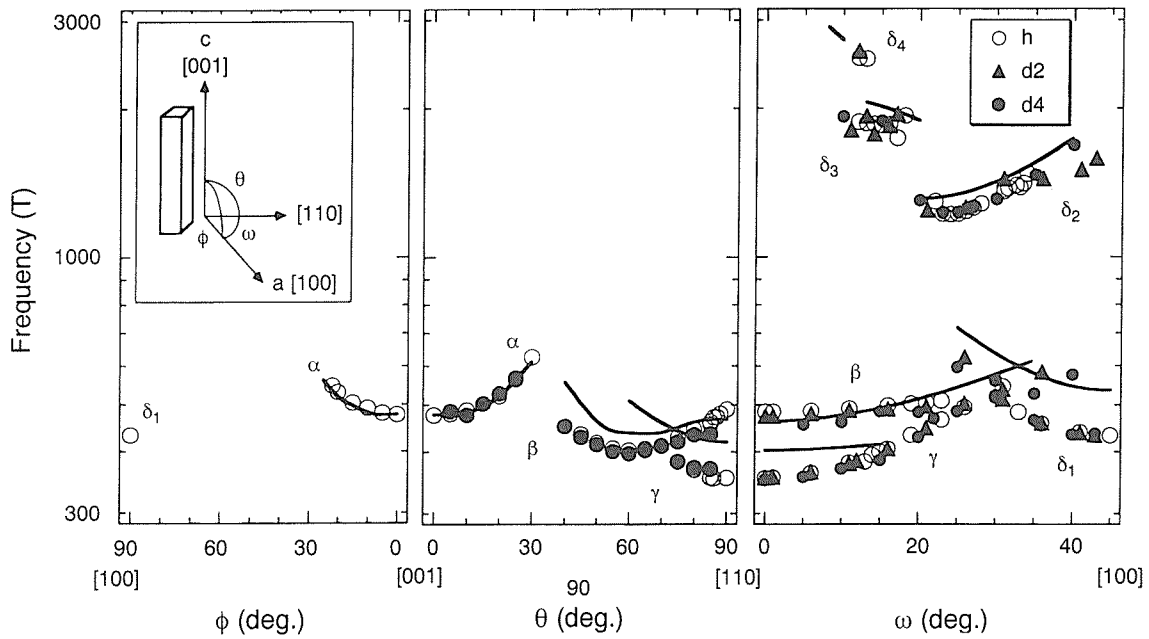

Fig. 3 Angular dependences of the low dHvA frequencies of the undeuterated (h) and deuterated (DMe-DCNQI)$_2$Cu salts (d2 and d4). The solid lines show the calculated results.

tron orbits on both the 1D and 3D FSs. They are observable only in limited angle ranges, which is ascribed to the characteristics FS structure. There are no appreciable differences in the frequencies between all the salts within the experimental error of about ±5%. Therefore, both the 1D and 3D FSs for all the salts are nearly the same in shape and in size.

The observed cyclotron mass m_c and the calculated band mass m_b are listed in Table 1. The cyclotron mass m_c is given by $m_c = m_b\,(1 + \lambda_{e\text{-}e})(1 + \lambda_{e\text{-}p})$, where $\lambda_{e\text{-}e}$ and $\lambda_{e\text{-}p}$ are the mass enhancement factors due to electron-electron interaction and electron-phonon interaction, respectively. The mass m_c of each oscillation is found to be the same for all the salts within the experimental error of about ±10%, and m_c is in good agreement with the band mass m_b. The agreement suggests that significant difference in the mass enhancement factors due to the many body effects is absent on both the 1D and 3D FSs in all the salts. Recently, the cyclotron resonance of the *d2* salt (H//c) was measured and the mass was determined to be 4.7 m_0, which is comparable to the mass of α.

The electronic specific heat coefficient γ for the alloy system $(DMe_{1-\chi}MeBr_{\chi}\text{-}DCNQI)_2Cu$ increases with increasing χ, and is steeply enhanced near the insulating phase. The similar behavior is observed for the alloy of the undeuterated and fully deuterated systems. The behavior of γ is consistent with the enhancement of the T^2 dependence in the resistance at low temperatures. Those results suggest that the mass of the conduction electrons is enhanced near the insulting phase. The possibility of the mass enhancement in this system has been predicted theoretically, considering strong electron correlation or strong electron phonon interaction.

Table 1 The calculated band masses m_b and the observed cyclotron mass m_c of the dHvA oscillations in the undeuterated (h) and deuterated salts (d2 and d4) of (DMe-DCNQI)$_2$Cu.

			h	*d2*	*d4*
label	**direction**	m_b/m_0	m_c/m_0	m_c/m_0	m_c/m_0
α	θ = 0°	4.0	3.5	-**)	3.3
β	ω = 0°	3.6	3.9	3.4	3.4
γ	ω = 0°	3.9	3.4	3.4	3.5
δ_1	ω = 45°	4.3	3.9	3.9	3.9
δ_2	ω = 25°	6.2	6.5	-**)	6.5
ε_5	ω = 25°	-*)	9.5	-**)	9.6
ε_6	ω = 25°	-*)	8.0	-**)	7.8

-*): not calculated
-**): not measured

However, even in the deuterated salts, such mass enhancement has not been observed by the dHvA experiments.

This work was performed in collaboration with R. Kato, H. Sawa, S. Aonuma, M. Tamura, and M. Kinoshita (ISSP, University of Tokyo), and J.S. Brooks (Florida State University).

❒ Field-induced Transition of f Electron Nature from Itinerant to Localized

H. Aoki, 4th Group & Tsukuba Magnet Laboratories

Keywords: heavy fermion, metamagnetic transition, f electron, Fermi surface

A class of cerium and uranium compounds are often referred as "heavy fermion" compounds. The name of "heavy fermion" comes from their enormously large masses of electrons which amounts to one hundred or even one thousand times as large as those of the normal metals. These compounds exhibit anomalous and interesting properties which originate from the highly correlated f electrons of cerium or uranium. The Coulomb interaction between the f electrons is significant in these compounds and the nature of the f electrons resides near the borderline between itinerant and localized. Although the heavy fermion compounds have been intensively studied in the past decade, many important issues have not been solved yet.

The properties of heavy fermion compounds are sensitive to external variables such as pressure and magnetic field. Most of the heavy fermion compounds exhibit metamagnetic transition in fields, i.e. the magnetization increases sharply at a certain magnetic field. $CeRu_2Si_2$ is one of the typical heavy fermion compounds which shows neither superconductivity nor magnetic order. It exhibits metamagnetic transition at about 7.7 T(Hm). The metamagnetic transition of the magnetic materials with well defined localized magnetic moments may be intuitively understood. For example in the antiferromagnetic materials the magnetic moments change their directions from antiparallel to parallel to the external magnetic field at the metamagnetic transition.

The mechanism of the metamagnetic transition of the heavy fermion compounds is very difficult to understand and closely correlated with the physics of heavy fermion. The f electrons of $CuRu_2Si_2$ behave at high temperatures as if they are localized. With decreasing temperature, the magnetic moments are thought to be suppressed via the Kondo effect. At lowest temperatures the magnetic moment is almost completely suppressed and behave like a paramagnetic material with large paramagnetic susceptibility. Almost at the same time a coherent state of the heavy electrons is formed. There is no phase transition between the high temperature state and the low temperature state. The question was what happens microscopically at the metamagnetic transition in this kind of materials.

The de Haas-van Alphen (dHvA) effect measurements have been performed in both field ranges above and below Hm to elucidate the microscopic nature of the metamagnetic transition. These studies have revealed a dramatic change of the electronic structure at the transition[1-3].

Figure 1 shows the angular dependence of the dHvA frequencies below and above Hm. The dHvA frequency is proportional to the extremal cross sectional area of the Fermi surface perpendicular to the field direction. From these measurements three dimensional Fermi surface shape can be derived. As is clear from Fig. 1, the Fermi surfaces below and above Hm are very different. It was found that Fermi surfaces below Hm can be explained by assuming that the f electrons are itinerant and those above Hm by assuming that the f electrons are localized.

Figure 2 shows the field dependence of the effective masses of the electrons responsible for the dHvA frequencies. The effective masses are nearly constant at low fields and is enhanced around Hm. Then, they decrease with increasing field above Hm. At sufficiently high fields the effective masses become nearly constant and much smaller than those below Hm. The behavior is qualitatively very similar to that of the electronic specific heat coefficient.

Summarizing the experimental results, the f electrons seem to change their nature from itinerant to localized at the metamagnetic transition and at the same time the masses of the electrons become smaller.

Above results gives valuable information of the microscopic nature of the metamagnetic transition. However, some important questions have not been

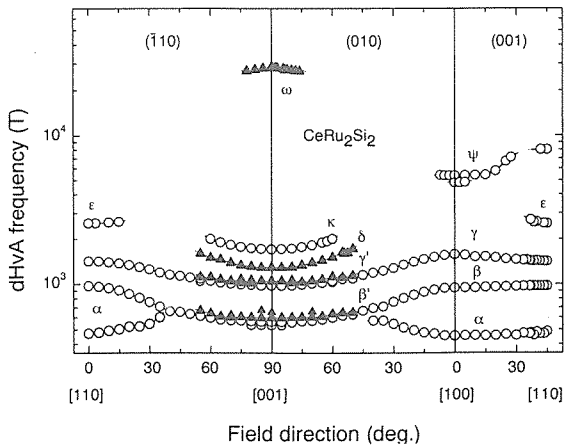

Fig. 1 Angular dependence of the dHvA frequencies. Open circles denote the frequency branch below Hm and closed triangles those above Hm.

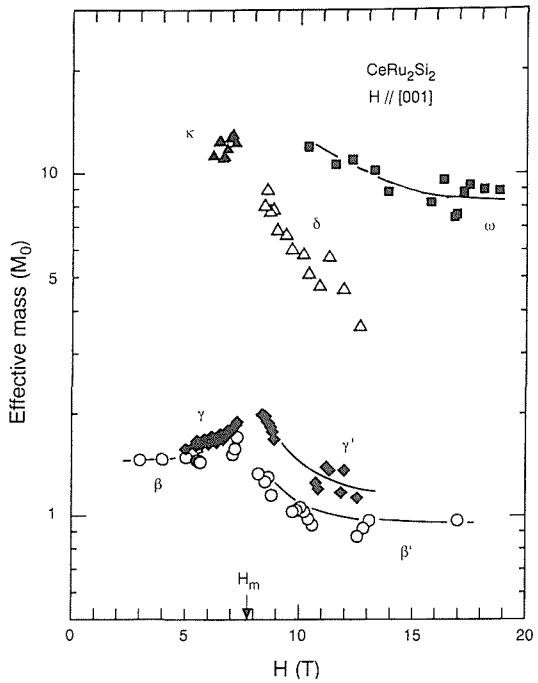

Fig. 2 Field dependence of effective masses.

solved yet. 1) The observed effective masses above Hm are much smaller than those expected from the specific heat measurements. This implies that the dHvA measurements miss to observe a part of the electrons. 2) The present observation also appears to violate the Luttinger sum rule. It states that the volume of the Fermi surface does not change irrespective of the interaction between the electrons unless phase transition takes place. Recent careful studies of the metamagnetic transition down to very low temperatures suggest that the metamagnetic transition is not likely to be phase transition. Then the volume of the Fermi surface should not change at the transition.

One of the possible interpretation is to assume that the dHvA measurements have not observed important and heavy Fermi surfaces above Hm. However, this interpretation is difficult to explain the fact that the observed Fermi surface above Hm is so close to that of the localized f electron model. Another possibility is that the dHvA effect observed above Hm could not be interpreted by the conventional semi-classical theory of the dHvA effect. Indeed many anomalous features of the dHvA effect, which is difficult to understand by the semi-classical formula, are observed above Hm. To answer the question, deeper understanding of the physics of the heavy fermion may be necessary.

References

1. *Transition of f Electron Nature from Itinerant to Localized: Metamagnetic Transition in $CeRu_2Si_2$ Studied via the de Haas-van Alphen Effect*, H. Aoki, S. Uji, A.K. Albessard and Y. Onuki, Phys. Rev. Lett. 71 (1993): 2110–2113.
2. *dHvA Effect Study of Metamagnetic Transition in $CeRu_2Si_2$*, H. Aoki, S. Uji, A.K. Albessard and Y. Onuki, J. Phys. Soc. Jpn. 62 (1993): 3157–3171.
3. *De Haas-van Alphen Effect Study of $CeRu_2Si_2$*, H. Aoki, M. Takashita, S. Uji, T. Terashima, K. Mawzawa, R. Settsai and Y. Onuki, Physica B 206 & 207 (1995): 26–28.

❒ Development of Powder Particle Assembly Technology

N. Shinya, T. Dan, M. Kobayashi, M. Egashira, T. Konno and H. Fudouzi, 5th Research Group

Keywords: particle assembly, manipulation, electrification

Multi-functional materials and intelligent materials are both new concepts in material science, and many efforts have been done in these areas. We proposed a new approach to create such materials as follows. It is possible to produce particles which have one primitive function such as sensor, actuator, processor, etc. Therefore, if we appropriately assemble several kinds of particles with different functions into a material, the material will have integrated and systematized functions which are derived from the component particles.

The key technology is an assembling technique of particles in our approach. Various methods to assemble particles are necessary according to its applications. Three different assembling techniques are investigated in our research group, i.e., ordered mixture of particles[1], particles assembly by electron beam[1, 2], and particles manipulation using probe[1, 3].

Ordered Mixture of Particles

We assume that particle A and particle B have a primitive function *A* and a primitive function *B*, respectively. If we can place particles B on the surface of particle A in order, this mixture may have an integrated and systematized function of *A* and *B*. This mixture is called an ordered mixture. The ordered mixture is expected to have a new function derived from the interface between particle A and particle B, besides the primitive functions *A* and *B*.

The method to produce the ordered mixture is as follows. Two kinds of particles are charged positively and negatively, respectively, by passing through the electric field formed between parallel electrodes. When both particles are mixed, an ordered mixture is produced by electrostatic force. Figure 1 shows a result of preliminary experiments using Au particles of 40 μm in diameter and SiO_2 particles of 5 μm.

In some cases, ordered mixtures produced by this method will be directly sintered to form bulk materials, and in other cases, they will be treated with assembling methods described below.

We have studied on improvement of electrification apparatus, mixing condition, variation of properties according to the ordered mixing, sintering condition, etc.

Particles Assembly by Electron Beam

This technique is to arrange particles on substrates and fit for less than about 10 μm of particles. The conceptual process of a particle arrangement consists of three steps, i.e., drawing, dipping and drying. The first step is to draw an electrified pattern on dielectric substrates with electron beam scanning. In the second step, the electrified substrates are dipped in a non-polar solvent, in which positively charged particles are dispersed. Particles in the suspension are attracted by the electrostatic force and adhered along the pattern. The third step, drying, is done as follows. The substrates are drawn up from the solvent, immersed in a volatile non-polar solvent for several seconds, and then dried in air. The repetition of this process using different kinds of particles will produce micro-devices and/or three dimensional structures. The three dimensional structures, produced artificially by the particles assembly, have the possibility to exhibit the systematized multifunction which may be safely called the intelligent function.

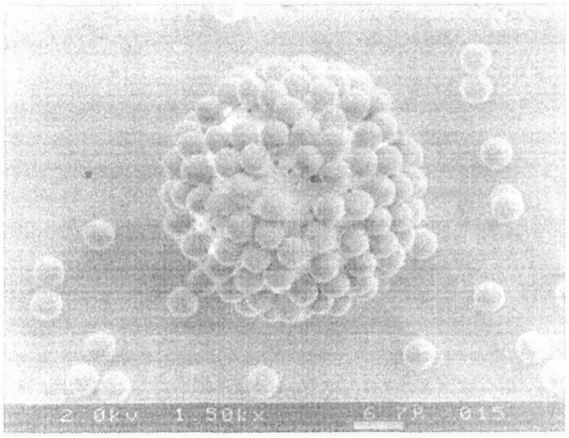

Fig. 1 Ordered mixture of Au and SiO_2 particles. The sizes of the Au and SiO_2 particles are 40 μm and 2.5 μm in diameter, respectively.

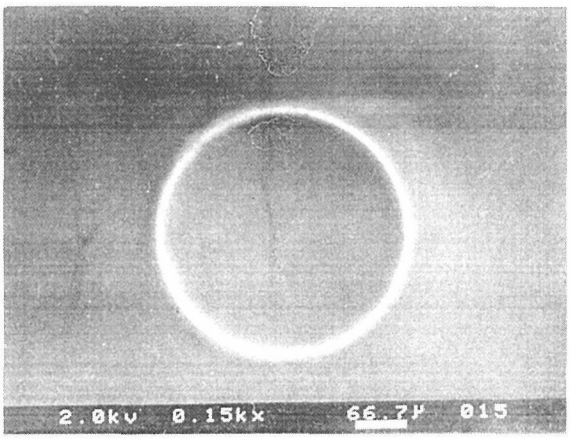

Fig. 2 Electrified circle pattern drawn on the $CaTiO_3$ substrate by electron beam. Diameter of the circle is 300 μm.

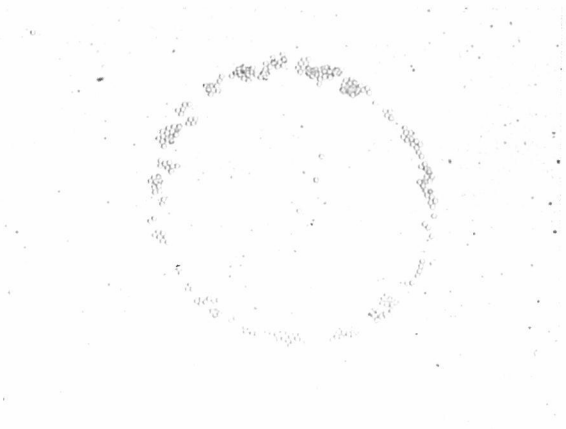

Fig. 3 SiO_2 particles (5.1 μmϕ) arranged on the electrified circle pattern shown in Fig. 2

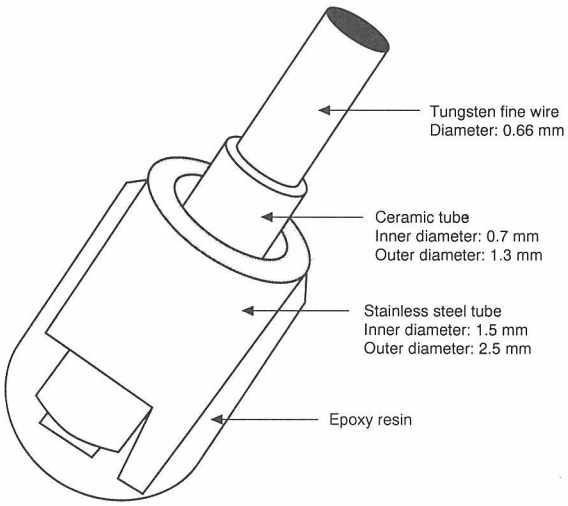

Fig. 4 Schema of the newly designed probe.

Experiments were carried out using spherical SiO_2 particles of 5 μm in diameter and polished $CaTiO_3$ substrates. An electrified circle pattern of 300 μm in diameter was drawn by scanning electron microscope (SEM) with CAD facilities. The charge distribution was visualized as secondary electron image at low energy primary electron beam (voltage contrast method), and shown in Fig. 2. Fluorinert (Sumitomo 3M) was used for dispersion solvent of SiO_2 particles, because of its non-polar and inert properties. Figure 3 is the results of the particles arrangement on the pattern shown in Fig. 2.

The effects of process parameters, such as primary electron beam energy and dose current for drawing, dipping time and suspension concentration for dipping, are investigated.

Particles Manipulation Using Probe

Manipulation using a probe handles one particle at a time, and size of the particles to be manipulated is about 10 to 100 μm. This method is, therefore, complementary to the assembly method described above.

The manipulation method of particles is, in general, classified into the mechanical method and the electrostatic method. We developed the latter by design of a new type probe. High voltage is applied between a substrate and a probe in the conventional electrostatic method. On the other hand, the new probe has two electrodes inside the probe and high voltage is applied between the two electrodes. The substrates do not suffer from high voltage in this manipulation. Therefore, this type of the probe can be used to the production process of IC chips in addition to the particle assembly.

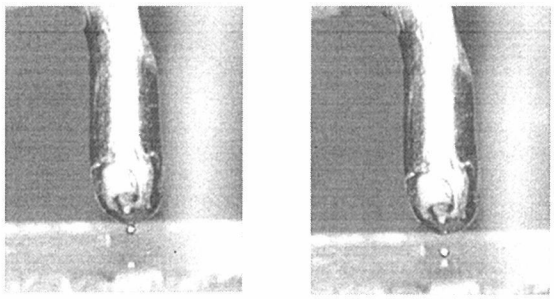

(a) (b)

Fig. 5 Manipulation of a single Au particle (400 μmϕ) with the probe. The particle is adsorbed by applying the voltage (a), and desorbed by cutting off the applied voltage (b).

Figure 4 is a schema of the probe, which size is about 3 mm in diameter. Au particles of 400 μm and styrene particles of 2.5 mm were manipulated with the probe. When voltages of 2–7 keV were applied between the dipole electrodes of the probe in the close vicinity of the particles, both Au particles and styrene particles jumped and adhered to the tip of the probe. The adsorbed particles were desorbed from the tip by cutting off the applied voltage. Figure 5 (a) and (b) show the manipulation of a single Au particle by this probe.

Conclusion

Our research group investigated various particles assembly techniques. Atom is an elemental unit of materials. A particle is also an elemental unit of materials from the practical view point. Thus, particles assembly will be improved in future work, and will become a key technology to create the multi-functional materials and intelligent materials.

References

1. *Powder Particle Assembly Using Electron Beam for Creation of Multi-Functional Materials*, N. Shinya, M. Egashira and H. Fudouzi, The 2nd Int. Conf. Intelligent Materials, Williamsburg (1994): 1741–1745.
2. *Powder Particles Assembly Technique Using Electron Beam*, H. Fudouzi, M. Kobayashi, M. Egashira and N. Shinya, The 3rd Asian-Pacific Workshop on Intelligent Materials, Tokyo, (1995): 94–96.
3. *Powder Particle Manipulation Using a Probe with Dipole Electrodes and Its Application*, T. Konno, M. Egashira and N. Shinya, The 3rd Asia-Pacific Workshop on Intelligent Materials, Tokyo (1995): 91–93.

❐ Cavitation Mechanisms in Superplastic Ceramics

K. Hiraga, Materials Strength Division

Keywords: superplasticity, zirconia, cavity nucleation and growth, damage accumulation

Introduction

Concurrent cavitation in superplastic ceramics is of practical importance because it limits both high temperature tensile ductility and subsequent room temperature strength. Earlier studies have revealed macroscopic trends in damaging behavior such as the evolution of cavitated area fraction and density loss during deformation[1]. However, in these studies conducted at relatively large strains, extensive cavity coalescence occurred to prevent detailed analysis, and hence there have been little information on the nature of cavitation in superplastic ceramics. In this study, we have intended to get more basic information available for cavity nucleation and growth mechanisms by examining cavity size distributions in an initial stage of superplastic deformation[2, 3].

Approach for Solving the Problem

We used a 3 mol% yttria stabilized tetragonal zirconia (3Y-TZP) because of its sluggish grain growth during deformation. For examining cavitation as explicit functions of stress, strain rate, and temperature, we conducted tensile creep tests under stress control between 16 and 40 MPa at 1548–1673 K in vacuum. Using an image processor combined with an optical microscope and SEM, we measured cavity size distributions on the polished surface of specimens deformed into prescribed strains. For reliable distribution statistics, more than 10^4 cavity sizes were measured for each deformed specimen. We developed programs for correcting the measured size distributions stereologically and for evaluating cavity growth rates. We confined the examinations to true strains smaller than unity, for which the cavity aspect ratios defined as (major axis length/minor axis length) were found to be smaller than 2 with a very little indication of coalescence.

Cavity Size Distribution and Nucleation Law

Figure 1 gives us the general characteristics of cavitation in the fine-grained TZP. The first point is the extremely high density of submicrometer-sized cavities resolved by SEM: more than 98% of cavity population is occupied by such fine cavities. The density decreases steeply as the cavity size exceeds those of the matrix grains resulting in bimodal distributions.

The second point is the shift of the size distribution towards higher density regime as strain increases, which is an indication of continuous nucleation. Though the micrometer-sized cavities were found to grow continuously from the submicrometer-sized cavities, their formation rate was about 50 times smaller than that of the latter ones. Such a situation and the bimodal nature in the size distributions indicate that different growth mechnisms work between the micrometer-sized cavities and the more finer ones.

The third point of Fig. 1 is the marked evolution in the distribution tail with increased strain, which suggests more active cavity growth in larger sizes. Cavitated area fraction cumulated from the tail of size distribution revealed that more than 95% of damage volume is occupied by the micrometer-sized cavities in spite of their low population and hence their growth plays central role in damage accumulation.

Growth Law of Micrometer-Sized Cavities

Assuming the micrometer-sized cavities as spheres, which is practically reasonable for cavities with aspects ratios smaller than 2, we evaluated their growth rates by applying the method given by Schneibel and Martinez[4] to the corrected distributions. The evaluation typically given in Fig. 2 reveals a growth law of $dR/dt \propto R$. For elucidating the growth law in more detail, we examined the growth rate as a function of stress, strain rate, strain, and temperature. The results confirmed that the cavities larger than about 1 μm obey the following growth law on strain(ε) and time(t) basis:

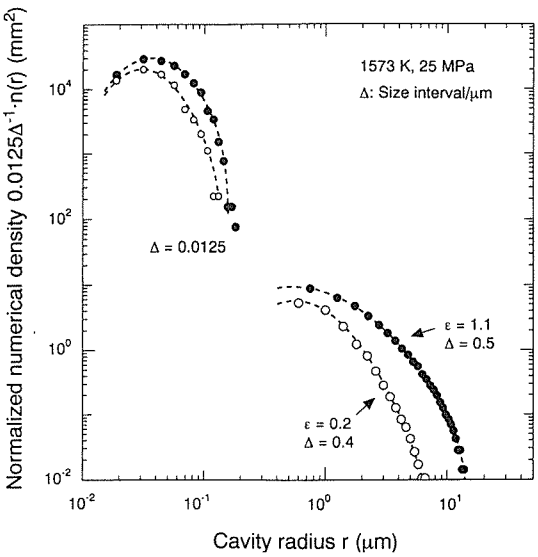

Fig. 1 Cavity size distributions on polished specimen surface.

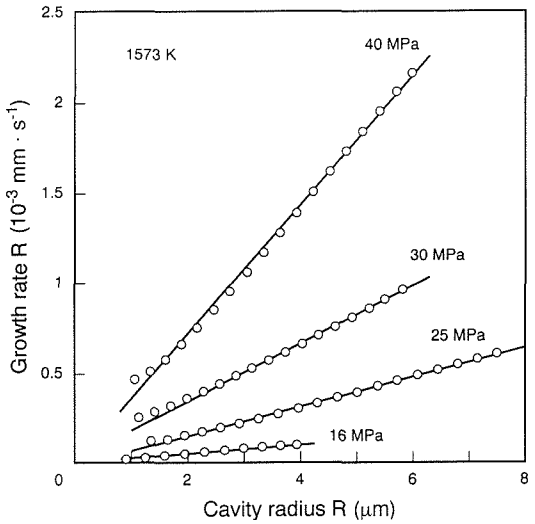

Fig. 2 Cavity growth rate as a function of cavity radius.

$$\text{strain bais}: \quad dR/d\varepsilon = R \tag{1}$$

$$\text{time basis}: \quad dR/dt = \dot{\varepsilon}R = k'\sigma^3 \exp\left(-600000/R_g T\right)R \tag{2}$$

where k is a material constant, σ is stress, R_g is the gas constant, and T is temperature. The growth law is exactly compatible with a model[5] of void growth in power-law creeping material. In addition, the stress exponent and the activation energy for cavity growth are consistent with those of matrix flow, respectively. Consequently, we concluded that the micrometer-sized cavities grow by the superplastic flow of the matrix.

Owing to a problem in the stereological size correction, we have not accomplished the analysis for the submicrometer-sized cavities yet. However, the steep decrease in the cavity density near the grain size indicates that their growth rates tend to decrease as their sizes increase. It suggests that diffusional mechanisms under constraints from the adjoining grains[5] may explain their growth behavior.

Damage Accumulation Model

On the basis of the clarified nucleation law and the growth mechanism of the micrometer-sized cavities, we derived a damage accumulation model represented as:

$$\begin{aligned} V_t(\varepsilon) &= V_0 + \Delta V_0(\varepsilon) + \Delta V_{nuc.}(\varepsilon) \\ &= V_0 + \int_0^{R_{max}} \int_0^{\varepsilon} 3N_0(R)V_0(R)\exp(3\varepsilon_x)d\varepsilon_x dR \\ &\quad + \int_0^{\varepsilon} V_C\left(dN/d\varepsilon_x\right)\exp\left[3\left(\varepsilon - \varepsilon_x\right)\right]de_x \end{aligned} \tag{3}$$

where $V_t(\varepsilon)$ is the total damage volume of strain ε, V_0 is the total initial volume of preexistent cavities, $\Delta V_0(\varepsilon)$ is the increment of V_0 by cavity growth, $\Delta V_{nuc.}(\varepsilon)$ is the increment of damage by nucleation and growth of new cavities, $N_0(R)$ and $v_0(R)$ are the size distribution function of the preexistent cavities and their initial volume, respectively, $\exp(3\varepsilon_x)$ arises directly from the cavity growth law, $V_c(= 4/3\pi\ \mu m^3)$ is the critical volume for the growth law, $dN/d\varepsilon$ is the formation rate of cavities larger than 1 μm, and $\exp[3(\varepsilon-\varepsilon_x)]$ represents the volume increment of a cavity nucleated at strain ε_x. As given in Fig. 3, the observed damage volume just follows the theoretical prediction. It can be also seen that though most of the damage consists of growing preexistent cavities at small strains ($\varepsilon <$ −0.5), the damage from newly nucleating cavities tends to overtake the former one at higher strains.

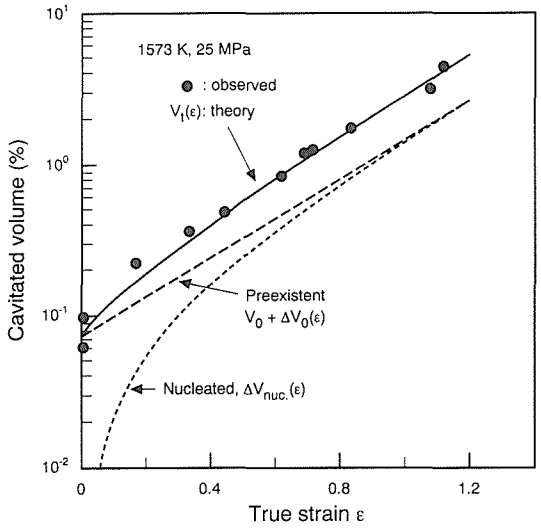

Fig. 3 Theoretical calculation of cavity damage accumulation.

References

1. *Superplasticity in Fine Grained Ceramics and Ceramic Composites: Current Understanding and Future Prospects*, A.F. Chokshi, Mater. Sci. Eng., A166 (1993): 119–113.
2. *Cavity Growth in a Fine-Grained Yttria-Stabilized Tetragonal Zirconia during Superplastic Deformation*, K. Hiraga, et al., *Strength of Materials*, Ed. by Oikawa et al., J. Inst. Metals, (1994): 843–846.
3. *Cavity Nucleation and Growth in a Fine-Grained Tetragonal Zirconia During Superplastic Deformation*, K. Hiraga, et.al., Abstracts of 7th Int. Conf. on Mech. Behavior of Mater., Ed. by A. Bakker, (1995): 169–170, to appear in Acta Metall, Mater.
4. *Determination of Cavity-Growth Rates from Cavity-Size Distributions*, J.H. Schneibel and L. Martinez, Phil. Mag., A, 54 (1986), 489–500.
5. *Fracture at High Temperature*, H. Riedel, Springer Verlag, (1987): 201–214 and 172–197.

❒ Extreme High Vacuum Integrated Process Using Magnetic Levitation Transports for Creation of Nano-structure Materials

M. Tosa, A. Itakura, Y. Yoshitake, M. Harada and K. Yoshihara, 4th Research Group

Keywords: extreme high vacuum, super conducting transport, magnetic levitation, linear motor drive, integrated process

Introduction

Development of advanced materials on an atomic scale manipulation in the near future demands the process to accumulate atoms one by one onto ultra clean substrates in ultra clean environment. The process comprises lots of continuous operations of substrate cleaning, deposition, etching, surface analysis, performance test and so on. It is difficult to carry out all operations in situ in the same chamber because each instrument for each operation has a number of its own high performance components and it is impossible to assemble all components in the same chamber.

The pressure less than 10^{-10} Pa (extreme high vacuum: XHV) can cause almost no surface contamination by the adsorption and can offer ideal ultra clean environment for a long time to artificially synthesize advanced materials with manipulation of atoms. Production of extreme high vacuum environment requires very low outgassing chamber, high sensitivity gauge system, high performance vacuum pumps and so on. Extreme high vacuum should be kept in using the transport system. Transport system to be used in extreme high vacuum should generate no particle because particles are sources of outgassing, therefore, it is essential to use no sliding components to keep extreme high vacuum system. A magnetic levitation transport system can meet the demand as it employs no sliding motion.

The purpose of this study, therefore, is to develop a XHV integrated process which can transfer specimens long distance from one XHV instrument to another XHV instrument without any contamination of gas adsorption on the ultra clean surface by means of XHV environment.

Generation of XHV

The XHV integrated process is composed of vacuum chambers, vacuum pumps, vacuum gauges, gate valves, specimen transports and instruments as shown in Fig. 1. Three chambers for instruments can join with the main chamber in transport through into chambers. Figure 2 shows the photograph of the whole system. The length of the main chamber is 2 m and a side of the square section is 0.3 m. The volume of the main chamber is about 0.2 m^3. Type 316 L stainless steel was employed as chambers material because it has no ferritic structure which causes magnetization and little intergranular corrosion for its low carbon content. The wall surface inside the chambers was electrolytically polished in phosphoric-sulfuric acid solution. All chambers were annealed at 830 K in a high vacuum. All components exposed to the extreme high vacuum environment of the main chamber use metal sealings for high temperature bakeout and can reduce outgassing remarkably.

Tandem turbo molecular pump system (pump speed: 0.2 $m^3\ s^{-1}$ and pump speed: 0.5 $m^3\ s^{-1}$) and two tantalum getter pump (speed: 1 $m^3\ s^{-1}$) evacuate each intro chamber, whole a tantalum getter pump and a bakable cryopump (pump speed: 1 $m^3\ s^{-1}$) evacuate the main chamber. The cryopump can be baked at 480 K because refrigerator system is separated from cryopanel housing in order to keep its cold head below 240 K during its bakeout. The

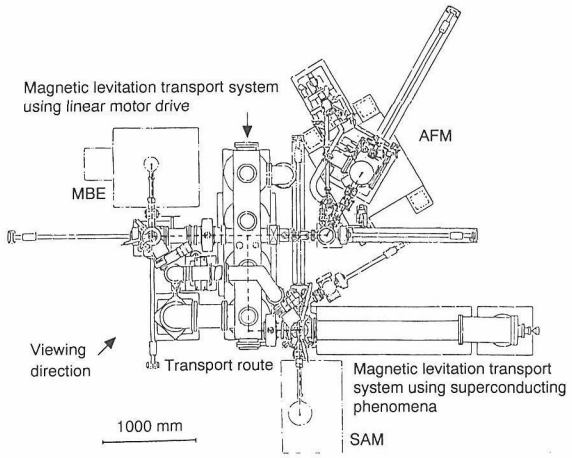

Fig. 1 Schematics of the XHV integrated process using levitation transports.

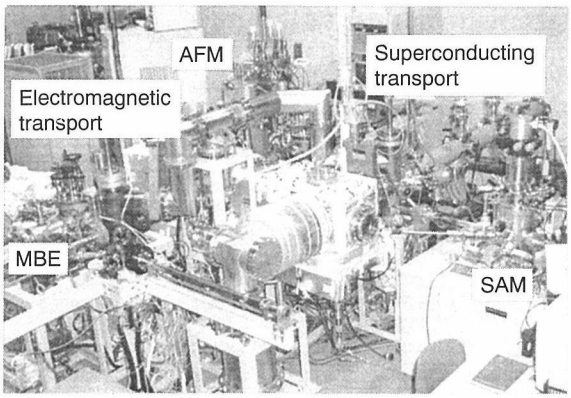

Fig. 2 Photograph of the XHV integrated process using levitation transports.

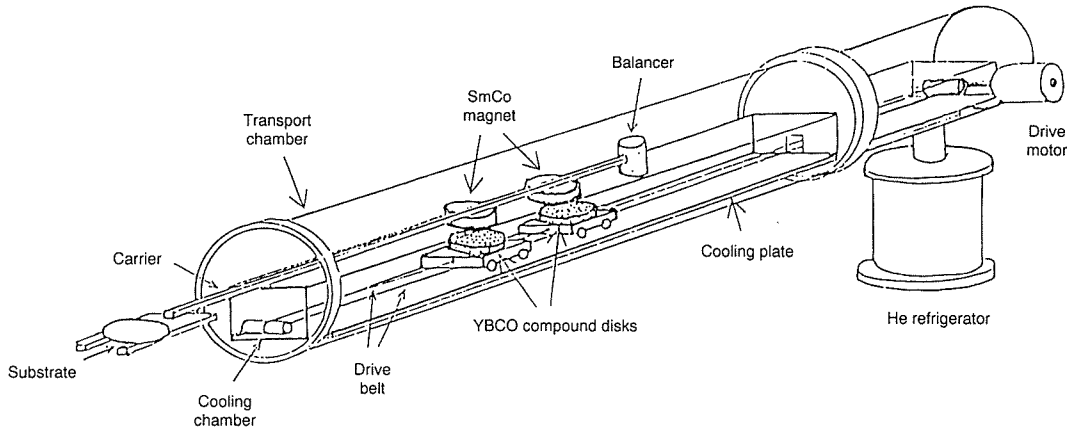

Fig. 3 Schematics of the superconducting levitation transport.

pressure in the main chamber was measured by an extractor gauge and a quadrapole mass spectrometer with separated ion source system.

The main chamber was annealed at 430 K for 67 hours and achieved pressure of less than 9×10^{-10} Pa about 300 hours in total after pumping start at atmospheric pressure of dry nitrogen gas purged into the chamber.

Levitation Transports

Two type of magnetic levitation transport systems were installed in the extreme high vacuum system because they have no sliding part and generate little dust particle and little outgassing. One transport system in the main chamber levitate a carrier with specimens about 2 mm above stators by electromagnet in four stators and transfer the carrier by linear motor drive. Combination of linear motor system and magnetic levitation system can transfer specimens smoothly through the junction connecting main chambers. A stator has electromagnets for levitation under the cooling plate and electromagnets for linear motor on the plate. Most part of the stator is occupied with electromagnets for antiroll because of poor stability of electromagnetic levitation and this antiroll system makes the whole transport system very large. The carrier can transport three specimen holders at variable speed from 10 mm s^{-1} up to 50 mm s^{-1} and can be positioned within an error of about 0.5 mm. Operation of the transfer system increased the base pressure from 2.4×10^{-9} Pa to 2.7×10^{-9} Pa in the main chamber.

The other transport system in an intro chamber could levitate the carrier with an specimen holder by two $YBa_2Cu_3O_{7-x}$ superconducting magnet discs and could transfer the carrier with permanent magnet discs of SmCo mechanically by a belt conveyor. Figure 3 shows a schematic model of the superconducting levitation transport system. Both Meissner effect for levitation and pinning effect for traction generated by superconductor discs provide the carrier with stable levitation transfer operation. This effect makes no necessity of antiroll system for the stable levitation and the whole system compact compared with the transport in the main chamber. The superconductor discs were installed in the chamber filled with cooled helium gas below 90 K which was separated vacuum atmosphere in transfer chamber. Operation of the transfer system increased base pressure of 8.4×10^{-9} Pa little and could transfer specimens at 10 mm s^{-1}.

The systems could successfully transfer a specimen from one intro chamber connecting with a scanning auger microprobe chamber to another intro chamber connecting with an atomic force microscope chamber through the intro chambers and the main chamber within the pressure change of 10^{-10} Pa.

Conclusion

We successfully developed a minimum unit for XHV integrated process which can transfer specimens from one XHV instrument to another XHV instrument without any contamination of gas adsorption on the ultra clean surface by means of levitation transports. The next phase is to develop advanced materials on an atomic scale manipulation by means of the XHV integrated process with more number of improved transport units and with more number of connected instruments.

References

1. *Extreme High Vacuum System for Long-Distance Transport*, M. Tosa, A. Itakura and K. Yoshihara, Vacuum 44 (1993): 549–551.
2. *Magnetic Levitation Transport for XHV Continuous Process*, M. Tosa, A. Itakura, M. Harada and K. Yoshihara, J. Vacuum S. Jp. 37 (1994): 789.

❒ Studies on the New Intermetallic Compound Superconductors of Borocarbide System

K. Togano, 1st Research Group

Keywords: borocarbide superconductor, intermetallic compound, thin film

Introduction

After the discovery of high temperature superconductivity in cupurate superconductors in 1986, most efforts of searching for new superconducting substances have been concentrated on the oxide materials. However, recent discovery of a new family of borocarbide intermetallic superconductors of RE-T-B-C, where RE = rare earth elements and T = Ni, Pd, Pt, attract again the interest in intermetallic compounds as a possible road to high temperature superconductivity. We started the study on this new materials immediately after the announcement by the collaboration group of ATT and Univ. of Tokyo, and succeeded to identify the superconducting phase in Y-Pd-B-C system which has the highest transition temperature of T_c of ~23 K. We are now studying on the phase stability of the borocarbide systems in order to establish the basis of processing high quality materials. We already succeeded to synthesize the thin film of borocarbide superconductor for Y-Ni-B-C system.

Identification of 23 K Superconducting Phase in Y-Pd-B-C System

Since the thin film of A15 Nb_3Ge recorded the highest T_c of 23 K in 1972, no new families of high T_c intermetallic compounds have been discovered. Therefore, the recent discovery that the Y-Pd-B-C alloy system has a superconducting onset temperature of 23 K in bulk form was exciting[1] and, hence, stimulated considerable interest in this new superconducting system of borocarbides. However, since the Y-Pd-B-C material could be synthesized only in the form of the multiple phases, the superconducting phase remained unidentified. In this work, we carefully investigated the relationship between the microstructure and superconducting properties of the Y-Pd-B-C system in order to identify the superconducting phase and determine its crystal structure[2].

Several samples with composition around $YPd_5B_3C_{0.3}$, which was reported as the optimal composition for superconductivity[1], were prepared by conventional arc melting technique. We carried out careful examinations comparing the results of superconductivity measurements by SQUID magnetometer, microstructure observations by optical microscope and scanning electron microscope (SEM), and x-ray diffraction (XRD). As a result, we found that the diamagnetic signal is largest for the

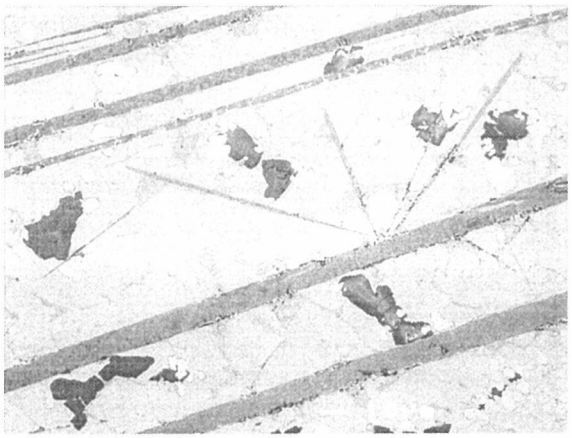

Fig. 1 Scanning electron micrograph for the arc melted $YPd_5B_3C_{0.5}$ ingot. The 23 K superconducting phase is embedded as plate like crystals in the matrix of other phases.

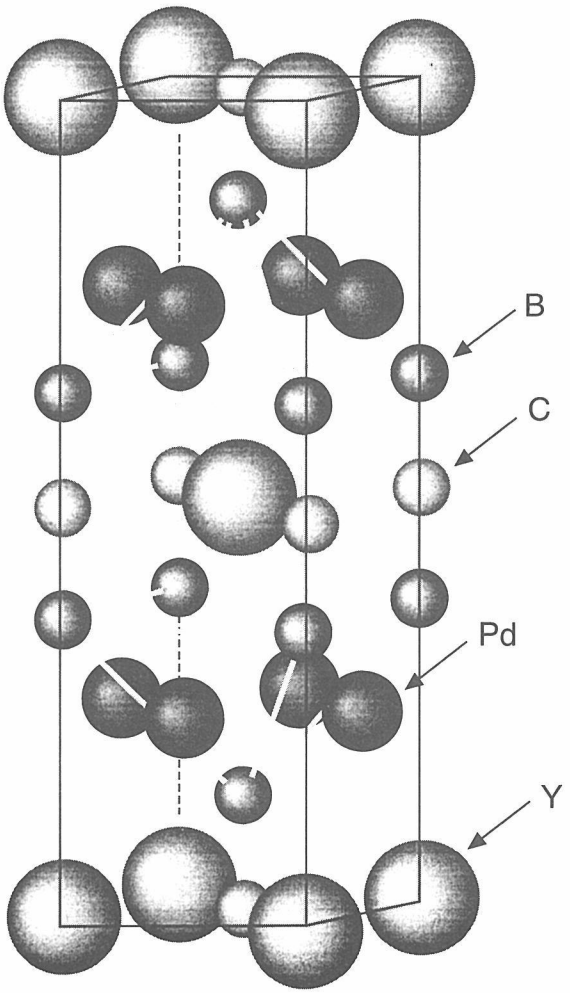

Fig. 2 Crystal structure of YPd_2B_2C compound.

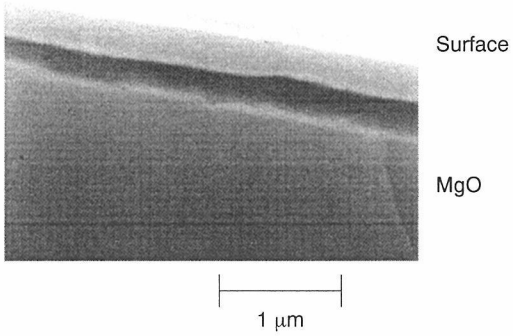

Fig. 3 Scanning electron micrograph of the YNi_2B_2C thin film synthesized by rf magnetron sputtering.

vicinity of $YPd_5B_3C_{0.3-0.5}$ composition and the large diamagnetism signal is always accompanied with the appearance of many platelike crystals in the microstructure (Fig. 1) and diffraction peaks of body-centered-tetragonal structure in XRD pattern. Electron probe X-ray microanalysis (EPMA) suggested that the platelike crystal has a stoichiometric composition of $Y_1Pd_2B_2C_{1.5}$, although there might be uncertainty in C concentration. These results of the microstructure and superconductivity studies led us to the conclusion that the platelike crystal with body-centered tetragonal structure is the 23 K superconducting phase. In order to obtain more detailed information on the crystal structure, we carried out transmission electron diffraction (TED) and high resolution transmission electron microscopy (HRTEM) studies[3]. As a result, we found that the crystal structure is very similar to that reported for the superconducting $LuNi_2B_2C$ intermetallic compound. Figure 2 shows the crystal structure when the stoichiometry is speculated as YPd_2B_2C.

Annealing experiment of the $YPd_5B_3C_{0.3}$ sample indicated that the superconducting phase is stable only at higher temperature. We are now studying on the stabilization of superconducting phase in Y-Pd-B-C system by the addition of other element such as Pt and rapid quenching from molten state.

Synthesis of Y-Ni-B-C Thin Film

The purpose of this experiment is to establish the technique to synthesize thin films of borocarbide superconductors in order to investigate the feasibility of their device application. The material we examined at first was Y-Ni-B-C system[4], since the superconducting phase in this system can be easily synthesized by conventional melting method, suggesting that it is thermodynamically stable.

The method we employed was conventional rf magnetron sputtering. The turget was powder of Y-Ni-B-C alloy prepared by arc melting and milling. The sputtered material was deposited on

Table 1 Parameters of Bi-2212/Ag coil

Tape length	7.3 m × 2
Cross section	15 μm × 22 mm × 2
(Bi-2212)	
Number of turns	154
Inner bore	13 mm
Outer diameter	46.5 mm
Potting materials	Epoxy

MgO(100) substrates maintained at room temperature under a pressure of 0.5 Pa of Ar. The substrates were arranged in on-axis geometry to the turget. The as deposited films were completely amorphous and showed no trace of superconductivity. However, by the post annealing at 1050 °C, the film was found to transform to the crystalline YNi_2B_2C phase with strong c-axis alignment. Figure 3 shows the SEM micrograph on the cross section of the cleaved sample. The film showed a sharp superconducting transition with the onset of 15 K, which was almost the same as the value reported for bulk sample. The results of critical current measurement indicated the anisotropy of pinning force and upper critical field B_{c2}.

This is the first success of synthesizing thin film of borocarbide superconductor. Synthesis of Y-Ni-B-C film without post annealing is also being investigated, because it is more practical for the application. We are also attempting the synthesis of YPd_2B_2C compound, which has higher T_c and is more thermodynamically unstable.

References

1. *Superconductivity at 23 K in Yttrium Palladium Boride Carbide*, R.J. Cava, H. Takagi, B. Batlogg, H.W. Zandbergen, J.J. Krajewski, W.F. Peck Jr., R.B. van Dover, R.J. Felder, T. Siegrist, K. Mizuhashi, J.O. Lee, H. Eisaki, S.A. Carter and S. Uchida, Nature 367 (1994): 146.
2. *Structure and Superconducting Properties of Y-Pd-B-C System*, H. Fujii, S. Ikeda, T. Kimura, S. Arisawa, K. Hirata, H. Kumakura, K. Kadowaki and K. Togano, Jpn. J. Appl. Phys. 33 (1994): L590.
3. *High Resolution Transmission Electron Microscopic Studies on a Superconductor YPd_2B_2C Compound*, S. Ikeda, H. Fujii, T. Kimura, H. Kumakura, K. Kadowaki and K. Togano, Jpn. J. Appl. Phys. 33 (1994): 3896.
4. *Synthesis of YNi_2B_2C Thin Films by Magnetron Sputtering*, S. Arisawa, T. Hatano, K. Hirata, T. Mochiku, H. Kitaguchi, H. Fujii, H. Kumakura, K. Kadowaki, K. Nakamura and K. Togano, Appl. Phys. Lett. 65 (1994): 1299.

❐ Generation of the Highest Field, 21.8 T, of Superconducting Magnet by the Hybridization of Metallic and Oxide Superconducting Coils

H. Kumakura, H. Kitaguchi and K. Togano, 1st Research Group

Keywords: Bi-based oxide superconductor, insert coil, critical current density

Introduction

Recently, a newly developed superconducting magnet system at NRIM accomplished the magnetic field generation of 21.1 T at 1.8 K[1]. However, it is very difficult to generate higher fields by conventional metallic superconductors, such as Nb_3Sn, because of its low critical current density J_c at ~20 T. Bismuth-based oxide superconductors, on the other hand, show excellent J_c vs magnetic field properties at low temperatures. Especially, grain oriented $Bi_2Sr_2CaCu_2O_x$(Bi-2212) layers prepared on Ag tapes by the melt-solidification method show excellent J_c values, higher than $10^5/cm^2$ even in magnetic fields above 20 T at 4.2 K. Hence, the Bi-2212/Ag composite tapes are expected as conductors of a high field superconducting magnet which can generate fields higher than 20 T. A new type hybrid superconducting magnet system can be constructed by the combination of conventional superconductors and an oxide superconductor. It is expected that a magnet made of this Bi-2212/Ag tape can be used as an insert magnet of a superconducting magnet system which can generate fields higher than 21 T. We have fabricated small pancake coils using the Bi-2212 tapes prepared by a continuous dip-coating process, and the coils were used as an insert coil of the superconducting magnet system.

Fabrication of Bi-2212/Ag Insert Coils

Bi-2212/Ag composite tapes were fabricated by applying the combination of continuous dip-coating process and slow cooling from a partially molten state[2]. The slurry for dip-coating was prepared by mixing fine Bi-2212 powder, organic solvent, binder and dispersant. The Bi-2212 powder was obtained by calcination of Bi_2O_3, $SrCO_3$, $CaCO_3$ and CuO. Nominal composition of Bi-2212 was 2.00(Bi): 2.00(Sr): 0.96(Ca): 2.00(Cu). Ag tapes with 30 mm width and 80 μm thickness were dipped into a slurry and pulled at a rate of 90 cm/min, and the tapes were coated with slurry on both sides. Each dip-coated tape was wound into a pancake coil with small gap between each turn, and then heat treated. At first, the coils were heated at 810 °C in air to remove organic materials and to decompose carbonates. Each pancake coil was, then, put on the powder mixture of $Bi_2Al_4O_9$ and Al_2O_3, covered with an alumina crucible and heat treated. During the heat treatment, bismuth was vaporized from $Bi_2Al_4O_9$. This heat treatment under bismuth atmosphere suppresses the vaporization of bismuth from oxide layers, which minimizes the precipitation of Bi-free impurity phases.

Melt-solidification was performed by heating up to 892 °C and cooling down to 835 °C at a rate of 5 °C/hr. By this heat treatment, highly grain-oriented Bi-2212 crystals with their c-axes perpendicular to the tape surface were formed on a Ag tape. The typical thickness of the superconducting layers after the heat treatment was ~15 μm on each side of a Ag tape. Current leads and voltage taps were soldered to the Ag tape. 100 μm thickness Ag plates and 20 μm thickness Ag tapes were used for current leads and voltage taps respectively. Organic films (Mylar tape) of 50 μm thickness were inserted into the gaps between turns for insulation. The coil was tightly wound around a stainless-steel pipe of 14 mm diameter which was inserted into the center of the coil, and then, encased in a stainless-steel frame of 46.5 mm outer diameter. Finally, the coil was impregnated with epoxy resin cured with acid anhydride. In this way, two pancake coils were fabricated. Two pancake coils were stacked coaxially and were electrically connected in series with Ag tapes. Figure 1 shows this double stacked Bi-2212/Ag coil. The parameters of the coil were listed in Table 1.

Performance Test

The double stacked pancake coil was inserted at the center of a conventional superconducting magnet[1]. The total magnet system used in this test was schematically shown in Fig. 2. The superconducting magnet used in this experiment consisted of four types of Nb-Ti and Nb_3Sn superconducting

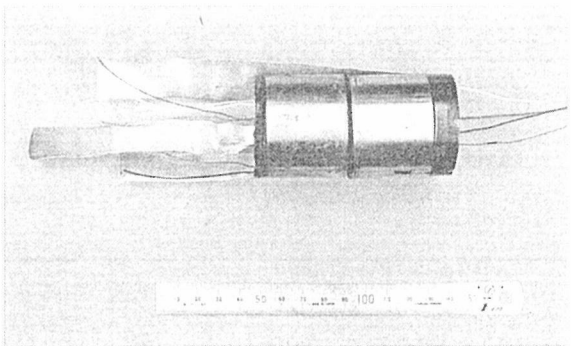

Fig. 1 Double stacked Bi-2212/Ag coil prepared by the continuous dip-coating process and melt-solidification method.

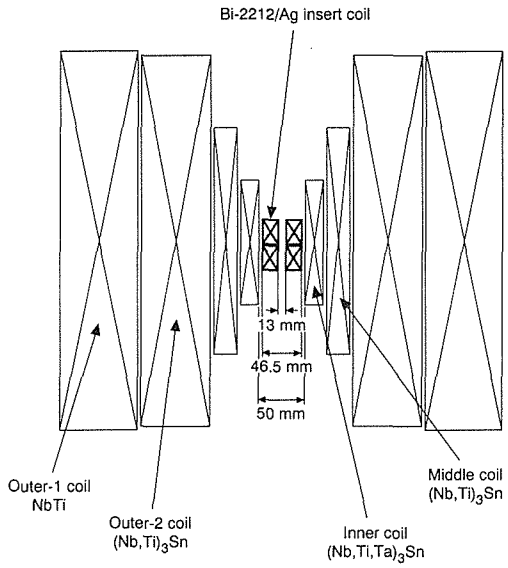

Fig. 2 The total magnet system used for the coil test.

coils. The outer-1 and outer-2 coils were made of stacked double pancakes with conductors of twisted multifilamentary NbTi strands and (Nb, Ti)$_3$Sn strands, respectively. The middle coil was also made of double stacked pancakes with monolithic conductors of multifilamentary (Nb, Ti)$_3$Sn. The inner coil was a solenoid wound of a monolithic conductor of multifilamentary (Nb, Ti, Ta)$_3$Sn. This magnet system successfully generated a magnetic field of 21.1 T in 50-mm bore of the inner magnet by cooling with saturated superfluid helium.

The performance test of the Bi-2212/Ag coil was also carried out at a saturated helium temperature (~1.8 K) under bias magnetic fields up to 20.9 T. I-V characteristics of the coil were measured by a four probe resistive method. The generated field of the coil was measured with a Hall probe. I_c depended on the sweep rate of the applied current. When the sweep rate was 300 A/min., I_c of the coil was 310 A with a criterion of 10^{-13} Ωm in a bias field of 20.9 T. This I_c of 310 A corresponded to the field generation of 0.9 T. Hence, the superconducting magnet system achieved generation of total magnetic field of 21.8 T. Measured resistivity of a Ag tape was ~5×10^{-9} Ωm in 20 T at 4.2 K. Because the temperature dependence of magnetoresistivity of Ag was small below 10 K, the I_c criterion of 10^{-13} Ωm was much smaller than the magnetoresistivity of Ag at 20.9 T and 1.8 K. Thus, current by-passing through the Ag tape was negligibly small for applied currents smaller than I_c.

J_c for the Bi-2212 layer was 4.7×10^4 A/cm^2 at 20.9 T. This J_c was higher than that of the Bi-2212/Ag coil reported before[3], but was still smaller than the highest J_c of Bi-2212/Ag short samples, ~10^5 A/cm^2. Furthermore, local I_c of the Bi-2212/Ag tape wound into a pancake was measured to be ~500 A which was larger than that of the whole length of the tape. These results indicated that there was I_c scatter along the tape length due to the inhomogeneity of the superconducting oxide layer. Another reason for the I_c degradation of the coil is the large Lorentz-force applied to the conductors in high magnetic fields. This large Lorentz-force introduces microcracks in oxide layers. Hence, the improvement of mechanical properties of the coil is very important for the application in high fields. Addition of small amount of second element to Ag significantly improves the mechanical properties of the conductors without serious degradation of J_c. We are now trying to fabricate pancake coils using the Ag alloy tapes.

This research program was performed in collaboration with Hitachi Cable Co. Ltd.

References

1. T. Kiyoshi, K. Inoue, K. Itoh, T. Takeuchi, H. Wada, H. Maeda, K. Kuroishi, F. Suzuki, T. Takizawa, N. Tada and H. Mori, Trans. Appl. Superconductivity, 3 (1993): 78.
2. H. Kumakura, H. Kitaguchi, K. Togano, H. Maeda, J. Shimoyama, T. Morimoto, K. Nomura and M. Seido, Cryogenics 32 ICMC Supplement (1992): 489–495.
3. N. Tomita, M. Arai, E. Yanagisawa, T. Morimoto, H. Fujii, H. Kitaguchi, H. Kumakura, K. Inoue, K. Togano, H. Maeda, K. Nomura, Appl. Phys. Lett. 65 (1994): 898–900.

❒ Silicon Isotope Enrichment by Infrared Laser Irradiation

T. Noda, Second Research Group

Keywords: isotopically controlled materials, silicon isotope separation, hexa-fluoro-disilane, silicon tetra-fluoride, infrared multi-photon decomposition

Most elements appearing on the periodic table consist of several stable isotopes. Advanced nuclear and physical properties are expected[1], if materials are composed of selected isotopes. In order to realize such so-called isotopically controlled materials, it is necessary to develop processes producing massively purified isotopes. Among elements, silicon is one of the important materials in nuclear and semi-conductor industries. Isotopically selected silicon or silicon compounds can be envisaged to have improved properties such as high uniformity in electric properties, high thermal conductivity, low transmutation, and low induced activity[1].

In the present study, isotopic selective decomposition of hexa-fluoro-disilane(Si_2F_6) by infrared laser has been examined to optimize the practical separation for silicon isotopes. Si_2F_6 with a purity of around 99.9% was prepared by the fluorination of Si_2Cl_6 followed by the low-temperature distillation in vacuum. The system consists of a CO_2 pulse laser, a reaction cell, a gas supplier and a vacuum pump, a distillation still, and a sample cylinder[2]. Reaction cells, 20 mmϕ × 100 mm long and 60 mmϕ × 2000 mm long, with respectively KCl and NaCl windows at both ends were used. CO_2 laser with the energy fluence range of 3–7 kJ/m^2 at the front window of the cell was irradiated at repetitions between 1 and 16 Hz. The full width at half maximum of the laser was 100 ns and the wavenumbers were set between 934.929 and 980.969 cm^{-1} by adjusting the grating mirror. The laser beam was slightly converged with a ZnSe lens with a focal length of 1.5 m. The Si_2F_6 was introduced into the cell in the ranges of 8.3-66.7 mm^3/s and 10.6–266.6 Pa. The silicon isotope composition in SiF_4 produced by the laser irradiation and residual Si2F6 was determined by a mass spectrometer.

Figure 1 shows the infrared spectrum of Si_2F_6 and emission lines of CO_2 laser between 900 and 1100 cm^{-1}. The absorption peak at around 990 cm^{-1} is assigned to the antisymmetric vibration of ^{28}Si-F bond. ^{29}Si-F and ^{30}Si-F absorption peaks are shifted to lower wavenumbers though these are very weak. Multi-photon decomposition of Si_2F_6 is therefore considered to occur in the wavenumber region of 10P and 10R branches of the CO_2 laser.

By irradiation of infrared laser with a fixed wavenumber, SiF_4, with enriched silicon isotopes was produced[2]. The enrichment of silicon isotopes depends on experimental parameters especially wavenumber and energy fluence of the laser. In Fig. 2, each isotope composition in SiF_4 produced is shown as a function of wavenumber under constant other parameters. The natural Si is composed of 92.23% of 28Si, 4.67% of 29Si and 3.10% of 30Si. As seen in this figure, ^{29}Si and ^{30}Si were enriched in the 940–970 cm^{-1} range while the concentration of ^{28}Si decreased. In the region of 975–980 cm^{-1}, ^{28}Si slightly concentrated in the SiF_4 vice versa. The maximum concentrations of ^{29}Si and ^{30}Si in the SiF_4 were 43% and 12% at 951.20 cm^{-1} and 956.20 cm^{-1}, respectively. The yield of SiF_4 increases with increasing wavenumber. $^{29}SiF_4$ and $^{30}SiF_4$ were continuously obtained at yields of 4 and 10% at maximum concentration. Such selective decomposition reactions were examined on the basis of

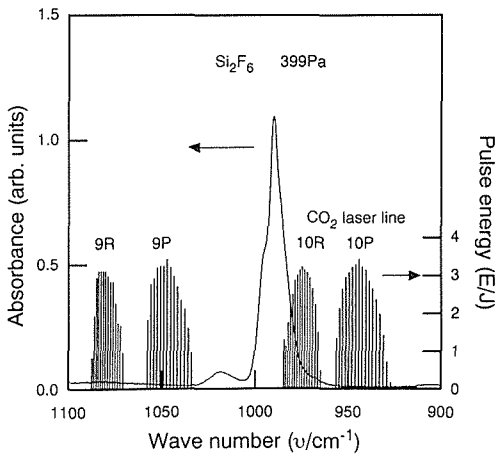

Fig. 1 Infrared spectrum of Si_2F_6 and CO_2 laser lines in the wavenumber region of 900–1000 cm^{-1}.

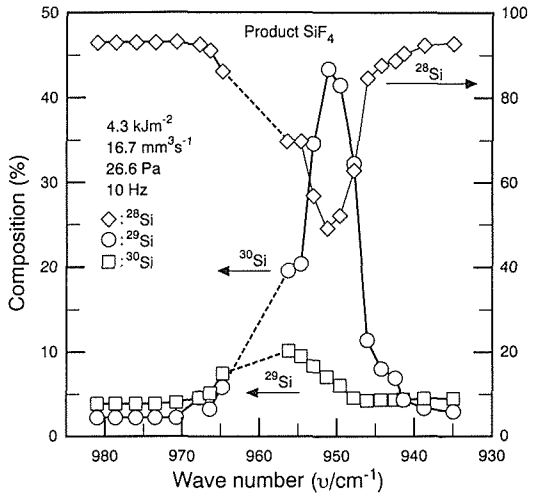

Fig. 2 Concentrations of ^{28}Si, ^{29}Si and ^{30}Si in the SiF_4 as a function of wavenumber of the laser.

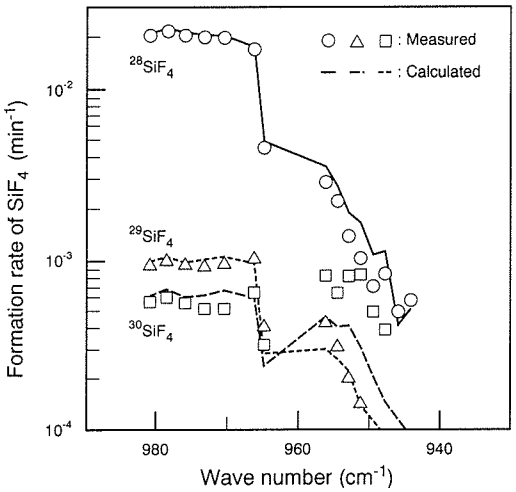

Fig. 3 Formation rates of $^{28}SiF_4$, $^{29}SiF_4$ and $^{30}SiF_4$ as a function wavenumber. The calculated values were obtained from the decomposition rate of Si_2F_6.

yields of isotopic SiF_4 and residual Si_2F_6 species assuming the following decomposition reaction.

$$Si_2F_6(gas) \rightarrow SiF_4(gas) + SiF_2(solid) \quad (1)$$

The reactions of isotopic species were expressed as

$$^{28.28}Si_2F_6 \rightarrow {}^{28}SiF_4 + {}^{28}SiF_2 \quad k1 \quad (2)$$

$$^{28.29}Si_2F_6 \rightarrow {}^{28}SiF_4 + {}^{29}SiF_2 \text{or} {}^{29}SiF_4 + {}^{28}SiF_2 \quad k2 \quad (3)$$

$$^{28.30}Si_2F_6 \rightarrow {}^{28}SiF_4 + {}^{30}SiF_2 \text{or} {}^{30}SiF_4 + {}^{28}SiF_2 \quad k3 \quad (4)$$

$$^{29.29}Si_2F_6 \rightarrow {}^{29}SiF_4 + {}^{29}SiF_2 \quad k4 \quad (5)$$

$$^{28.30}Si_2F_6 \rightarrow {}^{29}SiF_4 + {}^{30}SiF_2 \text{or} {}^{30}SiF_4 + {}^{29}SiF_2 \quad k5 \quad (6)$$

and

$$^{30.30}Si_2F_6 \rightarrow {}^{30}SiF_4 + {}^{30}SiF_2 \quad k6 \quad (7)$$

where ki is the decomposition rate constant which is experimentally obtained. It is found that k5 and k6 are larger than k1 by one order magnitude between 940 and 960 cm^{-1}. The order of magnitude of k is $k_6 > k_5 > k_3 > k_4 > k_2 > k_1$. Such difference in reaction rate constant leads to the enrichment of silicon isotope. Reaction rates increase with wavenumber. However, the tendency is reversed and k1 exceeds k5 and k6 in the region over 970 cm^{-1}. Eqs. 2–7 give the formation rates of $^{28}SiF_4$, $^{29}SiF_4$ and $^{30}SiF_4$.

Figure 3 shows the comparison of the formation rate of SiF_4 between calculated and measured values as a function of wavenumber. As seen in this figure, fairly good coincidence is observed. It is therefore found that the isotopically selective decomposition of Si_2F_6 occurs according to the above reaction.

As described above, ^{28}Si concentrates in the residual Si_2F_6 when ^{29}Si and ^{30}Si are enriched in the SiF_4. The concentration of ^{28}Si in the Si_2F_6 increases with increasing the laser power. In order to avoid the damage of windows of the reaction cell at high energy fluence, the 2 m-long cell was used so that the laser beam was focused at the half-length of the cell for ^{28}Si concentration. At present, Si_2F_6 with ^{28}Si content of 99.6% could be obtained at the yield of 5% under the laser conditions of 952.923 cm^{-1} and 2.81J.

As the summary, followings are concluded.

1. Maximum concentrations of 43% for ^{30}Si at 951.203 cm^{-1} and 12% at 956.205 cm^{-1} for ^{29}Si were obtained in the SiF_4 produced by the selective decomposition by the CO_2 laser irradiation.
2. The yields of $^{30}SiF_4$ and $^{29}SiF_4$ were 4 and 10%, respectively.
3. ^{28}Si with 5% yield was concentrated up to 99.6% in the residual Si_2F_6 at 952.923 cm^{-1}.
4. The decomposition of Si_2F_6 was explained by the reaction as $Si_2F_6 \rightarrow SiF_4 + SiF_2$, and the difference in decomposition rates between isotope species determines the enrichment of each silicon isotope.
5. Above results indicate the massive Si isotope separation can be easily performed.

References

1. T. Noda, Kinzoku, 7 (1993): 32–37 (in Japanese).
2. H. Suzuki, H. Araki, T. Noda, J. Japan Inst. Metals, 58 (1994): 1101–1102 (in Japanese).

❒ Developments of High Strength and High Conductivity Cu-Ag Alloy Wires and Sheets

Y. Sakai, T. Asano, K. Inoue and H. Maeda, High Magnetic Field Research Station

Keywords: high-field material, Cu-Ag alloy, microcomposite, pulsed magnet material, Bitter magnet material

Recently we successfully developed a new Cu-Ag alloy with a promising combination of high mechanical strength and high electrical conductivity, which is a microcomposite composed of a Cu matrix and a lot of ultrafine Ag filaments, as shown in Fig. 1. As a Cu-Ag alloy ingot including about 16% at Ag is cold-worked into a wire or a sheet with intermediate-annealing frequently at 350–450 °C, it turns into a microcomposite showing high conductivity of 75–83% IACS and high tensile strength of 0.7 - 1.1 GPa at room temperature. These values are much superior to those of a Cu-Nb microcomposite alloy which is one of the best high-field materials having high mechanical strength and high electrical conductivity.

The Cu-Ag microcomposite alloy shows the excellent mechanical strength with being slightly cold-worked over 93% areal reduction ratio, while a very heavy cold-work more than 99.97% areal reduction ratio is necessary for realizing such high mechanical strength in the Cu-Nb microcomposite alloy. A further advantage of the Cu-Ag microcomposite is easiness in melting and casting the alloy ingot due to its low melting point and poor chemical activity, resulting in excellent homogeneity of its microstructure and physical properties. Therefore the properties of the alloy wires and sheets are easily reproducible when we manufactured them on commercial basis.

In addition, the cold-rolled Cu-Ag microcomposite sheet scarcely shows anisotropy with respect to the rolling direction both in strength and conductivity. Although the Cu-Nb microcomposite shows excellent conductivity in a wire and poor conductivity in a sheet, the Cu-Ag microcomposite shows excellent conductivity both in a wire and a sheet. The Nb fine films in the Cu-Nb microcomposite sheet have very poor electrical conductivity and then prevent the current pass through them, resulting in increase in its resistivity through the increase in transport current pass length. On the other hand, the fine Ag films in the Cu-Ag microcomposite sheet have excellent electrical conductivity and does not increase in its resistivity without preventing the current pass through them. The tensile strength vs. electric conductivity curves at room temperature for the wires and the sheets of the Cu-Ag microcomposite alloys and the Cu-Nb microcomposite alloys are shown in Fig. 2.

The Cu-Ag alloy wire is a very promising material for solenoid-type high-field pulsed magnet, because both large hoop stress and large Joule heating are the most serious problems during operation of these pulsed magnet. In collaboration with Leuven University of Belgium, we wound the Cu-Ag microcomposite rectangular wires of 2 mm × 3 mm cross-section into several small pulsed magnets, which were cooled down to 77 K and energized by the large pulsed-discharge currents from a capacitor bank system of 250 kJ. One of them could generate non-destructively 73.4 T with duration time of 5 msec in a 10 mm bore. With developing a new powerful winding machine we became able to wind relatively thick Cu-Ag microcomposite rectangular wires of 4 mm × 6 mm

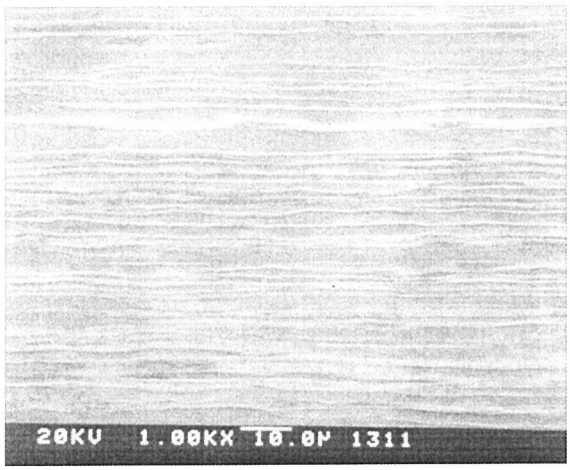

Fig. 1 Microstructure of cold-drawn Cu-Ag microcomposite wire observed by a SEM.

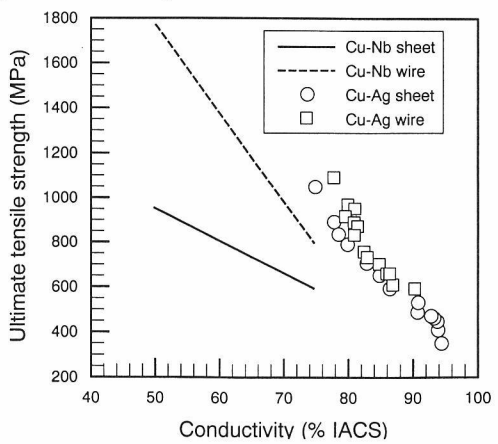

Fig. 2 Comparison of tensile strength vs. electrical conductivity for the wire and the sheet of Cu-Ag microcomposite and those of Cu-Nb microcomposite.

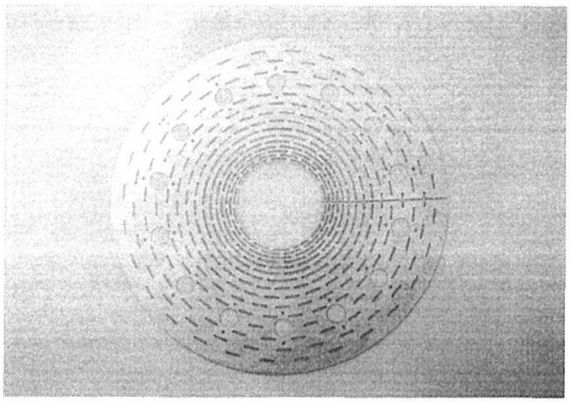

Fig. 3 A Bitter plate of Cu-Ag microcomposite for 34 T class water-cooled magnet.

cross-section into relatively large pulsed magnets. One of them could generate non-destructively 65.3 T with duration time of 100 msec in a 16 mm bore by connecting with a capacitor bank system of 1.6 MJ. These non-destructive pulsed fields are the present world records, considering the bore sizes and the duration times.

The Cu-Ag alloy sheet is also a promising material for Bitter-type water-cooled magnet, because both the large hoop stress and large Joule heating are the most serious problems in the high-field water-cooled magnets. The water-cooled magnet is energized by a large dc power supply and cooled by a large water- cooling system. Bitter-type water-cooled magnet is composed of many conductor plates (Bitter plates) and many inserted insulator plates, which have a lot of holes at the same positions, as shown in Fig. 3. With piling up the Bitter plates and insulator plates, their integrated holes form many cooling channels of water in a water-cooled magnet. On the other hand, every Bitter plates electrically contacts each other at the each edge, where there is no insulation, and electrically forms a helical structure in a Bitter-type magnet.

The feasibility study of the Cu-Ag microcomposite alloy sheet as Bitter magnet sheets is progressing now in collaboration with the Francis Bitter National Magnet Laboratory, the National High Magnetic Field Laboratory of USA, and the National Research Institute for Metals. The maximum field, generated by the water-cooled magnet, is determined by the conductor material, the magnet design, and the power for energizing and cooling. There is the most powerful power supply and cooling system of 24 MW in the NHMFL. By using these large facilities we are now progressing to develop a 34 T class Bitter-type magnet made of Cu-Ag microcomposite alloy sheets by the end of 1995. Fig. 3 shows a Bitter plate made of the Cu-Ag microcomposite sheet in the 34 T class Bitter-type magnet. The value of 34 T will be the world record generated by a water-cooled magnet.

There is a hybrid magnet system of Hybrid III at the FBNML, of which the former highest-field record was 34.0 T. A steady field of 35.3 T was generated on May, 1994, by inserting the Cu-Ag microcomposite alloy Bitter sheets into the highest-field region in the Hybrid III of the FBNML, which is composed a 22.8 T Bitter-type water-cooled magnet and 12.5 T outer superconducting magnet. The steady field of 35.3 T was the highest field record till we succeeded in generation of 35.8 T at the end of March, 1995, using a hybrid magnet composed of a 21.7 T inner polyhelix-type water-cooled and a 14.1 T outer superconducting magnet. Polyhelix-type magnet is composed of many co-axial helical coils with different outer and inner diameters. The cooling water flows between each helical coil in the polyhelix-type magnet. It is more expensive to fabricate the polyhelix-type magnet due to its complicated structure, but more suitable to generate higher field than Bitter-type magnet because the optimized current distribution can be more easily attained in the polyhelix-type magnet. We are now studying on the application of the Cu-Ag microcomposite alloy to the polyhelix-type water-cooled magnet for developing a 45–50 T class hybrid magnet.

References

1. *Development Of 40 Tesla Hybrid Magnet System*, K. Inoue, T. Takeuchi, T. Kiyoshi, K. Itoh, H. Wada, H. Maeda, T. Fujioka, S. Murase, Y. Wachi, S. Hanai and T. Sasaki, IEEE Trans. on Mag. Vol. 30 (1994): 493–496.
2. *40 T Class Hybrid Magnet System*, K. Inoue, T. Takeuchi, T. Kiyoshi, K. Itoh, K. Takehana, H. Wada, H. Maeda, T. Fujioka, S. Murase, Y. Wachi, S. Hanai, Y. Dozono and T. Kojo, Physica B 201 (1994): 517–520.
3. *High-Strength and High-Conductivity Cu-Ag Alloy Sheets: New Promising Conductor for High-Field Bitter Coils*, Y. Sakai, K. Inoue and H. Maeda, IEEE Trans. on Mag. 30 (1994): 2114–2117.
4. *Copper-Silver Wire Coils for Pulsed Magnet*, T. Asano, Y. Sakai, M. Oshikiri, K. Inoue, H. Maeda, G. Heremans, L.V. Bockstal, L. Liang and F. Herlach, Physica B 201 (1994): 556–559.
5. *Design of a Poly-Bitter Magnet at the NHMFL*, M.D. Bird, S. Bole, Y.M. Eyssa, B.J. Gao, H.J. Schneider-Muntau, to be published in Proc. of MT-14. (1996).
6. *Hybrid Magnets—a Magnet Engineer's Experience*, Y. Iwasa, to be published in Physica B (1996).

❒ New High Field Magnets and Facilities

H. Maeda, High Magnetic Field Research Station

Keywords: high-field magnet, long-pulsed magnet, hybrid magnets, high-field superconducting magnet, high resolution magnet

In order to measure and evaluate high-field properties of high-T_c oxide superconductors, we have been developing several extremely-high field magnets since 1988, such as 80 T class long-pulsed magnets, a 40 T class hybrid magnet, and a 20 T class superconducting magnet, etc. Recently, most of these magnets were completed and are being used for measuring various kinds of high-field properties.

It is easier and more economical to generate a pulsed high magnetic field than a steady high magnetic field. However, the measurements in pulsed fields are difficult due to the large noise induced by rapid field change and the delayed penetration of quickly-varied field into a conductive sample. Therefore it is necessary for the high-field measurements of conductive materials to develop a long pulsed magnet with a duration time longer than 1 msec. We recently developed a Cu-Ag microcomposite wire with high mechanical strength and high electrical conductivity. Large hoop stress and large Joule heating are the most serious problems in fabricating a high-field long-pulsed magnet. However, it is very difficult to wind the thick Cu-Ag microcomposite wire into a small solenoid coil, because of very large spring-back force caused by bending the Cu-Ag micro-composite. With developing a new powerful winding machine at first, we could wind the Cu-Ag microcomposite rectangular wires into several pulsed magnets with internal reinforcements of glass fibers, which were cooled down to 77 K and energized by the large pulsed-discharge currents from a capacitor bank systems, as shown in Fig. 1. One of them, a relatively small coil wound of a 2 mm × 3 mm rectangular wire, could generate non-destructively 73.4 T with duration time of 5 msec in a 10 mm bore with being connected with a 250 kJ capacitor bank. The other hand, a relatively large coil wound of a 4 mm × 6 mm wire, could generate non-destructively 65.3 T with duration time of 100 msec in a 16 mm bore with being connected with a 1.6 MJ capacitor bank. We have used these pulsed fields for measuring the superconducting critical currents of various superconductors, the de Haas-van Alphen effects of heavy fermion compounds and the far-infrared cyclotron resonances.

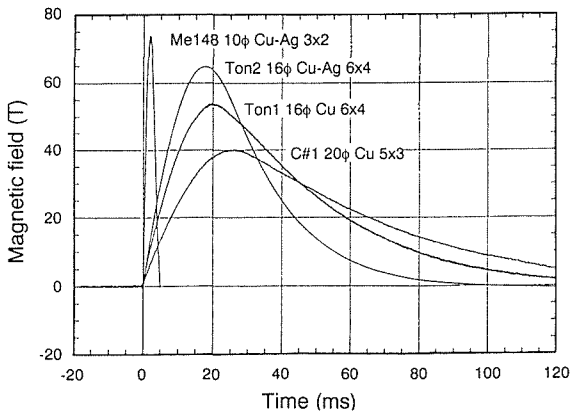

Fig. 1 Pulsed magnetic fields generated by various types of Cu-Ag multilayered coils with internal reinforcements of grass fibers.

We have developed a 20 T class large bore superconducting magnet, which can supply several kinds of high-field experimental spaces by changing the combination component coils as shown in Fig. 2. The cryostat of this magnet system is separated into two coaxial chambers with thermal insulator. The outer-1 and the outer-2 coils in the outer chamber are operated at 1.8 K, connected in series, and generate fields up to 15 T in the inner temperature-variable chamber, the diameter is 314 mm. The middle coil in the inner chamber generates 18.06 T at 1.8 K in a 160 mm cold-bore. An inner coil is inserted into the bore of the middle coil, and excited at 1.8 K with an independent power supply. We have already fabricated four coils as the inner coils. By using the No. 4 coil developed this year, we have been succeeded in generating 21.5 T in a clear bore of 61 mm without quenching. The field is also a new world record

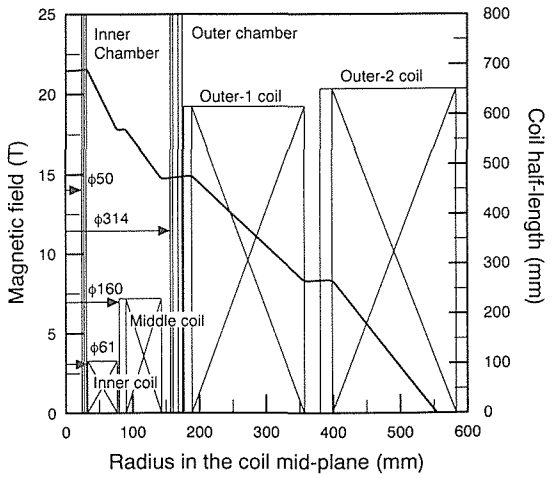

Fig. 2 Magnetic field distribution and bore sizes in the middle plane of 20 T class large bore superconducting magnet with the component coil locations.

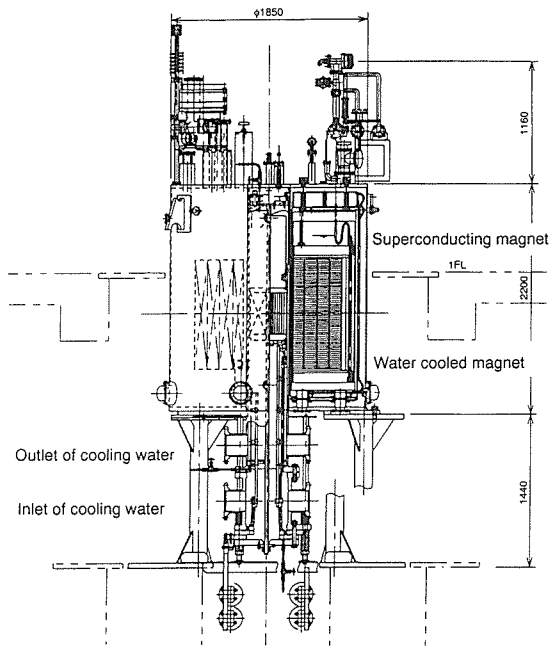

Fig. 3 Whole view of 40 T class hybrid magnet.

generated by a metallic superconducting magnet. This improvement seems to be caused by using an advanced $(Nb, Ti)_3Sn$ conductor with low Cu ratio of 0.25 for the No. 4 coil. The Cu ratio of the conductor in the No. 3 coil is 0.48. The 21 T superconducting magnet system is now being used, for instance, for the coil tests of high T_c oxide superconductors. Under a background field of 20.9 T a small test coil of Bi-2212 oxide double pancake coil has generated totally 21.8 T in a 13 mm clear bore, which is also the highest field record generated by a full superconducting magnet system.

We have completed the fabrication of the 40 T class hybrid magnet system including a 15 MW dc power supply (maximum voltage of 430 V and maximum current of 35 kA), a 15 MW water-cooling system (inlet temperature below 10 °C, mass flow rate of 700 t/hr, pressure loss of 147 MPa), a helium liquefier/refrigerator (150 1/hr in liquefaction mode and 450 W at 4.4 K in refrigeration mode), and a hybrid magnet composed of an outer superconducting magnet and an inner water-cooled magnet. Figure 3 shows the whole view of the 40 T class hybrid magnet. The outer superconducting magnet consists of 58 double pancake windings with 470 mm inner diameter; each pancake is wound with four kinds of superconductors (G1, G2, G3, and G4), where the grading depends on the experienced field distribution. Th G3 and the G4 conductors, used in lower fields, are Nb-Ti multifilamentary monoliths. The G1 and the G4 conductors, used in higher fields, are composite conductors of Cu-housings and $(Nb, Ti)_3Sn$ multifilamentary monoliths. The outer superconducting magnet is designed to generate background fields up to 15 T in a room temperature bore of 400 mm. The operation temperature, the maximum operation current, and the maximum stored energy of the outer superconducting magnet are designed to be 4.2 K, 1476.1 A, and 63.37 MJ, respectively.

This year we have been progressing the test operation of the whole hybrid magnet system. At first the outer superconducting magnet was cooled down gradually from room temperature to 4.2 K by flowing cold helium gas and by pouring liquid helium supplied from the helium liquefier/refrigerator into the crostat. It took about 150 hrs. to cool down the outer superconducting magnet. Then the test operation of outer superconducting magnet up to 14.2 T has been performed successfully without quenching.

We have fabricated two kinds of inner water-cooled magnets (Insert A and Insert B), which are designed to generate incremental fields up to 25 T and 20 T in clear bores of 30 mm and 50 mm with consuming electric power of 13.3 MW and 10.8 MW, respectively under a background field of 15 T. The Insert A is a polyhelix coil composed of 18 helices made of a $Cu\text{-}Al_2O_3$ alloy. The Insert B is also a polyhelix coil composed of 15 helices made of Cu-Cr alloy (6 inner coils) and $Cu\text{-}Al_2O_3$ alloy (9 outer coils). Test operations of hybrid mode have been performed up to 32.1 T and 35.7 T with using the Insert B and the Insert A under the background field of 14.1 T, respectively. Considering the clear bore sizes, these values are both the new world records of steady magnetic fields. We will try to generate the designed maximum fields within the next 1–2 years.

In addition, we have installed commercially available best superconducting magnets including two 16 T high-homogeneous-field magnets, 11.75 T-NMR magnet, 15 T split magnet, and several small superconducting magnets, which are also being used for measuring high field properties of superconductors; semiconductors, organic conductors and magnetic materials.

References

1. *High Field Installations at the Tsukuba Magnet Laboratories of NRIM*, K. Inoue, T. Takeuchi, T. Kiyoshi, T. Asano, Y. Sakai, K. Itoh, and H. Maeda, to be published in Physica B (1995).
2. *Present Status and Future of the Tsukuba Magnet Laboratories*, H. Maeda, K. Inoue, T. Kiyoshi, T. Asano, Y. Sakai, T. Takeuchi, K. Itoh, and G. Kido, to be published in Physica B (1995).

❐ Cytotoxity Evaluation of Metal Salts and Its Compound Effects — Toxicity Decreasing Due to Titanium and Iron Salts —

A. Yamamoto and M. Sumita, 2nd Research Team

Keywords: biomaterials, biocompatibility evaluation *in vitro*, metal salts

Toxicity Evaluation of Metallic Biomaterials

Stainless steels, cobalt-chromium alloy and titanium alloy are generally used for the replacements of structural components of the human body such as bones, joints, and tooth roots. These materials have been originally developed for industrial uses, so they have some troubles on biocompatibility, mechanical strength, resistance to corrosion or wear inside a living body. It is important for biomaterials to have no toxicity against a living body, like cancer, allergy, inflammation and developmental malformations.

Though toxicity of biomaterials has been surveyed using whole-animals, it is also tested in cultures of human or mammalian cells, since the latter method, called cytotoxicity evaluation, is simple, well-reproducible and saves money and time compared with the former one. According to the results of the toxicity tests both in whole-animals and cultured cells, the toxicity of metallic elements seems to depend upon their chemical species or states[1–3]. Regardless, the mechanism of their toxicity appearances or the relation between their toxicity and their concentrations or chemical states has not been elucidated. Furthermore, a systematic and quantitative estimation of the toxicity of the metallic elements is required for the development of new metallic biomaterials with superior biocompatibility.

Cytotoxicity of Metal Salts

Cytotoxicity of 13 metal salts were evaluated by colony formation method using murine osteoblastic cell line, MC3T3-E1. Figure 1 shows dose-response curves of the metal salts, which indicate the relationship between the amount of each salt and its toxicity against the cells. The x axis represents the concentration of each salt in medium and the y axis represents the relative plating efficiency (r.p.e.) which means the ability of cells to proliferate: 0 indicates dead cells. The metal salt's relative toxicity is ranked by comparing the concentration of the salt that produces 50 percent r.p.e., known as the IC50 (for "inhibitive concentration"), to each other. According to the results shown in Fig. 1, VCl_3 has the highest toxicity followed by $CoCl_2$ > $CuCl_2$ > $SnCl_2$ > $MnCl_2$ > $NiCl_2$ > $ZnCl_2$ > $FeCl_3$ > $TiCl_4$ > $NbCl_5$ > $MoCl_5$, $Al(NO_3)_3$, $Cr(NO_3)_3$.

Compound Effects on Cytotoxicity

The cytotoxicity of metal salts described above is the result of the tests in which the cells were reacted only with a kind of the salts. However, most of the materials indeed implanted into the human body are not pure metals but alloys, and several metallic elements were detected in the pseudo-body fluid used for the environment of fretting fatigue tests of SUS316L stainless steel or Ti-6Al-4V alloy[4]. In order to estimate the compound effects on cytotoxicity induced by several metallic elements released inside a body from im-

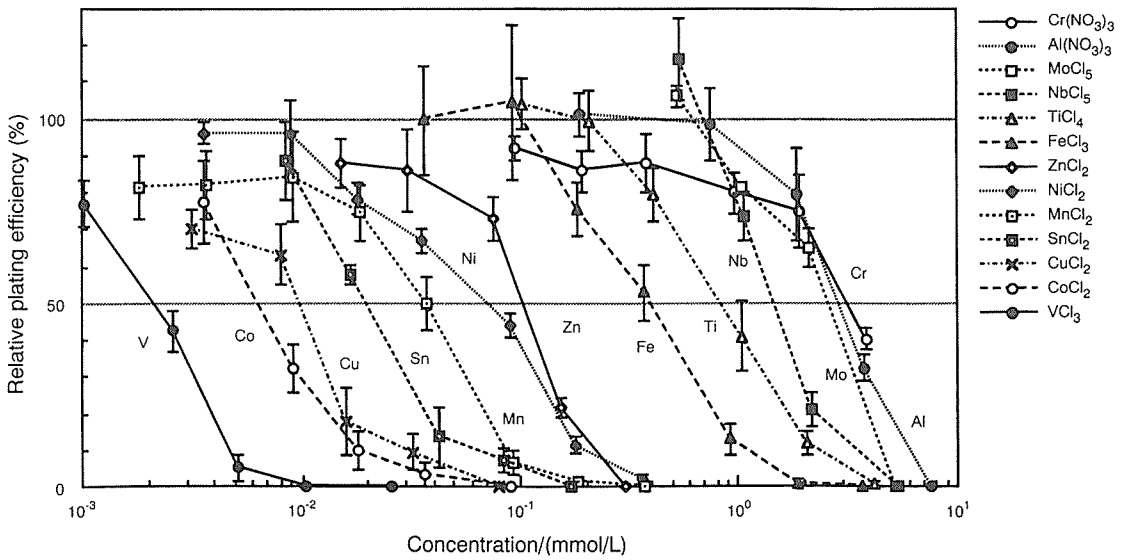

Fig. 1 Cytotoxicity of metal salts investigated by colony formation method. Relative plating efficiency is one of the parameters to express cell viability.

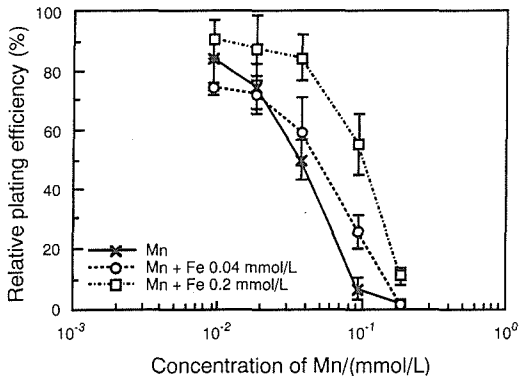

Fig. 2 Effect of $FeCl_3$ on cytotoxicity of $MnCl_2$.

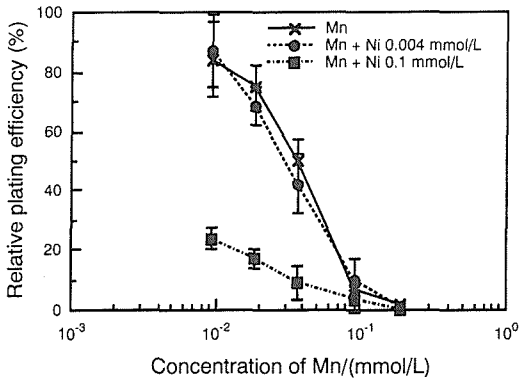

Fig. 3 Effect of $NiCl_2$ on cytotoxicity of $MnCl_2$.

planted materials, cytotoxicity of some combinations of two metal salts were investigated.

Dose-response curves of $MnCl_2$ with/without another metal salt are shown in Fig. 2 and 3. The line with cross as plot symbol is the dose-response curve of $MnCl_2$ without any other metal salts. The open circle and square in Fig. 2 show the curves of $MnCl_2$ with 0.04 and 0.2 mmol/L of $FeCl_3$, respectively. The curves slide to the right from the curve in the case of continuous line, indicating that the toxicity of $MnCl_2$ is decreased by the addition of $FeCl_3$. The phenomenon is also observed in the combinations of $MnCl_2$ added by $TiCl_4$, and VCl_3 added by $FeCl_3$.

The closed circle and square in Fig.3 show the dose-response curves of $MnCl_2$ with 0.004 and 0.1 mmol/L of $NiCl_2$, respectively. The curves tend to move to the left from the curve in the case of continuous line with the increase of the $NiCl_2$ concentration, indicating that the toxicity in this case becomes stronger than that in the case of $MnCl_2$. Compound effects on cytotoxicity of other combinations of the metal salts are now under investigation.

The data presented here suggest that cytotoxic behavior of the combination of two or several metal salts is different and complicated compared with that of each metal salt investigated separately. Further investigation of the compound effect on cytotoxicity of metal salts or other kinds of metallic elements, such as wear debris or particulate metals, is considered to contribute the estimation of the biocompatibility of metallic biomaterials and also to offer useful information to the elucidation of the mechanism of their toxicity appearances in human being or other organisms.

References

1. *Biological Safety of Metallic Materials,* A. Sato, Zairyo-Kagaku, 19 (1982): 193–199 (in Japanese).
2. *Biological Testing of Dental Materials by Means of Tissue Culture,* H. Kawahara, A. Yamagami and M. Nakamura Jr, Int. Dent. J., 18 (1968): 443–4467.
3. *Cytotoxicity of Pure Metals,* S. Takeda, H. Kakiuchi, H. Doi and M. Nakamura, J. of Jpn. Soc. for Dent. Mater. and Devices, 9 (1989): 648–652 (in Japanese).
4. *Fretting Fatigue Properties of Ti-6Al-4V Alloy in Pseudo-Body Fluid and Evaluation of Biocompatibiling by Cell Culture Method,* A. Yamamoto, T. Kobayashi, N. Maruyama, K. Nakazawa and M. Sumita, Jpn. Inst. Metals, 59 (1995): 463–470 (in Japanese).

Research in Progress 1994–1995

❐ List of Research Subjects

Numbers with circle indicate subjects newly started from April 1995.

Numbers with square indicate subjects ended by March 1995.

Characterization/Properties

Electronic and nuclear properties

(1) 2-Dimensional Photoelectron Spectroscopic Study on Solid Surface and Structure

(2) A Quest for the Pinning of Vortices in High Temperature Superconductors

(3) Fabrication and Evaluation of Physical Properties of Intrinsic Josephson Junctions

(4) Studies on the Highly Correlated Electron Systems under Multiple Extreme Conditions

5 Pressure Effects on Physical Properties of Magnetic Materials

6 Structure and Electronic Properties of Silicides

7 First-Order Phase Transitions in Magnetic and Superconducting Materials at Low Temperatures

8 Fundamental Research on Electromagnetic Materials with Strong Electron Correlations

9 Research on Low Dimensional System in High Magnetic Field

[10] Electronic Structure and Superconducting Mechanism in High-Temperature Superconductors

[11] Development of Magnetic Measurement System under Low Temperature and High Pressure

[12] Synthesis of New Functional Materials by the Application of Host-Guest Reactions (II)

[13] Development of Common Interface to Two Different Types of Numerical Database

[14] Database Development in Assistance of New Superconducting Materials Research

Atomistic arrangement

(15) Infrared and Raman spectroscopy of transition metal oxides

16 Atom Probe Microanalysis and its Use in Materials Design

17 Quantification Study on High Resolution Transmission Electron Microscopy

18 Study on Detection and Evaluation of Radiation Damages in Extreme Particle Fields

19 *In situ* TEM Observation and Structural Analysis of High T_c Superconductors for Fusion Reactors at Low Temperature

[20] Structures of Transition Metal Oxides from the Bonding View Point

[21] Synthesis and Characterization of Oxide Superconductors

[22] Study on Fabrication Processes of High-T_c Oxide Superconductors

Phase transformation and microstructures

(23) Effect of High Magnetic Field on Phase Transformations in Fe-based Alloys and Its Application to Structure Control

(24) Hydrogen Behaviors at Interfaces in Alloys

25 A Molecular-Dynamics Study of the Initial Process of Fracture

[26] Super-Microscopic Study on the Mechanism of Martensitic Transformation in Shape Memory Alloys

[27] Evaluation of Magnetomechanical Instability of Metastable Austenitic Steels

Surface and interface properties

(28) The Evaluation of Super Structures on Ultra Clean Solid Surface and the Creation of Dimensional Controlled Nano-materials

(29) Self-control of Surface Composition of Thin Film and Its Application to Field Emitter

30 Theory of Thermal Reaction on Solid Surfaces

31 Research on Electrode Reactions between Metallic Ions and Carbonaceous Materials/Research on Electrochemical Characteristics of TiAl-base Alloys

32 Fabrication of Quantum Well Box Systems by Droplet Epitaxy for Advanced Optoelectronic Devices

33 Fabrication and Characterization of Compound Semiconductor Nanometer Structures

34 Basic Study on Reaction between Materials and Bacteria

35 Electrochemistry and Modelling of Corrosion of Metals under Thin Water Layer

36 Evaluation of High-Performance Triazinedithiols as a Corrosion Inhibitor

[37] Effect of Oxidation on Mechanical Degradation of Metallic Materials

[38] Evaluation of Atomic Level Damage on Material in Aqueous Solution

[39] Reaction Phenomena Related to Tunnel Current

Mechanical properties

(40) Temperature Strength and Fracture of Reinforced Oxide- and Nitride-Base Ceramics

(41) Long-term Creep-fatigue Properties of 316 FR Stainless Steel for Fast Breeder Reactor

(42) Generalized Rule and Guide for Use of Fatigue Data

43 Cyclic Deformation in a Corrosive Environment

44 Fatigue Behavior of Brittle Materials at Elevated Temperatures

45 Study on Deformation and Fracture of Structural Materials at Cryogenic Temperatures

46 Toughness Improvement of Ceramics and Brittle Steels by Control of Precipitation and Phase Transformation

47 Transient Behaviour of Creep Deformation and Fracture at the Elevated Temperature

48 Relationship between Fatigue Crack Propagation and Cyclic Deformation of Small Specimens

49 NRIM Creep Data Sheet Project-IV

50 Study on Deformation and Fracture of Materials under Irradiation

51 Fundamental Research for Intelligent Materials (Formation Process and Recovering Method of Creep Damage)

[52] High Temperature Deformation and Fracture in Polycrystalline Oxide Ceramics

[53] NRIM Fatigue Data Sheet Project–IV

Measurement and evaluation

(54) Observation of Fine Metallurgical Structure with a Comnputer-Image Analysis

(55) Study on Flat and Mirror Finishing by Glow Discharge Plasma Using Rare Gas

56 Self-organizing Information-base System Used for Creative Research and Development

57 *In situ* Measurement of Local Strain in High Temperature Range of Material and Detection of Defects by the Laser Speckle Method

58 Correlation between Plasma Parameters and Evaporation in Free-burning Arcs

59 Fundamental Study on Advanced Techniques of Physical Characterization of Metallic Materials and their Application

60 Research on the Development of Chemical Analysis And Characterization Techniques for Metallic Materials

61 Fundamental Study for Electromagnetic Evaluation of Materials

62 Research on Quantitative and Intelligent Nondestructive Evaluation Techniques for Materials and Structures of High Reliability, Stage II

63 Modeling and Evaluation of Advanced Materials—A Coordinated Interlaboratory Research

64 Nanoscopic Materials Damage Evaluation

65 Chemical Analysis of Organotin in Marine Environmental Samples

66 Determination of Order Parameters in Alloys from Electron Diffraction Intensities using CCD Camera System and Its Application to Examination of Ordering Process

67 A Database for Surface Chemical Analysis

68 Development of Analytical Techniques for Characterization of Nuclear Materials using New Generation Synchroton X-rays

[69] Study on the Trend of Application of New Super Conductors

[70] Development of Advanced Technologies for X-ray Microtomography

[71] Evaluation of Metallurgical Structure with a Fuzzy Logic

[72] Study on Mechanism of Ion Production in Low Temperature Plasma

[73] Control of Surface Atomic Layer and Technological Development of Surface Electron Spectroscopic Tomography

Simulation and theory

(74) Development of Knowledge Databases for High-T_c Superconducting Materials

(75) Understanding of the Superconducting Mechanism of High Temperature Superconductivity

76 Establishment of Multidimensional Evaluation of Human Senses for Materials Design

77 Thermodynamic Analysis of Transition Process from Metastable to Stable Phases

78 Assessment of Strength and Structural Materials Database for Weldment in FBR (Fast Breeder Reactor) Components

79 Modelling and Simulation for Material Strengths Properties

Materials

Non-ferrous materials

80 Relationships between Fatigue Softening/Hardening Behavior and TEM Structure of Titanium Alloys

Intermetallic compounds

(81) Diffusion in Ordered Alloys and Preparation of Composition Gradiented Materials

(82) Characterization of Creep-Damaged Microstructure of Stainless Steels by Computer Aided Quantitative Metallography

(83) Development of Porous Ceramics Impregnanted with Ionic Conductive Materials

84 Fundamental Study of Microstructures and Properties to Develop High Performance Materials for Severe Environment (II-High Temperature Intermetallic Compound)

85 Improvement of Mechanical Properties of Intermetallic Compounds by Crystal Growth Control

86 Basic Research on Intermetallic Compounds for Structural Applications

87 High Performance Materials for Severe Environments-I (Microstructure and Properties of Intermetallic Compounds with High Specific Strength)

[88] High Ionic Conductivity of Solid Electrolyte

Composites

89 Thermal Stability of Intermetallic-Compound Matrix Composites Reinforced with Fibers

[90] Development of High Strength Metal Base Composites with Excellent Physical Properties by the Advanced Bronze Method

Materials for mechanical application

91 High Temperature Mechanical Properties of Particulate Reinforced Titanium-based Metal Matrix Composites

[92] Intelligent structural Materials

[93] Fracture Mechanism of Ceramic Particulate-Reinforced Titanium Matrix Composites

Materials for electronics application

(94) Characterization and Application of Superconducting Thin Films Synthesized by Atomic Layer-by-layer and Epitaxial Growth Methods.

(95) Development of Tapes and Wires Using New High-T_c Oxide Superconductors

(96) Development of High Strength/High Conductivity Materials for High Field Magnets

(97) Developments of High Strength Oxide Superconductors for High Magnetic Field Applications

(98) Performance Evaluation on Long Oxide Superconductors

(99) Development of 1 GHz NMR System

100 Thermal and Electrical Properties of II–IV and V–VI Thermoelectric Semiconductors

101 Energy Conversion Materials Fabricated with Functionally Gradient Structure

102 Study on Design and Assessment Technology for Ecomaterials

103 Structure Control and Electromagnetic Properties of High Temperature Superconductors

104 Microstructure and Electromagnetic-Characteristics Studies on V_3Si Multifilamentary Superconductors

105 Stabilities of Superconducting Materials

106 Purification of Active Metals for the Preparation of Superconductive Materials

[107] Development of Bismuth Oxide Superconducting Tapes and Coils

[108] Fabrication and Characterization of Ag-I Intercalated $Bi_2Sr_2CaCu_2O_y$

[109] The Formation Mechanism of Textured $Bi_2Sr_2CaCu_2O_y$ on Ag Tapes

[110] Developments of High-T_c Superconducting Thick Films and Tapes by Various Spraying Methods and by Internal Oxidation

[111] Development of Extremely High Field Magnets

[112] Fabrication of Oxide superconductors Using YAG Laser Irradiation

[113] Developments of High-Field Multifilamentary Superconductors Made of Intermetallic Compounds

Magnetic materials

(114) Development of a Superconducting Magnet for Magnetic Separation

115 Research on Materials Synthesis to Control of Magneto-Thermal Properties by Changing Size

Materials for energy application

(116) Design of Refractory Superalloys

(117) Research on Utilization Technique of "Data-Free-Way" System for Nuclear Materials

118 Development of Third-Generation Nickel-base Single Crystal Superalloys

119 Environmental Degradation of Structural Materials for Light Water Reactors

120 Computational Mechanical Property Analysis with Consideration to Microstructures of Nuclear Reactor Materials

121 Real-Time Investigation on Surface Reaction and Defect Growth Processes under Irradiation

[122] Fundamental Research on Application of New Functional Materials to Passive Components

[123] Research on Distributed Database for Advanced Nuclear Materials

Materials for environmental performance

124 Fundamental Study on Creation of Micro Stereom Fabrics by Powder Technology

Bio-Materials, etc.

125 Spectroscopic and Electrochemical Investigations of the Metal Complexes with an Unusual Electronic Structure

126 Fundamental Study on Biocompatibility of Materials

Processing

Separation and synthesis

(127) Development of Magnetic Separation Control System

128 Extraction from Metal to Gas Phase

Gaseous process

129 Study on Atomic Scale Engineering of High Performance Films

130 Processing and Development of Isotopically Controlled Materials (ICM)

131 Development of Shape Memory Thin Films Formed by PVD Method

[132] Precise Composition Control of Ordered Alloys by Chemical Transportation Techniques

Liquid state process

(133) Solidification in the Strong Magnetic Field

134 Basic Study on Refining of Molten Metal and Controlling of Solidification by Electromagnetic Force

135 Investigation on Nucleation and Crystal Growth Mechanism under Heterogeneous Ambient Phase

136 Solidification Processing For Particle Dispersed Unidirectionally Grown Composites

137 Metastable Phase Solidification from Undercooled Liquid by Inducing External Nucleation Seed

[138] Basic Technology Development of Materials Procession in a Short-Duration Microgravity Environment

Solid state process

139 Metallurgical Analysis of Micro-Machining Region

[140] Cooperative Phenomena of the Transformation Variants

Powder processing

141 Study on Solid State Chemical Reaction, its Propagation and Materials Synthesis

142 Sintering of TiAl Intermetallic Compounds

143 Synthesis and Characterization of advanced Materials Utilizing Colloidal Dispersed Systems

144 Characterization of Composite Ultrafine Particles

145 Development of Particles Assembly Technology for Integration of Functions

[146] Preparation and Characterization of Ultrafine Powders Used for Making Oxide Superconductors

[147] Study on Properties of Raw Powder of Superconductor using High Pressure Forming

[148] Study on Rapidly Solidified Powders for Superconductive Materials

Joining

(149) Influence of Surface Composition on Joining of Materials

150 Corrosion of Dissimilar Metals Joints in Reactor Fuel Reprocessing Plants

151 Fundamental Research on Brazing and EB Welding in Space Environment

[152] Low Energy Joining with Controlled Surface Composition

Composite process

(153) Coatings Formation by Powder Deposition Processes

154 Forced infiltration process for making composite structures

[155] Coating Formation by Molten and Electrified Powders

Process with aid of beam technology

(156) Study on the Efficiency of Resonance Photoionization Process

(157) Analysis/Evaluation of Atomic Scale Compositional Change in Materials Due to The Radiation Damage

(158) Characterization and control of the optoelectric properties of small crystalline materials with electron probe analysis

159 Synthesis of Superconducting and Supermagnetic Ultrathin Films by Use of Ion Implantation

160 Study on Evaporation Processes by High Energy Density Beams

[161] Diagnostics of Laser Photoionization Induced Plasma

[162] *In Situ* Analysis/Evaluation of Radiation Damage in Materials

[163] Control of Surface Reaction and Synthetic Processes Using "State-Controlled" Molecular Beams

[164] R & D of Advanced Heat-Resistant Structural Materials for Very High Temperature Gas-Cooled Reactors

Processing in special environment

(165) Study on Effects of Aging in Magnetic Field on Properties of Thin Films

(166) Study of regenerator for ultra-low temperatures

[167] Development of Quantum Microstructure un Ultra Clean Vacuum

❒ Research Programme

Characterization/Properties

Electronic and nuclear properties

① 2-Dimensional Photoelectron Spectroscopic Study on Solid Surface and Structure

April 1995 to March 1996
M. Shimoda, Materials Physics Division
Keywords: angle resolved photoelectron spectroscopy, band gap

Our main goal is to draw the energy band structure at both the normal and superconducting states, especially to observe the band gap anisotropy of superconducting oxides, which is widely accepted as a key factor in revealing the secret of the high T_c. The target material is $Bi_2Sr_2CaCu_2O_{8+x}$, which is comparatively easy to get a single crystal large enough and stable in a high vacuum.

For that purpose, we have developed an angle scanned type Angle Resolved Photoelectron Spectroscopy system, which enables us to observe 2-dimensional images of a band structure at constant energies using ultraviolet radiation as well as diffraction patterns reflecting the lattice structure using X-ray radiation.

Related Paper

Complete Fermi Surface Mapping of $Bi_2Sr_2CaCu_2O_{8+x}$ (001): Coexistance of Short Range Antiferromagnetic Correlation and Metallicity in the Same Phase, P. Aebi, J. Osterwalder, P. Schwaller, L. Schlapbach, M. Shimoda, T. Mochiku, and K. Kadowaki, Phys. Rev. Let., 72 (1994): 2757.

② A Quest for the Pinning of Vortices in High Temperature Superconductors

April 1995 to March 2000
K. Kadowaki, 1st Research Group
Keywords: pinning center, vortex dynamics

After the 7 year research of high temperature superconductors, it became clear in part that the nature of the vortex state in high temperature superconductors is distinctly different in many aspects from that in low temperature metallic superconductors. These differences have been understood to originate from the essential differences in the superconducting properties of them: the short coherence length, the large anisotropy, the quasi two dimensional electronic state and the strong thermal effect due to the high superconducting transition temperature. Although the physical properties at low temperatures such as the critical current density and the upper critical field are substantial and are even superior to the low temperature intermetallic superconductors, these features fade away rapidly with increasing temperature, resulting in valueless superconductors in practical use at high temperatures. Since the most fruitful application of high temperature superconductors is in liquid nitrogen temperature region at 77 K, the improvement of the high temperature performance near 77 K are crucial and essential for the future applications.

In this five year project, it is aimed that the pinning properties of the high temperature superconductors at high temperature region are investigated in order to understand the fundamental nature of pinning behaviors in these materials. It is also aimed that the effective pinning mechanism in these materials will be sought for by using well characterized single crystals as well as bulk materials processed by various techniques. By changing type of defects in a controlled manner the physical properties related to the characteristic features necessary for the high performance superconductor will be investigated as functions of the number of defects, type of defects, temperature, magnetic field, etc. From these studies, the key parameters determining the effective pinning strength will be elucidated and understood both experimentally and theoretically. Furthermore, by applying these ideas obtained from the fundamental study of the vortex state in these materials, the pinning performance in real materials will be tested.

③ Fabrication and Evaluation of Physical Properties of Intrinsic Josephson Junctions

April 1995 to March 2000
K. Kadowaki, 1st Research Group
Keywords: intrinsic Josephson Junctions, electromagnetic devices, Josephson devices

The superconducting electronic structure of high temperature superconductors has been known to be composed as a stack of superconducting CuO_2 layers sandwiched by the other structural units, which exhibit an insulating or a less-conducting nature electrically. Because of this structural characteristics, some of the compounds possess an extremely large electronic anisotropy in the superconducting state. From the previous results of high quality single crystals, the effective two dimensional anisotropy—parameter, γ, of $Bi_2Sr_2CaCu_2O_{8+\delta}$ as an extreme example, amounts to 200–500, which is far beyond the values ever

found in the traditional superconducting materials. In addition, the coherence length perpendicular to the CuO_2 layers is very short (~1 Å or less). Therefore, it has long been believed that the superconducting state in such a highly two dimensional anisotropic superconductors may behave as a stack of Josephson Junctions.

This prediction has recently been proved by measuring the current voltage relation along the perpendicular direction to the two dimensional superconducting plane in high quality single crystalline $Bi_2Sr_2CaCu_2O_{8+\delta}$. This important experimental finding provides us wide possibilities of application as Josephson devices, which will become one of the most important application field of high temperature superconductors. These Josephson devices have superior advantages to the ones fabricated by MBE deposition techniques, which has been considered as the most advanced high technology for the fabrication of the Josephson junction in thin films. In this five year project, it is aimed to fabricate Josephson junctions by using the idea of intrinsic Josephson coupling naturally existing in the single crystals. Since the quality of the junctions will be reflected by the quality of single crystals, it is of necessity to produce large and high quality single crystals. Based on these single crystals, fundamental properties related to the wide device applications such as the microwave responses, characteristics of filters, etc. will be studied.

④ Studies on the Highly Correlated Electron Systems under Multiple Extreme Conditions

April 1995 to March 2000

H. Aoki, 4th Research Group and Tsukuba Magnet Laboratories

Keywords: high magnetic field, low temperature, high pressure, highly correlated electron system

The highly correlated electron systems, such as high-T_c oxides, heavy fermion compounds and organic conductors, have been the most important subjects of materials science and have been intensively studied in the past decade. However, many central issues have not been solved yet. A magnetic field is very useful and powerful to study the physical properties and electronic structures of these materials, particularly when it is combined with other experimental environments such as low temperatures and high pressures. NRIM has developed several types of high field magnets, i.e. a hybrid magnet, a large-bore-size magnet, pulsed magnets, high resolution magnets whose capabilities are of the highest class in the world. The purpose of this project is to develop several types of high precision detection systems under low temperatures and high pressures for the high field magnets and is to apply them to the study of the highly correlated electron systems.

A part of the program has been accomplished in a preceding project. We have developed high precision detection systems of transport, magnetic and nuclear magnetic resonance measurements for the high resolution magnets. These systems have been used for many cooperative researches with more than 15 universities, research institutes and companies. Particularly, the Fermi surface properties of more than 20 materials of highly correlated electron systems have been revealed through these collaborations. The present project will provide broader ranges of magnetic fields, temperatures and pressure for several types of experiments and will give opportunities to reveal the properties and electronic structures of the highly correlated electron systems which are not obvious under normal ecperimental conditions.

5 Pressure Effects on Physical Properties of Magnetic Materials

April 1993 to March 1996

T. Matsumoto, Materials Physics Division

Keywords: magnetic properties, Kondo effect, pressure dependence

We have been pursuing for a number of years a program in high pressure physics, centering around the magnetic and transport properties of heavy-fermion and high-T_c compounds. We have constructed a cubic anvil high pressure apparatus which is available for both powder X-ray diffraction and transport properties measurements in the pressure range 0–10 GPa. One of current research interests focuses on the transport properties of Pr-Ba-Cu-O compounds using this apparatus. These compounds are isostructural to their superconducting Y-Ba-Cu-O counterparts but do not exhibit superconductivity because charge carriers redistribute to the hybridized state between Pr4f and 02pπ orbitals. Last year we found an interesting pressure dependence of resistivity in these compounds below 2 GPa which implies the conduction through this hybridized state. We are expecting that higher pressure possibly gives rise to an appearance of new physical properties originating from the hybridized state.

Another current interest centers on the effects of pressure on the magnetic ordering temperature in dense-Kondo materials, such as $CePd_2Al_3$, CePdAl and so forth. In these materials magnetic ordering temperature strongly depends on pressure because of the competition between Kondo effect and RKKY interaction. We have showed that the ordering temperature displays a universal curve as a function of the exchange interaction parameter J which was estimated from the compressibilities obtained by the cubic anvil apparatus mentioned above.

6 Structure and Electronic Properties of Silicides

April 1993 to March 1996

T. Hirano, Chemical Processing Division

Keywords: silicides, single crystal, interface, high-pressure

The purpose of the study is to investigate structure and electronic properties of metal disilicides. We study those under two circumstances, i.e., at silicon/disilicide interface and under high-pressure.

In the former, the interface is formed by the growth of Si on single-crystalline substrates of transition-metal disilicides (M_TSi_2). M_TSi_2 is selected for the following reasons; (1) there are few experiments about semiconductor/metal interface formed on metal surface, and (2) Schottoky barrier height (SBH) of Si/disilicide interface is sensitive not only to the kind of metal but also to the structure of the interface. The structure of the interface is observed using transmission electron microscope, TEM. The electronic property will be studied using SBH measurements.

Structural phase transition is induced under high-pressure condition. Therefore, we synthesize metastable phases of alkaline-earth metal disilicides (M_ASi_2, M_A = Ca, Sr, Ba) under high-pressure and high-temperature conditions, and study structure and electronic properties of these phases. M_ASi_2 is chosen as samples because of their unique atomic configurations and large compressibilities of M_A atoms. We synthesized $BaSi_2$ with a cubic structure and a trigonal structure, and found that trigonal $BaSi_2$ is a hole metal while cubic $BaSi_2$ is an n-type semiconductor. It is rarely known that high-pressure metallic phase is quenched at ambient condition. Furthermore, it is found that trigonal $BaSi_2$ is a superconductor with onset temperature of 6.8 K. We also observe pressure-induced structural phase transition with *in situ* X-ray diffraction measurements. Furthermore, we are going to discuss about the similarity among the transformation sequence under pressure in three M_ASi_2.

Related Papers

Electrical Resistivity of Metastable Phases of $BaSi_2$ Synthesized under High Pressure and High Temperature, M. Imai and T. Hirano, to be published in J. Alloys and Compounds.

Superconductivity of Trigonal $BaSi_2$, M. Imai, K. Hirata, and T. Hirano, to be published in Physica C.

7 First-Order Phase Transitions in Magnetic and Superconducting Materials at Low Temperatures

April 1993 to March 1996

M. Uehara, Surface and Interface Division

Keywords: first-order phase transition, metastable state, quantum tunneling, magnetic relaxation

Recently, much attention has been given to the dynamical nature in magnetic and superconducting systems due to the first-order phase transition in which the fluctuations of systems of either thermal or quantum mechanical origin play an essential role and in a macroscopic system a metastable state undergoes transitions to a lower state. In disorder magnetic systems like $SmCo_{3.5}Cu_{1.5}$ magnetic domain walls move between pinning centers provided by the disorder. At high temperature this is known to occur via thermal activation: at low temperature we have shown previously that there is a crossover to quantum tunneling. It is expected that such behavior of the decay of the metastable state is also observed in type II superconductors. We have shown that the concept of mean activation energy leads to coherent results on the mixed state nature in several high-T_c superconductors (HTSCs). We have found that the time decay of the zero field cooled diamagnetic magnetization of $YBa_2Cu_3O_{7-d}$ and $Bi(Pb)_2Sr_2Ca_2Cu_3O_y$ can be explained in terms of a mean activation energy E which is found to be proportional to the reciprocal magnetic field. The temperature variation of the penetration and exclusion rate of vortices obeys an Arrhenius type equation with an effective temperature $T^*=(\theta/2)\coth(\theta/2T)$. Here, θ is a characteristics temperature closely related to the crossover from thermal process to quantum tunneling of vortices. The studies on magnetic relaxation in conventional superconductors such as $Ti_{50}V_{50}$ and A15 compound V_3Si single crystals are currently in progress. This study has partly been carried out within cooperative scientific research program between STA (Japan) and CNRS (France).

Related Papers

Noncoherent Quantum Effects in the Magnetization Reversal of a Chemically Disordered Magnet, M. Uehara and B. Barbara, J. Physique 47 (1986): 235–38.

Field and Temperature Dependence of the Mean Penetration Rate of Fluxons in the Mixed State of High T_c superconductors, M. Uehara and B. Barbara, J. Phys. I France 3 (1993): 863–70.

Decay of Metastable States of High-T_c and Conventional Low T_c Superconductors, M. Uehara, T. Numazawa, T. Hirano, and B. Barbara, Physica C 235 (1994): 2905–06.

8 Fundamental Research on Electromagnetic Materials with Strong Electron Correlations

April 1993 to March 1996

K. Kadowaki, 1st Research Group

Keywords: heavy fermions, Kondo effect, unconventional superconductivity

There has been a growing interest in the intermetallic compounds with rare earth or actinides elements, because they often exhibit anomalous behaviors in many of physical properties. Appearance of unusual magnetic order and complex superconductivity in highly correlated electron systems with extremely heavy quasiparticles is one of most striking examples in these systems.

In order to study such an interesting area of physics, it is important to have high quality single crystal samples. In many cases, the quality of samples is very crucial to understand underlaying physics, which is, in most cases, covered by the spurious effect of dirtiness of the sample. Therefore, we have firstly planned to set up facilities, in which we are able to grow high quality single crystal samples of these compounds.

In the past two years, the fund is mostly devoted to set up the high quality single crystal grwth facilities such as the tetra arc-furnace and multipurpose single crystal furnace with a high frequency power generator. These two main furnaces in combination with the glove box system with ultra-pure atmosphere are now in operation for the systematic production of high quality single crystals such as $CeCu_6$, $CeRu_2Si_2$, $CeRu_2(Si_{1-x}Ge_x)_2$, $CeRu_2$, RET_2B_2C(RE = rare earth element, T = Ni, Pd, Pt) etc. These single crystals are currently under investigation of various physical properties at low temperatures down to 10 mK using a dilution refrigerator, which was newly installed last year.

Related Papers

Magnetism and Superconductivity in RET_2B_2C (RE = Y and T = Ni, Co), K. Kadowaki, H. Takeya, T. Hirano, and Mochiku, Physica B 206 & 207 (1995): 555–58.

Single Crystal Growth of Quaternary Superconductor YNi_2B_2C by Floating Zone Method, H. Takeya, T. Hirano, and K. Kadowaki, submitted to Physica C.

Anomalous Magnetization Behavior of Single Crystalline $CeRu_2$, K. Kadowaki, K. Hirata, and H. Takeya, submitted to Phys. Rev. B.

9 Research on Low Dimensional System in High Magnetic Field

April 1993 to March 1996

G. Kido, The 4th Research Group

Keywords: low dimensional, spin Peierls, high magnetic field, sub-millimeter, electron spin resonance

The quantum spin effect is one of the most interesting phenomena in the physics of low dimensional magnetic system. The existence of finite energy gap is predicted by Haldane in one-dimensional Heisenberg antiferromagnet system with S = 1 spin, whereas no energy gap accompanies for S = 1/2 spin system. The spin-Peierls transition takes place in the S = 1/2 spin system by descending the temperature due to the dimarization of spin sites in one-dimensional antiferromagnet chain, which has been found in several organic conductors (TTF-CuBDT, $MEM(TCNQ)_2$, etc.) and in inorganic materials $CuGeO_3$. The high magnetic field is quite effective to investigate the magnetic materials since it controls the degree of quantum effect. Particularly, we are interested in the magnetic phase of the spin-Peierls materials, which appears above 12 T for $CuGeO_3$ and 20 T for $MEM(TCNQ)_2$, respectively, at helium temperature. The 40 T hybrid magnet and the 80 T pulsed magnet will be employed in the experiments. We are building apparatuses to measure the AC and DC susceptibility, far-infrared electron spin resonance and phonon spectra in wide temperature range at high magnetic fields. For the measurement of electron spin resonance, a standard technique is used with an optically pumped molecular gas laser (or Gunn diode) and a pulsed magnet. At present, magnetic field dependence of phonon spectra and g-values is investigated using a Fourier-transform spectrometer in the energy region between 3 and 60 cm^{-1}, using 14 T superconducting magnet instead of the hybrid magnet. This research will clarify the phase boundary between the magnetic phase and uniform phase and the property at the magnetic phase.

The two-dimensional electron system realized at the interface in semiconductor is planned to study by the precision transport measurements at very low temperature in the high magnetic field.

10 Electronic Structure and Superconducting Mechanism in High-Temperature Superconductors

April 1988 to March 1995

T. Sasaki, Materials Physics Division

Keywords: high-temperature superconductor, theory, electronic structure

The high-temperature superconductor (HTSC) is a potential material for a variety of applications. Despite a great deal of effort of basic research on electronic structure and properties of HTSC, the superconducting mechanism has not been clarified yet. In this work, we have studied electronic structure of HTSC based on band-structure calculations with the local-density approximation (LDA).

So far, LDA band calculations have been performed for $YBa_2Cu_3O_y$ (y = 6 or 7) and $YBa_2Cu_4O_8$, as abbreviated as Y123 and Y124, respectively. The calculations have shown that overall characteristics of electronic structure of these compounds are

quite similar to each other, in accordance with the similarity of the crystal structures. Several characteristics aspects have been derived by comparing with other HTSC's. Importance of the energy separation between Cu-*d* and O-*p* states was pointed out in connection to photo-emission experiments. The present calculations have provided the physical aspect into the differences in the properties of these compounds. Especially, we have found a large energy-level lowering of oxygen *p*-states at chain sites in the electronic structure of Y124. This fact can be considered to explain the relative stability of the oxygen content in Y124.

The Fermi surfaces of these Yttrium compounds have been obtained from the LDA calculations. The calculated Fermi surfaces will be utilized not only to clarify the electronic structure by comparing them with the experimental data but also to obtain the transport properties theoretically. In this research, the Hall coefficients have been calculated. An agreement between the calculated result and the experimental data can be seen, and the discussion on the remained disagreement has been done.

Related Papers

Implication of Band Structure Calculations for High-T_c Related Oxides, K.T. Park, K. Terakura, T. Oguchi, A. Yanase, and M. Ikeda, J. Phys. Soc. Jpn., 57 (1988): 3445–56.

Electronic Band Structure of $YBa_2Cu_4O_8$, T. Oguchi, T. Sasaki, and K. Terakura, Physica C, 172 (1990): 277–81.

Local Density Band Structure of Y-Ba-Cu Oxides, T. Oguchi, T. Sasaki, and K. Terakura, Physica C, 185–189 (1991): 1733–34.

Fermi Surface and Transport Properties of $YBa_2Cu_4O_8$, T. Oguchi and T. Sasaki, J. Phys. Chem. Solids, 53 (1992): 1525.

[11] Development of Magnetic Measurement System under Low Temperature and High Pressure

April 1994 to March 1995

T. Naka, Materials Physics Division

Keywords: high pressure, low temperature, magnetization

We investigated the pressure dependence of magnetic property in the heavy fermion (HF) system which exhibits metallic behavior in low temperature region. The effective-mass of conducting carrier in this system is anomalously enhanced. We focus on the substances in HF-system showing unconventional superconductivity, magnetic ordering and, especially, the high-sensitive properties to magnetic field and pressure at very low temperature. A study of the pressure effect of magnetic susceptibility in rare-earth compounds including HF system, e.g. Ce, CeP, was performed. We found the rapid increases of transition temperature and magnetization with pressure in CeP. Also a critical pressure of where magnetization exhibits maximum at low temperature was found in CeP.

In this study, we developed magnetic measurement system at low temperature down to 1.5 K, high pressure up to 2.0 GPa and high magnetic field up to 6 T. This system consists of 5 units; (1) magnetic (Faraday) balance, (2) superconducting magnet, (3) 1.5 K cryostat, (4) control device, (5) pressure (piston-cylinder clamp) cell. The unit of superconducting magnet consists of a main coil for a DC-field and a supplemental coil generating a field gradient at a sample position. We can perform a study of magnetization in HF-compounds using this system under multi-extreme-condition (low temperature, high pressure and high field).

Related Papers

Magnetic State of α- and γ-Ce at High Pressure, T. Naka, T. Matsumoto, and N. Mori, Physica B, 205 (1995): 121–26.

Magnetization at High Pressure in CeP, T. Naka, T. Matsumoto, Y. Okayama, N. Mori, Y. Haga, and T. Suzuki, Physica B, 140–144 (1995): 1253–54.

[12] Synthesis of New Functional Materials by the Application of Host-Guest Reactions (II)

April 1993 to March 1995

M. Amano, Physical Properties Division

Keywords: insertion/extraction reaction, ionic conductor, antimonic acid, proton conduction, water absorption

The aim of this project is to synthesize new functional materials by applying insertion/extraction reactions. We are trying to synthesize new ionic-conductor materials by using ion exchange process.

Two kinds of antimonic acid with a cubic structure ($HSbO_3 \cdot 1.OH_2O$: c-SbA) and a monoclinic structure ($HSbO_3 \cdot 0.15H_2O$: m-SbA) have been prepared by acid treatment of $KSbO_3$ and $LiSbO_3$, respectively. Their altenating impedance and FTIR were measured. They are proton conductors. The conductivity of m-SbA is smaller and more sensitive to the amount of water than that of c-SbA. The conductivity is closely related to the absorption state of hydroxyl groups and water molecules. It has been found by the analysis of micropore using water vapor and nitrogen gas that there are micropores in c-SbA, where water molecules can enter and nitrogen molecules cannot.

It has been found that $LiSbO_3$, $NaSbO_3$ and $KSbO_3$, which are the starting materials for antimonic acid, are ionic conductors, and their activation energy for conductance are 70.3 kJ/mol, 68.2 kJ/mol and 59.8 kJ/mol. These starting ma-

terials were synthesized by a dry process. The film of $LiSbO_3$ could be also prepared by a sol-gel method using lithium propoxide and antimony propoxide.

The ion exchange velocity of Li^+ to H^+ in $LiSbO_3$ has been found to increase markedly by substituting small amount of Li by K.

[13] Development of Common Interface to Two Different Types of Numerical Database

April 1994 to March 1995
Y. Asada, Material Design Division
Keywords: oxide superconductors, database, network

We have developed two types of numerical database for new high T_c superconducting materials. One is for the data from the published papers. There are so many fields that it is arranged to store any kind of data. Key item is sample number; If samples with different compositions appear in a same paper, then they have different sample numbers. Samples from different papers have different sample numbers even if they have the same composition. Using this key item, data are treated as individual data. This is important for data processing.

The other is for original data which we produced in our working group. We prepared samples well-characterized and measured many superconducting and normal state properties. The raw data are stored together with their detailed measuring conditions. We can make comparison among the data in various aspects.

These two databases are constructed using the same DBMS (DataBase Management System), but different in the database structure. We have introduced BBN/Cornerstone as a common tool for statistical processing. Using this tool one can access the database constructed by using different DBMS (ingres, oracle, sybase). Now any user with password can access to two types of our databases mentioned above using the same interface via network. The system is expected to contribute to the effective usage of the numerical databases with different database structure.

[14] Database Development in Assistance of New Superconducting Materials Research

April 1988 to March 1995
Y. Asada, Material Design Division
Keywords: oxide superconductors, database, graphic data, material design

Since the discovery of high-T_c oxide superconductors an enormous amount of research papers have been reported. Numerical database on these superconducting materials, therefore, is necessary for the researchers in this field. We developed in this study a numerical database "SUPERCON:" The data on superconducting properties (T_c, higher and lower critical magnetic fields, coherence length, penetration depth, energy gap, etc) and related properties (Hall coefficient RH, thermopower s, thermal conductivity k, specific heat C, etc) are collected from the published papers. More than 5000 records of data are stored up to now in our database "SUPERCON." Graphic data of temperature dependence of RH, s, k, C are also stored in the form of digital data.

We investigated the doping effect of T_c in Y1-xRxBa2Cu3Oz, YBa2-xMxCu3Oz and YBa2Cu3-xMxOz by retrieving the data from "SUPERCON." For each alloying system T_c depends on the oxygen content z. At first T_c of the fully oxygenated samples is fitted to the polynomial equation of x. Then the effect of oxygen content on T_c was investigated for samples with the same doping level. We obtain the approximate equation of $T_c(x, z)$. To construct a T_c calculation system these equation have been stored as basic data for superconducting materials design.

Related Paper

Numerical Database of High-T_c Oxide Superconductors, Y. Asada, Cryogenic Engineering (in Japanese), 28 (1993): 298.

Atomistic arrangement

(15) Infrared and Raman spectroscopy of transition metal oxides

April 1995 to March 1998
T. Hirata, Materials Physics Division
Keywords: Phonons, infrared/Raman spectroscopy, transition metal oxides, solid solutions, phase transition

It is well-known that phonons play a significant role in many phenomena in solid state physics. Infrared spectroscopy as well as Raman scattering are useful techniques, providing with information to understand the underlying mechanism of phenomena from the view-point of phonons. Using both spectroscopic techniques, we are concerned with the following issues:

1. The compositional effect on phonons in mixed oxides, where another metal cations with different radius and/or charge are substituted for the constituent cations to form a series of solid solutions; a study of the mode behavior can throw light on lattice distortions and/or force-constant changes upon substitution.
2. Transition metal oxides with intersticially incorporated ions-interstitial solid solutions; this issues covers a field of interest "optical phonons of disordered system." Structural and property changes upon ion-incorporation are of another interest from a spectroscopic point of view.

3. Phase transitions in some metal oxides; the infrared and Raman spectra of transition metal oxides are measured as a function of temperature to investigate their phase transition(s) in detail, as the significant role of electron-phonon coupling in superconductivity for cuprates is somewhat elucidated from the temperature dependence of Raman and infrared spectra.

16 Atom Probe Microanalysis and its Use in Materials Design

April 1994 to March 1997

H. Harada, Materials Design Division

Keywords: Ni-base superalloy, NiTi-base alloy, Ni_2TiAl precipitate, phase equilibrium, atomic configuration, computer modelling

Microstructures of third generation Ni-base single crystal (SC) superalloys developed in NRIM are being analyzed by an Atom Probe Field Ion Microscope (APFIM) equipped with a Three Dimensional Atom Probe (3D-AP). The state of γ/γ' phase equilibrium, including atomic configuration in the γ' phase, has been determined in the alloys. The results have been compared with estimations by computer modelling using Cluster Variation Method (CVM) and a very good agreement has already been obtained between them. CVM is now being applied to the development of Ni-base SC superalloys with further superior temperature capabilities.

A series of Al-containing NiTi-base intermetallic alloys newly developed in NRIM for possible applications as gas turbine discs have also been investigated. The precipitation behavior of Ni_2TiAl phase which is coherent with NiTi matrix is thought to be the key to understanding the very high strength of the alloys. The APFIM/3D-AP has been again used to analyze the precipitates in terms of size, distribution and chemical composition. It has been possible to detect a very early stage of the Ni_2TiAl precipitation. 3D-mapping of the chemical composition clearly showed an evolution of the cuboidal precipitates during aging.

Related Papers

The Location of Atoms in Re- and V-containing Multi-component Nickel-base Single-crystal Superalloys, H. Murakami, H. Harada, and H.K.D.H. Bhadeshia, Applied Surface Science, 76/77 (1994): 177–83.

Phase Decomposition in NiTi-Ni_2TiAl Alloy System, P.J. Warren, Y. Koizumi, H. Murakami, and H. Harada, Proc. 3rd International Charles Parsons Turbine Conference, 25–27, (April 1995), Newcastle upon Tyne, UK.

17 Quantification Study on High Resolution Transmission Electron Microscopy

April 1993 to March 1996

S. Ikeda, Surface and Interface Division

Keywords: HRTEM, superconductor, cross sectional TEM method, slow scan CCD camera

In the present study, we have tried quantify the high resolution electron microscopic images and the electron diffraction intensity, with the aid of SSC camera, and to obtain much more information than the conventional use with photographic films. Light atoms, for example, oxygen atoms in a ceramic specimen cannot be recorded on the film, in contrast with heavy atoms. A slow scan CCD camera-image processor with a dynamic range of 10^4 is attached to the high resolution electron microscope, JEM-4000EX, with a point to point resolution of 0.17 nm. The intensity distribution can be drawn as a contour map in detail finer than the positional accuracy of 0.02 nm. Therefore, it will be possible to detect the intensity contribution from oxygen atoms in oxides by image taken by the CCD camera.

We applied the HRTEM technique to identify the structure of recently discovered superconducting compound YPd_2B_2C. We performed electron diffraction experiments using the tilting stage and obtained 3D structure of the reciprocal lattice. We compared the high resolution images for the [100], [110] and [001] zones with the computed ones using MacTempas software and found that the structure of this compound is basically the same as that of $LuNi_2B_2C$.

It is known that ion irradiation enhances the irreversibility field of the superconducting material and increases intragrain critical current densities. We have examined irradiation induced structural damages in the BSCCO tapes with 15 μm thick using the cross-sectional TEM method. The results revealed that the long continuous cylindrical columnar defects with a diameter of 2 to 8 nm were produced by ion irradiations and the core of columns is surrounded by an anisotropic strain field.

Related Papers

High Resolution Transmission Electron Microscopic Studies on a Superconductor YPd_2B_2C Compound, S. Ikeda, H. Fujii, T. Kimura, K. Kumakura, K. Kadowaki, and K. Togano, Jpn. J. Apply. Phys., 33 (1994): 3986–99.

HREM Observation of the Effects of 180 MeV Cu^{11}+ Ion-Irradiation on the Crystal Structure of $Bi_2Sr_2CaCuO_x$, B. Chenevier, S. Ikeda, H. Kumakura, K. Togano, S. Okayasu, and Y. Kazumata, Materials Research Forum, 129 (1993): 17.

18 Study on Detection and Evaluation of Radiation Damages in Extreme Particle Fields

April 1992 to March 1999

N. Kishimoto, Materials Characterization Division

Keywords: extreme particle field, high current, negative ion source, *in situ* measurement

Combined particle fields of ion and photon exert strong interactions with materials and are potent not only to detect elementary processes but to explore novel properties of materials. Especially if both high energy and high density of ion and photon are attained, unexplored non-equilibrium effects will be expected, by virtue of their contrasting effects of momentum, energy, excitation modes. The extreme particle field is also an important aspect for practical environments of high energy devices, such as fusion reactors, MHD generators, etc. The main purpose of this research program is to detect and evaluate non-equilibrium processes of materials in the extreme particle fields, associated with radiation damage.

In order to attain the extreme particle field, the key technology is an ion injector of high current and low emittance, and the negative ion source is requisite for the tandem acceleration. We accordingly have concentrated on the development of a high-current negative ion injector of plasma-sputter type, since this method recently has attracted attention as a promising candidate for the intense negative-ion source. The technological issues are 1) optimization between the sputtering and the negative ionization processes at the metal surface, 2) optimization of beam extraction conditions, i.e. spatial distribution of electric field, etc. and 3) control of space charge effects for the beam transport. Above all, the space charge effects are essential and our goal value of more than 1 mA/cm^2 is considerably difficult for heavy ions in principle. After orbit analyses and parameter adjustments of the beam, we have accomplished a beam current of 3 mA for Cu-ion. The current value for the heavy ion is the highest in the world, as the values transported outside from the ion chamber.

The beam properties including the emittance are further measured by the injector test-stand, and the data will be used for the development of a high-current MeV accelerator. Thus, technological feasibility of the extreme particle field is now in our prospect.

Related Papers

Resonant Irradiation Creep of 316 Stainless Steel Under Pulsed Deuteron Bombardment, N. Kishimoto and H. Amekura, J. Nucl. Mater., 212–215 (1994): 535.

Resonant Creep Enhancement of Austenitic Stainless Steels Due to Pulsed Irradiation at Low Doses, N. Kishimoto, H. Amekura, and T. Saito, Fusion Eng. & Design., 29 (1995): 391.

19 *In situ* TEM Observation and Structural Analysis of High T_c Superconductors for Fusion Reactors at Low Temperature

April 1994 to March 1999

T. Kimoto, 1st Research Group

Keywords: resolution limit of TEM at low temperature, high T_c superconductors, high intensity electron gun, short-time TEM imaging, MCP, CCD camera, electron holography

Few principles for the development of high T_c superconductors for fusion reactors have been found because their mechanism of superconducting is not yet understood. Development of the systems for the *in situ* analysis of high T_c superconductors at low temperatures, which includes high-resolution TEM imaging of atomic scale, on-line analysis of electron diffraction patterns and direct observation of fluxoid quantum by electron holography, is aimed in the present research in order to obtain experimental information for the understanding of the mechanisms for superconducting. The development of the systems will be performed by developing both software and hardware which includes the high intensity electron gun for TEM, short-time imaging devise with cold CCD camera and effective utilization of laser beam for temperature control.

The resolution limit of TEM of low temperatures is about ten times lower than that at room temperature because a TEM specimen is apt to drift easily due to the instability of temperature or vibrate due to liquid helium evaporation. To resolve the reduction of resolution limit of TEM at low temperature, short-time imaging device were developed in 1994. The device was consisted of microchannel plate (MCP), cooled CCD camera, YAG scintillator, optical lenses and computer system. The short-time imaging is realized by reducing the pulse time of voltage pulse on MCP. The minimum exposure time for imaging is 5 nano-second (5×10^{-9} sec) and the taken TEM images are fed to the computer system through A/D convertor at real time. By combining the developed short-time imaging device, high intensity electron gun and temperature control by laser beam, high resolution TEM observation at atomic scale will be realized even at low temperature.

Specimen preparation techniques for TEM observation from arbitrary orientation from thin-filmed $Bi_2Sr_2CaCu_2O_8$ single crystal were developed in 1994. The system development for the determination of the order parameters of high T_c superconducting oxides from electron diffraction intensities was started in 1995 based on the successfully developed system for dualistic alloy.

20 Structures of Transition Metal Oxides from the Bonding View Point

April 1993 to March 1995

M. Okochi, Metals Properties Division

Keywords: transition metal oxides, binding nature, γ-Mo_4O_{11}, Fermi surface map, $Bi_2Sr_2CaCu_2O_{8+x}$, infrared-reflectance spectra, $Zr_{1-x}Hf_xO_2$

Transition metal oxides are characterized by the structures of crystalline coordination compounds with interatomic bonds by sharing of electrons between metallic atoms and the neighboring oxygen. The bonding view point is a potential conception to make the microscopic binding nature clear in the compounds.

We have estimated valence electrons of molybdenum in γ-Mo_4O_{11}, having metallic conductivity, by analyzing bond-strength bond-length relationships. The relationhships have decided merit to be able to estimate valence electrons of covalent bonds between two atoms in a system of more complicated interactions between atoms and electrons. The crystal structure of γ-Mo_4O_{11} consists of octahedra and tetrahedra, where the tetrahedra have shorter interatomic distances between oxygen and less valence electrons than octahedra. We have newly taken account of coordination numbers and metallic bonds in the relationships. Our results show that conduction electrons in metallic bonds are 1.81 per formula and valences of molybdenum are 4.93, 5.52, and 5.12 for octahedral sites and 4.72 for tetrahedral site. These results are in good agreement with band scheme of color properties of γ-Mo_4O_{11}.

We have succeeded to draw the complete Fermi surface map of $Bi_2Sr_2CaCu_2O_{8+x}$ over the whole Brillouin zone with an angle-scanning data aquisition technique, the UPS version of the x-ray photoelectron diffraction experiment. The map shows features which are basically in good agreement with the local density calculation, as well as a c(2*2) structure which suggests the existence of short range anti-ferromagnetic correlations.

Infrared-reflectance spectra of $Zr_{1-x}Hf_xO_2(0 < x < 1)$ have been measured at room temperature in the frequency region 50–4000cm^{-1} by Fourier transform spectroscopy. Infrared-active modes of 5 A_u and 7 B_u varied systematically with x, with changes in the frequency, line-width, and intensity. It was concluded that the stiffening of the B_u modes is associated with the bond reinforcement by substituting the Hf^{4+} ions of smaller radius for the Zr^{4+} ions.

[21] Synthesis and Characterization of Oxide Superconductors

April 1988 to March 1995

K. Nakamura, 1st Research Group

Keywords: high-T_c oxide superconductors, thin film, MBE, cation disorder, super-lattice

Among the various technique in synthesizing films with multi-component layered structure, an alternate sequential deposition method using multi-evaporation sources and accurate shutter control is most promising in controlling the structure of such systems. We have successfully controlled the number of CuO_2 layered in the $Bi_2Sr_2Ca_{n-1}Cu_nO_{2n+4}$ (22(n-1)n) films with n up to 7 and have synthesized superlattice films with $(2212)_m(2234)_{m'}$, × L and $(2201)_m(2245)_{m'}$, × L structure, where m, m' = 1 and L 1 to 16. We have also measured superconducting properties of these films to investigate the mechanism governing the T_c of these films, i.e., charge transfer or proximity effect model. The observed T_c's of these superlattice films were higher than those of the component phases and seem to suggest that the charge transfer model is valid when m and m' are less than 2.

The structural disorder generated during the vapor deposition of $YBa_2Cu_3O_{7-\delta}$ films has been investigated in detail. The ordering process of these films with disordered defects has been also investigated using *in situ* x-ray diffraction technique. The growth mechanism and kinetics of compound films in molecular beam epitaxy (MBE) process is also an important target in this study. We have also successfully synthesized thin films of YNi_2B_2C compound, a member of recently discovered Pd_2YB_2C family which has the highest T_c among the non-oxide superconductors.

Related Papers

Structural Certification and Superconducting Properties of Artificially Layered 22(n-1)n/22(n'-1)n' Superlattice, T. Hatano, K. Kadowaki, and K. Nakamura, Physica B, 194–196 (1994): 2307.

Systematic Study of the Growth-Temperature Dependence of Structural Disorder and Superconductivity in $YBa_2Cu_3O_{7-\delta}$ Thin Films, J. Ye and K. Nakamura, Phys. Rev., B50 (1994): 7099.

Self-Annihilation of Surface Precipitates on Compound Films by Alternate Impinging of Molecular Beams, M. Yata, K. Nakamura, and K. Ogawa, Phys. Rev., B51 (1995): 2473.

Synthesis of YNi_2B_2C Thin Films by Magnetron Sputtering, S. Arisawa, T. Hatano, K. Hirata, T. Mochiku, H. Kitaguchi, H. Kumakura, K. Kadowaki, K. Nakamura, and K. Togano, Appl. Phys. Lett., 65 (1994): 1299.

[22] Study on Fabrication Processes of High-T_c Oxide Superconductors

April 1992 to March 1995

Y. Tanaka, High Magnetic Field Research Station

Keywords: YBaCuO film, deposition, BiSrCaCuO, AgCu sheath-tape, powder-in-tube technique

Fabrication processes for YBaCuO films and for Bi(Pb)SrCaCuO tapes have been studied. To obtain high critical current density, J_c, of YBCO films problems of weak-links at high angle grain boundaries must be solved. Particular attention has been given to preparing highly in-plain textured YSZ buffer layer in addition to c-axis align-

ment. An attempt was made to deposit in-plain aligned YSZ thin buffer layers on both sides of metallic tape by modifying the bias sputtering technique. Using these substrates, it has been demonstrated that $YBa_2Cu_3O_y$ films having J_c of around 10^5 A/cm^2 (77 K, 0 T) can be successfully deposited on both sides of the tape simultaneously by laser ablation technique. A high degree of in-plain grain alignment was observed in our $YBa_2Cu_3O_y$ films, which resulted in high J_c values for the polycrystalline films. The proposed technique is pointed out as a potential method towards the fabrication of a tape conductor.

Bi-2223 superconducting tapes were fabricated by the powder-in-tube technique using AgCu-alloy-sheaths doped with a small amount of Ti, Zr or Hf. The doping of the elements modified grain morphorgy and phase alignment probably due to an enhancement of Bi-2223 formation. The doped samples showed larger and more flat shaped Bi-2223 grains than those for the non-doped sample of small and containing many sub-grains. The alignment of the Bi-2223 phase is also greatly increased for the doped samples. Furthermore, recently it has been found that the doping can introduce many disc-like amorphous regions into the Bi-2223 crystal lattice. Investigations have been continued to examine whether these amorphous regions become effective flux pinning centers in the magnetic field. If the amorphous regions act as effective pinning centers for Bi-2223 we will have a new metallurgical technique for introducing flux pinning centers correlated with high J_c property.

Phase transformation and microstructures

(23) Effect of High Magnetic Field on Phase Transformations in Fe-based Alloys and Its Application to Structure Control

April 1995 to March 1998

S. Kajiwara, Physical Properties Division

Keywords: kinetics, thermodynamics, transformation mechanism

Investigation of the effect of high magnetic field on phase transformations is very important to understand the mechanism, kinetics, and thermodynamics of the phase transformations in Fe-based alloys. There exists a difference in magnetic moment between the austenitic parent phase and the transformation products in Fe-based alloys. Therefore it is expected that the transformation temperature, nucleation and growth rates and their mechanisms and transformation kinetics are changed by applying the high magnetic field, and it may possible that the microstructures can be controlled by the magnetic field. There are also thermodynamic effects of high magnetic field on the martensitic transformation, which are well described by the three factors; (1) Zeeman effect, (2) high field susceptibility and (3) forced volume magnetostriction. All these effects of high magnetic field can contribute to the formation of unique transformation structures. The similar effects are also expected for the other phenomena, such as recovery, recrystallization, segregation, ordering, clustering, spinodal decomposition and precipitation.

(24) Hydrogen Behaviors at Interfaces in Alloys

April 1995 to March 1998

C. Nishimura, Physical Properties Division

Keywords: hydrogen, intermetallics, grain boundary, interface, trapping

Recent studies have demonstrated that a number of promising $L1_2$-ordered intermetallics suffer from environmental embrittlement at room temperature: the ductility is drastically reduced via intergranular fracture caused by atomic hydrogen originated from the moisture in air. Our previous studies have suggested that the main reason of the embrittlement lies in the peculiarity of the grain boundaries in ordered intermetallics. In order to clarify this point, in this project, hydrogen behaviors at grain boundaries are investigated for Ni_3Al and $(Co,Fe)_3V$. We can control the grain boundary characters of Ni_3Al by a floating zone method. We can prepare both ordered and disordered $(Co, Fe)_3V$ by selecting an appropriate heat treatment. Diffusion behavior along grain boundaries can be evaluated by comparing the permeation data determined at room temperature by an electrolytical hydrogen permeation method and the data determined at higher temperatures by a gas permeation method. Hydrogen trapping behaviors can be observed using tritium autoradiography.

Our previous studies have suggested that a breakthrough in the field of hydrogen energy applications could be brought about by composite materials. The composite materials are composed of main materials with high hydrogen permeation or storage performance, and overlayers which keep the main materials from oxidation or accelerates the hydrogen penetration. In such composite materials, interfacial trapping of hydrogen must be minimized. In this project, in order to obtain a guideline for developing such composite materials, hydrogen permeation characteristics through interfaces are investigated using palladium-coated membranes of vanadium-based alloys, and magnesium-based alloys. The effects of argon-sputtering and deposition of interface modifying elements on the hydrogen permeation characteristics are examined.

25 A Molecular-Dynamics Study of the Initial Process of Fracture

April 1994 to March 1997
K. Kusunoki, Materials Physics Division
Keywords: molecular dynamics, fracture, atomistic models, crack

Fracture of material takes place through an irreversible process and the movement of atoms in the very early stage of the process affects greatly the ultimate morphological aspect of the fractured material. Conventional fracture theories, which are based on continum models, cannot treat the microscopic forces acting on each of atoms and atom displacements under stress. Recent experimental techniques such as STM and FIM cannot also reveal the dynamical movement of atoms inside the material. On the contrary, the molecular-dynamics simulation can, using appropriate configurational models and interatomic potentials, demonstrate the whole time evolution of the microscopic forces, the momenta and the atom positions of a system under applied stress.

The present study aims to elucidate how the microscopic forces and displacements of atoms develop into the macroscopic ones. It also aims at an atomistic description of the macroscopic concepts such as crack, stress and strain.

We made a simulator by which we can make both tensile and compression test of single crystals. We also made an equipment by which we can separate the non-vibrational movement of atoms from the vibrational one in a crystal lattice. A preliminary study, which uses modified Lennard-Jones type interatomic potentials for both pure and solid solution of fcc crystals, revealed that perfect crystals as well as crystals containing one vacancy cannot be fractured by crack initiation but by plastic deformation. In this case, the stress-strain curves are fairly similar to those obtained by actual tensile tests of fcc whiskers.

We are planning to investigate how to generate cracks inside a crystal under tensile stress.

[26] Super-Microscopic Study on the Mechanism of Martensitic Transformation in Shape Memory Alloys

April 1992 to March 1995
S. Kajiwara, Physical Properties Division
Keywords: martensitic transformation, shape memory effect, high resolution electron microscopy, structure image, lattice image, stacking fault

The mechanism of improvement of shape recovery of an Fe-based shape memory alloy has been studied by using high resolution electron microscope. Among a few Fe-based shape memory alloys, an Fe-14Mn-6Si-9Cr-5Ni (mass%) alloy is regarded as the most promising shape memory alloy, because the alloying elements are not expensive and yet the alloy has a property of corrosion-resistance. However, this alloy can not be used unless the so-called "training" treatment or a kind of thermomechanical treatment is done to improve the shape recovery, for the shape recovery in the as-solution treated state is only about 50%. In the present work, the following thermomechanical treatment was performed. Specimens solution-treated at 1320 K for 30 min was first cold rolled by 10% at room temperature and then heated at 970 K for 10 min. The martensitic transformation involved in exhibiting shape memory effect in this alloy system is the f.c.c to h.c.p. transformation induced by deformation at room temperature and its reverse transformation (h.c.p. → f.c.c.) on heating. In order to elucidate the transformation mechanism which leads to the improvement of shape recovery, we have examined the distribution of martensites plates with various widths in the as-solution treated specimen and the thermomechanically treated specimen. By taking lattice images and structure images with a high resolution electron microscope, it was possible to measure the width of martensite plate in the sub-nano-metric scale up to 0.2 nm (the interval of two neighboring close-packed layers.) The histogram of number of martensite plates against width of martensite plate was obtained by examining along a total length of 1600 nm perpendicular to the $(111)_{f.c.c.}$ habit plane, and it was found that there is a remarkable difference in the histograms for the thermomechanically treated specimens and non-thermomechanically treated specimens; that is, in the former case, the number of martensite plates with extremely small widths (less than 4 nm) is very large and it decreases rapidly with increasing width, while, in the latter case, the number of existing martensite plates is not dependent on plate width. This fact means that the f.c.c. to h.c.p. transformation in the former case is accomplished by the random stacking fault mechanism, while, in the latter case, the transformation proceeds mainly by the pole mechanism. As a result, a large number of parent f.c.c. crystals are mixed with h.c.p. martensite in the former case and hence, there is no need for nucleation of f.c.c. phase in the reverse transformation, and furthermore, there are many Shockley partial dislocations associated with the tips of those thin martensite plates, which are suffering the back stress field from the neighboring austenite phase. These two facts greatly promote the reverse transformation, and accordingly, increase the shape recovery on heating.

[27] Evaluation of Magnetomechanical Instability of Metastable Austenitic Steels

April 1994 to March 1995
K. Nagai, Mechanical Properties Division

Keywords: martensitic transformation, magnetic field, tensile stress

Mechanism of magnetomechanical instability, which is caused by both mechanical instability through deformation or stress and magnetic instability, has been investigated. Alloys used in this study are an Fe-31Ni-0.4C and an Fe-27Ni-0.8C (wt%), which were vacuum melted and hot rolled. Specimens for the tensile test have a parallel portion of 20 mm length and a cross section of 3 mm by 3 mm, and sealed in the evacuated silica capsules. They were solution treated at 1273 K for 3.6 ks, and quenched rapidly by breaking the capsules in the brine. The 13T superconducting magnet equipped with tensile machine of the maximum load of 1 t was used for the following tests; (1) cooling to 4 K, (all the following tests were carried out at 4 K) (2) the magnetic field of 10T was applied, (3) the stress of 220 MPa was applied, (4) the stress of 220 MPa was applied under the magnetic field of 10T, (5) the magnetic field up to 10T was applied under the tensile stress of 220 MPa. The experimental results by the test (1) shows that both specimens are stable parent phase at 4 K, but martensitic transformation is induced by applying either the magnetic field or the stress. Here the parent phase is f.c.c. austenite and the transformed phase is thin plate type b.c.t. martensite. The surface relief formed by martensitic transformation was observed by an optical microscope and it was found that the amount of martensite induced by magnetic field was larger than that induced by stress. The load-elongation curves show that martensitic transformation is induced in the magnetic field by a stress lower than that without magnetic field, and this tendency is remarkable in an Fe-27Ni-0.8C alloy. When the magnetic field is increased under the constant stress, serration appears due to the stress relaxation by the martensitic transformation. Since the elongation is proportional to the amount of martensite, the load-elongation curves show that the amount of martensite induced by magnetic field under the constant stress is larger than that induced by stress under the constant magnetic field.

Surface and interface properties

(28) The Evaluation of Super Structures on Ultra Clean Solid Surface and the Creation of Dimensional Controlled Nano-materials

April 1995 to March 2000

H. Nejoh, Surface and Interface Division

Keywords: STM, STS, nano-scale, atoms manipulation

These days nano-scale science brought various interesting results. In 1982 Binning and Rohrer invented Scanning Tunneling Microscope (STM). The nano-scale science has been making rapid progress. Recently the aim of STM isn't only to see atoms but also to manipulate ones. The manipulation means moving, supplying, picking up and so on. A STM isn't only used for observing atomic-scale structures on surfaces but also processing them. We can observe not only nano-meter structure on surface to use STM but also the density of states. Especially, the new method is called Scanning Tunneling Spectroscopy (STS). One of the most impressing technique was Eigler group's work. They made a corral of Fe atoms on Cu(111) using atom manipulation and observed standing waves on it using STS technique.

In this background, the aims of this research are observing quantum waves and controlling them. Since we expect that we create new techniques and materials using atom manipulation and our extreme high vacuum technique which have been researched in our group. Concretely, we are going to advance along two themes. First one is the development of technique to control spin polarized interaction on solid surface. It is the aim of this theme that we order spins in atomic-size area array on surface, so we can use the memory devices and we can get information from ones using spin polarized interaction. Second one is the development of system to detect quantum effect on solid surface. It is the aim of this theme that we control the phases of quantum waves, so we make a phase interference devices.

(29) Self-control of Surface Composition of Thin Film and Its Application to Field Emitter

April 1995 to March 2000

K. Yoshihara, Surface and Interface Division

Keywords: surface segragation, saturated surface compositon, self-compositon control, work function, field emitter

When deposited metal film on substrate was heated in a vacuum, it was observed that substrate element diffused to the surface of film. The surface concentration of segregant was always constant. Even if the segregated layer was removed by argon ion sputtering, the segregated layer of the saturated concentration was formed again by re-heating. Therefore, the surface composition of the segregated layer on metal film is expected to have a self-controlling property.

It is well-known that the surface adsorption of metal changes the work function of a solid surface. Therefore, it is expected to change the work function by the surface segregation. If the work function of materials can be lowered, we can produce a field emitter of high performance. Fowler-Nordheim relation shows that a half eV decrease in work functions brings approximately 10 times in-

crease in field emission current. The work function varies with a coverage of adsorbed materials. However, if we use the self-controlling property of segregation behavior on metal film, then the stable work function on the surface, i.e., stable field emission current can be expected.

In this study, the stability of surface composition will be quantitatively analyzed in the wide range of temperature, and the change of work function by segregation will be measured. The recovering rate of the surface composition during Ar ion sputtering will be measured. The reproducibility and the stability of work function on segregated surface will be also examined. Furthermore, the effect of contaminant adsorption on work function and the method to solve contamination problem will be searched.

30 Theory of Thermal Reaction on Solid Surfaces

April 1994 to March 1997

T. Ohno, Materials Physics Division

Keywords: structural stability, chemisorption, reaction, solid surface

The purpose of this study is to clarify theoretically the thermal reaction processes on several solid surface systems. The analysis is based on the density-functional electronic theory within local-density approximation, which provides a powerful tool to determine the dynamical behavior as well as the stable atomic arrangement of solid surfaces.

Particular attention will be paid on the structural stability and optimum atomic arrangment of semiconductor and metal surfaces, the chemisorption of atoms and molecules such as chlorines on semiconductor surfaces, and the self-adsorption on simple-metal and transition-metal surfaces.

In order to make it possible to perform numerical calculations for large-scale systems, we will also try further developments on methodological and numerical techniques.

Related Papers

Energetics of As Dimers on GaAs(001) As-Rich Surfaces, T. Ohno, Phys. Rev. Lett., 70 (1993): 631–34.

Barrierless Dimer Breaking at Semiconductor Surfaces by Chlorine Atoms, T. Ohno, Phys. Rev. Lett., 70 (1993): 962–65.

Chlorination of Ga-Rich and As-Rich Reconstructed GaAs(001) Surfaces, T. Ohno, in Proc. 22nd International Conference on the Physics of Semiconductors, ed. by D.J. Lockwood (World Scientific Publishing, (1995): 545–48.

31 Research on Electrode Reactions between Metallic Ions and Carbonaceous Materials/Research on Electrochemical Characteristics of TiAl-base Alloys

April 1994 to March 1996

I. Tomizuka, Physical Properties Division

Keywords: electrode reaction, metallic ion, carbonaceous material, TiAl-base alloy

The activities are characterized by reactions on electrodes. They are concerned with the following three fields.

1. Cathodic reaction of carbonaceous material: This subject deals with elimination of metallic ions from their dilute solution. Whereas the ions are known to be deposited on an electrode under an appropriate cathodic potential, simple application of a potential is often not practical, because bonding force of the crystals to the electrode material is too weak to handle. The research is aimed at solving this problem by employing active carbon (AC) for the cathode. Then, reduced anions are expected to be adsorbed on AC in an amorphous state, not in a crystalline one. Experiment data so far secured imply that the metal adsorbed on AC in amorphous state would be more stable in a thermodynamic sense than that attached to AC in crystal states, but that the rate of adsorption would be fairly slower than that of deposition when the potential is deeply cathodic in comparison with the concentration of the solution.
2. Anodic reaction of carbonaceous material: An attempt has been made to fabricate inexpensive carbon fiber from lignin, a by-product of pulp industry. A problem of the carbon fiber based on this material is that it contains a considerable amount of sodium and its compounds. The research is aimed at developing an electrochemical process to eliminate the impurities by applying an anodic potential to the fiber in aqueous solution of sulfuric acid. Experimental results have revealed that content of the impurities can be reduced to the level in which their peaks are not discerned in the x-ray diffractogram. The mechanism of the elimination is currently under study.
3. Electrochemical reaction of TiAl: Hydrides are formed within TiAl when the latter is retained for a sufficiently long time under a cathodic potential in sulfuric acid. Even in the cases where the cathodic treatment is so short that peaks of no hydride are discerned in x-ray diffractogram, they can appear if an anodic treatment follows the cathodic treatment. A research was performed by x-ray diffractometry to check if the hydrides were different depending on the simple cathodic treatment or on the anodic treatment preceded by a cathodic one. The experimental results have shown that the diffractograms can be accounted for not by a single compound but by two which are identical in both cases. One was tetragonal and the other was hexagonal.

32 Fabrication of Quantum Well Box Systems by Droplet Epitaxy for Advanced Optoelectronic Devices

April 1991 to March 1996

N. Koguchi, Surface and Interface Division

Keywords: quantum well boxes, molecular beam epitaxy, GaAs, scanning tunneling microscopy

Predictions of an enhanced electron mobility device and and advanced semiconductor laser with highly-monochromized and low threshold current density have been made in the quantum well box structure. Although the molecular beam epitaxy (MBE) method is known to be successful in growing finely layered structures and quantum well wires, it has not yet been successful to obtain the quantum well box structure.

We have proposed a new MBE growth method named Droplet Epitaxy for the fabrication of some III-V compound semiconductor quantum well box structures. This method is based on incorporating V-column elements with III-column elements in the periodic table droplets which were deposited on an inert surface of the subtrate for monolayer adsorption of the III and V-column elements. Some III-V compound semiconductor surfaces terminated with a VI-column element like S, Se or Te have been reported to provide an inert surface with appropriate dangling bonds suitable for supporting the adhesion of foreign atoms. Such surfaces are thought to be suitable for the growth of epitaxial microcrystals by the Droplet Epitaxy method.

We have demonstrated three dimensional growth of GaAs epitaxial microcrystals on an S-terminated GaAlAs substrated by Droplet Epitaxy. At the end of the process of Droplet Epitaxy the GaAs microcrystals are covered by an MEE (migration enhanced epitaxy) grown GaAlAs layers. By this technique a number of epitaxial microcrystals with a pyramidal shape were successfully obtained on the S-terminated substrate. The base size of each epitaxial microcrystals was about 10 nm × 10 nm with standard deviation of about 5% and the average distance between microcrystals was about 10 nm in the case of substrate temperature of 50 °C and the Ga molecular beam intensity of 3.3×10^{14} cm^{-2} s^{-1}. The size and distribution of microcrystals correspond to those of Ga droplets. The measurements of the Ga droplet saturation density as functions of Ga molecular beam intensity and substrate temperature revealed the nucleation mechanism of Ga droplets on the S-terminated GaAs. The size of the smallest stable nucleus is one Ga-Ga pair on the substrate. It is necessary to fabricate nucleation sites for Ga droplets to arrange the site of each GaAs microcrystal. The selective deposition using finely focused Ga ion beam is also a promising method to arrange the site of each microcrystals.

Related Papers

New MBE Growth Method for InSb Quantum Well Boxes, N. Koguschi, S. Takahashi, and T. Chikyow, J. Crystal Growth, 111 (1991): 688–92.

Growth of GaAs Epitaxial Microcrystals on an S-terminated GaAs Substrate by Successive Irradiation of Ga and As Molecular Beams, N. Koguchi and K. Ishige, Jpn. J. Appl. Phys., 32 (1993): 2052–58.

New Selective MBE Growth Method for Direct Formation of GaAs Quantum Dots, N. Koguchi, K. Ishige, and S. Takahashi, J. Vac. Sci. Technol., B11 (1993): 787–90.

33 Fabrication and Characterization of Compound Semiconductor Nanometer Structures

April 1994 to March 1997

N. Koguchi, Surface and Interface Division

Keywords: nanometer structure, molecular beam epitaxy, GaAs, scanning tunneling microscopy

With the continuous reduction in the dimension of electronic devices, quantization effects become dominant and may disturb the function of the device. Nanometer research, however, makes constructive use of quantum effects. Tunneling, single-electron transfer and wave interference can be used as a basis for novel devices. In 1994, Science and Technology Agency has organized several institutes and universities for new research project, named Nanospace Laboratory Project. The target of this project is to fabricate and characterize the material structures with dimensions down to a few nanometers. In this project, we are now researching the fabrication and characterization of compound semiconductor nanometer structures. In order to fabricate these structures, we are researching three methods; self-organized formation by using adsorption phenomena, microfabrication using metal fine particle deposited on semiconductor quantum wells and Droplet Epitaxy combined with lithography by scanning tunneling microscopy (STM).

We have designed and introduced a new system suitable for the self-organized formation of nanometer structures. This system is composed of molecular beam epitaxy equipment combined with STM and optical measurement instruments. We can perform *in situ* observation of surface, during formation of nanometer structures using this new system.

It is necessary to investigate the S-terminated GaAs (001) to fabricate nanometer structures by Droplet Epitaxy combined with STM lithography. We have observed the S-terminated GaAs (001) with (2 × 6) surface reconstruction by STM and found out this reconstruction originating from the cell which contains five S-S adatom dimers and one missing dimer for the first time. Also we have estimated the structural stability of this (2 × 6)

reconstruction by the first principles pseudopotential calculation and confirmed the phenomena of electron transfer from S-S to missing dimer.

Related Papers

New Selective MBE Growth Method for Direct Formation of GaAs Quantum Dots, N. Koguchi, K. Ishige, and S. Takahashi, J. Vac. Sci. Technol., B11 (1993): 787–90.

Arsenic Adsorption on GaAs (001), H. Noerenberg and N. Koguchi, Sur. Sci., 296 (1993): 199–212.

2 × 6 Surface Reconstruction of in situ Sulfur-Terminated GaAs (001) Observed by Scanning Tunneling Microscopy, S. Tsukamoto and N. Koguchi, Jpn. J. Appl. Phys., 33 (1994): L1185–88.

Observation of Sulfur-Terminated GaAs (001)-(2 × 6) Reconstruction by Scanning Tunneling Microscopy, S. Tsukamoto and N. Koguchi, Appl. Phys. Lett., 65 (1994): 2199–201.

34 Basic Study on Reaction between Materials and Bacteria

April 1993 to March 1996

H. Masuda, Failure Physics Division

Keywords: Bacteria, FeS, Redox potential

It is well known that some bacteria have special ability to oxidize metals. This ability of oxidizing metals is very useful for refining materials if the reaction rate is comparatively fast. This year we studied the bacteria (Thiobacillus ferroxidans) reactions on FeS as a function of the redox potential and the activity of bacteria. Good correlation was observed between the redox potential and the activity of bacteria as shown in the figure. The number of bacteria increased according to logarithmic law at first stage and then kept constant after 4 days. FeS decreased with time and S showed maximum after 20 days. The reaction process of bacteria was found very complicated. We study the possibility of producing new material by bacteria reaction.

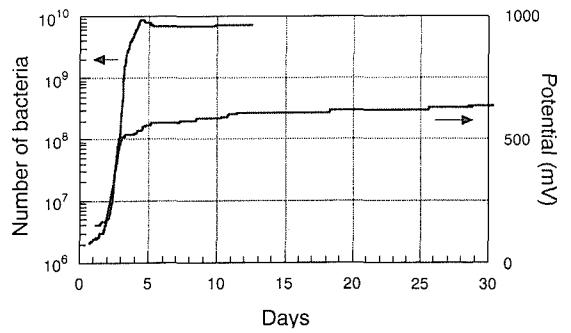

Fig. 1 Relation between number of bacteria and redox potential

35 Electrochemistry and Modelling of Corrosion of Metals under Thin Water Layer

April 1993 to March 1996

T. Kodama, Environmental Performance Division

Keywords: thin water layer, kelvin probe, potential distribution, atmospheric corrosion

Corrosion of Metals Under Thin Water Layer

Several types of corrosion reaction occur through thin layer of water on metal surfaces in such cases as atmospheric corrosion and indoor corrosion. Electrochemical reactions occur on the boundary between thin layer of water and metal surface. The reaction rate in this case is generally larger than that in bulk solution because of higher activity of mass transfer or accelerated diffusion. Little information has been available on the mass-transfer and distribution of local electrochemical potential or current in the water layer because of experimental difficulties in the measurements.

To measure the distribution of local electrode potential of metal, we prepared non-contact electrodes (kelvin probe) of gold wires of 1.0 and 0.5 mm diameter. The probe was oscillated sinusoidally by a piezoelectric vibrator. Electrode potential is converted from sinusoidal current flowing through the probe and sample electrode.

To examine the performance of above prove, we prepared a sample of iron-zinc couple. Potentials were measured on dry and wet (pure water, about 500 μm thickness) surfaces of the metal couple using the probe with 1.0 mm diameter. On the dry surface, potential on zinc was about –0.85 V, while that on iron was about –0.65 V. The zone of potential transition was 6.0 mm wide at boundary iron and zinc. The width was not influenced by a probe diameter. On the wet surface, the potential of zinc shifted to about –0.8 V, and that of iron to –0.4 V. The zone of potential transition was wider than that on dry surface.

Atmospheric Corrosion in Tropics of Southeast Asia

The JAPAN-ASEAN cooperation programme on materials science and technology (atmospheric corrosion project) was completed in May 1994 after two years follow-up of atmospheric weathering tests in Thailand and the Philippines.

In tropical environment, it was demonstrated that deterioration of polymer layer is more prominent than that of metals. Among polymer coatings tested fluoride-resin showed the highest resistance to ultraviolet degradation, followed by polyurethane coating. The corrosion rate of bare metals in Southeast Asia was the same level as that of world average.

36 Evaluation of High-Performance Triazinedithiols as a Corrosion Inhibitor

April 1993 to March 1996

H. Baba, Environmental Performance Division

Keywords: triazinedithiole, corrosion, inhibitor, copper

The project of surfactants of triazinedithiole (RTDT) has started in cooperation with universities, governmental research institutes and industry under the auspices of Science and Technology Agency. The general targets of the project are designing molecular structure of high performance RTDT's with fluoride and siliceous functional groups, and establishing synthetic methods of the compounds that give highly protective interfacial layers on surfaces of metals, rubbers and plastics. In NRIM we take part in clarifying the mechanism of corrosion inhibition and the nature of chemical bonding between metals and RTDT's. Thiole radicals (-SH) are known to react readily with copper and other metals following strong chemisorption. When metals are treated in solutions of properly selected triazinedithioles with variety of hydrophobic substitution groups (represented by R), stable and protective surface films are expected to be formed. In the second year of the project our concern is focused on the performance of highly sophisticated RTDT's with fluoride groups and the effect of conventional RTDT's on copper corrosion.

Copper specimens were electrochemically treated in several RTDT solutions with various radicals (-R), such as $-N(C_4H_9)_2$, $-N(CH_2CH = CH_2)_2$, -SH, $-N(n-C_8H_{17})_2$, $-NHC(CH_3)_2CH_2C(CH_3)_3$, $-N[CH_2CH(CH_3)_3]_2$, $-NHC_{18}H_{35}$, $-N(CH_2C_6H_5)_2$, $-N[CH_2(C_2H_5)CH(CH_3)_3CH_3]_2$, and $-NC_7F_{15}CH_2CH_2CH = CH_2$. The treated metal specimens were then subjected to the characterization of surface layers and evaluation of corrosion resistance. We have also studied the electrochemical behavior of copper in aqueous solutions of triazinedithiole for the purpose of obtaining the optimum electrolysis conditions for surface treatment. The highest protection was attained when copper was treated potentiostatically at the potential of current peak, E_p. We evaluated the corrosion resistance of anodized copper ny electrochemical methods. Potentiokinetic polarization curves in 3% NaCl showed that corrosion current was suppressed with increasing number of carbon in the hydrophobic radicals, such as $-N(n-C_8H_{17})_2$, $-N[CH_2(C_2H_5)CH(CH_2)_3CH_3]_2$, $-NC_7F_{15}CH_2CH_2CH = CH_2$. The performance of thiols as a corrosion inhibitor has been evaluated for a special type of localized corrosion of copper, the case of so-called "ant-nest" corrosion that occurs in wet acetic or formic acids. The performance of thiols as an inhibitor was improved with increasing number of carbon in hydrophobic radicals; e.g., such radical as $-N[CH_2(C_2H_5)CH(CH_2)_3CH_3]_2$ showed the highest performance. Among the groups of the same C number, iso-structure showed better performance than normal structure.

37 Effect of Oxidation on Mechanical Degradation of Metallic Materials

April 1991 to March 1995

Y. Ikeda, Failure Physics Division

Keywords: oxidation, thermal spray coating, Y_2O_3 dispersion, mechanical alloying, S segregation

Some questions arose from our previous works and were elucidated separately.

1. Is a thermal spray coated layer doped with Y_2O_3 so effective as Y_2O_3 dispersed alloys for suppressing high temperature oxidation?
   Type 304 stainless steel samples were coated with stainless steel powder implanted with Y_2O_3 by means of thermal spray coating technique. The resulting Y_2O_3 dispersed layer was much more resistant to cyclic oxidation than steels without coating. This result shows that a Y_2O_3 alloy composite coating can be substituted for mechanical alloying for the purpose of high temperature oxidation resistance.
2. Is the high temperature oxidation mechanism of mechanically alloyed materials different from that of cast alloys?
   Surface morphology was observed with AFM on several ODS alloys through mechanical alloying and cast alloys in early stages of oxidation. Oxide growth was found to be retarded at a number of dispersed points on ODS alloys, while oxide grew relatively uniformly on cast alloys. This result suggests that oxidation mechanism is different between ODS and cast alloys from a very early stage.
3. Is oxide spalling suppressed by interfacial roughening?
   It is plausible that oxide film spalls more easily at a flat interface than roughened. Spalling test of Al2O3 coating film, however, shows that the interfacial roughening suppresses very little the spalling on a steel where surface segregation of S is rapid. By contrast, the spalling is suppressed even at a flat interface on a steel in which S is trapped by La.
4. Is P trapped by rare earth metal (REM) or Y_2O_3?
   Y_2O_3 traps P to some extent but REM does not.

38 Evaluation of Atomic Level Damage on Material in Aqueous Solution

April 1992 to March 1995

H. Masuda, Failure Physics

Keywords: tip effect, SPM image, image convolve

When we study the nanometer range of corrosion by the scanning probe microscopes (SPM), such as STM and AFM, we always meet the problem of the accuracy of the SPM image. On of the biggest factor for the accuracy of the image is the shape of the SPM tip. Recently the SPM tip of

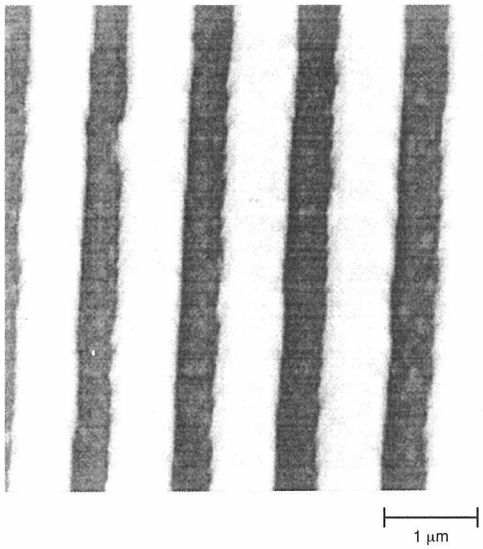

Fig. 1 Original AFM image

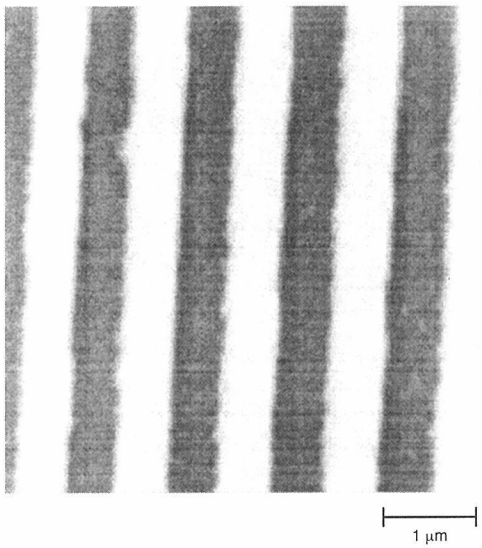

Fig. 2 Reconstructed AFM image

10 nm in radius of curvature can be made according with the development of nano-fabrication technology. However even we use these very sharp SPM tip, we cannot get rid of the influence of the tip shape if we take the image of very sharp particles. In order to reduce the effect of the SPM tip we develop an image treatment method.

The principle of this method is as follows; First we took the AFM image of the standard specimen (0.5 μm pitch) as shown in Figure 1. The difference of shape in real and observed is due to the influence of the tip shape. We estimated the tip shape by this image and placed this virtual tip on the image. We removed the overlapped part of the tip and the image repeatedly and finally got a better image as shown in Fig. 2. This kind of process should become the standard method to get rid of the influence of the tip shape.

[39] Reaction Phenomena Related to Tunnel Current

April 1994 to March 1995
H. Masuda, Failure Physics

Keywords: moire interference, piezo actuator, hysteresis, AFM

We observed reaction phenomena related to tunnel current and applied this phenomena for the nano-fabrication. However, the accuracy of the image of the scanning probe microscope (SPM) is usually unknown around the range between 50 and 500 nm, because no proper standard material exists to correct the hysteresis of the piezo actuator. When we observe the atomically flat surface by these microscopes, we often find noise-like moire patterns around the scanning range of 50 to 200 nm. The moire interference phenomenon caused by atoms or molecular is applied for the improvement of the accuracy of scanning probe microscope around the scanning range between 50 and 500 nm.

We first took the AFM image of mica molecular. The period of molecular at the horizontal direction was evaluated about 0.55 nm by the image. The moire pattern usually appeared when the sampling interval is nearly equal to the molecular space, that is, 0.55 × 256 = 140.8 nm. The moire pattern can be clearly seen at the scanning range of 130 nm.

The moire pattern spacing should be the same in all scanning range if no hysteresis exists in the piezo actuator. The change of moire pattern spacing is caused by the hysteresis property of the piezo actuator. The strain of the piezo actuator was found to exceed more than 4% by the moire pattern. In this way, we can calibrate the very small range of hysteresis on the piezo actuator.

Mechanical properties

(40) Temperature Strength and Fracture of Reinforced Oxide- and Nitride-Base Ceramics

April 1995 to March 1997
K. Hiraga, Mechanical Properties Division

Keywords: creep, cavitation, toughening microstructure

Though polycrystalline ceramic materials are typically brittle at room temperature, most of them show plasticity at high temperature under the aid of grain boundary sliding accomodated by matter transport through and/or across the boundaries. Concurrent damage accumulation occurs by cavitation and/or diffusional crack growth, both of which are related closely to the abovementioned deformation mechanisms. The basic information of such deformation and damge process, which are quite different from those at lower temperatures, are important when the materials are used in high temperature machinery. The present study is conducted to examine the high temperature deformation and fracture of oxide- and nitride-base ceramics. The special attention is placed on the constitutive behavior and cavitation

damage of reinforced composites at relatively low tensile stresses (σ/E~10^{-4}), at temperatures higher than 1500 K.

㊶ Long-term Creep-fatigue Properties of 316 FR Stainless Steel for Fast Breeder Reactor

April 1995 to March 2000

K. Yamaguchi, Failure Physics Division

Keywords: low cycle fatigue, fast breeder reactor, 316 FR stainless steel

The 316 FR stainless steel has been developed as a candidate material for fast breeder reactor of twenty first century. For the structural design of components of the reactor, a simple and accurate analysis method for evaluating the low cycle fatigue life of the 316 FR steel is required, because the main components of the reactor are subjected to cyclic thermal stresses. One of the objects in this research is to develop the analysis method for time-dependent low cycle fatigue life of 316 FR steels. At present, the author has an idea to apply a parametric analysis for temperature and strain rate dependences of the fatigue life, and to predict and evaluate the fatigue life of very slow strain rate up to 10^{-6}/sec. This method was developed by the author and was successful to apply to many kinds of conventional engineering heat resisting materials at the strain rate up to 10^{-5}/sec.

Second is to evaluate monotonic creep and cyclic fatigue properties for modified 316 FR steels which is now developing by a steel maker and fabricators. So the testing data would be useful to the materials design. In the first half of this research the tests will be carried out for eight heats of the materials with different chemical compositions variating the elements such as C, N, Mn and P. In the second half a prediction method of the fatigue life will be developed by using the data of monotonic creep rupture properties such as creep rupture ductility.

This research is performed in collaborations with Mitsubishi Heavy Industry Ltd., Nippon Steel Corp. and The Japan Atomic Power Co.

Related Paper

Parameter Analysis for Time-Dependent Low-Cycle Fatigue Life, K. Yamaguchi, K. Kobayashi, K. Ijima and S. Nishijima, Trans. ASME, J. Eng. Mater. Tech., 116 (1994): 479–82.

㊷ Generalized Rule and Guide for Use of Fatigue Data

April 1995 to March 1997

S. Nishijima, Failure Physics Division

Keywords: fatigue, steels and alloys, aluminum alloys, welded joints, NRIM Fatigue Data Sheets

NRIM has been conducting a series of project researches since 1975 to establish standard reference data on fundamental fatigue properties of typical Japanese materials being used for building machines and structures. The program of work has been accomplished most successfully in March 1995 by the publication of 83 Data Sheets.

Table 1 NRIM Fatigue Data Sheet Technical Document

No.	Subjects	Issued
1	Fundamental Fatigue Property for Carbon, Cr and Cr-Mo Steels	1981
2	Fatigue Strength for Welded Joints of High Strength Steels	1983
3	Crack Growth in Arc-Welded Butt-Joints of High Strength Steels	1984
4	Strain Rate Effect in Low Cycle Fatigue of Alloy Steels at High Temperatures	1985
5	Fundamental Fatigue Property of JIS Steels for Machine Structures	1989
6	High Cycle Fatigue of Alloy Steels at Elevated Temperatures	1990
7	High Cycle Fatigue Property of Carburized Steels	1992
8	High Cycle Fatigue Property of Hard Steels	1995
9	Fatigue Crack Propagation in Welded Joints of Structural Steels	1995
10	Time/Temp Effect in High Cycle Fatigue of Steels at Intermediate Temps.	(1996)
11	Time-Dependent High Temperature Fatigue of Steels and Alloys	(1996)
12	Fatigue Property of Aluminum Alloys for Welded Structures	(1996)
13	Intermediate Temperature Fatigue of Steels for Welded Structures	(1997)
14	Low/High Cycle Fatigue Properties of Steels and Aluminum Alloys	(1997)
15	Intermediate Temperature Fatigue of Steels for Pressure Vessels	(1997)
16	Elastic Moduli of Steels for Machine Structures	(1997)

The present research aims at the presentation of generalized rules found in different fatigue properties that can be explained from view point of fundamental mechanisms of fatigue and, therefore, are substantially important for correct use of those fatigue data. It is, in other words, to offer a guide for understanding the change in various properties and for applying the data to engineering requirements. Selected data from related Data Sheets are collectively analyzed to be fit to theoretical models, for some cases, and additional experiments are performed to verify theories, for other cases.

The effort to show the generalized rule on fatigue property data has actually been continued in the Fatigue Data Sheet Project. The outputs have been published in Japanese as Fatigue Data Sheet Technical Documents, as shown in Table 1, and

will be completed further by the present 2 year program.

43 Cyclic Deformation in a Corrosive Environment

April 1994 to March 1997
R. Hamano, Mechanical Properties Division
Keywords: stage I fatigue, stage II fatigue

The growth of fatigue crack nucleated along the slip bands of PSBs or PLBs occurs over two successive propagation stages—Stage I (sheer mode) and Stage II (normal mode). The past data on the effect of environments on crack growth in Stage II fatigue region have been reported in previous works. Comparatively little attention has been paid to the effect of hydrogen-related environments on Stage I crack propagation and the transition of crack growth from Stage I to Stage II.

We present experimental results suggesting that the transition of fatigue crack growth from Stage I to Stage II is accelerated in a hydrogen environment and discuss whether the early transition of the stages of fatigue crack growth is caused by the localized deformation of the decohesion at a notch root, carrying out fatigue tests on U-notch specimens of SNCM439 steel and Al-2 Li alloy in laboratory air with or without water vapour and in a 3.5% NaCl aqueous solution. Fatigue tests were performed on a closed loop servo-hydraulic machine, using a sinusoidal wave and a load ratio of 0.1. The cyclic loads were set to produce after 10 cycles a crack extension of about 2.0 mm. The testing temperature was 293 ± 1 K. A frequency of 15 Hz in laboratory air with a relative humidity of about 50% and a frequency of 1 Hz in a 3.5% NaCl aqueous solution were employed. After fatigue testing, fracture surfaces, were observed with scanning electron microscope (SEM).

The observation of the early transition of fatigue crack growth from Stage I to Stage II and the appearance of striation on the fracture surfaces in a 3.5% NaCl aqueous solution suggests that secondary slip plays an important role in the transition of fatigue crack growth and the fatigue crack grows by the operation of two more slip systems leading to macroscopically brittle (transcrystalline) fractures bisecting the two active slip planes. Further work to make clear the possibility is left.

Related Paper

Transition of Fatigue Crack Growth from Stage I to Stage II in a Corrosive Environment, R. Hamano, submitted to Metall. Mater. Trans., A, 26, (1995): 1.

44 Fatigue Behavior of Brittle Materials at Elevated Temperatures

April 1992 to March 1996
Y. Kawabe, Mechanical Properties Division
Keywords: cyclic fatigue, static fatigue, elevated temperatures, ceramics

The development of ceramics is being watched with knee interest, because they are very promising as structural components for engineering applications where metallic materials are not available. Since many of them are subjected to static or cyclic loading at elevated temperatures for prolonged periods, it is important to understand fatigue behavior at elevated temperatures. Nevertheless, there are very few studies on the cyclic fatigue behavior of ceramics at elevated temperatures.

In prior study, we investigated cyclic and static fatigue behavior in ceramics at room temperature and showed that lifetimes are shortened and crack growth rates are significantly accelerated by cyclic, compared to static loading. In addition, it was found that cyclic fatigue behavior is affected by factors such as fracture toughness, environment, stress ratio, and variable amplitude loading. However, it is little known whether these factors affect cyclic fatigue behavior at elevated temperatures.

In this study, cyclic and static fatigue behavior in silicon nitride have been investigated over a range of room temperature to 1200 °C. As a result, it is found that fatigue behavior depends strongly upon fracture toughness and/or viscous flow of glass phase.

Related Papers

Cyclic Fatigue in Silicon Nitride Ceramics, G. Choi, S. Horibe, and Y. Kawabe, Acta Metall. Mater., 42 (1994): 1407–12.

Cyclic Fatigue Crack Growth from Indention Flaw in Silicon Nitride: Influence of Effective Stress Ratio, G. Choi, S. Horibe, and Y. Kawabe, Acta. Metall. Mater., 42 (1994): 3837–42.

45 Study on Deformation and Fracture of Structural Materials at Cryogenic Temperatures

April 1993 to March 1996
K. Nagai, Mechanical Properties Division
Keywords: cryogenic temperature, subsurface fatigue crack initiation, titanium alloy

In titanium alloys, subsurface initiation of fatigue crack is seen at room temperature and more often at lower temperature. The subsurface or internal initiation is attributable to cracking of specified microstructure by localized cyclic deformation. Therefore, this initiation crack is identified as the origin of Stage I crack. By the aid of SEM, the size and the location of the subsurface Stage I crack can be measured; the size and the location are varied from specimen to specimen.

In the present study, multiple fatigue tests were done at the two cyclic stress levels to clarify the relationship between the Stage I crack size or loca-

tion and the fatigue life. An Fe-alloyed Ti was tested at 77 K and the fatigue specimen was hourglass type with a waist of 4.5 mm in diameter. The alloy showed the subsurface crack initiation at all the stress level tested. The number of multiple tests was about ten for each level. The number of cycles to failure (Nf) scattered almost within one order, between 10^6 and 10^7 at 905 MPa and between 10^4 and 10^5 at 1033 MPa. The size varied from 25 to 100 μm at 905 MPa and from 25 to 50 μm at 1033 MPa. The location in terms of the distance from the nearest surface varied from 500 to 1000 μm at 905 MPa and from 0 to 2000 μm at 1033 MPa. However, no apparent interrelation between the size and Nf and also between the location and Nf was observed. In all the stress levels, the size tended to be larger at lower stress but the location was not stress-dependent.

Related Paper

High Cycle Fatigue Properties of Ti-6Al-4V Alloys at Cryogenic Temperatures, K. Nagai, T. Yuri, O. Umezawa, K. Ishikawa, Y. Ito, and T. Nishimura, Titanium '92, Science and Technology, edited by F.H. Froes and I. Caplan, The Minerals, Metals & Materials Society, (1993): 1827–34.

46 Toughness Improvement of Ceramics and Brittle Steels by Control of Precipitation and Phase Transformation

April 1993 to March 1996
F. Abe, Environmental Performance Division
Keywords: toughness, zirconia ceramics, martensitic steels, phase transformation

The purpose of the present research is to investigate the microstructural evolution and to improve toughness by microstructural control for partially stabilized zirconia ceramics and neutron-irradiated martensitic steels.

The atomic arrangements at interfaces between a lenticular precipitate of monoclinic phase and the cubic matrix, at twin boundaries in the m-phase and at surface of a transformation-induced microcrack along grain boundaries have been investigated by means of high-resolution electron microscopy for a sintered ZrO_2 containing 9.7 mol% MgO. The microcrack has propagated along the (110) plane of the m-phase. A few edge-dislocations were also observed to have formed beneath the microcrack surface. This suggests that transformation-induced strain was partially accommodated by the formation of dislocations, although it was mainly accommodated by microcracks.

Fracture properties of the reduced-activation martensitic 9Cr steels for fusion reactor have been investigated by carrying out instrumented Charpy impact tests and tensile tests at temperatures below room temperature, after irradiation in the Japan Materials Testing Reactor at 493–573 K. The irradiation caused an increase in ductile-to-brittle transition temperature, which resulted primarily from the irradiation-induced increase in yield stress.

Related Papers

Tetragonal to Monoclinic Transformation in ZrO_2-9.7 mol% MgO During Cyclic Annealing, F. Abe, S. Muneki, and S. Ikeda, Proc. PTM '94, (1994): 823–28.

Phase Transformation and Interfaces in a MgO-Partially-Stabilized-Zirconia, F. Abe, S. Ikeda, S. Muneki, and K. Yagi, Proc. Japan-US Workshop on Functional Fronts in Advanced Ceramics, (1994): 216–19.

Development of Reduced-Activation Martensitic 9Cr Steels for Fusion Reactor, F. Abe, T. Noda, H. Araki, and M. Okada, J. Nucl. Sci. Technol., 31 (1994): 279–92.

47 Transient Behaviour of Creep Deformation and Fracture at the Elevated Temperature

April 1994 to March 1997
F. Abe, Environmental Performance Division
Keywords: creep deformation, inherent creep strength, creep crack growth, microstructural evolution

Complex transient behaviour which does not obey classical form, is observed on both creep deformation and creep crack growth of heat resisting steels and alloys at the elevated temperature. Creep deformation and creep crack growth are influenced by the changes in microstructure of materials. This study aims at giving a role of microstructural change in the transient behaviour.

Abnormal creep deformation behaviour at 823–973 K has been investigated on SUS 316 stainless steel. Complex creep deformation behaviour which reveals several peaks and local minima in creep strain rate, that differs from classical one which consists of transient, steady-state and tertiary creep stages, has been clearly observed. Correlation between irregular changes in creep strain rate and precipitation of second phases such as carbide and Laves phase has been found. It has been revealed that unusual marked increase in creep strain rate observed at 823 K and about 1000 h is caused by annihilation of large amounts of dislocations accumulated by a strengthening effects due to very fine carbide particles.

The evaluation method of creep crack growth rate da/dt at transient creep stage have not been established. The da/dt-C* relation shows the nose-part at this stage. In this research, the change of creep strain distribution, creep damaged zone and microstructures at the crack tip during transient

and steady-state creep stages are investigated for creep ductile and brittle materials. Based on these results, the evaluation method of da/dt will be increased.

The theoretical transition time from small-scale creep to transient creep and steady-state creep have been calculated based on the strain-hardening law for several kinds of heat resisting materials that have ever tested. The theoretical transition time does not always correspond to the initial nose-part for some materials.

48 Relationship between Fatigue Crack Propagation and Cyclic Deformation of Small Specimens

April 1994 to March 1997

A. Ohta, Environmental Performance Division

Keywords: fatigue crack, fatigue properties, cyclic deformation

The fatigue crack propagation property of steels in higher stress ratio is unique in spite of the difference of stress ratio. This property is obtained in a fatigue crack closure free condition, and defined as the fundamental fatigue crack propagation property.

This fundamental fatigue crack propagation property for aluminum alloy and titanium alloy which received STA heat treatment was measured by two levels of the maximum load hold tests. Those tests gave the fatigue crack propagation property for different stress ratio which were confirmed to be unique. These properties for different materials increased with the increase of the Young's modulus when the properties were compared in the relationship between the fatigue crack propagation rate, da/dn, and the range of stress intensity factor, ΔK.

The fundamental fatigue crack propagation properties for different materials become unique in the relationship between the fatigue crack propagation rate and the strain intensity factor, $\Delta K/E$, where E is the Young's modulus. This means that the fatigue crack propagation is controlled by the elastic strain range around the crack tip.

However, the property for titanium alloy which was annealed was superior to that for above property near the fatigue threshold. The relationship between the fatigue crack propagation and cyclic deformation of small specimens by measuring the variation of the mean strain during the cycling of small smooth specimens for titanium alloys of STA treated and annealed is going to be investigated.

49 NRIM Creep Data Sheet Project-IV

April 1991 to March 1996

K. Yagi, Environmental Performance Division

Keywords: long-term creep, stress relaxation, microstructural evolution

The major objectives of the NRIM Creep Data Sheet Project are to generate long-term creep and rupture data including 10^5 h data for heat-resisting steels and alloys, which were produced in Japan, and to publish the data as a series of NRIM Creep Data Sheets. This project has been continued since 1966 and the series of NRIM Creep Data Sheets have been distributed not only in Japan but also in abroad. In fiscal year 1994, we published three sheets for the steels listed in Table 2.

Table 2 Summary of NRIM Creep Data Sheets in fiscal year 1994.

Material	Number	Issued
1.25Cr-0.5Mo-Si steel plate for boilers and pressure vessels	21B	September 30, 1994
High strength steel (class 590 MPa) plate for pressure vessels	25B	September 30, 1994
18Cr-8Ni (base metals, weld metals and welded joints)	32A	March 31, 1995

In parallel with the testing and publishing program, we have made researches on long-term creep and rupture behavior of heat-resisting steels and alloys. Abnormal creep deformation behavior that reveals multiple local minima in creep rate was investigated for 0.2% carbon steels, from viewpoints of a decrease in creep strength and the advent of an inherent creep strength at long times. Stress relaxation behavior was investigated for NCF 800H (20Cr-30Ni steel). Complicated stress relaxation behavior, such as a rapid decrease in residual stress followed by an increase in residual stress, was related to a reduction of creep resistance resulting from the coarsening of $M_{23}C_6$ and to a shrinkage of the lattice of austenite matrix caused by the precipitation of $M_{23}C_6$. The creep curves of martensitic 12Cr steels were analysed based on a concept of modified θ-projection. The creep rupture strength and the softening of the steels during creep were correlated with a rate constant α in the modified θ approach.

Related Papers

Abnormal Creep Deformation Behaviour and Inherent Creep Strength of Carbon Steel, K. Kimura, H. Kushima, and K. Yagi, Proc. ISCMA-10, (1994): 645–48.

Long-term Stress Relaxation Behaviour of NCF 800H Alloy, T. Ohba, O. Kanemaru, K. Yagi, and C. Tanaka, Proc. ISCMA-10, (1994): 649–52.

Characterization of Long-Term Creep Strength for 12Cr Steels, H. Kushima, K. Kimura, K. Yagi, andK. Maruyama, Proc. ISCMA-10, (1994): 653–56.

50 Study on Deformation and Fracture of Materials under Irradiation

April 1993 to March 1998

J. Nagakawa, 2nd Research Group

Keywords: irradiation, radiation damage, deformation, fracture

Changes in mechanical properties induced by irradiation are critically important to the

structural materials for nuclear application. These materials are exposed to alternate stress or strain loading during the shut-off and start-up periods as well as almost constant loading during the steady operation. The former loading may cause fatigue fracture and the latter can impose very significant radiation-induced deformation. Therefore, the synergistic loading of alternate and constant types under irradiation is quite essential to investigate the mechanical response of the nuclear reactor materials, although it's not been tried until the present research project. During the fiscal year 1994, the following research activities were accomplished.

It is inevitable to use thin and small specimens for the deformation testing under light-ion irradiation so as to assure uniform radiation damage and less radioactivation of the specimen. Small specimen testing technique was examined using the creep-fatigue machine, specially designed for the irradiation experiments, the small specimens, 100–150 μm thick, 1.2 mm wide and 5 mm long in gage. The materials used were solution-annealed stainless steels, either SUS 304 or 316. Accuracy of the deformation measurement by the high resolution LVDT was evaluated by comparing it with the actual elongation of the specimens. The difference in each test was only of the order of microns and within the accuracy of the measuring microscope used. The machine successfully produced triangular and sinusoidal loading patterns of up to 1 Hz. The synergistic loading was accomplished in both stress- and strain-controlled modes. Larger stress relaxation was observed in the strain-controlled mode with 10 s holding at both high and low strain compared with the steady loading mode. Also higher creep strain rate was observed under cyclic loading in the stress-controlled mode.

The creep-fatigue machine will be connected to the NRIM Small Cyclotron in 1995 and used for the testing under irradiation.

51 Fundamental Research for Intelligent Materials (Formation Process and Recovering Method of Creep Damage)

April 1994 to March 1999

N. Shinya, 5th Research Group

Keywords: intelligent materials, electron Moiré method, creep deformation, self-recovering of creep cavity, life extension

In this work, high temperature damage formation process and recovering method of high temperature damage are being studied for creating self-repair materials.

Creep Damage Formation Process

Using the electron Moiré method, the micro creep deformation such as grain boundary sliding, coarse slip and localized strain in pure copper and 321 stainless steel specimens have been measured. The results show that the local deformation after secondary creep is non-uniform, while the deformation up to beginning of secondary creep is comparatively uniform, and the high longitudinal tensile strain and transverse compressive strain are formed at the same area. This strain distribution has a close relationship to grain boundary sliding and grain boundary properties.

Recovering of Creep Damage

For the purpose of recovering creep damage and life extension on heat resisting steels, a sintering mechanism of cavities and precipitation behaviour of stable compounds on cavity surface are studied.

The progressive sintering of the cavities due to some treatments (compressive creep, hot isostatic pressing and annealing) is monitored using highly sensitive density measurement technique. The results show that sintering rates under compressive creep are rapid and depend proportionally on compressive creep rate, whereas annealing causes only slight sintering. Therefore compressive creeps remove completely the cavities and extend the rupture life considerably.

Cavity surface by precipitation of a stable compound like BN is expected to suppress the surface diffusion and the cavity growth remarkably. The austenite stainless steel with high B, high N and low S showed the precipitation of BN at cavity surface, rare formation of cavity and high rupture ductility. It is thought that these properties are due to the precipitation of BN.

52 High Temperature Deformation and Fracture in Polycrystalline Oxide Ceramics

August 1992 to March 1995

K. Hiraga, Mechanical Properties Division

Keywords: oxide ceramics, superplasticity, cavitation

Concurrent cavitation in fine-grained superplastic ceramics is of practical importance because it degrades high temperature tensile ductility and subsequent room temperature strength. Since earlier studies based on cavitated volume fraction have failed to obtain information available for the cavitation mechanisms, we have examined cavity nucleation and growth behavior in tetragonal zirconia (3Y-TZP) by analyzing cavity size distribution in an early stage of deformation where cavity inter-linkage can be ignored.

Stereological measurements by SEM and optical microscopy have revealed that cavities nucleate continously at grain multiple junctions and grow into grain-sized polyhedra followed by further growth in micrometer-sized rounded cavities. From the analysis of cavity size distributions, the submicrometer-sized cavities were suggested to grow by a diffusional mechanism under con-

straints from adjoining grains. The cavities with radii (R) greater than 1 μm were found to obey a growth law, $dR/d\varepsilon=R$, which indicates that they grow by superplastic flow of the matrix. The damage accumulation process during superplastic deformation can be predicted by the cavity nucleation and growth behavior described above.

In the present study we have also examined the constitutive behavior of the 3Y-TZP as a function of the amount of grain boundary glassy phase and hard dispersoids such as mullite.

Related Papers

Cavity Growth in a Fine-Grained Yttria-Stabilized Tetragonal Zirconia During Superplastic Deformation, K. Hiraga and E. Takakura, Proc. ICSMA 10, Fundamental Physical Aspects of Strength of Crystalline Materials, Sendai, 1994.

Cavity Nucleation and Growth in a Fine-Grained Tetragonal Zirconia During Superplastic Deformation, K. Hiraga and K. Nakano, Proc. ICM7, Hague 1995, and will appear in Acta Metall. Mater.

[53] NRIM Fatigue Data Sheet Project–IV

April 1990 to March 1995

S. Nishijima, Failure Physics Division

Keywords: fatigue of metals, standard reference data, steels and alloys, aluminum alloys

The project aims at the establishment of standard reference data on the fundamental fatigue properties of Japanese engineering materials most commonly used for machines and structures under fatigue conditions. There are successive five-year-term programs since 1975 and the present term IV accomplishes whole of the programs. Emphasized research areas are: ambient temperature properties of high strength steels and aluminum alloys, intermediate temperature properties of steels for pressure vessels, and high-temperature time-dependent properties of heat-resistant alloys. Table 3 gives a brief summary of NRIM Fatigue Data Sheets.

Table 3 Summary of NRIM Fatigue Data Sheets (Total 83 issues)

Subtheme	Items Investigated	Issued
Machine Structural Materials	High/Low-Cycle Properties on: Carbon/Low-Alloy Steels, Stainless Steels, Carburizing Steels, Spring Steels, Tool Steels, Aluminum Alloys	38
Welded Joints of Structural Materials	High/Low-Cycle and Crack Growth Properties Looking at the Effect of: Specimen Size, Welding Procedure, Stress Ratio, Weld/HAZ Materials, for Steels and Aluminum Alloys, as well	23
Elevated Temperature Materials	Time Dependences in High/Low-Cycle Properties for: Carbon/Low Alloy Steels, Stainless Steels, and Heat Resisting Alloys	22

In parallel with the testing program, series of fundamental researches are conducted to understand materials behavior and mechanisms of degradation under fatigue environment. Some of the latest concerns are: quantitative evaluation of the effect of non-metallic inclusions in hard materials, equivalence of steels and aluminum alloys in terms of strain based fatigue strengths, cyclic softening mechanism of weld metals, elaboration of a new time-temperature parameter for predicting long-term creep-fatigue interaction effects, and development of a new test method of crack growth at intermediate temperatures with large CCT specimens, and so on.

The output data validated by the fundamental researches are published and exchanged worldwide with scientific and technical organizations. An on-line data service is also available from the Japan Information Center of Science and Technology. The NRIM Fatigue Data Sheets are contributing for long time to the safe and effective use of engineering metallic materials.

Related Papers

Fatigue Properties of Butt-Welded Joints for 5083-O Aluminum Alloy, H. Hirukawa, S. Matsuoka, E. Takeuchi, and S. Nishijima, Transactions of Japan Society for Mechanical Engineers, 58 (1992): 676–82, in Japanese.

Fatigue Strength of Non-Load Carrying Cruciform Welded Joints by a Test Maintaining Maximum Stress at Yield Strength, A. Ohta, et al., Engineering Fracture Mechanics, 49 (1994): 639–45.

Parameter Analysis for Time-Temperature Dependent Low-Cycle Fatigue Life, K. Yamaguchi, K. Kobayashi, K. Ijima, and S. Nishijima, ASME Journal of Engineering Materials and Structures, 116 (1994): 479–82.

Measurement and evaluation

(54) Observation of Fine Metallurgical Structure with a Comnputer-Image Analysis

April 1995 to March 1998

M. Fukamachi, Materials Characterization Division

Keywords: improvement of resolution with computer-image analysis, electron-probe microscopy, phase identification, distribution of chemical elements in sub-micron region

In order to reveal fine metallurgical structures, an analytical method to improve the resolution of electron-probe microscopy is going to be studied with an application of a computer-image processing. Several methods reported to be effective to improve resolution are to be examined systemati-

cally. The present study is intended to improve the resolution of image-data obtainable with the commercially-available ordinary instruments with the application of a computer-image processing.

The identification of the phases in sub-micron meter size and the observation of their distribution, and the segregation of chemical elements in sub-micron region will be studied. Thus the characterization of the metallurgical structures in sub-micron meter size will become easily attainable with the results of this study.

(55) Study on Flat and Mirror Finishing by Glow Discharge Plasma Using Rare Gas

April 1995 to March 1997

M. Saito, Materials Physics Division

Keywords: mirror finishing, direct current glow discharge, mass spectrometry, rare gas

In general, the mirror finishing for the surface of metals and semiconductors is very difficult by using the plasma-etching (dry-etching) technique. In order to overcome the difficulty of this technique, the following experiments are carried out.

1. In a plasma gas for direct current glow discharge plasma, the most suitable kinds of the mixed gas consisting of the rare gas such as Ar, Ne, Ke, Xe, He and the optimum ratios of the mixed gas are investigated.
2. In direct current glow discharge, the optimum conditions such as discharge current, voltage and vacuum in the plasma source are studied.
3. The method developed to obtain a mirror-like-metal surface is also applied to a glow discharge mass spectrometry, and the influence of the surface state of metals analyzed on the precision for the composition determination is investigated.

56 Self-organizing Information-base System Used for Creative Research and Development

April 1992 to March 1996

K. Hoshimoto, Materials Design Division

Keywords: self-organizing, information-base, materials design, dictionary, knowledge converter

In the domain of metals and alloys one can never find any two species that have precisely identical internal structure even if the chemical composition and outer shape are the same; which means that one cannot specify the object exactly in the database of material properties. Therefore the specification of materials has inevitably somewhat ambiguity. Specialists create new materials by combining basic theories, factual data and qualitative knowledge with their full skill and experiences, while the information on materials today is increasing day by day beyond the quantity which one person can deal with. The objective of the present study is to develop a self-organizing information-base system for materials design. To realize the system, the investigation on fundamental procedures has been made to select and organize various types of information automatically with the aid of computer for producing new materials. Because the knowledge on materials being fuzzy ones, the information which the system can offer contains fuzziness inevitably to some extent. For this reason, a knowledge retrieval system has been constructed in the preceding study, by which the knowledge included in relative research articles are collected and stored in the computer, and in the response to queries expressed by user in his natural language (Japanese in this case) the system retrieves and shows the related knowledge to the user. Information on the data sources and experimental procedures are also stored together with the experimental results and conclusions.

The system to be accomplished in the study will treat collectively the fundamental knowledge on materials and the actual data of materials properties along with the above mentioned information.

In the first three years of the study, two tools for gathering information into the computer has been developed; the first one searches for new words from the text fed into the computer by using OCR and put them automatically in the internal dictionary. It also assists to construct a thesaurus in consultation with the user. The other one is a knowledge converter by which a text cut out from a document is transformed to a knowledge treatable by the computer.

On the basis of collected information, a prototype conversational system has been designed and realized to retrieve the information from the knowledge base by using natural English languages.

Description of information has been done by using so called object oriented procedures. In spite of the recent advances in object-oriented database system, there are many problems in the application for scientific database because of the lack of flexibility for changing the description of object. An Object Management System (OMS) has been developed which can successfully deal with the change of modelling of information.

Related Paper

Development of a Knowledge base System for Computer-Assisted Alloy Design, K. Hoshimoto, Advanced Materials '93, III, Proceedings of the Symposium of the 3rd IUMRS Int. Conf. on Advanced Materials, Tokyo, (1993): 173–76.

57 *In situ* Measurement of Local Strain in High Temperature Range of Material and Detection of Defects by the Laser Speckle Method

April 1993 to March 1996

Y. Muramatsu, Advanced Materials Processing Division

Keywords: laser speckle method, dynamic strain, *in situ* strain measurement, high temperature, phase-transformation

We have been examining the applicability of the laser speckle strain measurement to the welding process. We already proved that it was possible to perform the *in situ* strain measurement in a high temperature range such as in welding using SUS304 thin plate by a gas tungsten arc. A problem was pointed out whether the formation of oxide films on an object surface and local expansion in the thickness direction had effects on the measuring accuracy or not.

A lot of measurements for several conditions of the sampling rate and the heat input were carried out to examine the effects of the factors mentioned above. It was clarified that the formation of oxide film has little effect on the measuring accuracy. The local expansion in the thickness direction, however, has a possibility to reduce the accuracy especially in a case that a heat source is in the vicinity of the measuring spot. Consequently, it was also clarified that the deterioration of the measuring accuracy relates closely to the refreshing of the reference frame which is used for converting the sampling data into the strains. During almost all range of heating, however, the strain behavior can be detected smoothly. Several surface conditions of the specimen were examined for accurate measurement and no relation was found out between the surface condition and the accuracy.

Moreover, we are examining a contact-free detection of the phase-transformation by a local heating using the laser speckle method. Some kinds of steels, for example 9%Ni, high tensile and mild steels, were used for the tests. The strain behavior due to phase-transformation in each steel is clearly detected for many cases of heat input. Now, we are examining the effect of microstructure on the detected expansion by the phase-transformation.

58 Correlation between Plasma Parameters and Evaporation in Free-burning Arcs

April 1993 to March 1996

K. Hiraoka, Advanced Materials Processing Division

Keywords: anode, material element, vaporization, heat input, radiation, mixed gas

In this research, firstly, the effect of an alloy element in an anode material on the anode behavior is discussed. Whether the anode area on the molten pool tends to concentrate or disperse is investigated on several materials. Some elements in the material which have higher vapor pressure have influence on the anode behavior. The anode area depends on distributions of metal vapors on the molten pool and those ionization potentials. Degree of the influence of an element can be estimated by the relative position of elements in a diagram whose X axis is the ionization potential and the Y axis is the vapor pressure. The current and vaporization distributions on the molten pool of a material can be expected from the direction between the two main alloy elements in the material on the diagram.

Secondly, the effect of the shielding gas composition on the vaporization rate of an anode materials was discussed. Anode heat input and the vaporization rate of an anode material were measured at the same time. It was found that the amount of vaporization of the anode material was slight and held constant up to He contents of 75% from pure Ar, although anode heat input steepy increased as introducing He gas into Ar arcs. The vaporization rate in the pure He gas arc was clearly increased. Moreover, it was confirmed that the thermal efficiency at the anode decreased with the remarkable vaporization of the anode material in the pure He arc. From the measurement using the radiative power meter, it is made clear that the decrease in anode heat input in He arc is mainly caused by recombination radiation and Bremsstrahlung of plasma including anode metal vapor in front of the anode.

59 Fundamental Study on Advanced Techniques of Physical Characterization of Metallic Materials and their Application

April 1994 to March 1996

R. Hasegawa, Materials Characterization Division

Keywords: EPMA, XRD, HRTEM, SEM

Advanced techniques and systems for the characterization of metallic materials by routine physical analysis are studied.

1. Electron probe microanalyzer (EPMA)
   A data treatment system with high precise and rapid acquisition is being constructed by using a workstation and local area network (LAN). Using the system, analyzed was the interface of a stainless steel and Zr metal contact; the formation of three kinds of reaction phases and the grain boundary diffusion of iron atoms have been confirmed. Furthermore, distribution of iodine dopant in a BiTe single crystal was observed.
2. X-ray diffraction (XRD)
   For the crystal structure analysis of the samples to which preliminary observation by TEM is not applicable, the method which can be conducted only by XRD is studied. Firstly, the performance of various commercial software for the x-ray structure analysis was tested. It was found that the commercial software is applicable to the determination of crystal system of single phase samples, but not necessarily to that of mixed phase samples.

3. High resolution transmission electron microscope (HRTEM)
   A digital electron microscope system which consists of a 200 kV HRTEM equipped with a lens camera, a IP camera, a SSCCD camera, a PIX system and a workstation is being built up for time-saving and accurate analysis of HRTEM images. Using a part of the system, the mechanism of the martensitic transformation of the shape-memory alloy (Fe-Mn-Si-Cr-Ni) was studied.
4. Scanning electron microscope (SEM)
   An automatic analytical system of electron channeling pattern (ECP) is being built up to determine the crystal orientation of a small crystall grain. A convenient data-treatment software which can identify cubic BCC crystals with high accuracy has been already completed. However, the software is yet unsatisfactory for the identification of cubic FCC crystals and tetragonal system.

60 Research on the Development of Chemical Analysis And Characterization Techniques for Metallic Materials

April 1994 to March 1997

R. Hasegawa, Materials Characterization Division

Keywords: GF-AAS, ICP-AES, GD-MS, gas analysis

Taking account of the recent progress of metallic materials, studies were carried out on the expansion of the kinds of the elements to which instrumental analytical methods are applicable, as well as on the improvement of the detection limits and precision.

Elemental Analysis I

1. In order to determine trace selenium in nickel-base heat-resisting alloys by graphite furnace atomic absorption method (GF-AAS), direct atomization of the sample solution prepared only by the acid decomposition was studied; a rapid determination procedure with a detection limit of 0.12 ppm was established.
2. A high-sensitivity determination procedure by fluoride separation-molybdosilicic spectrophotometry was established for sub-ppm level silicon in high-purity titanium and chromium.

Elemental Analysis II

1. A high-sensitivity simultaneous determination procedure of trace impurity elements (Ca, Cd, Co, Cu, Mg, Mn, Ni, Pb and Zn) in high purity iron was established by using inductively coupled plasma-atomic emission spectrometry (ICP-AES) and preliminary concentration by cation exchange.
2. End-on observation in ICP-AES was examined using a long torch and a significant increase in sensitivity was found for Al, Mn, Cr and Na.

Solid Analysis I

1. In order to apply glow discharge mass-spectrometry (GD-MS) to the analyses of nickel-base heat-resisting alloys, reliable relative sensitivity factors (RSFs) of the analytes were estimated by analyzing fifteen standard samples.
2. In order to utilize the high sensitivity and the rapidity of total reflection x-ray spectrophotometry (TR-XRF) in the analyses of the solution samples, mounting of the solution on a silicon wafer was studied.

Solid Analysis II

Determination of oxygen in pure lead and solder alloy is being studied. First, extraction of oxygen from molten baths with various chemical compositions was examined; it was found that high recovery is obtained when a mixture of Ni, Sn and graphite powder is used.

61 Fundamental Study for Electromagnetic Evaluation of Materials

April 1994 to March 1997

I. Uetake, Failure Physics Division

Keywords: non-destructive evaluation, materials evaluation, electromagnetic method, magnetic flux, leakage testing, surface flaw

Flaws in structural materials decrease remarkably the materials strength. The detection of eventual flaws and material degradation is especially important for the security of important structures such as reactor pressure vessels and/or large consructions. In this study the basic phenomena of electromagnetic evaluation method is investigated.

The target of detection is surface flaws. Test material used is a low alloy steel SM50A (220L × 50W × 10H mm) for structural use. Applied magnetization frequency is selected in the range between 0.05 to 10 kHz. Magnetic flux leakage caused by the surface flaw is detected with a flux meter using a sensor with Hall element. Normal component of leakage flux signal is detected as the amplitude and phase values using a lock-in amplifier.

The magnetization state of material is variable according to the magnetization current and frequency. The measurement is therefore carried out after having controlled the surface magnetic field and flux density. The change in flaw signal determined on the voltage vector plane displays similar trends that have two peak points as generally observed for the time domain waveform. The magnitude of this peak-to-peak change and the phase varies according to the magnetization frequency. The dependence of these signals on the flaw size is

under examination and will give interesting results.

62 Research on Quantitative and Intelligent Nondestructive Evaluation Techniques for Materials and Structures of High Reliability, Stage II

April 1994 to March 1996

C. Masuda, Failure Physics Division

Keywords: nondestructive evaluation, frequency response, laser-ultrasonic, composite materials, computer simulation, anisotropic microstructure

In this research, it is planned to develop nondestructive measurement technique and systems based on ultrasonic techniques to evaluate the properties of metal matrix composite. This research is sponsored by STA and supported by members of various institutions, universities and companies. The previous stage (stage I) of this project was the development of an advanced ultrasonic measurement technique and supporting procedures, using ultrasonic spectrum analysis, velocity measurement with a scanning ultrasonic microscope, the laser-ultrasonic technique and computer simulation for ultrasonic wave propagation. In the stage II, the ultrasonic techniques will be applied to evaluate the microstructure, damage and defects in metal matrix composites. The first year of stage II produced two major results, as follows.

1. Development of ultrasonic wave measurement techniques

   The ultrasonic frequency response technique has been widely approved in the quantitative measurement of microstructural parameters such as grain size and inclusion contents. An improvement of the accuracy of this technique has been achieved in this work. Theoretical analysis indicated the influence upon frequency spectrum of different factors, such as specimen surface roughness, thickness of ultrasonic couplant, ultrasonic wave form and sound fields. This analysis enables precise identification of the change of microstructural properties through variations of the frequency response of materials. The analysis also clarified mechanisms of the wave form inversion of the tip echo and the peak frequency shift of ultrasonic spectrum.

   During the stage II, application of the laser-ultrasonic technique is attempted. An ultrasonic imaging system is developed in order to detect small subsurface defects by noncontract ultrasonic imaging technique. Detection principle relies on the optical heterodyne interferometry, that brings in a new development for conventional measurement of ultrasonic waves. The transmission is assured by a pulsed laser light, guided by optical fiber with a large core. Ultrasonic generation and detection are performed at two points 1 mm apart each other on the specimen surface. The model specimens used are bonded metal plates with hallmarks of 1.5 mm wide 0.2 mm depth between layers simulating sub-surface defects. Despite the 1 mm distance between the transmission and detection points, it is possible to distinguish shapes of hallmarks. Resolution is about 0.2 mm. The results show the applicability of this imaging technique for the evaluation of layered materials.

2. Effect of anisotropic structure on ultrasonic wave propagation in composite materials.

   Macroscopic elastic properties of long SiC fiber reinforced titanium alloy matrix composites were obtained using ultrasonic velocity measurement. The density of the composite was 4092 kg/m^3. The volume fraction of SiC fiber was estimated to be 39%, that was in agreement with metallurgical measurement of 38.8 ± 2%. The macroscopic elastic properties of the composite could be modeled by a hexagonal crystal, when the directional distribution was examined for shear and longitudinal ultrasound velocity. The elastic properties of composite were analyzed by this modeling, and found to be a good agreement with experimental result.

   Using the stiffness matrix obtained from the velocity measurement, mechanical properties such as Young's modulus and Poisson's ratio were calculated. They were also in good agreement with those obtained by mechanical testing, for the orientation parallel to the fibers. For the orientation normal to the fibers, Young's moduli was greater than that obtained by mechanical testing. On the other hand, Poisson's ratio parallel to the fibers was twice the value perpendicular to the fiber. Moreover, the same results were also obtained for SiC reinforced aluminum alloy matrix composite.

   Anisotropy of microstructures in composites can be evaluated by measuring the transmitted ultrasonic intensities in C scan mode. The frequency response analysis technique described above can be applied also to quantitative microstructural anisotropy in composites.

   A 3-dimensional simulation technique has been developed to visualize the complicated ultrasonic wave propagation in composites. It allows to analyze damages such as interfacial debonding and cracks in strengthening elements and/or matrix. The method requires to established stiffness matrix data for matrix alloy as well as for reinforcements. Tentative results for steels including voids at different volume fractions revealed strong effect of voids to the shear wave propagation. This suggests one of the possible ways to evaluate damages

in composites by means of ultrasonic measurement.

63 Modeling and Evaluation of Advanced Materials—A Coordinated Interlaboratory Research

April 1992 to March 1996

S. Nishijima, Failure Physics Division

Keywords: advanced materials, property evaluation, modeling, VAMAS project, interlaboratory testing

One of the targets of this work is to study models describing the behavior and properties peculiar to selected advanced materials such as composites of high performance. It covers the establishment of rationalized test methods for evaluating the performance of advanced materials, as a part of the international research cooperation: Versailles Project on Advanced Materials and Standards (VAMAS).

NRIM takes initiative with its 35 research staffs to harmonize the efforts of more than 50 other groups from industrial, university and national laboratories. Whole the work is organized as a coordinated research project of the Science and Technology Agency (STA). Following is some topics illustrating the NRIM contributions.

Intermetallic Compounds

Titanium aluminides are light-weight and heat-resisting material expected for high temperature applications. Two of NRIM laboratories are collaborating with Daido Steel Co., Ltd., to develop models explaining respectively the monotonic strength, fatigue strength and fracture toughness properties of TiAl.

Figure shows the fatigue strength variation according to the volume fraction of γ phase in α_2 grains. Fatigue crack initiates inside of isolated γ grains for lower volume fractions and a rule of mixture holds in the region 1 in the figure. It initiates at γ grain boundaries when the volume fraction is higher and the strength becomes constant in the region 2.

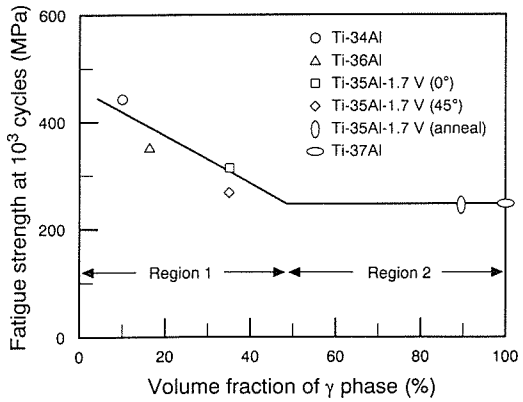

Fig. 3 Variation of fatigue strength with microstructure in Ti-Al.

Similar researches are in progress on *Metal Matrix Composites* (MMC) in collaboration with Mitsubishi Heavy Industries and Tokyo University, in one hand, and on *Ceramic Matrix Composites* with Toshiba Corporation and Tokyo Institute of Technology, on the other.

International Project VAMAS

There are 16 Task Working Areas (TWA), spreading from metals, polymers and ceramics, and their composites, as well, to test methods and problems related to materials classification and data. NRIM offers international chairpersons for 3 TWAs respectively on: superconducting materials, cryogenic structural materials and materials property databases. Leading members are also from NRIM for other 4 TWAs: method of evaluating MMC, method of creep crack growth test, method of low cycle fatigue test, and method of surface chemical analysis.

Related Papers

Low-Cycle Fatigue Properties of Ti-Al Intermetallic Compounds, K. Yamaguchi, M. Shimodaira, and S. Nishijima, Tetsu-to-Hagane, 78 (1992): 134–40.

Effect of Temperature on Tensile Properties of TiAl Base Alloys, K. Hashimoto, S. Kajiwara, T. Kikuchi, and M. Nakamura, Scripta Metall. Mater., 32 (1995): 417–22.

Microtomography Using Conventional X-ray Sources, Y. Yamauchi, N. Kishimoto, and T. Ikuta, *Non-destructive Characterization of Materials VI*, ed. R.E. Green Jr. et al., Plenum Press (1994): 129.

64 Nanoscopic Materials Damage Evaluation

April 1994 to March 1996

S. Matsuoka, Environmental Performance Division

Keywords: materials damage, STM, AFM, molecular dynamics

It is important to examine the materials damage in the vicinity of crack tip or grain boundary to improve the reliability of structural materials. Recently, the damage in small-size structural components has also become a subject of much concern, as seen from an example of the stress or electromigration for aluminum thin-film conductors in the technology of integrated circuits.

This research has been conducted to develop the materials damage evaluation technique in the nanoscopic region. At first, the damage of metallic materials such as fatigue and creep, including the stress- and electro-migration for aluminum thin-film conductors, is investigated by a scanning tunneling microscope (STM) and atomic force microscope (AFM) which has two excellent abilities of atomic-scale imaging and nano-fabricating. On the basis of AFM, in particular, a nano-indentation method is developed to measure the hardness

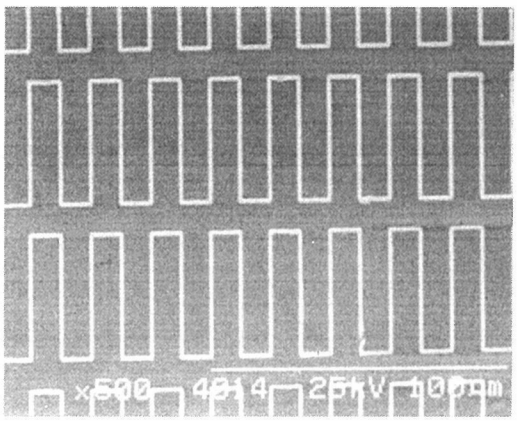

(a) SEM image

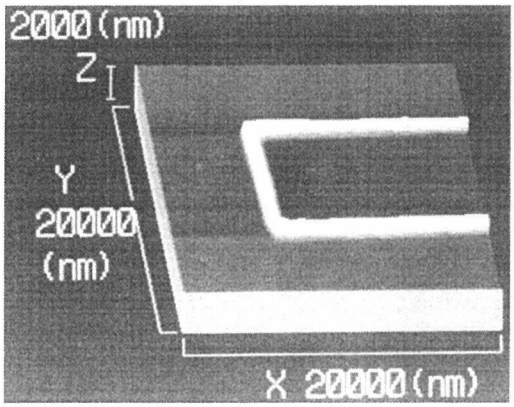

(b) AFM 3D image

Fig. 4 Fig. 1 SEM and AFM images of aluminum thin-film conductors.

ahead of the crack tip or on the surface of thin films. Secondary, the process of damage or indentation is simulated, using a molecular dynamics. Finally, the nanoscopic materials damage evaluation is established by comparing the experiment and simulation.

In the current year, nano-indentation hardness tests were started for aluminum thin-film conductors of integrated circuits. Figure 4 shows SEM and AFM images of aluminum thin-film conductors. Indentation force versus penetration depth curves were obtained at the minimum force and depth levels of 500 μN and 25 nm, respectively, by a nano-indentation hardness apparatus which was developed on the basis of AFM. The apparatus is being improved so that the minimum force level is smaller by two figures.

65 Chemical Analysis of Organotin in Marine Environmental Samples

April 1991 to March 1996

H. Okochi, Team of Director of Special Research

Keywords: organotin, solid phase extraction, sea water, deep sea sediments, MLC/ICP-MS, GF-AAS

Speciation of Organotin

For the speciation of ultra trace organotin compounds, batch technique for solid phase extraction (SPE) has been developed using Excelpack SPE-GLF as a solid phase sorbent. The recovery of organotin compounds was measured by MLC/ICP-MS. The SPE sorbent in 10 ml methanol was added into a seawater (0–3L). After shaking, the solution with sorbent was pored into an 8 ml reservoir. The effluent was evaporated to 0.25 ml at ca.35 °C under Ar flow. After 0.25 ml of ultra pure water was added, 100 μl of the solution was injected to MLC/ICP-MS. The limit of detection (LOD, 3 σ) was 3ng l^{-1} for TBT and 4ng l^{-1} for TPT, respectively. The SPE of organotin in shell samples was also investigated using the same SPE sorbent. The optimum conditions has been investigated.

The determination of total tin in shell samples by GF-AAS has been established. Samples were decomposed with nitric acid. The stabilized temperature platform furnace technique was applied. Nickel was used as a matrix modifier.

Deep Sea Environmental Analysis

The deep sea sediments of box cores of ca.30 cm length were collected at the Iheya Ridge and the Izena Hole in Okinawa Trough by the submersible "SHINKAI 2000" of the Japan Marine Science and Technology Center. The depth analysis of them was performed by x-ray fluorescence spectrometry using bead samples of low dilution fusion. The correction of matrix effect was by the fundamental parameter method. The analytes under investigation were main components (Si, Ti, Al, Fe, Mn, Mg, Ca, K and P) and trace elements (V, Rb, Cl, Ba, Zr, Br, Cr, Sr, Pb, Zn, Cu, Y, and Nb).

Related Papers

Solid Phase extraction of Organotin Compounds in Seawater, M. Kohri, Y. Inoue, K. Ide, K. Sato, and H. Okochi, BUNSEKI KAGAKU, 43 (1994): 933–38.

X-ray Fluorescence Analysis of Submarine Sediments by Low Dilution Fusions and Matrix Correction using theoretical alpha Coefficients, K. Sato, M. Kohri, K. Ide, H. Hotta, and H. Okochi, BUNSEKI KAGAKU, 44 (1995): 143–50.

66 Determination of Order Parameters in Alloys from Electron Diffraction Intensities using CCD Camera System and Its Application to Examination of Ordering Process

April 1993 to March 1996

T. Kimoto, 1st Research Group

Keywords: order parameter, multi-slice method, cooled CCD camera, fluctuation of order parameter, grain boundary

The objectives of our research is to develop the system for determination of a long-range or-

der parameter in an alloy from the ratio of superlattice reflection and fundamental reflection intensities in electron diffraction pattern, which are detected by cooled CCD camera of highest dynamic range of 64,000, and its application to the examination of ordering process.

In 1994, we successfully developed the ordering determination system for the first time in the world. The computer program for the system was developed with C compiler (Think C) by applying successive approximation to multi-slice (Cowley-Moodie) method, which is based on dynamical theory of electron diffraction. Thickness of diffracted area, which is necessary for the calculation of electron diffraction intensities, was performed by using convergent beam electron diffraction (CBED) method and transmitted electron beam current method. The long-range order parameter S of Cu_3Au aged at 250 °C for 1369 hours was determined by the developed system to be S = 0.957, which is approximately in good accord with the value S = 0.972 determined by x-ray diffraction.

The developed system for order parameter determination from electron diffraction is the only method to determine an order parameter in a microscope area because x-ray and neutron diffraction can not provide microscopic information. It was found in 1994 by using the developed system that order parameter near grain boundary is much lower than that in matrix in Cu_3Au which was aged at 250 °C for 3 hours after rapid quenching from 850 °C or 930 °C. The reduction of order parameter near grain boundary is thought to be caused by the decrease of concentration of vacancies which promote ordering. It was also found that fluctuation of order parameter is significantly large at the early stage of ordering in Cu_3Au which was aged for ordering after rapid quenching from 850 °C or 930 °C.

Related Papers

Quantitative Examination of Radiation-induced Disordering in Precipitates with a Cooled CCD Camera Attached to a TEM, T. Kimoto and T. Saito, J. Nucl. Mater., 212–215 (1994): 275.

Development of CCD Camera System for On-line and Precise Measurement of Electron Diffraction Intensities and its Application to the Investigation of Ordering in Cu_3Au Alloy, T. Kimoto and T. Saito, Proceedings of 13th International Congress on Electron Microscopy (1994): 981.

67 A Database for Surface Chemical Analysis

April 1994 to March 1997

K. Yoshihara, Surface and Interface Division

Keywords: database, AES, XPS, spectrum, data transfer

Since 1994, Science and Technology Agency (STA) has started to construct Inter Ministry Computer Network System (IMNet) which connects Tsukuba-Tokyo-Osaka by 6 MB digital cables. On this network system, STA intends to incorporate database, one of which is Surface Analysis Database. When we construct a spectral database by collecting spectral data from different machines, the spectral data format of the data capture computer must be translated to a common format (VAMAS-SCA Standard Data Transfer Format), and intensity and energy scales must be converted to standard scales. We started to program software in Visual Basic for the IBM-PC or NEC-PC with Windows to translate spectral data acquired on different machines to VAMAS Format and to process AES and XPS spectra in a standard manner. This software has been named the Common Data Processing System.

Surface Analysis Society of Japan (SASJ) kindly offers the cooperation with NRIM, and is now taking spectra for the database. The quality of spectra is controlled by SASJ. The spectral and physical property data retrieved from the database will be displayed on Common Data Processing System. A workstation for the database will be connected to computers by network systems. The spectral data taken on different machines will be sent to this workstation by computer network or modem line, and stored in the spectral database. We hope all computers of surface analysis machines will be connected by computer network, and every surface analyst can use the surface analysis database and common data processing software to identify the surface properties.

68 Development of Analytical Techniques for Characterization of Nuclear Materials using New Generation Synchroton X-rays

April 1993 to March 1997

K. Sakurai, 1st Research Team

Keywords: synchroton radiation, surface and interface analysis, x-ray fluorescence, materials characterization

The 3rd generation storage ring, SPring-8 is now under construction at Harima science park city. It provides extremely highly collimated strong photon flux in x-ray region. Basic and applied x-ray sciences are stimulated again and significant progress in new experimental trends is expected. Another advantage of SPring-8 is the use of high energy x-rays, typically, 40–100 keV, where any other appropriate x-ray source has not been developed so far. In the present program, we study both features of new synchroton radiation from a point of analytical use for materials characterization.

1. Surface and interface study using interference effect in grazing incidence x-ray experiments (Use of collimated strong x-rays)

Grazing incidence synchroton x-ray techniques are powerful tools for the surface study of materials. As is often the case in multilayers, specular reflectivity, fluorescent x-rays and other signals from thin films sometimes show the complicated angular dependence because of interference. In the present program, we have studied the analytical use of this interference effect, i.e., the strong modulation of the x-ray electric field in a film caused by multiple reflection at each interface. It has been found that the fluorescent x-rays can be used to determine the depth position of trace impurities in the specific layer, even when the thin film has not periodicity and regular standing wave is not generated. Enhancement of the specific interface is expected to facilitate to analyze a role of the trace element in the property of thin films.

2. High energy x-ray fluorescence analysis (Use of high energy x-rays)
   We have developed a prototype x-ray fluorescene equipment with high energy x-ray tube (160 kV, 10 mA). It has been found that x-ray fluorescence spectroscopic analysis of heavy elements using high energy K lines is promising from a point of high sensitivity especially for bulk analysis.

Related Paper

M. Wormington, K. Sakurai, D.K. Bowen and B.K. Tanner, Mat. Res. Soc. Symp. Proc., 332 (1994): 525.

[69] Study on the Trend of Application of New Super Conductors

April 1988 to March 1995

K. Hoshimoto, Materials Design Division

Keywords: High T_c superconductors

The development of High T_c Superconductors will give revolutional influences not only to the field of science but to the economy or social affairs. The investigators of the new superconductors should recognize this fact. From this point of view, studies have been started on the trend of application of new super conductors, which include the investigation of the possibilities of application of new superconductors to the industries of energy and also to the future technology.

[70] Development of Advanced Technologies for X-ray Microtomography

April 1992 to March 1995

Y. Yamauchi, Materials Characterization Division

Keywords: CT, tomography, microtomography, x-ray, three-dimension

X-ray computerized tomography has been widely utilized in the applications for relatively large objects, such as in medical diagnostics of human bodies or in industrial inspection of manufactured components. In those applications, the required spatial resolution is usually in the order of 1 or 0.1 mm at most and is limited by the number of pixels on the image. The effective number of pixels is circumscribed by the dynamic range of detected x-ray signal or the steepness of x-ray absorption. Further a mass of data storage and computational power have to be considered. However, if it is allowed to restrict the size of objects fairly small, the constraints would be alleviated. The limited number of pixels may not affect the pixel size nor the resolution of image. Based on this idea, we are developing the x-ray microtomography device. In the previous project, high resolution tomographies of a small object were accomplished with the parallel beam projection using a conventional point x-ray source. Then we extended the function of the device to three-dimensional. In this project we have been studying advanced technologies which improve the spacial resolution of tomographs and which provide another function to analyze chemical composition.

Asymmetric reflection seems to be a promising technique to magnify x-ray images. We obtained magnified image of factor 10 by Si(511) reflection with a normal focus Cu tube source. A lead glass capillary plate which consists of channels of 2 μm in diameter and 2 mm in length was used to reduce the diverging angle of primary beam.

Also, we had tried to introduce filtering technique into x-ray microtomography using conventional poly-chromatic sources for elemental evaluation of objects. It was found that the filter modulation of incident beam yields slight modification of contrast in tomographs and that the post-reconstruction subtraction between those tomographs extracts elemental information qualitatively.

[71] Evaluation of Metallurgical Structure with a Fuzzy Logic

April 1992 to March 1995

M. Fukamachi, Materials Characterization Division

Keywords: computer-image analysis, fuzzy logic, electron microscopy, distribution of chemical elements on metallurgical structures

In order to carry out an accurate and rapid computer-image analysis of metallurgical structures, the feasibility of an application of a fuzzy logic to a computer-image simulation has been studied. Fine metallurgical structures can be revealed with the electron microscopy. Usually, the numerical computer-image simulation is necessary to analyse and to evaluate the fine metallurgical structures. It is difficult to give accurate numerical values to many parameters which characterize the geometry of parts of electron microscopes and the operating conditions to obtain a satisfactory image simulation.

The method to simulate microscope images of the secondary and the reflected electrons has been studied with an application of the fuzzy logic. Only two parameters are used in the image simulation. These are the parameters to represent the amount of generation of signal electrons and the efficiency of detector to collect these signal electrons. With this method, the distribution of chemical elements on metallurgical structures can be obtained rapidly by separating the image contrast caused by the local distribution of chemical elements from that of the geometry of a specimen surface.

[72] Study on Mechanism of Ion Production in Low Temperature Plasma

April 1991 to March 1995
M. Saito, Materials Characterization Division
Keywords: laser, rf glow discharge, mass spectrometry, ion intensity

The interaction between the laser beam and the rf glow discharge plasma was examined using the double focus mass spectrograph with an Ilford Q_2 photoplate ion detector. The laser used was a ruby laser (power: 80–90 MW/cm^2) and the rf glow discharge (frequency: 3000 Hz) was operated in the presence of Ar buffer gas. The ion intensity of elements in copper standard and low alloy steel standard samples obtained by the combination of the two sources showed the maximum value under the condition of the vacuum of about 1.0 Pa, and this value was higher than that obtained by the laser alone. However, the repeatability of the measurement for this method was above 100% with the relative standard deviation because of the instability of the laser used in this study. Further study will be necessary.

[73] Control of Surface Atomic Layer and Technological Development of Surface Electron Spectroscopic Tomography

April 1992 to March 1995
K. Yoshihara, Surface and Interface Division
Keywords: surface, electron spectroscopy, tomography

The control of the surface atomic structure will be the key technology to develop modern new materials. Therefore, it is very important to develop the technology on creating very thin films and analyze the layered structure of the very thin film with atomic scale. Especially, the analytical technique must be a non-destructive one, because the properties of very thin films will be strongly affected by the interface structure between thin films and substrates.

The main objectives of the project is to develop the new technique called "Surface Electron Spectroscopic Tomography: (SET)." SET is the technique to make the surface atomic structure visible by analyzing the whole angle of energy spectrum of the elctrons exited in the films. The display-type spherical mirror analyzer has been developed and characterized in regard to the performance of the analyzer and the spectra taken by this analyzer. The analyzer was originally designed by H. Daimon. The main feature of this analyzer is to display the 2-dimensional electronic structure directly onto the screen. We used the micro-electron beam which was located outside the analyzer to excite the Auger electron. To use the electron beam, however, has some problems because there exists interface between the electron beam and the analyzer. We solved this problem by varying the various analyzer conditions and could present the results of the analyzer characteristics together with AES spectra.

To analyze the displayed spectra, it is necessary to use the energy loss functions of electrons in various materials. Therefore, we developed an angle resolved x-ray photoelectron spectrometer which was operated in extreme high vacuum. By this spectrometer, we are now collecting energy loss spectra of electrons emitted from thin films.

Simulation and theory

(74) Development of Knowledge Databases for High-T_c Superconducting Materials

April 1995 to March 2000
Y. Asada, Material Design Division
Keywords: oxide superconductors, database, knowledgebase, network

We have already developed numerical database for high-T_c oxide superconductors. It will be opened publicly via network. All the data in it are extracted from the papers reported in journals. The papers contain much useful informations as well as numerical date. These informations are written in text style in abstract, summary or conclusion. It is desirable that researchers employed in designing new products and searching new materials retrieve these informations from database and apply them to their purposes.

In this project, we study how to store the informations and how to construct knowledgebase for high-T_c superconductors. The knowledge base contains the information induced by processing the data from numerical database: empirical relations between physical properties. Conclusions and informations obtained in studies of multi-core project are also included in the knowledgebase. We have a plan to introduce NEURALNET as a tool to process numerical data statistically and EXPERT SYSTEM as a tool to store and process the informations.

(75) Understanding of the Superconducting Mechanism of High Temperature Superconductivity

April 1995 to March 2000

K. Kadowaki, 1st Research Group

Keywords: mechanism of superconductivity, electronic structure

Immediately after the discovery of high temperature superconductors, a number of the exotic mechanisms for the superconductivity has been proposed, which essentially do not rely on the electron-phonon interaction as a superconducting pair formation, and, most of which are outside the scope of the BCS theory for the traditional superconductivity established in 1957. Although these theories are very attractive as new concepts of superconductivity, it is too premature to be established. In order to understand the real physics in these materials, it may be useful to classify the available theories into several categories: theories which are purely based on magnetic interactions such as RVB (Resonating Valence Bonds) theory, antiferromagnetic spin fluctuation theory, etc., and on non-magnetic interactions such as bi-polaron theory, strong charge fluctuation theory, etc. In any cases, it is rather common agreement by now that the successful theory needs new concepts, which may be additional to or may be even beyond the BCS theory.

On the other hand, it seems that from accumulating experimental facts the normal state of high temperature superconductors is highly anomalous in the sense that they do not possess the characteristics features associated with the conventional metals, and they strongly violate the basic concept underlaying in the BCS theory. The proper understanding of the electronic state of these materials even now is poor, when the doping is progressed from antiferromagnetic insulator to doped metals.

In this five year project, it is planned to study, firstly, the electronic structure of these superconductors and much effort will be focussed on to understand properly the electronic structure. In order to do so, the difference in the electronic structure between superconducting and non-superconducting compound will be studied by various experimental techniques in collaboration with other laboratories. Secondly, by establishing the physical picture in the normal state, the currently available theories classified above will be re-examined critically and they will be re-considered based on the various experimental results. By repeating these processes of consideration it is finally aimed to meet or, at least, to predict the essentials necessary for the occurence of high temperature superconductivity.

76 Establishment of Multidimensional Evaluation of Human Senses for Materials Design

April 1994 to March 1997

Y. Kurihara, Materials Design Division

Keywords: human senses, materials properties, relation matrix, multivariate statistical analysis, function of human beings

Recently, there are increasing demands for materials developments from new aspects such as environment consciousness, amenity, and so on. When we investigate such new needs, most of information are provided mainly by language and human senses. Thus, the target of this study is to construct a quantitative evaluation method which can incorporate sensory information into materials design.

For this purpose, we inquired 81 persons from 20 to 50 years old about the relationship between human sense and technical terms for materials properties such as mechanical, chemical and physical ones using a relationship matrix. Three characteristics vectors representing "warmth," "cleanliness" and "splendidness" were extracted from multivariate statistical analysis on collected sensory data. From the present analysis, it is concluded that we understand and express materials properties in comparison with functions and properties of human beings. Thus, at the next stage in this study, we will list up all functions and properties of human beings, and make a relationship matrix of these functions and materials properties. Such a relationship matrix can be used as an effective tool to find new needs for materials. If there would be no materials which could be correlated with a given function of human beings, there should be a possibility to develop new materials.

77 Thermodynamic Analysis of Transition Process from Metastable to Stable Phases

April 1994 to March 1997

H. Onodera, Materials Design Division

Keywords: $Ti_{48}Al_{52}$ amorphous alloy, metastable phase, CVD, fluidized bed

Rapid solidification, mechanical alloying, and other non-equilibrium processing techniques have been employed to improve mechanical properties of various materials by refining the microstructure. These techniques produce metastable phases such as supersaturated solid solutions and amorphous phase. For the effective utilization of these metastable phases to improve mechanical properties of materials, it is necessary to reveal the transition process from metastable to stable phases on the heat treatment. The target of this study is to construct a kinetic model which can describe the transition processes quantitatively.

The crystallization process of sputter deposited $Ti_{48}Al_{52}$ amorphous alloy was studied by high resolution transmission electron microscopy (HRTEM) and X-ray diffraction. An unknown phase having spherical morphology precipitates in amorphous matrix in the early stage of crystallization. Electron diffraction patterns from this phase can be identified by supposing that the phase has primitive cubic or tetragonal symmetry and the lattice parameter of a (=c) = 0.69 nm. The analysis on prototype structure and/or atom positions is in progress. In the final stage of the crystallization, the appearance of stable γ-TiAl and α-Ti(Al) are confirmed by X-ray diffraction.

Coating of HfC on W powder was tried by a fluidized bed CVD as a new process to manufacture sintered W-Hf-C alloys. A HfC coated layer of 8 nm thickness is obtained by a fluidized bed CVD at 1553 K for 900 s, which corresponds to 0.4 mol% of HfC in bulk. The sintered material shows a large scattering of hardness from 500 to 1700 VHN. A microstructural evolution in sintering HfC coated tungsten powders will be analyzed in terms of process conditions such as time, temperature and partial pressure of oxygen.

Related Paper

Crystallization of Sputter Deposited Amorphous Ti-52at%Al, T. Abe, S. Akiyama, and H. Onodera, ISIJ Int., 34 (1994): 429.

78 Assessment of Strength and Structural Materials Database for Weldment in FBR (Fast Breeder Reactor) Components

April 1991 to March 1996

Y. Monma, Failure Physics Division

Keywords: creep, database, FEM, stainless steel, welded joint

This study deals with creep-rupture and stain-time behavior of welded joint for FBR reactor vessel. So far we have generated creep strain-time data with accumulated times of about 230,000 h for the base metal of 316FR (0.01C-0.07N-18Cr-11Ni-2Mo) stainless steel and its narrow-gap GTAW (gas tungsten arc welding) joints. On the basis of the creep data obtained with small specimens cut from a welded joint plate of 50 mm thick, the creep behavior of full-thickness specimens has been estimated by use of the FEM (finite element method) calculation. A moir interferometry using a CCD camera was applied to map the strain distribution of the welded joint subjected creep loading at 550 °C for a certain period. The key issue we are trying to clarify is the performance of creep strength in undermatching and overmatching joints. Surely the relative strength of weld metal to the parent metal plays important role in the joint. We want to identify the location of crack initiation and propagation by creep exposure in a large welded joint.

We are also interested in the creep behavior of modified 9Cr-1Mo steel weldment. Prior to the testing program of high-Cr steel, we examined the creep-rupture behavior of 2.25Cr-1Mo steel plate. Usually the HAZ (heat affected zone) of welded joint of 2.25Cr-1Mo steel contains duplex structure coarse and fine grain regions. The location of the creep crack initiation for 2.25Cr-1Mo steel joint was in the fine grained region of HAZ where the surface and the back beads meet unlike traditionally believed coarse grain region.

With regards to the prediction of creep behavior of large welded joint, the accuracy of creep strain-time curve we achieved so far by the FEM is the factor of two. We think it is needed to extend the current two-dimensional model to more rigorous three-dimensional one and more detailed behavior of the local variability of creep properties in the weld metal. We are testing sub-sized specimens of the weld metal in order to obtain the dependency of the anisotropy in weld metal.

Related Paper

Prediction of Creep Lifetime for Butt-Welded Joint of Type 304 Stainless Steel by Finite Element Method Incorpolating Damage Variable, J. Kinugawa, M. Yamazaki, H. Hongo, T. Watanabe, and Y. Monma, Q. # J. of Japan Welding Soc., 13 (1995): 19–27.

79 Modelling and Simulation for Material Strengths Properties

April 1994 to March 1999

M. Nihei, 4th Research Team

Keywords: computer simulation, modelling, material strength

Researches with a view of developing new evaluation technologies of materials through the utilization of high performance computer and database are being conducted in two approaches. The one is the computer simulations and aims to develop the modelling algorithm where the influence of crystallographical factors, such as anisotropy of crystals and the grain boundary et al., on the materials strength is evaluated by means of computational scientific approach, assuming materials as aggregates of crystals. As a first stage of this research program, the relationship between the grain size and the materials strength such as hardness and tensile properties was investigated by a mechanical testing using steels with an appropriate heat treatment. A good correlation between the grain size and the tensile properties was obtained. From this result, the development of the prototype modelling schemes for the materials strength is being attempted. The other is the empirical systematization approach based on the combining the

scientific and empirical understanding for materials strengths. For the purpose of this systematization, the computerized expert system for the researcher assist, DIMS (Dialogical Integrated system for Materials Strength database) was developed in the previous study. This system can analyze the desired data set extracted from the factual database of materials strengths and can make the new combinations among characterized items of materials on that strength property. It was already found that a good result for the fatigue life prediction was obtained by using this approach for many heat treated structural steels. The same approach by this systematization procedure is being conducted for the creep rupture properties for heat resisted steels.

Materials

Non-ferrous materials

80 Relationships between Fatigue Softening/ Hardening Behavior and TEM Structure of Titanium Alloys

April 1994 to March 1997

T. Kainuma, Mechanical Properties Division

Keywords: Ti-3-8-6-4-4, pure titanium, Ti-6Al-4V, TEM structure, fatigue softening, fatigue hardening

The change of the width or area of the hysteresis loop during the fatigue testing of materials at constant stress amplitude is taken usually as a measure of dynamical changes in mechanical properties. By testing at stress amplitudes higher than yield stress, fatigue hardening only takes place in alloys as well as pure metals (decrease in the width of hysteresis loop). While at stress amplitudes lower than the yield stress, fatigue softening occurs. Details of fatigue softening behavior have been reported for the materials such as aluminum(1), copper(2), silver and iron(3). The aim of this work is to reveal the mechanisms of fatigue softening and hardening behavior of titanium alloys in connection with the characteristics of crystal structures, using transmission electron microscope (TEM).

Fatigue Softening and Hardening Behavior

We determined at first the specimen shape most suitable for tension-compression fatigue testing, then examined the crystal structure dependence of fatigue softening and hardening behavior using Ti-3Al-8V-6Cr-4Mo-4Zr alloy (β-type titanium alloy, Ti-3-8-6-4-4), pure titanium (α-type) and Ti-6Al-4V alloy ($\alpha + \beta$ type). The experiments for the fatigue softening and hardening phenomena were carried out on work-hardened and annealed materials, respectively.

Relation between Fatigue Behavior and Electron Microscopic Structure

We have shown previously that hydrogen absorption and subsequent formation of dislocation structures (ghost structure) occur in the beta-type titanium alloy during the specimen preparations, such as cold rolling, emery paper polishing, diamond blade cutting snd water quenching.

In this work, we have established the preparation method for thin foils which are without ghost structures by the TEM observation; for example, the specimen cutting and mechanical polishing were performed either in argon gas atmosphere or in vacuum. The thin foils were prepared from the fatigue-tested bulk specimens by cutting, mechanical polishing and jet-electropolishing. The TEM observation has been aimed to reveal the mechanisms of fatigue softening and hardening in the three type titanium alloys.

Related Papers

Substrate and Fatigue Fracture in Aluminum, J.C. Grosskreutz and P. Waldow, Acta Metallurgica, 11 (1963): 717–24.

Fatigue of Copper Polycrystals at Low Plastic Strain Amplitudes, K.V. Rasmussen and O.B. Pedersen, Acta Metallurgica, 28 (1980): 1467–78.

Cyclic Deformation of Ferritic Steel-I. Stress-Strain Response and Structure Evolution, H.J. Roven and E. Nes, Acta Metall. Mater., 39 (1991): 1719–33.

Intermetallic compounds

(81) Diffusion in Ordered Alloys and Preparation of Composition Gradiented Materials

April 1995 to March 1998

H. Sasano, Physical Properties Division

Keywords: ordered alloy, diffusion, chemical transportation, shape memory alloy

Diffusion in ordered alloy is strongly affected by their composition. One of purposes of this research program is to clarify the composition dependency of diffusivity in ordered alloys such as NiAl, TiAl and Ti_3Al. Based on the results, particular attention will be paid on diffusion mechanism and phase stability in the alloys. A chemical transportation technique developed by us will be applied to the measurement of diffusion coefficient.

Another purpose of the program is to develop the preparation method of composition gradiented materials. The properties of ordered alloys are very

sensitive to the composition. If the composition is delicately changed along the longitudinal direction of the materials of the ordered alloys, we can obtain the materials possessing unique properties. We try to prepare the composition gradiented Cu-Al-Zn and NiTi shape memory alloys by the chemical transportation technique.

(82) Characterization of Creep-Damaged Microstructure of Stainless Steels by Computer Aided Quantitative Metallography

April 1995 to March 1998

F. Abe, Environmental Performance Division

Keywords: creep-damaged microstructure, computer aided metallography, stainless steels

In the NRIM Creep Sheet Project, we have published the long-term creep and rupture data containing 10^5 h data for heat-resisting steels and alloys as a series of NRIM Creep Data Sheets. We are now making a plan publishing the data on microstructural evolution during creep of the heat-resisting steels and alloys as another series of NRIM Creep Data Sheets. The microstructural data sheets will include not only microstructure but also relating data such as time-temperature-precipitation diagrams, distribution of precipitates and creep-voids, and creep damage parameters.

The purpose of the present research is to characterize the creep-damaged microstructure of type 304, 316, 321 and 347 stainless steels by computer aided quantitative metallography and to analyze the creep damage of the steels based on the characterized microstructures. The part of the results of the present research will be published as the microstructural data sheets described above. The characterization of the creep-damaged microstructure is carried out at different levels of creep strain with emphasis on the distribution of creep-voids and σ phase precipitates along grain boundaries, and on the relationship between the distribution of creep-voids and remaining creep-life.

(83) Development of Porous Ceramics Impreganted with Ionic Conductive Materials

April 1995 to March 1998

H. Nakamura, Environmental Performance Division

Keywords: ionic conductor, solid electrolyte, charge carrier, electrical conductivity

Recently, research works on solid high ionic conductor have been mainly focused on oxygen ion conductor such as ZrO_2, proton conductor such as $SrCeO_3$ and sodium ion conductor such as β-Al_2O_3.

One of the reasons why no other solid electrolytes have been developed as high ionic conductor is that cracks caused by grain growth or voids along grain boundaries tend to initiate in the sintered materials prepared for the solid electrolyte.

The objective of this study is to develop a new type of solid electrolyte in which grain boundaries or voids are extremely decreased by impregnation of liquid compounds (M_2O - B_2O_3 - M_2SO_4, M = Li, Na, K) into the porous oxides. Subsequently, its electrical properties will be evaluated by the measurement of electrical conductivity, the investigation of polarizing behavior and the determination of charge carrier. Furthermore, the thermal characteristics will also be evaluated using various thermal analysis methods.

84 Fundamental Study of Microstructures and Properties to Develop High Performance Materials for Severe Environment (II-High Temperature Intermetallic Compound)

April 1990 to March 1997

T. Yamagata, Materials Design Division

Keywords: Nb_3Al+Nb two phase structure, mechanical properties

The purpose of this research is to develop high temperature Niobium Aluminaide intermetallic compound which has the properties of 3 percent tensile elongation at room temperature and 75 MPa tensile strength at 2073 K. Intermetallic compound Nb3Al (A15) is a typical brittle materials, therefore, two phase alloys composed of Nb3Al and ductile Nb(A2) phase and in equilibrium at 2073 K, are searched in binary and Nb-Al-X ternary (X: Mo, Ta, W, Zr, Ti, Cr, Si, Co, Ni) alloys. Two phase structure was obtained on Nb-18at%Al in binary, and on Nb-18Al-4X ternary alloys (X: Ta, W). Mechanical properties of two phase alloys were examined at RT and 2073 K by compression test. At 2073 K, strength at 10% strain increased by addition of Ta and W, but even the maximum strength obtained in Nb-18Al-4W alloy was only 20% of the target value. At RT, three different stress-strain curves were observed, therefore, phase of each specimen was analized by x-ray diffractometer with powder made from compressed specimen. Compressive strain was very sensitive to the ratio of A2 and A15 phases. Few percent of strain, about 1.5% was observed on alloy with almost equal volume fraction of A15 and A2 phase.

85 Improvement of Mechanical Properties of Intermetallic Compounds by Crystal Growth Control

April 1992 to March 1997

T. Hirano, Chemical Processing Division

Keywords: unidirectional solidification, floating zone method, Ni_3Al, room-temperature ductility

The objective of this study is to improve the mechanical properties of intermetallic compounds by crystal growth. We have found that

unidirectional solidification using a floating zone method remarkably enhances the room-temperature ductility of Ni_3Al without addition of alloying such as boron. We call this method FZ-UDS. Stoichiometric Ni_3Al exhibits more than 60% tensile elongation at room temperature. It is found that FZ-UDS can enhance even the ductility of Al-rich Ni_3Al which can not be ductilized by the alloying method. This indicates that FZ-UDS is a new promising method to improve brittle intermetallic compounds.

In this study three subjects are stressed. First, crystal growth technique is developed in detail. Columnar-grained structure of Ni_3Al which is closely related to the large ductility is obtained by selecting the growth rate, depending on the deviation from the stoichiometry. Secondly, the solidified columnar structure is characterized, paying attention to the grain boundary structure. It is found that this structure consists of low energy grain boundaries. Thirdly, the mechanical properties and deformation behaviors are studied.

Related Papers

Unidirectional Solidification of Ni_3Al by a Floating Zone Method, T. Hirano and T. Mawari, Acta Metall. Mater. 41 (1993): 1783–89.

Effects of Unidirectional Solidification Conditions on the Microstructure and Tensile Properties of Ni_3Al, T. Mawari and T. Hirano, Intermetallics 3 (1994): 23–33.

Texture and Grain Boundary Character Distribution (GBCD) in B-Free Ductile Polycrystalline Ni_3Al, Mater. Sci. Forum 157–162 (1994): 1103–08.

86 Basic Research on Intermetallic Compounds for Structural Applications

April 1993 to March 1996

M. Nakamura, 3rd Research Group

Keywords: intermetallic compound, TiAl, elongation, creep behavior, grain morphology control, thermal shock, TiB_2

TiAl base intermetallic compounds have become of major interest as a candidate for high temperature structural applications. Although they have advantages of high melting point, high strength at high temperatures, high elastic moduli and reasonable oxidation resistance, improvement of both room temperature ductility and strength at temperatures above 1273 K is required.

Stoichiometric TiAl and Al-rich TiAl alloys were tested in tension in a temperature range from room temperature to 773 K in order to study the brittle-ductile transition behavior in elongation. The elongation increased from 1% at room temperature to about 3% at 473 K for the stoichiometric alloy with a γ single phase structure, while the increase of elongation was observed at about 573 K for the γ phase Al-rich alloy. Now, we are studying the mechanism of the elongation increase, which was observed at 473 and 573 K for the stoichiometric and Al-rich alloys, respectively.

The knowledge of creep behavior at high temperatures is also required for high temperature structural applications, but there are not many researches on tensile creep behavior TiAl base alloys. Thus, the creep rupture behavior in tension was studied at 1273 K and 1373 K in a He atmosphere with various impurities and other atmospheres for a Ti-46at%Al alloy consisting of lamellar grains with a small amount of γ grains. The surface of the specimen which has tested in air and a He atmosphere is considerably corroded, and the surface layer with a thickness of more than 1 mm peeled off for the specimen ruptured in about 200 h. The ordinary creep behavior with three stages was observed in He and in vacuum, while the accelerating creep was followed by the steady-state creep with a lower creep rate in air. This is because the oxides which were formed on the specimen surface became thicker. The longer creep rupture life was thus obtained in air than in He and in vacuum.

The microstructure control of TiAl base alloys was also studied for improvement of mechanical properties at high temperatures using thermo-mechanical processing. It is konwn that a large aspect ratio of grains improves remarkably high-temperature strength. Thus, the recrystallization structure which was obtained using a furnace with temperature-gradient was studied for a TiAl alloy. In the surface region and the central part of a Ti-50at%Al specimen, recrystallized lamellar grains with lamellar interfaces oriented at about 30 degree and parallel to the temperature-gradient direction were formed, respectively. The grain growth stopped at coarse grains of more than 100 μm, but it continued across fine grains. Thus, the furnace with the larger temperature-gradient and the specimen with a fine grain structure will be required for the formation of the elongated grain structure.

The wear properties of TiAl base alloys were studied. The wear resistance of three types of microstructures, i.e γ single phase, duplex and lamellar structures, was compared at room temperature using an Ohgoshi-type wear testing machine, which was an improved type of a Scoda Savan one. The resistance of the lamellar structure is two times higher than that of the γ single phase structure, and that of the duplex structure was intermediate. The hardness of the specimen surfaces after wear test with a low wear rate was about 530–655 H_v and decreased to 250–384 H_v with increasing wear rate and load. The decrease of the hardness was the largest in the lamellar structure and small in the γ phase structure. These results

may indicate that the formation and peeling of the hardened layer on the specimen surface result in the difference in the wear resistance of the three types of microstructure.

The resistance to thermal shock of transition metal carbides and borides with a much higher melting point was also studied for much higher temperature structural applications using HIP'ed mixture of W and TiB_2, etc.

Related Papers

Thermal Shock Behavior of Metal-Ceramics Mixtures for Ultrahigh Temperature Use, M. Fujitsuka, I. Mutoh, H. Nagai, and T. Tanabe, Proc. of the 3rd Japan Int. SAMPE Symp.*Advanced Materials-New Processes and reliability,* ed. by T. Kishi, N. Takeda, and Y. Kagawa, SAMPE, Chiba, Japan, (1993): 641–46.

Effect of Temperature on Tensile Properties of TiAl Base Alloys, K. Hashimoto, S. Kajiwara, T. Kikuchi, and M. Nakamura, Scripta Metall. Mater., 32 (1995): 417–22.

Wear Properties of Oxide Dispersion Strengthened Nickel Alloys, S. Ikeno, M. Siota, M. Nobuki, and M. Nakamura, J. Mater. Sci, in press.

87 High Performance Materials for Severe Environments-I (Microstructure and Properties of Intermetallic Compounds with High Specific Strength)

April 1990 to March 1997

M. Nakamura, 3rd Research Group

Keywords: Intermetallic Compound, TiAl, Microstructure, elongation, thermomechanical processing, high temperature strength, oxidation

Light-weight, heat-resisting intermetallic compound TiAl is a candidate for a structural use in severe environments for a space plane, etc., and the knowledge of various properties of TiAl base alloys is required for a practical use in such an environment. In this research program, the mechanical properties are systematically studied for TiAl base alloys whose composition and microstructure are well controlled, and then the fundamental methods to control microstructure which gives the optimum properties for a practical use to materials are discussed.

TiAl base alloys with Sb additon from 0.1 to 0.4 at.% were prepared by argon arc melting and heat-treatment, and the effect of solute Sb on yield strength and hardness above 1273 K, and ductility at room temperature were studied. The addition of solute Sb up to 0.4 at.% increased the yield strength of TiAl from 160 and 80 MPa to 260 and 160 MPa at 1273 K and 1373 K, respectively. The alloy containing 0.4 at.% Sb also exhibited an elongation of more than 2% at room temperature. The Vickers hardness, H_v at 1373 K for the alloy with solute Sb varied from about 110 to 160 with Sb content from 0 to 0.4 at.%. For the alloys with the addition of Sb from 3 to 9 at %, the microstructure was examined and Sb-rich phase precipitates of 10 to 40 vol.% were observed, irrespective of heat treatment. It was found that the Sb-rich phase had a $D8_m$ structure using high resolution-electron microscopy and x-ray diffraction. The hardness, H_v of 460 was obtained at 1373 K for the Sb-rich phase. Although the hardness at 1373 K varied to 260 with the volume fraction of the Sb-rich phase to 40 vol.% for the alloys with Sb addition, the yield strength increased to 160 MPa at 1373 K, and was approximately equal to that of the alloy containing solute Sb of 0.4 at.%. The room temperature elongation of the alloys decreased considerably with increasing Sb-rich phase precipitates.

The effect of microstructure on room temperature elongation was also studied for TiAl base alloys prepared by thermomechanical processing. V-containing TiAl alloys with a equiaxed fine grained and $\gamma + \beta + \alpha_2$ phase structure were prepared using isothermal forging above 1273 K. The alloys have exhibited an excellent elongation of more than 8% at room temperature in vacuum. A binary Ti-50Al alloy with a fine grained structure also have a good elongation of about 5% at room temperature.

The microstructure change caused by quenching from the α phase field and then tempering at relatively high temperatures was also investigated for Ti-48 at.% Al, and it was found that the equiaxed γ grain structure with a fine α_2 phase precipitates could be obtained only by heat treatment. The morphology of the α_2 precipitates was able to change from a fine particle to a platelet with tempering temperature.

The oxidation behavior of TiAl containing various rare earth elements at 1173 K have been studied, and it was found that the addition of a small amount of rare earths prevented the oxide layers on the specimen surface from breaking and peeling off.

Related Papers

High Temperature Strength and Room Temperature Ductility of TiAl Base Alloys with Antimony, K. Hashimoto, M. Nobuki, H. Doi, E. Abe and M. Nakamura, Proc. Int. Symp. on Gamma Titanium Aluminides, ed. by Y–W. Kim, R. Wagner, and M. Yamaguchi, TMS, (1995) in press.

High Temperature Mechanical Properties of Vanadium Alloyed γ Base Titanium-Aluminides, M. Nobuki, D. Vanderschueren, and M. Nakamura, Acta Metall. Mater., 42 (1994): 2623–32.

Environmental Effect on Room-Temperature Ductility of Isothermally Forged TiAl-Base Alloys, M. Nakamura, N. Itoh, K. Hashimoto, T. Tsujimoto, and T. Suzuki, Metall. Trans. 25A (1994): 321–30.

[88] High Ionic Conductivity of Solid Electrolyte

April 1992 to March 1995

H. Nakamura, Environmental Performance Division

Keywords: ionic conductor, solid electrolyte, charge carrier, electrical conductivity

Recently, research works on solid-high ionic conductor have been mainly focused on oxygen ionic conductor such as ZrO_2, proton conductor such as $SrCeO_3$ and sodium ionic conductor such as β-Al_2O_3.

One of the reasons why no other solid electrolytes have been developed as high ionic conductor is that cracks caused by grain growth or voids along grain boundaries tend to initiate in the sintered materials prepared for the solid electrolyte.

The purpose of this study is to synthesize a new solid electrolyte consisting of oxides and sulfates (M_2O - B_2O_3 - M_2SO_4, M = Li, Na, K) of which grain boundaries or voids were decreased by a rapid quenching method, and to investigate the suitable composition of the compound in solid-liquid coexisting composition range by various thermal analytical methods.

Furthermore, the electrical properties of the electrolyte can be evaluated by the measurement of electrical conductivity, the investigation of polarizing behavior, the determination of charge carrier, the comparison of electron motive force for concentration cell with that for theoretical one, etc.

Related Papers

Electrical Conductivity of Solid Berryllium Sulfide, H. Nakamura, Y. Ogawa, A. Kasahara, and S. Iwasaki, Mater. Trans., J. Japan Inst. Metal., 56 (1992): 1408–13.

A. Kasahara, Y. Ogawa, S. Iwasaki, and H. Nakamura, Mater. Trans. JIM, 34 (1993): 786–91.

Electrical Conductivity of II a and III a Metal Sulfide in Solid, H. Nakamura, Y. Ogawa, and A. Kasahara, Mater. Trans., J. Japan Inst. Metal., 58 (1994): 519–25.

Composites

89 Thermal Stability of Intermetallic-Compound Matrix Composites Reinforced with Fibers

April 1993 to March 1996

Y. Shinohara, Physical Properties Division

Keywords: TiAl, B fiber, W fiber, protection layer, BN, TiB_2

Heat resistive materials which can be applicable over 1373 K are essential for developing a space plane, a fusion reactor and a high performance turbine engine. TiAl and Ni_3Al intermetallic compounds (IMCS) have higher strength and toughness than ordinal metals and ceramics at elevated temperatures. Therefore the IMCS are suitable for matrixes of composites. The TiAl matrix composite reinforced with fiber is a promising structural material for a space plane.

SiC, B or W fibers are candidates as reinforcement for TiAl matrix. B and W fibers are tougher than SiC fiber, while they are more reactive to the matrix. We have studied the reactivity between TiAl matrix and the fibers of B and W. In order to protect the fibers, the suitability of BN and TiB_2 as protection layer has also been investigated.

The coating treatments of BN and TiB_2 on the B and W fibers were carried out by using the following methods, respectively. The B fiber was coated with Ti using PVD method and then heat treated to change Ti to TiB_2. On the other hand, BN was deposited on an electrically heated W fiber by using a CVD method, which was specially designed for W. fiber.

Both the layers could prevent the interfacial reaction, however they caused deterioration when the layers were too thick. It is essential to control thickness and compactness of the layer. The study for controlling the thickness and forming a compact layer is in progress.

[90] Development of High Strength Metal Base Composites with Excellent Physical Properties by the Advanced Bronze Method

April 1994 to March 1995

H.G. Suzuki, Mechanical Properties Division

Keywords: bronze method, composite, Cu alloy, iron base alloy, high strength

The demand for high strength materials is increasing in many fields. High strength metal base composite with high conductivities such as Cu-Cr alloys is one example. Another is cendust which has high strength with superior magnetic properties. However, these materials have difficulty with hot and cold workability. So, there has been no practical usage of these materials until now.

The Bronze method (Tachikawa method) was developed at NRIM to produce a superconductive Nb_3Sn which is too brittle to obtain a wire product for high magnetic field uses. Starting materials are ductile boith a Cu-Sn alloy (bronze) and a pure Nb rod. Holes, into which the Nb rods are inserted, are drilled mechanically in the Cu-Sn matrix. The combined materials are cold rolled or extruded to get final size of less than 1 mm dia wire. A diffusional heat treatment is then performed to yield Nb_3Sn fibers in the Cu matrix.

Based on this idea, the present theme is planned and is undergoing now.

Materials for mechanical application

91 High Temperature Mechanical Properties of Particulate Reinforced Titanium-based Metal Matrix Composites

April 1994 to March 1997

M. Hagiwara, Mechanical Properties Division

Keywords: particulate-reinforced, titanium, MMC's, mechanical properties, powder metallurgy

One of drawbacks of Ti alloys is that the service temperature is limited to 600 °C due to a degradation of tensile strength, creep resistance, thermal stability and environmental resistance. Moreover, Ti alloys exhibit lower stiffness and poor abrasion-related properties than nickel-based alloys. The dispersion of ceramic particulates into Ti matrix is expected to overcome these drawbacks. These particulates metal matrix composites (MMC's) have isotropic properties and can be processed more cheaply using the conventional near net shape methods.

The advanced powder metallurgy (P/M) such as rapid solidification and blended elemental techniques can provide a flexible method for producing particulates MMC's with tailored microstructure. However, information on the processing conditions and mechanical property data available for this type of MMC's are still lacking.

This research program has firstly been aimed to obtain information on processing conditions in more detail. Secondly, Ti-based MMC's reinforced with both large-sized ceramic particulates (1~10 μm in diameter) such as TiC and TiB and very fine oxide particulates (below 1 μm) such as Er_2O_3 have been produced using the best processing conditions obtained, and high temperature mechanical properties, especially creep and fatigue, have been evaluated quantitatively.

Related Papers

Mechanical Properties of Particulate Reinforced Titanium-Based Composites produced by the Blended Elemental P/M Route, M. Hagiwara, S. Emura, Y. Kawabe, N. Arimoto, and H.G. Suzuki, ISIJ Int. 32 (1992): 902–16.

Properties of P/M Processed Titanim Alloy/Particulate Composites, M. Hagiwara, S. Emura, Y. Kawabe, N. Arimoto, and S. Mori, Metallurgy and Technology of Practical Titanium Alloys, edited by S. Fujishiro, TMS, (1994): 363–70.

92 Intelligent structural Materials

April 1991 to March 1995

S. Matsuoka, Environmental Performance Division

Keywords: intelligent materials, materials damage, self-sensing, self-restoring, nanotechnology

Recently, a new material concept, known as intelligent material or smart material, has been proposed and developed to establish the reliability of engineering structures such as air crafts, space structures and nuclear power plants. The intelligence of the material is defined as self-detectibility for environmental changes and feasibility of sensing, processing and actuating.

In this study, fundamental research has been carried out in order to impart the intelligent functions to the metallic materials for structural use. Small cavities which do not deteriorate the mechanical properties exist in the materials. An attempt has been made to implant the sound-emitted material, phase-transformed material or surface-film-controlled material into the cavities. The implantation could make the material possible to self-sense and self-restore the damage during operation. A nanotechnology based on a scanning tunneling microscope (STM) and atomic force microscope (AFM) has also been developed to evaluate the intelligent functions of the materials from atomic scale viewpoint.

Y_2O_3 particles in Fe-20Cr alloy and Pb particles in two stainless steels, SUS304 and SUS403, have been found to arrest the elevated-temperature fatigue crack growth. In the current year, a small addition of Zr in 0.17 wt% in Fe-27Cr-35Ni alloy also showed the arrest function in the elevated-temperature fatigue crack growth. The mechanism was related to the fact that the strength properties of oxide film at the crack tip could be improved by precipitating ZrC or ZrO_2 between oxide film and matrix.

93 Fracture Mechanism of Ceramic Particulate-Reinforced Titanium Matrix Composites

April 1994 to March 1995

Y. Kawabe, Mechanical Properties Division

Keywords: particulate, composites, titanium, mechanical properties

This study is a part of "Investigation of High Temperature Titanium Alloys at above 600 °C," which is a joint research project determined by Chinese-Japanese Science and Technology Cooperation Committee. It was decided to be carried out by Northwest Institute for Non-ferrous Metal Research (NIN) and National Research Institute for Metal (NRIM).

The purpose of this program is (1) to study the techniques of preparing particulates-reinforced Ti-based metal matrix composites (MMC's) by both powder metallurgy (P/M) and ingot metallurgy (I/M) processes, (2) to evaluate the high temperature mechanical properties of these composites and (3) to discuss the strengthening mechanism by particulates.

The joint research contents and discussion done in two institutes are as follows:

Research Contents

Both sides have produced Ti-based MMC's with their own procedures and provided samples to the other side for evaluating their properties. Chinese side have tested the creep properties of the Japanese P/M samples and Japanese side have evaluated the room and high temperature high cycle fatigue properties of Chinese I/M samples.

Discussion

The experimental results obtained in both institutes have been exchanged, and fracture mechanism have been discussed in terms of microstructural variables such as the shape of reinforcements, matrix microstructure, structure of interface and change of Young's modulus during the exchange of researchers from both insitutes. Both side have expressed satisfaction with research results.

Materials for electronics application

(94) Characterization and Application of Superconducting Thin Films Synthesized by Atomic Layer-by-layer and Epitaxial Growth Methods.

April 1995 to March 2000

K. Nakamura, 1st Research Group

Keywords: atomic layer epitaxy, superlattice, oxide superconductor, Boro-carbide superconductor, textured buffer layer, microwave cavity, high temperature plasma

In the preceding project on high T_c superconductors, we have investigated on the following subjects:

1. a. Application of atomic layer-by-layer deposition technique to the grown of $Bi_2Sr_2Ca_{n-1}Cu_nO_{2n+4}$ (n=1 to 7) and their superlattice films.
   b. Control of oxygen potential in $YBa_2Cu_3O_{7-\delta}$ (YBCO) thin films and structural analysis related to the oxygen deficiency and structure disorder.
   c. Synthesis of boride-carbide superconductors, i.e., families of Pd_2YB_2C which has the highest T_c among the metallic superconductors.
2. a. Application of a modified bias sputtering technique to the preparation of in-plane textured buffer layers on metallic substrate for the epitaxial growth of YBCO thick films
   b. Development of flash evaporation method using high temperature plasma for the growth of thick YBCO films.

In the present project we attempt a further development based on the above mentioned results. For examples, in the atomic layer-by-layer growth we are planning to investigate surface defects by scanning tunneling microscope *in situ* and aim to get a controlled surface morphology in the atomic scale. To deposit large area superconducting films on non planar substrates for their application to microwave devices and accelerating cavities is also an important application aspect in this project.

Related Papers

Analysis of Intergrowth Structure and Growth Model of $(Bi_2Sr_2CuO_y)_m(CaCuO_2)_m$, Superlattices Synthesized by Alternate Deposition, K. Nakamura and T. Hatano, J. Appl. Phys., 77 (1995): 6402–10.

Structure and Properties of $Bi_2Sr_2Ca_{n-1}Cu_nO_{2n+4}$ Films Prepared by Sequential Deposition, T. Hatano and K. Nakamura, to be published in Bismuth-based High Temperature Superconductors, ed. by H. Maeda and K. Togano, Marcel Dekker (N.Y., 1995).

Laser Deposition of YBa_2Cu_3Oy Thin Films on a Metallic Substrate with Biaxially Texture YSZ Buffer Layers Prepared by Modified Bias Sputtering, M. Fukutomi, S. Aoki, K. Komori, R. Chatterjee, and H. Maeda, Physica C 219 (1994): 333.

(95) Development of Tapes and Wires Using New High-T_c Oxide Superconductors

April 1995 to March 1999

H. Kumakura, 1st Research Group

Keywords: grain boundary, grain alignment, critical current density

In general, polycrystalline oxide superconductors show weak coupling at grain boundaries. This weak coupling significantly restricts the superconducting current transfer across the grains. Grain orientation is effective to improve this coupling and to increase transport critical current density J_c. Grain oriented microstructure can be easily obtained for Bi-based oxide superconductors because of their strong two dimensionality. However, this strong two dimensionality brings about low irreversibility field B_{irr} at elevated temperatures, and hence, low J_c values.

II_b-metal based oxides show much more excellent flux pinning properties than Bi-based oxides at high temperatures due to weaker two dimensionality of the systems. However, grain alignment for these oxides is more difficult because of this weaker two dimensionality. The elimination of weak couplings by a conventional heat treatment and/or mechanical working is not successful for II_b-metal based oxides, and excellent J_c has not attained yet.

In this research program, we develop II_b-metal based oxide tape and wire conductors which show excellent J_c at high temperatures. We investigate the mechanism of weak coupling between grains of oxide superconductors including II_b-metal based oxides in order to establish the method to eliminate the weak coupling. Tape conductors are fabricated by several methods including a precursor method. Ba-Ca-Cu-O precursor is deposited on a

Hastelloy or Ag tapes coated with buffer layer, and then, the precursor is converted to II_b-metal based oxide superconductors by heating the precursor under II_b-metal vapor atmosphere. The relation between microstructure and current carrying capacity will be investigated. For this purpose, grain boundary observations with high-resolution electron microscope and precise J_c measurements with a resistive method and a magnetization method will be carried out for many samples prepared under various condition.

(96) Development of High Strength/High Conductivity Materials for High Field Magnets

April 1995 to March 1998

K. Inoue, High Magnetic Field Research Station

Keywords: Cu-Ag microcomposite alloy, high-strength/high-conductive material, conductor materials for high-field magnets

In this study we will develop new high-strength/high conductive materials for resistive high-field magnets, such as polyhelix-type water-cooled magnets and pulsed magnets. Recently, we successfully developed a new Cu-Ag microcomposite alloy having a promising combination of high mechanical strength and high electrical conductivity. When a Cu-16at.%Ag alloy ingot was cold-worked into a wire or a sheet with several times of intermediate annealing at 350 450 °C, it shows not only high conductivity of 75–83% IACS but also high tensile strength of 0.7–1.1 GPa at room temperature. However, it should be necessary to optimize the fabrication process further more for obtaining excellent characteristics in a bulk or a large hollow cylinder of Cu-Ag microcomposite alloy, which is very suitable for making polyhelix-type water-cooled magnets. We will also perform a feasibility study on several pure metals as the conductor materials for pulsed magnets in this study. Several pure metals are well known to have a promising combination of high strength and high conductivity. Their electric conductivity, magnetic resistance, mechanical strength, elongation, and heat capacity will be investigated as the feasibility study.

(97) Developments of High Strength Oxide Superconductors for High Magnetic Field Applications

April 1995 to March 1997

Y. Tanaka, High Magnetic Field Research Station

Keywords: Bi(Pb)SrCaCuO, AgCu alloy sheath, multifilamentary wires

Fabrication process for Bi(Pb)SrCaCuO wires and superconducting properties were studied. In order to meet high magnetic field applications, requirements such as high critical current density. J_c high critical current, I_c, long lengths and high mechanical strength, must be fulfilled. In the present study both the Bi-2212 and Bi-2223 wires were prepared by using AgCu-alloy sheaths.

The Bi-2223 superconducting tapes prepared by the powder-in-tube technique using AgCu alloy sheaths doped with a small amount of Ti, Zr or Hf have been found to show considerably larger J_c value than those of the pure Ag sheathed or the non-doped AgCu alloy sheathed samples. This may be attributed to two reasons; one is macroscopic grain morphogy improvements and the other is microscopic defect introduction. The doping of the elements modifies grain morphogy and phase alignment probably due to an enhanced formation of Bi-2223 phase. The doped sample showed larger and more flat-shaped grains than those for the pure Ag sheathed or the non-doped samples containing many small sub-grains. The alignment of the Bi-2223 phase is also greatly increased for the doped samples. Recently, in the doped samples many disc-like amorphous regions have been found which are expected to be effective magnetic flux pinning centers for the Bi-oxide superconductors.

Based on these recent results the fabrication and superconducting properties of a variety of multifilamentary wires will be investigated towards making several test-coils for high magnetic field applications.

(98) Performance Evaluation on Long Oxide Superconductors

April 1995 to March 1999

K. Itoh, Strong Magnetic Field Research Station

Keywords: oxide superconductor, evaluation, measurement technique, long length

To realize the high-temperature oxide superconductors for a magnet use, it is indispensable to have a long wire with high quality and homogeneity. We often use short-length specimens cut from the different positions of the whole wire to check the quality and homogeneity. However, such technique does not only waste long length of wire but also disable to use it for the magnet winding.

In this study we develop techniques to measure superconducting properties such as the critical current, ac losses, thermal and electro-mechanical properties, of a long wire without giving any damage to the wire. In addition, we develop measurement techniques on a coil shaped specimen, and compare the results with those obtained by the techniques on short- and long-length specimens. Such comparison would be efficient for the development of wire fabrication and winding techniques.

⑨⑨ Development of 1 GHz NMR System

April 1995 to March 2000

H. Maeda, High Magnetic Field Research Station

Keywords: high-field superconducting magnet, high resolution superconducting magnet, oxide superconducting magnet, 1 GHz NMR system

Bi-system oxide superconductors have become very interesting superconducting materials, because they show very high critical currents in extremely high magnetic field and in relatively low temperature. However, the extremely high J_c values are obtained for only short oxide-superconducting samples, while long samples (coil samples) show relatively small J_c values due to having local defects. Therefore the application of oxide superconductors have not been established yet. However the J_c of long sample is now being improved gradually.

Recently, NMR system using high/homogenous-field superconducting magnet has become the most popular method to determine the detailed structures of high molecular compounds, such as proteins, nucleic acids, and polysaccharides. The S/N ratio of NMR measurements increases with increasing the NMR frequency, which is proportional to the magnetic field for NMR. Therefore many efforts have been performed to develop higher field NMR systems. Up to date 750 MHz NMR system has been commercialized. Since the J_c of high-field metallic superconductor (Nb_3Sn) rapidly decreases in higher fields, it has become very difficult to develop higher-field NMR system with using only metallic superconductor. On the other hand, the J_c of Bi-system oxide superconductor scarcely decreases in higher fields.

In this study, we will develop 1 GHz NMR system including a 23.5 T homogeneous-field magnet and NMR measurement system. At first we will determine the primary design of the 23.5 T homogeneous-field magnet, which will be composed of an outer metallic superconducting magnet and an inner oxide superconducting magnet. We will perform several fundamental coil testa of Bi-system oxide superconductors under high magnetic fields up to 21 T for developing the inner oxide superconducting magnet. We will also develop a high-strength Nb_3Sn conductor for the outer superconducting magnet this year.

100 Thermal and Electrical Properties of II–IV and V–VI Thermoelectric Semiconductors

April 1993 to March 1996

I.A. Nishida, Physical Properties Division

Keywords: thermal conductivity, thermoelectric property, energy conversion, $Bi_{2-x}Sb_xTe_{3-y}Se_y$, $Pb_{1-x}Sn_xTe$, $Mg_2Sn_{1-x}Ge_x$

Thermoelectric (TE) materials have been widely used for the direct energy conversion systems. These materials convert thermal energy to electric power with quick response and without noises and mechanical vibration. Recently, the thermoelectric generators are mainly used for the electric source in space, marine and polar regions, and the thermoelectric cooling systems are mainly used for the precise temperature control in the semiconductor processing, and in the use of optical and electronic devices. Therefore, it is important to develop TE materials with high efficiency.

The TE materials with high efficiency are given by the three characteristics, i.e., high thermoelectric power (α) and electric conductivity (σ) and low thermal conductivity (κ). For the TE materials with very low values of κ, such as the case of $Bi_{2-x}Sb_xTe_{3-y}Se_y$, $Pb_{1-x}Sn_xTe$ and $Mg_2Sn_{1-x}Ge_x$, it is very difficult to obtain the reliable value of κ, which is necessary for developing TE materials.

The aim of this study is to establish a technique for the precise measurement of κ by means of the static comparative method, Harman's method and PAS (Photo Acoustic Spectroscopy).

Related Papers

Anisotropic Galvanomagnetic and Thermoelectric and Thermoelectric Properties of n-Type Bi_2Te_3 Single Crystal with the Composition of a Useful Thermoelectric Cooling Material, H.T. Kaibe, Y. Tanaka, M. Sakata, and I.A. Nishida, J. Phys. Chem. Solids, 50 (1989): 945–50.

Preparation and Thermoelectric Properties of $Mg_2Sn_{1-x}Ge_x$, Y. Noda, T. Sugawa, I.A. Nishida, and K. Masumoto, Proc. 12th Int'l. Conf. Thermoelectrics (XII ITC), Yokohama Japan, November (1993): 142–44.

101 Energy Conversion Materials Fabricated with Functionally Gradient Structure

April 1993 to March 1996

I.A. Nishida, Physical Properties Division

Keywords: energy conversion, thermoelectric materials, functionally graded materials (FGM)

Thermoelectric (TE) materials have been widely used for the purpose of direct conversion of thermal energy to electric power without noise and mechanical system. For a given TE material system with homogeneous matrix and dopant distribution, the optimized figure of merit Z can only be obtained in a narrow temperature range. In other temperature range, the TE conversion efficiency η becomes comparatively small. Since the temperature of the thermocouple legs changes continuously from the top (high temperature) end to the bottom (low temperature) end, the large value of η will be obtained if the carrier concentration in the TE material changes continuously along the thermocouple legs, i.e., functionally graded TE materials. By preparing these materials, the effective

value of η is estimated to double or more. In addition, Z can be increased by controlling the composition and grain size of the FGM, because the lattice contribution to the thermal conductivity can be decreased by phonon scattering at the lattice defects such as crystal distortion and grain boundary.

The goal of this study is to establish the fabrication technology of functionally graded TE material with high η by controlling carrier concentration, composition, texture and grain size.

Related Paper

Highly Efficient Thermoelectric materials in FGM program, I.A. Nishida, Proc. Japan-Russia-Ukraine Int'l. Workshop on Energy Conv. Materials (ENCOM 95), Sendai Japan, (January 1995): 1–10.

102 Study on Design and Assessment Technology for Ecomaterials

April 1993 to March 1996

K. Yagi, Environmental Performance Division

Keywords: evaluation of environment load, ecomaterials data base, structural design of solid solution alloys, recyclable materials design, multiphase structure

Recent environmental problems in a global scale originate from strains existing in a large amount of materials and energy consumption. Although man-made materials have supported the society bringing advantages and conveniences to human life, they also impose a wide variety of burdens on the environment through each and every step of production, processing, consumption, use, recycling and disposal. Ecomaterials which would harmonize with the environment and minimize environmental load have to be developed as a new concept of materials design and materials technology. In this project, the study on three subjects as follows are being conducted;

Construction of Ecomaterials Data Base

MLCA (Materials environmental Life Cycle Analysis) is investigated to evaluate the environmental load of materials through whole processes of their life cycle. The data of environmental burden in each sage and practical material-flow data are collected in a meta-database of MLCA. From this meta-database, environmental burdens of each metals and alloys are calculated and arranged with detailed description of alloys, such as 12Cr steel, 18Cr-8Ni steel etc., in a database named "Material Eco-sheet." This Eco-sheet will provide the quantitative relation between the properties of a material and its environmental load by using with a database of mechanical or other properties of materials.

Structural Design of Solid Solution Alloys for High Temperature Applications

Effect of solute elements in the ferrite matrix on the Inherent creep strength of carbon steels was studied from a view point of atomic configurations such as atomic pairs. The equilibrium concentrations of solute elements and atomic pairs in the ferrite matrix were estimated by thermodynamic calculations with the sublattice model (Thermocalc.) and the central atoms model, respectively. A good correlation is observed between the Inherent creep strength and the concentrations of Mn-C and Mo-C atomic pairs, suggesting that the Inherent creep strength of carbon steels is controlled by these atomic pairs in the ferrite matrix.

Fracture Criterion for Multiphase Structure

A tramp element, Cu, deteriorates the hot deformability of steels. However, the small addition of Cu is not said to be harmful to the mechanical properties. A SM50C (weldable structural steel with 500 MPa strength) showed the best balance of strength and ductility with 0.5 mass% Cu addition. The high-cycle fatigue strength was also remarkably improved by the Cu addition. In the further study, the feasibility of microstructural adjustment is taken into account for improved combination of the mechanical properties.

New specimen cooling system was developed by utilizing a gas refrigerator. A low temperature below 20 K was accomplished.

Related Papers

MLCA (Materials environmental Life Cycle Analysis) for ECOMATERIALS, K. Halada, Proceedings of International Conference of EcoBalance, Tsukuba (1994): 288–93.

Environmental Life Cycle Analysis of PM Products, K. Halada, K. Minagawa, and K. Yagi, Funtai Oyobi Funmatsu Yakin, 41 (1994): 1388 (in Japanese).

Effect of Minor Alloying Elements on Inherent Creep Strength Properties of Ferritic Steels, K. Kimura, H. Kushima, K. Yagi, and C. Tanaka, Tetsu-to-Hagane, in press.

103 Structure Control and Electromagnetic Properties of High Temperature Superconductors

April 1993 to March 1998

K. Togano, 1st Research Group

Keywords: high temperature superconductors, critical current density, flux quantum, tape, film, vapor deposition

New superconductors, such as high-T_c oxides are not only in scientific interest but also key materials for further progress of superconductivity applications in various advanced technological fields. From this point of view, the research pro-

gram conducts following researches to establish the base of superconductivity applications.

Study on the Relationship between Microstructure and Critical Properties

The objective of this research is to study the effects of various microstructural features, such as grain alignment, phase distribution and defects produced by irradiation, on critical current density J_c of high temperature superconductors (HTSC). Attempts of producing long tape and its coil test of HTSC are also carried out in order to study the possibility of power application of HTSC.

Understanding of the Electromagnetic Behavior of HTSC

The objective is to understand the origin of peculiar behavior of flux quantum in HTSC. For this purpose, high quality single crystal of HTSC is prepared, from which precise information on electromagnetic properties can be drawn. New model of flux quantum state is proposed and discussed with possibility of J_c improvements.

Structure Control by Film Depositon Techniques

Structure control in atomic layer level is carried out for HTSC by using MBE and alternative sputtering techniques. New techniques of film analysis such as RHEED-TRAXS and RBS-PIXE are also developed. Those techniques of deposition and analysis are essential to achieve well control of crystal structure, which is one of the keys to realize electronic applications of HTSC.

Microstructure Control by Vapor Deposition Techniques

The objective is to apply vapor deposition techniques to the conductor fabrication of HTSC. Films are synthesized by various deposition techniques of laser ablation, sputtering and thermal flash plasma, using metallic tape substrate with buffer layer of ceramic. A new sputtering technique to achieve three dimensional grain alignment for buffer layer is developed.

104 Microstructure and Electromagnetic-Characteristics Studies on V_3Si Multifilamentary Superconductors

April 1994 to March 1997

T. Takeuchi, High Magnetic Field Research Station

Keywords: flux pinning, ac loss, V_5Si_3, image analysis

A V_3Si multifilamentary conductor has been developed as a new A15-type AC superconductor. V_5Si_3 layers are preferentially formed between the bronze and V_3Si filaments at the early stage of diffusion reaction. The resistivity of V_5Si_3 is reported to be ~15 μΩcm at 4.2 K, which is expected to be high enough to separate the filaments from each other for electromagnetic decoupling. The combination of adjusting the total proportion of V to Si in the Cu-Si/V composite to ~3 and reducing V filaments to ~1 μm enables the completion of the reaction in a short time; the initially formed V_5Si_3 appropriately decomposes and mostly V_3Si probably without grain growth is produced to achieve a high overall J_c (1.3×10^9 A/m$_2$ at 5 T). Magnetic properties, in correlation with cross-sectional microstructures, were examined in order to check the potentiality of V_3Si multifilamentary superconductors for AC use. Irregular deformation of V filaments was likely to bring about the bridging between filaments after heat treatments, and thus the effective filament diameter D_{eff} was 2–3 times larger than the designed V core diameter before heat treatment D_f. D_{eff} of 2.3 μm is, however, one of the smallest D_{eff} reported so far (excluding NbTi). At long heat treatments, the V_5Si_3 layer initially forming around V_3Si filaments disappeared, and then proximity coupling occurred additionally to the bridging. The proximity coupling caused the two peaks to appear in the magnetization curves and D_{eff} to increase at low fields. The existence of V_5Si_3 was confirmed to be quite effective in reducing D_{eff} and hence hysteresis loss.

Related Papers

V_3Si Multifilamentary Superconductor Produced by a Modified Bronze Process, T. Takeuchi and K. Inoue, J. Appl. Phys., 74 (1993): 6454–56.

Magnetic Properties and Microstructure of V_3Si Multifilamentary Superconductors, T. Takeuchi, Y. B. Kim, K. Itoh, Y. Nemoto, Y. Iijima, M. Kosuge, K. Inoue, andH. Maeda, IEEE Trans. Appl. Superconductivity, 5 (1995).

105 Stabilities of Superconducting Materials

April 1994 to March 1999

H. Wada, High Magnetic Field Research Station

Keywords: Nb-matrix Nb_3Sn wires, critical current, stress/strain sensitivities

The main purpose of this study is to define stabilities of superconducting materials under various conditions they may experience when wound to superconducting magnets. Stabilities of new, promising superconducting materials including high-temperature oxide superconductors are examined in terms of mechanical stress/strain, temperature and magnetic field.

In fiscal year 1994 effects of axial tensile and transverse compressive/strains/stresses on critical currents of Nb-matrix Nb_3Sn wires were studied. These wires showed 0.2% proof stresses of 550 MPa, 3.4 times larger than those of conventional bronze-matrix Nb_3Sn wires. It was found that the axial tensile strain sensitivities of critical currents were almost the same for both Nb-matrix and bronze-matrix Nb_3Sn wires. On the other hand,

sensitivities of critical currents to transverse compressive stresses were much smaller in Nb-matrix wires than in bronze-matrix wires. In Nb-matrix wires irreversible stresses where critical currents on unloading no longer recover to initial values in the unstressed state were larger than 300 MPa, which is several times larger than those in bronze-matrix wires. Based on these results, it is concluded that Nb-matrix Nb_3Sn wires are of higher tolerance to transverse compressive stresses compared to conventional bronze-matrix Nb_3Sn wires.

106 Purification of Active Metals for the Preparation of Superconductive Materials

April 1987 to March 1994
T. Fujii, Chemical Processing Division
Keywords: sintering method, melt-growth method, $YBa_2Cu_3O_x$

In order to examine in more detail the superconducting characteristics of $YBa_2Cu_3O_x$ ceramics, effects of impurity contents in starting mateials on superconductivity such as the critical transition temperature, T_c, and the critical current density, J_c, were investigated. Specimens for measurements of T_c and J_c were fabricated by the sintering and the melt-growth techniques using refined alloy powders of various purity grades. Superconducting properties were affected with the purity of starting materials as well as the preparation techniques. As far sintered specimens, T_c and J_c values increase 87.4–89.6 K and 207–317 A/cm^2 (at 77 K, OT), respectively, with a decrease in impurity contents in starting materials. In melt-grown specimens, both T_c and J_c values were improved to be 90.0–92.9 K and 777-1040 A/cm^2, respectively. In these specimens, with lowering impurity contents, T_c values increase whereas J_c values decrease. All the sintered specimens show similar microstructures with randomly oriented plate-like 123 grains irrespective of impurity contents. On the other hand, fine grained needle-like 123 crystals and spherulitic microstructures were observed in the melt-grown specimens, in which the 123 grains became smaller with an increase in impurity contents.

107 Development of Bismuth Oxide Superconducting Tapes and Coils

April 1994 to March 1995
H. Kumakura, 1st Research Group
Keywords: melt-solidification, grain orientation

We have developed Bi-2212/Ag tape conductors applying the combination of a continuous dip-coating process and a melt-solidification method. C-axis grain alignment was attained by the slow cooling from the partially molten state of the oxide. The change of phases in oxides during the slow cooling was observed, and the mechanism of the grain alignment was investigated. It was found that the smoothness of the oxide surface is very important for the good grain alignment of the Bi-2212. The grain oriented Bi-2212 tapes showed excellent critical current density J_c. J_c higher than 10^5 A/cm^2 was obtained at 4.2 K even in fields above 20 T. The results indicate that the tape conductors are promising for high field applications such as superconducting magnets.

Small pancake coils were fabricated using the Bi-2212/Ag tapes. Wind & react method was applied for the coil fabrication. The dimension of the coils were 40–100mm outer diameter and 13–20mm bore. The coils were tested at various temperatures and fields. A double stacked pancake coil inserted in a hybrid magnet generated 1.1 T at 4.2 K in a bias field of 20 T. One of the serious problems in the high field applications is that the mechanical properties of the tape conductors are not strong enough to sustain strong electro-magnetic force. This electromagnetic force introduced damage in the oxide layer and the J_c values of the coils decreased in high applied fields. In order to improve mechanical properties of the tape, alloying an Ag substrate was performed. We prepared Ag-Mg, Ag-Mg-Ni, Ag-Mg-Zr, Ag-Ti and Ag-Mn alloy tapes. Addition of small amount of Mg, Mg-Ni or Mg-Zr to Ag significantly improved the mechanical properties of the conductors without serious degradation of J_c. The improvement of the mechanical strength of the alloy tapes was attributed to the fine grain structure and precipitation of small oxides. Then we made small coils using the Ag-Mg-Zr alloy tapes, and the coils were tested in high fields. J_c values of the coils were higher than that of the coil made with pure Ag tape due to the improvement of the mechanical properties.

Related Papers

Formation and Growth Mechanisms of $Bi_2Sr_2CaCu_2O_y$ on an Ag Substrate in the Partial Melting Method, T. Hasegawa, H. Kobayashi, H. Kumakura, and K. Togano, Supercond. Sci. Technol. 7 (1994): 579–82.

Development of Superconducting Coil Using Bi-2212/Ag Tapes, N. Tomita, J. Shimoyama, H. Kitaguchi, H. Kumakura, K. Togano, H. Maeda, H. Fujii, and K. Nomura, Adv. Cryogenic Engr. 40 (1994): 297–303.

108 Fabrication and Characterization of Ag-I Intercalated $Bi_2Sr_2CaCu_2O_y$

April 1994 to March 1995
H. Kumakura, 1st Research Group
Keywords: transition temperature, irreversibility field

We obtained a new group of (Ag-I) intercalated $IBi_2Sr_2CaCu_2O_y$(Bi-2212) as well as the iodine-intercalated Bi-2212 using Bi-2212/Ag

tapes. Samples were textured thick films prepared on Ag substrate. Intercalation was performed by heating the samples with iodine at ~170 °C in air or under vacuum. Heat treatment in air brings about intercalation of Ag-I into Bi-2212 with stoichiometric composition of $AgI_2Bi_2Sr_2CaCu_2O_y$. By this intercalation, c-axis was significantly expanded from 30.9 to 45.6(= 22.8 × 2)A. Heat treatment under vacuum, on the other hand, introduced iodine intercalated Bi-2212, $IBi_2Sr_2CaCu_2O_y$ with c-axis of 38.2(= 19.1 × 2)A. The change of ac susceptibility due to superconducting transition for $(Ag\text{-}I)_xBi_2Sr_2CaCu_2O_y$ is almost equal to those of host Bi-2212 and $IBi_2Sr_2CaCu_2O_y$, indicating that $(Ag\text{-}I)_xBi_2Sr_2CaCu_2O_y$ is also a bulk superconductor.

Transition temperature T_c was measured by the resistive method. Before T_c measurements, $IBi_2Sr_2CaCu_2O_y$ was heated in air at 170 °C in order to introduce oxygen which was removed by the heat treatment under vacuum. T_c(zero resistivity) of $(Ag\text{-}I)_xBi_2Sr_2CaCu_2O_y$ is 72 K, which is lower by 15 K than that of the host materials. However, this T_c is slightly higher than that of $IBi_2Sr_2CaCu_2O_y$. This indicates that intercalation of silver and additional iodine into $IBi_2Sr_2CaCu_2O_y$, which expands lattice parameter from 19.1A of $IBi_2Sr_2CaCu_2O_y$ to 22.8A, has small influence on the superconducting transition. Irreversibility field B_{irr} was measured by the dc magnetization method. Magnetic field was applied parallel to the c-axis. No change of B_{irr} – t (t= T/T_c) curves was observed after the intercalation although the c-axis was significantly expanded. It seems that flux dynamics or flux pinning is almost independent of the distance between Cu-O layers. This suggests that the increase of the distance between Cu-O layers has little influence on the coupling of the layers. Because the coupling of Cu-O layers is very weak and each pancake vortex behaves almost independently even for host Bi-2212, the increase in the distance between Cu-O layers has no effect on the behavior of panacake vortices.

Related Papers

Preparation of Ag-I Intercalated $Bi_2Sr_2CaCu_2O_y$ Superconductor, H. Kumakura, J. Ye, H. Kitaguchi, K. Togano, and J. Shimoyama, Jpn. J. Appl. Phys. 32 (1993): L894–L896.

Superconducting Properties of Ag-I Intercalated $Bi_2Sr_2CaCu_2O_y$, H. Kumakura, H. Kitaguchi, N. Tomita, and K. Togano, Physica C 235–40 (1994): 939–40.

109 The Formation Mechanism of Textured $Bi_2Sr_2CaCu_2O_y$ on Ag Tapes

April 1994 to March 1995

H. Kumakura, 1st Research Group

Keywords: high temperature x-ray diffraction, oil quenching

Melting and subsequent slow cooling of Bi-Sr-Ca-Cu-O layer on Ag substrate brings about precipitation of grain oriented $Bi_2Sr_2CaCu_2O_y$(Bi-2212). This textured Bi-2212 shows high critical current density J_c at low temperatures, and is promising for high field applications. For the further improvement and better reproducibility of J_c values, it is very important to investigate the mechanism of this grain alignment. In this experiment, we observed the phase evolution of a Bi-Sr-Ca-Cu-O/Ag composite tape during cooling from a molten state applying the high-temperature x-ray diffraction method and oil-quenching technique. At the partially molten state (~900 °C), the solid phases of $(SrCa)_2CuO_3$(21) and Cu-free-phase were observed. During the slow cooling from the molten state, the amount of (21) and Cu-free phases decreased, and at ~880 °C another impurity phase of $(SrCa)CuO_2$(11) appeared. At around 860 °C, Bi-2212 phase appeared and grew rapidly. First nucleation of Bi-2212 occurred at the surface of the liquid phase. However, the appearance and growth of the Bi-2212 phase on the surface was too fast to catch the early stage of Bi-2212 crystal growth. All of the x-ray diffraction peaks from Bi-2212 phase corresponded to (00l) diffraction, suggesting that c-axis grain alignment occurred at the first stage of the Bi-2212 precipitation. This initial grain alignment at the surface seems to be very important for the texturing of the whole oxide layer. With decreasing temperature the Bi-2212 crystal growth slowly proceeded from the surface to the inner area with the a-b plane almost parallel to the surface. The amount of (11) and Cu-free phases decreased with decreasing temperature, however, these impurity phases did not disappear completely. The amount of these impurity phases should be reduced as small as possible for the good grain alignment of Bi-2212, because they obstruct the Bi-2212 growth along the surface.

Related Papers

Effect of Ag on Microstructure and Superconducting Properties of $Bi_2Sr_2CaCu_2O_x$, H. Kumakura, T. Hasegawa, H. Kobayashi, H. Kitaguchi, K. Togano, and H. Maeda, Adv. Cryogenic Engineering 40 (1994): 1–8.

Formation and Growth Mechanisms of $Bi_2Sr_2CaCu_2O_y$ on an Ag Substrate in the Partial Melting Method, T. Hasegawa, H. Kobayashi, H. Kumakura, and K. Togano, Supercond. Sci. Technol. 7 (1994): 579–82.

110 Developments of High-T_c Superconducting Thick Films and Tapes by Various Spraying Methods and by Internal Oxidation

April 1988 to March 1995

H. Maeda, High magnetic Field Research Station

Keywords: high-T_c superconductor, thick film, plasma spraying, flame spraying, flame spraying, internal oxidation, magnetic shielding

We studied superconducting properties and microstructures of Bi-based and Y-based high-T_c oxide thick films and tapes prepared by plasma spraying, flame-spraying, and internal oxidation. Especially, we have fabricated a prototype vessel for superconducting magnetic shielding, which is very useful for medical application such as neuromagnetics.

$(Bi,Pb)_2Sr0_2Ca_2Cu_3O_{10}$ oxide thick films with 770 μm in thickness were deposited by plasma spraying on the outer surface of a Ni-based alloy pipe with 320 mm in diameter and 660 mm in length. The films have a silver buffer layer to prevent the interdiffusion between the oxide and substrate. The films were post-annealed for 100 h at 1110 K. The superconducting properties and microstructures of the films are strongly affected by plasma power; the best is 11 kW. The best film obtained so far has a T_c of 101 K and a J_c of 170 A/cm^2 at 77 K. For the film we measured the magnetic shielding factor, S, which is (applied magnetic field)/(detected magnetic field inside the pipe), by a RF-SQUID magnetometer at an applied field of 4×10^{-4} parallel to the pipe axis. The facter, S shows above 10^3 at the center of the pipe, which is the positon almost equal to the pipe diameter from the pipe end. The value of S is in good agreement with the calculated value, suggesting that the film gives the ideal magnetic shielding. Furthermore, we detect no difference in S in the low frequency range of 0.1 to 10 Hz, which is very important for the measurement of neuromagnetics.

Flame spraying using a mixed gas of oxygen and propylene (or acetylene) was applied to fabricate $Bi_2Sr_2Ca_1Cu_2O_8$ thick films. The films with 300 μm to 1 mm in thickness were deposited on a silver plate substrate heated at 673 K. The films have a T_c of 90 K without post-annealing.

Three kinds of Ag alloys including the compositons of $Y_1Ba_2Cu_3$, $Bi_2Sr_2Ca_1Cu_2$ and $(Bi,Pb)_2Sr_2Ca_2Cu_3$ were prepared by melting. Small plate-like specimens of the alloys were initially oxidized at temperatures of 973 to 1023 K in oxygen atmosphere, and annealed at various temperatures. For all the samples continuous high-T_c oxide layers are formed in the Ag matrix, and their T_c's almost equal to those of bulk samples. The best Ic obtained so far is about 50 A for $Bi_2Sr_2Ca_1Cu_2O_x$.

111 Development of Extremely High Field Magnets

April 1988 to March 1995

H. Maeda, High Magnetic Field Research Station

Keywords: high-field magnet, long-pulsed magnet, hybrid magnets, high-field superconducting magnet, high resolution magnet

In order to measure and evaluate the high-field properties of high-T_c oxide superconductors, we have developed several high-field facilities, such as 80 T class long-pulsed magnet, a 40 T class hybrid magnet, a 20 T class large-bore superconducting magnet, and high-resolution magnets. We also fabricated an automatic helium refrigeration/liquefier for cooling down the large superconducting magnets and several measuring facilities used in these magnetic fields.

We have successfully developed A Cu-Ag microcomposite wire, which is very promising material with high strength and high conductivity for high-field long-pulsed magnet, because both large hoop stress and large Joule heating are the most serious problems for operating the pulsed-magnet. We wound the Cu-Ag microcomposite rectangular wires into several pulsed magnets, which were cooled down to 77 K and energized by the large pulsed-discharge currents from capacitor bank systems. One of them could generate non-destructively 73.4 T with duration time of 5 msec in a 10 mm bore. The other one could generate non-destructively 65.3 T with duration time of 100 msec in a 16 mm bore. We have measured the Haas-van Alphen effects of heavy fermion compounds and far-infrared cyclotron resonance by using these pulsed fields.

A new insert magnet, No. 4 coil, has been developed for the 20 T class large-bore superconducting magnet system. By using the No. 4 coil, we have been succeeded in generating 21.5 T in a clear bore of 61 mm without quenching. The field is also a new world record generated by a metallic superconducting magnet. The 21 T superconducting magnet system is now being used, for instance, for the coil tests of high T_c oxide superconductors. Under a background field of 20.9 T a small test coil of Bi-2212 oxide double pancake coil has generated totally 21.8 T in a 13 mm clear bore, which is also the highest field record generated by a full superconducting magnet system.

We have completed the fabrication of the 40 T class hybrid magnet system including a 15 MW dc power supply, a 15 MW water-cooling system, a helium liquefied/refrigerator, and a hybrid magnet composed of an outer superconducting magnet and inner water-cooled magnet. The outer superconducting magnet is designed to generate a background fields up to 15 T in a clear bore of 400 mm. The test operation up to 14.2 T has been performed successfully without quenching. We have fabricated two kinds of inner water-cooled magnets (Insert A and Insert B), which are designed to generate incremental fields up to 25 T and 20 T in clear bores of 30 mm and 50 mm, respectively. Test operations of hybrid mode have been performed up to 32.1 T and 35.7 T with using the INsert B and the Insert A, respectively. Considering the clear

bore sizes, these values are both the new world records of steady magnetic fields.

In this year we moved all the high-resolution magnet systems from Tokyo to Tsukuba. We have already completed the installation, the piping, the cabling, and the adjustment of the systems. By using the high-resolution magnet systems, we progressed the studies on the high field properties of the oxide superconductors, the heavy fermion matters, the graphite intercalations, the catalyzers, and the organic conductors. In particular, we succeeded in observations of new interesting high-field properties about UPt_3 and CeSb.

Related Papers

High Field Installations at the Tsukuba Magnet Laboratories of NRIM, K. Inoue, T. Takeuchi, T. Kiyoshi, T. Asano, Y. Sakai, K. Itoh, and H. Maeda, to be published in Physica B (1995).

Present Status and Future Plan of the Tsukuba Magnet Laboratories, H. Maeda, K. Inoue, T. Kiyoshi, T. Asano, Y. Sakai, T. Takeuchi, K. Itoh, and G. Kido, to be published in Physica B (1995).

[112] Fabrication of Oxide superconductors Using YAG Laser Irradiation

April 1986 to March 1995

H. Wada, High Magnetic Field Research Station

Keywords: critical current, pinning center, yttrium-based superconductor

Research efforts are being made at NRIM to fabricate oxide superconductors which may be used above liquid nitrogen temperature. It is known that the most practical superconducting property, critical current, strongly depends on the process based on which the superconductor has been fabricated. Critical current is essentially determined by pinning centers introduced into the superconductor during the fabrication process. Thus, ion or neutron irradiation has been adopted to induce appropriate microstructures. YAG laser irradiation may have these both possibilities by rapidly changing the sample temperatures in the heat treatment temperature range and creating a desirable superconducting phase with different non-super-conducting phases as pinning centers.

A sintered mixture of powders corresponding to yttrium-based superconductor compositon (123 phase) was placed on a movable stage and irradiated in the following conditions; irradiation power = 10 to 60 W, laser beam diameter = 34 to 500 mm ϕ, sample moving speed = 0.025 to 10 mm/s. Based on x-ray diffractometry it turned out; (1) that samples were heated above 1273 K and Y_2O_3 phase was observed, (2) that non-superconducting 211 phase was formed by subsequent quenching, and (3) that superconducting 123 was not formed since the sample failed to stay at the appropriate temperature range long enough.

Heat treatment of irradiated sample at 1173 K resulted in the formation of the superconducting 123 phase. Thus, the present process could not directly produce a superconducting phase, but introduced pinning centers. The process was applied to bismuth-based superconductors as well and similar results were obtained. The process was then refined by adopting a thermal imaging technique precisely monitoring sample temperature and temperature distribution.

[113] Developments of High-Field Multifilamentary Superconductors Made of Intermetallic Compounds

April 1992 to March 1995

K. Inoue, High Magnetic Field Research Station

Keywords: multifilamentary superconductor, Nb_3Al, rapid-quench, deposition

Stoichiometric Nb_3Al (A15 phase) is one of the promising superconductors having superior high-field properties to those of the commercially produced Nb_3Sn. However, it is very difficult to fabricate a Nb_3Al multifilamentary conductor, showing excellent high-field properties, through diffusion reaction process. We proposed a new fabrication process of Nb_3Al multifilamentary wire, in which a composite wire, composed of Nb matrix and Nb/Al microcomposite filaments, is rapid-heated by direct current transport and then rapid-quenched into a Ga bath continuously. Through this process, Nb/Al microcomposite filaments are changed into Nb-Al super-saturated bcc filaments, which is not superconductor above 4.2 K. However, as the rapid-quenched wire is heated at 700–850°C, Nb_3Al A15 phases are deposited from the supersaturated bcc filaments and show excellent high-field superconducting properties. We found that the finer microstructure of Nb/Al microcomposite filaments results in the better high-field properties. The best values of T_c, H_{c2} (4.2 K), and J_c(4.2 K, 20 T) obtained for the Nb_3Al multifilamentary wire are 17 K, 26–27 T, and 3–4 × 10^4 A/cm^2, respectively. The J_c values are 2–3 fold larger than those of the commercially available Nb_3Sn multifilamentary wire. We fabricated a Nb_3Al multifilamentary wire with about 10 m length, which was cut into many pieces for measuring the I_c dispersion on position. The I_c dispersion was less than 20%. Bending effects on this wire were also studied and made clear that the Nb_3Al multifilamentary wire has a excellent tolerance to mechanical strain. We are now fabrication a long Nb_3Al multifilamentary wire of 120 m length for making a Nb_3Al small test coil.

This research was performed in collaboration with Hitachi Cable Co. Ltd.

Related Papers

Nb_3Al Multifilamentary Wires Continuously Fabricated by Rapid-Quenching, Y. Iijima, M. Kosuge, and K. Inoue, Advances in Cryogenic Engineering, 40A (1994): 899–905.

Superconducting Properties of Nb_3Al Multifilamentary Wires Fabricated Continuously by Rapid-Quenching, Y. Iijima, M. Kosuge, T. Takeuchi, and K. Inoue, to be published in Advances in Cryogenic Engineering.

Magnetic materials

(114) Development of a Superconducting Magnet for Magnetic Separation

April 1995 to March 1999
H. Kumakura, 1st Research Group
Keywords: Bi-based oxide superconductors, critical current density, helium-free magnet

Magnetic separation has been used for many years to correct magnetic particles such as iron ore. For the efficient magnetic separation, field gradient ∇B should be large because the magnetic force is proportional to ∇B. High Gradient Magnetic Separators (HGMS) use a finely divided ferromagnetic matrix to create large gradient and to correct even paramagnetic materials. In most case, however, conventional copper electromagnets are being used for HGMS, and the magnetic fields available are limited to ~2 Tesla by the saturation of iron. In addition, generation of magnetic fields in a large volume is costly in terms of electric power, iron and copper. For example, a large electromagnet for kaolin separation may consume as much as 500 kW electric power, all of which is converted into heat. For these reasons superconducting magnets for magnetic separation were proposed as early as 1970. The advantage of superconductivity is the lack of electric power dissipation at a constant field. However, conventional metallic superconducting magnets usually require expensive liquid helium for cooling, which hinder the significant decrease of the running cost. High-T_c oxide superconductors that have transition temperatures, T_c, of 90–110 K may be used in liquid nitrogen whose cost is an order of magnitude lower than liquid helium. Cryocooler may also be used effectively to cool down an oxide superconducting magnet. This cryogen-free magnet should be very convenient for separator magnet users because they are not accustomed to use liquid helium. Among the many oxide superconductors, grain oriented Bi-based oxides ($Bi_2Sr_2Ca_2Cu_3O_x$ and $Bi_2Sr_2CaCu_2O_y$) prepared by the powder in tube method or oxide-coating method show excellent critical current density J_c.

In this research program, we will develop a superconducting magnet for magnetic separation which can be operated without liquid helium. Bi-based oxide seems to be most promising for the magnet. But we will also investigate the feasibility of Tl-based oxides that show more excellent J_c-B properties at elevated temperatures.

115 Research on Materials Synthesis to Control of Magneto-Thermal Properties by Changing Size

April 1993 to March 1996
M. Sato, Physical Properties Division
Keywords: low temperature, fine magnetic particles, garnet solid solution

Several nanocomposite magnetic materials were synthesized by sol gel processing. The nanocomposites containing 10–20 wt% Fe were prepared by adding the appropriate amounts of an aqueous solution of ferric nitrate to a 50 mol% solution of tetraethoxysilane and ethanol, with a few drops of HF added as a catalyst. The nanocomposite containing 12 wt% Gd was also prepared by the similar processing without the catalyst. The magnetization measurements show the paramagnetic behavior between 4.5 and 77 K. This suggests the evidence of nano-scale magnetic composites, especially for the Fe base sample. Further direct measurements of the magnetocaloric effect are in progress.

Rare-earth distribution behaviors and lattice parameter changes on rare-earth substituted garnet single crystals grown using the Czochralski technique were studied in order to control magnetic properties as solid solution. Furthermore, properties of Czochralski-grown $RAlO_3$ (R: Dy, Ho and Er) single crystals were measured as magnetic refrigerants. Larger magnetic entropy change were obtained for ErAlO3 single crystal than that for $Dy_3Al_5O_{12}$ and $Gd_3Ga_5O_{12}$ which were used for the current magnetic refrigeration system to produce liquid helium.

This research was performed in collaboration with the Institute for Materials Research, Tohoku University.

Related Papers

Rare-Earth Distribution Behaviors and Lattice Parameter Changes on Rare-Earth Substituted Garnet Single Crystals, H. Kimura, T. Numazawa, and M. Sato, J. Meter. Sci. Lett. 13 (1994): 1164–68.

Properties of Czochralski-grown $RAlO_3$ (R: Dy, Ho and Er) Single Crystals for Magnetic Refrigeration, H. Kimura, T. Numazawa, M. Sato, T. Ikeya, and T. Fukuda, J. Appl. Phys. 77 (1995): 432–34.

Materials for energy application

(116) Design of Refractory Superalloys

April 1995 to March 2000
H. Harada, Materials Design Division

Keywords: computer modelling, refractory superalloy, creep strength, oxidation resistance

The temperature capability of the Ni-base superalloy has been improved by 400 °C since it was introduced in 1945; the capability of our latest single crystal superalloys is approaching 1100 °C. However, it is obvious that there will be a limitation which comes from the melting point of Ni(1453 °C) as long as the alloys are based on it.

In this new project we design "Refractory Superalloys" with help of computer modelling based on a statistical thermodynamics calculation. Metallic elements with high melting points are examined for possible use as the base metal as well as the alloying elements in the Refractory Superalloy. Characterization of the micro-structure and evaluation of the ultra-high temperature (~2000 °C) creep strength / oxidation resistance will also be carried out.

(117) Research on Utilization Technique of "Data-Free-Way" System for Nuclear Materials

April 1995 to March 2001

M. Fujita, 2nd Research Group

Keywords: Data-Free-Way, distributed database, advanced nuclear materials, data share, transmutation

Data systems having a huge material database and effective computer utilized tools are required for the alloy design or selection of advanced nuclear materials. However, there are limitations in storing numerous material properties into the database and developing a variety of tools for material design in each research laboratory. Under the cooperation among National Research Institute for Metals (NRIM), Japan Atomic Energy Research Institute (JAERI) and Nuclear Fuel Development Corporation (PNC) with different special field, the pilot distributed database system for development of nuclear materials called "Data-Free-Way" has been built since April of 1990.

In order to complete the "Data-Free-Way" system, the project on the second stage was started in 1995 under the cooperation among NRIM, JAERI, PNC and Japan Information Center of Science and Technology (JICST). The aim of this project are to store the data in the database and to develop useful computer utilized tool for data analysis and simulation codes for various phenomena under irradiation environments.

In NRIM, the data systems having a statistical analysis on materials properties and a simulation of behavior including nuclear transmutation and radioactivation are created in addition to the completion of the database. The system will be easily used mutually through the network and aid operate for the nuclear materials design and selection.

118 Development of Third-Generation Nickel-base Single Crystal Superalloys

April 1994 to March 1997

T. Yamagata, Materials Design Division

Keywords: alloy design, SC-alloy, low density, lattice misfit

The purpose of this research is to develop new type single crystal superalloys which has relatively low density (8.5) and excellent high temperature strength, by the use of alloy design computer program developed in NRIM. As the first step, alloy with high strength at intermediate temperature was searched with TMS-63 as the base alloy. Optimum alloy composition was searched by alloy design computer program on the conditions limited by structural parameters such as lattice misfit, γ' volume fraction, composition of alloy elements such as Cr and Re content, solubility index, density, heat treatment window. Single crystal of designed alloy was directionally solidified and mechanical properties and structural parameters were evaluated after solution heat treatment, and these data are fed back to the alloy design program to improve predictive accuracy of alloy design program. In order to study the creep mechanism of SC-alloy at temperature higher than 1300 K, new type of creep test machine equipped with Non-contact type elongation measuring apparatus was developed and creep test was started.

Collaboration Research

Computer modeling of alloys (Rolls-Royce plc, U. K.)

Single crystal superalloys for future (IHI, Japan)

119 Environmental Degradation of Structural Materials for Light Water Reactors

April 1991 to March 1996

T. Ishihara, Failure Physics Division

Keywords: low cycle fatigue, crevice, stress corrosion cracking, database

The purpose of this research is to clarify the elemental process of environmentally assisted cracking (EAC) of structural materials for LWR in high temperature water and systematize the related data for life prediction of components. In this year, the effect of crevice on low cycle fatigue behavior in high temperature water, and systematization of elemental process of damages based on a related database have been conducted.

The effect of crevice on low cycle fatigue behavior of low alloy pressure vessel steels was investigated in high temperature water by means of applying a spill collar made from the same material onto the round bar specimen. From the comparison of both specimens with and without collar, it was found that in the case without collar relatively large corrosion pits were formed and the crack length was longer than in the case with collar. It

resulted in that the fatigue life of specimen with collar was longer than that without collar due to a poor dissolved oxygen (DO) concentration in the crevice water.

A relational database has been constructed mainly about properties for stress corrosion cracking (SCC) in high temperature water. It has a capability to analyze any correlation between damage parameters such as percentage of cracked specimens, ratio of intergranular SCC (IGSCC) on the fracture surface, and environmental parameters such as temperatures, pH, DO, etc.: a function very useful for the construction of a damage map for related materials in the relevant environments.

For example, the correlation was investigated between the percentage of cracked specimens obtained by U-bend test and the ratio of IGSCC by slow strain rate test (SSRT) in terms of DO concentration and temperature. It was found that high DO concentration gave severe damage for both tests, and that the maximum damage in the U-bend tests was revealed at middle or low temperature, while the damage in the SSRT tests was increased with increasing temperature. These trends could be well explained in terms of the difference of oxide films and the stress conditions for both specimens.

120 Computational Mechanical Property Analysis with Consideration to Microstructures of Nuclear Reactor Materials

April 1994 to March 1996

*H. Shiraishi, M. Tabuchi and Y. Nakasone**

Keywords: helium embrittlement, computer simulation, finite element method, bubble morphology, work hardening ability

The helium embrittlement was analyzed by applying two dimensional elastic-plastic finite element method based on continuum mechanics. It was shown that the mechanical properties such as uniform elongation, total elongation and tensile strength can be evaluated by assuming the yield stress, the work hardening coefficient and the helium bubble morphology at grain boundary.

This program was written by author and treat large scale plastic strain. In this program, triangular mesh elements were used assuming plain stress condition. Mises yield condition and work hardening law of Swift type are applied here. The helium embrittlement was assumed here to be caused by local necking of region between grain boundary bubbles and the infinite arrangement of helium bubbles along grain boundary is approximated by repeated boundary condition. The effect of work hardening ability and bubble morphology at grain boundary are estimated.

The case of bubble size of 1.0^{-8} m, bubble density of 10^{7} /m and grain size of 2.0^{-5} m was investigated at first. The effect of work hardening is divided into three categories. When n is more than 0.1, no helium embrittlement was observed. This is because the multiaxiality due to existence of bubbles resulted in the increase of hydrostatic stress component and a kind of notch strengthening. When n is less than 0.03, the grain interior remained in elastic state except the neighborhood of grain boundary and severe embrittlement occurred. For the intermediate n value, the elongation decreased from more than 50% to about 0.1% sharply. Thus, calculation revealed the work hardening ability plays essential role and why the helium embrittlement is limited to high temperature.

121 Real-Time Investigation on Surface Reaction and Defect Growth Processes under Irradiation

April 1994 to March 1999

M. Kitajima, 2nd Research Group

Keywords: irradiation, surface reaction dynamics, growth process of surface defect, real-time observation

We are studying on reaction dynamics of material surface, under irradiation of ions, plasma, molecular beams and light. The purpose of this research is to elucidate mechanisms of the irradiation activated surface reaction including surface damage process and to develop the fast analytical techniques with emphasis of real-time observation of dynamic process. Investigations on cluster reactions in gas phase and with surface are also targets. From this viewpoint, we have started studies on reactive scattering of molecular beam with solid surfaces using a resonance enhanced multiphoton ionization (REMPI) spectroscopy, in order to get direct information on molecular dynamics during surface chemical reaction. In the REMPI measurements, the desorbing molecules from the surface are ionized with a YAG-pumped dye laser, introduced into the TOF chamber and detected by a multichannel plate. We have obtained a rotational-vibrational state distribution of the SiO molecule desorbing from Si surface in reaction with O_2 beam. The REMPI result obtained here gives a clue for further development of the study on surface chemical reaction dynamics. For real-time Raman measurements during ion irradiation, we are investigating time-dependent changes in phonon correlation length of crystal surfaces of graphite, silicon, and gallium arsenide, and recently have got a new result supporting an idea of phonon confinement due to defects produced by ion irradiation. Plasma-solid interaction is also being studied by using *in situ* real-time ellipsometry.

*Tokyo Science University

We have found a strong sample bias dependence of growth rate of ultra thin oxide film in oxygen plasma. A basic study of technique on the generation of cluster beams is now in progress.

Related Papers

Resonance Enhanced Multiphoton Ionization Detection of SiO Desorbing from a Si(111) Surface in Reaction with O_2, K.G. Nakamura and M. Kitajima, Appl. Phys. Lett. 65 (1994): 2445–46.

Real-Time Measurements of GaAs under Low Energy He+ Irradiation, K.G. Nakamura, E. Asari, and M. Kitajima, J. Mater. Sci. Lett. 13 (1994): 1767–68.

Phonon Confinement in GaAs by Defect Formation Studied by Real-Time Raman Measurements, K. Ishioka, K.G. Nakamura, and M. Kitajima, Phys. Rev. B, in press.

Effects of DC-bias on Plasma Oxidation Rate of Solid Surface, M. Kitajima, I. Kamioka, K.G. Nakamura, and T. Kawabe, Proc. 1994 Int. Conf. Plasma Physics, in Iguaz (Brazil), Nov. 1994.

122 Fundamental Research on Application of New Functional Materials to Passive Components

April 1990 to March 1995

T. Ishihara, Failure Physics Division

Keywords: shape memory alloy, SCC, shape recovery

In this study, (1) stress corrosion cracking (SCC) susceptibilities of Ni-Ti alloys in high temperature water and (2) the mechanisms of improvement of shape recovery in Fe-based shape memory alloy were evaluated.

1. The effects of composition, heat treatment and test temperature on the SCC behavior of Ni-Ti shape memory alloys in the high temperature pure water were determined. The tests were conducted by using slow strain rate test machine. The 50–50.9 at.% Ni-Ti shape memory alloys were subjected to SCC which was initiated from the scratches. The 50 at.% Ni-Ti was less susceptible to SCC than 50.5 % Ni-Ti or 50.9% Ni-Ti alloys. The solution treated specimens revealed severe cracking than tempered or tempered-after-annealing specimens. Under the aerated condition at 473 K, SCC occurred in all of Ni-Ti alloys tested and their susceptibilities to SCC were similar to those at 573 K. The cracks were initiated from scratches at 473 K as well as at 573 K. The fracture mode at 473 K was the same to that tested at 573 K.
   In the case of Fe-based shape memory alloy, specimens at martensitic phase were susceptible to SCC for low temperature and low oxygen concentration environment. The martensitic Ni-Ti alloys, however, did not crack in the deaerated water at 287 K.
2. The following thermomechanical treatment was performed for Fe-14Mn-6Si-9Cr-5Ni(mass %) alloy. Specimen was first solution-treated at 1320 K for 1.8 ks, cold rolled by 10% at room temperature and then heated at 970 K for 0.6 ks. By this treatment, the shape recovery strain is increased to 80% from 50% in the as-solution treated state.
   The martensitic transformation involved in exhibiting shape memory effect in this alloy system is the f.c.c. to h.c.p. transformation induced by deformation at room temperature and its reverse transformation (h.c.p. → f.c.c.) on heating. In order to elucidate the transformation mechanism which leads to the improvement of shape recovery, we have examined the distribution of martensite plates with various widths in the as-solution treated specimen and the thermomechanically treated specimen.
   By taking lattice images and structure images with a high resolution electron microscope, it was possible to measure the width of martensite plate in the subnanometric scale up to 0.2 nm.
   The histogram of number of martensite plates against width of martensite plate was obtained by examining along a total length of 1600 nm perpendicular to the $(111)_{fcc}$ habit plane. It was found that there is a remarkable difference in the histogram for the thermomechanically treated specimens and non-thermomechanically treated specimens. In the former case, the number of martensite plates with extremely small widths (less than 4 nm) is very large and it decreases rapidly with increasing width, while, in the latter case, the number of existing martensite plates is not dependent on plate width. This fact means that f.c.c. to h.c.p. transformation in the former case is accomplished by the random stacking fault mechanism, while, in the latter case, the transformation proceeds mainly by the pole mechanism. As a result, a large number of parent f.c.c. crystals are mixed with h.c.p. martensite in the former case and hence, there is no need for nucleation of f.c.c. phase in the reverse transformation. Furthermore, there are many Shockley partial dislocations associated with the tips of those thin martensite plates, which are suffering the back stress field from the neighboring austenite phase. These two facts greatly promote the reverse transformation, and accordingly, increase the shape recovery on heating.

123 Research on Distributed Database for Advanced Nuclear Materials

April 1991 to March 1995

M. Fujita, 2nd Research Group

Keywords: Data-Free-Way, distributed database, advanced nuclear materials, data share

New material-searching using database systems is required for nuclear technology. But it is very difficult at present to describe numerous nuclear materials properties because of their complexity in nature and pre-standardized status of information on new materials. The stored data consist of the properties under environments from normal to severe states, such as high temperature, stress loading and/or corrosive ones under heavy irradiation. Therefore, a wide spectrum of special knowledge of different fields is necessary.

A distributed database system, for designing and selecting has been built under the cooperation of National Research Institute for Metals (NRIM), Japan Atomic Energy Research Institute (JAERI) and Power Reactor and Nuclear Fuel Development Corporation (PNC). In 1993, other three research organizations: National Research Laboratory of Metrology (NRLM), Ship Research Institute (SRI) and the Japan Information Center of Science and Technology (JICST); were connected to this system. The system is called as "Data-Free-Way" and has been built since April of 1990. This project is to build the system within five years, focusing on advanced nuclear materials, such as new structural metals, intermetallic compounds, ceramics and composites. Input data will be captured from results of Fundamental Research on Nuclear Materials supported by Science and Technology Agency of Japan.

The data for the database is collected from several research organizations under a certain cooperation to collect sufficient data and to maintain quality of data. An utilization technique of the system are also required to get refined information from the stored data. An example of the merit by using the system is discussed about tensile and creep properties in Type 316 stainless steel.

Related Papers

Some Computer Utilized Alloy Designed, M. Fujita, Y. Kurihara and T. Noda, Proc. Japanese Polish Seminar on Advanced Computer Simulation, Tokyo (1993): 103–09.

Data System of Transmutation and Radioactivation for Nuclear Material Design, M. Fujita, T. Noda, and H. Shiraishi, 2nd Japan China Symp. on Mat. for Advanced Energy Sys. & Fission and Fusion Eng. (1994): 454–59.

Present Status and Prospect of "Data-Free-Way" (Distributed Database for Advanced Nuclear Materials, H. Nakajima, N. Yokoyama, F. Ueno, S. Kano, M. Fujita, Y. Kurihara, and S. Iwata, J. Nucl. Mater. 133 (1994): 1171–74.

Development of "Data-Free-Way" Distributed Database System for Advanced Nuclear Materials, F. Ueno, S. Kano, M. Fujita, Y. Kurihara, H. Nakajima, N. Yokoyama and S. Iwata, Nucl. Sci. Technol no. 12 (1994) 1314–1334.

Materials for environmental performance

124 Fundamental Study on Creation of Micro Stereom Fabrics by Powder Technology

April 1993 to March 1996

K. Halada, 5th Research Team

Keywords: powder, structure control, ecomaterial, Fe-Fe composite, LCA

Minerals of biological origin have the microstructure to perform functions efficiently. It is well-known that spicules or echinoderms have three dimensional framework and porous structures, to perform efficient mechanical properties. Powder technology is noteworthy artificial technology for inorganics to create the mimetic microstructure of natural materials, because the powder can be divided to small elemental particles and can be synthesized under optional controllings. As the first step of this study, we apply the powder-technology to the creation of Fe-Fe composite for structure-controlled recyclable materials.

Fe-Fe composite consists of strongly-drawn Fe fibers and porous matrix of sintered Fe. Strongly-drawn Fe fiber has high strength by filament structure in itself. Sintered Fe porous-matrix supports fibers and gives bending strength. As fiber and matrix have same composition of Fe and its mechanical properties are obtained by microstructure control, this composite is expected to have simultaneously good property and recyclability. As the microstructure inside of the fiber is easily damaged by heating, ultra fine powder of Fe is used in order to combine fibers and powders at lower temperature. Fe-fiber is coated with UFP, arranged in Fe powder in parallel, and sintered below 500 °C above which strengthened structure of the fiber sustains damage. This Fe-fiber-reinforced porous Fe composite has better deflective strength than sintered Fe of the same density. MLCA analysis is conducted on this composite to assess the achievement of ECOMATERIALS.

Related Papers

A Trial for Ecomaterials; Possibility of Manufacturing of Fe-Fe Composite, N. Itsubo, K. Halada, K. Minagawa, and R. Yamamoto, Funtai oyobi Funmatsuyakin, 41 (1994): 1361–66 (in Japanese).

Environment Life Cycle Analysis of PM Products, K. Halada, K. Minagawa, and K. Yagi, Funtai oyobi Funmatsuyakin, 41 (1994): 1383–88 (in Japanese).

Bio-Materials, etc.

125 Spectroscopic and Electrochemical Investigations of the Metal Complexes with an Unusual Electronic Structure

April 1994 to March 1997

H. Isago, Chemical Processing Division

Keywords: metal complex, antimony, phthalocyanine, electronic structure

The fabrication of molecular devices, where one molecule functions as one device, is one of the most attractive and challenging theme in current and future science. Some materials in biological systems, such as proteins (including enzymes), can be considered as well-designed molecular devices. In numbers of such materials in biological systems, unusual electronic structures have been often observed. Therefore, it is a key step to the fabrication of molecular devices to find out compounds with an unusual electronic structure. In this meaning, metal complexes are particularly of interest as model compounds for such materials in biological systems because numbers of such materials contain some metal ions(s) in their reaction centers which have an unusual electronic structure.

We have investigated some metal complexes of phythalocyanine, which have attracted much attention as a group of new advanced materials in recent years. For example, it was found in this laboratory that bis(phthalocyaninato)lanthanoids(III) exhibited remarkable electrochromic properties in organic solvents and in solid state as thin film. In these compounds, unlike normal molecular compounds, a hole is created in the complex molecule. This work is intended to understand the unusual electronic structures of the above-mentioned bis(phthalocyaninato)lanthanoids(III) complexes from the view points of $\pi - \pi$ interaction between the two cofacial phthalocyanine chromophores mainly by using spectroscopic, electrochemical, and spectro-electrochemical techniques. Furthermore, we will try to prepare previously unknown antimony-phythalocyanine complexes. It is because that antimony is stable in trivalent oxidation state and has a close ionic radius to those of lanthanoids(III), and hence, bis (phthalocyaninato)antimony(III), which has a hole in the molecule, is expected to form.

The results of this work will serve not only for the fabrication of molecular devices but also for further understanding of supramolecular chemistry.

126 Fundamental Study on Biocompatibility of Materials

April 1994 to March 1999

M. Sumita, Biomaterials Research Team

Keywords: biomaterials, cytotoxicity, cell adhesion force, fretting fatigue, bio-simulator, in vivo tests

Towards 21st century, the aged society progresses, and requirements for affluent quality of life are getting stronger. Numbers of the aged and the physically challenged implanted in their bodies increase. It is important that artificial organs and medical devices exist and function in their bodies without any trouble for many years until they die. Release of metallic ions and debris from materials implanted in body should be avoided, because they always or infrequently cause carcinogenicity, physical deformity enhancement and allergies. Unexpected failure of artificial organs and medical devices implanted also should be avoided, because the reluctant re-operation forces the patient physical and mental pains. Therefore, non toxicity, adhesion to tissue, control in bioreaction caused by foreign bodies, sufficient resistance to corrosion and wear, and long fatigue life are considered as necessary characteristics for the used in vivo conditions.

As metallic materials had the higher strength and the higher toughness than all of the other materials, 316L stainless steel, Co-Cr-Mo alloy, Ti-Al-V alloy, etc. have experimentally been used as biomaterials, though those alloys had been developed for other applications. Therefore, a capability exists in development of other materials with higher biocompatibility than those being used as biomaterials. The research conducted here is the accumulation of fundamental data to develop new biomaterials, which are superior in biocompatibility in living bodies.

The content of the present research subject is as follows:

1. Quantitative evaluation and systematic interpretation of cytoxicity of bio-materials.
2. Measurements of cell adhesion force to various materials and observations of cell response to mechanical stimulation by a modified atomic force microscope.
3. Measurements of corrosion, wear, fatigue, and fretting fatigue properties of biomaterials under a quasi-biological environment.
4. Reliability tests and standardization of artificial hip joints by a simulator having been developed.
5. Corrosion and fretting fatigue tests of biomaterials in animal bodies, being carried out by cooperative researches.

Processing

Separation and synthesis

⑫⑦ Development of Magnetic Separation Control System

April 1995 to March 2000
T. Ohara, Strong Magnetic Field Research Station
Keywords: fine particles, magnetic separation, magnetic chromatography

Progress in applied superconductivity technologies has resulted in the development of superconducting magnets with excellent operability. Consequently, the dream of applying superconducting magnets to many different areas has been broadened. In particular, magnetic separation is a promising application field for strong magnetic field occupying large areas. The primary advantages of magnetic separation, those being energy saving, compact size, and increased speed become visible only after the system is superconductorized. The full-scale application of this process will also contribute greatly to the preservation of global environments.

We will develop the key system technologies of application of high T_c superconducting magnets to magnetic separation. Moreover, we will verify our feasibility study on magnetic chromatography which can separate chemically similar but magnetically dissimilar materials, such as lanthanide and actinide elements. The feasibility study suggests the potential of separating very weak paramagnetic materials which we have not been able to deal with through the conventional high-gradient magnetic separation techniques.

This research is performed in collaboration with the Electrotechnical Laboratory, AIST, MITI.

Related Paper

Feasibility of Using Magnetic Chromatography for Ultra-fine Particle Separation, T. Ohara, S. Mori, Y. Oda, Y. Wada, and O. Tsukamoto, IEE Japan of Power & Energy '95, (1995): 161–166.

128 Extraction from Metal to Gas Phase

April 1992 to March 1994
A. Fukuzawa, Chemical Processing Division
Keywords: thermal plasma, low pressure plasma jet, vaporization

Thermal plasma produced by transfer or non transfer type torch is widely used for melting metals and surface lining. However, its operating pressure is usually at atmospheric pressure because of the existence of plasma jet. In some case low pressure plasma jet is used, but its pressure is not less than 100 torr.

This research work is to investigate the behavior of plasma jet in lowered pressure of 10 torr order and apply to the gaseous extraction of tramp elements like Cu, Sn, Ga or Cr from liquid iron or steel by the help of ultra high temperature of plasma jet. To get the aimed pressure rotary pump of 6000 l/min was attached with plasma furnace. However, in the hot run, glow discharge was observed around 10 torr by gage. Extraction rate of above elements is investigated by varying the pressure, gas composition and power supply.

This technology can be applied for the extraction of various kinds elements from molten metals and alloys, and especially from recycled scrap.

Gaseous process

129 Study on Atomic Scale Engineering of High Performance Films

April 1994 to March 1997
T. Hatano, 1st Research Group
Keywords: thin films, atomic scale characterization, x-ray total reflection

The atomic scale engineering has been developed in the semiconductor field. The high performance materials are designed based on the prediction of quantum mechanics which rules the properties of materials in this dimension. The aim of this study is to extend this technique to the other materials such as high T_c superconducting oxides and molecular crystals. However, in these materials, the crystal structure is much more complicated and especially the molecules show a quite different characteristics in course of the film synthesis. The molecular beam epitaxy technique under ultra high vacuum and the electron diffraction technique are not the most suitable technique for these materials. To solve these problems, synthesis technique having higher selectivity and reactivity is necessary and the other probe should be installed instead of electron. As a new fabrication technique for these materials, we introduce a reactive deposition technique equipped with x-ray analysis system in the total reflection region.

X-ray analysis technique was applied to the artificially layered $Bi_2Sr_2Ca_{n-1}Cu_nO_{2n+4}$ films prepared by sequential sputter deposition. In the $\theta/2\theta$ diffraction spectrum at the grazing incidence, the oscillatory pattern can be observed which is due to the interference of the reflected x-ray from the surface and interface of the films. Such pattern can be observed between the Bragg peaks which exactly corresponds to the number of units in the films. The thickness of the films can be analyzed in the scale of one atomic layer by this analysis. The

atomically layer-by-layer synthesis can be established by this analysis. The superstructure of $Bi_2Sr_2Ca_{n-1}Cu_nO_{2n+4}$ system was successfully synthesized by applying these results. This technique can be extended in another two ways. One is the *in-plane* x-ray diffraction which reveals the surface structure and the texture of the films. The other is the fluorescent x-ray analysis of the surface. The composition of the film surface can be analyzed. We are planning to apply these techniques for the *in situ* analysis during synthesis of high T_c superconducting oxide films.

Related Papers

Structure and Properties of $Bi_2Sr_2Ca_{n-1}Cu_nO_{2n+4}$ Films Prepared by Sequential Sputter Deposition, T. Hatano and K. Nakamura, in Bismuth based High Temperature Superconductors, ed. H. Maeda and K. Togano, Marcel Dekker, New York, 1995.

Superconductivity in Bi-based Oxide Thin Films, T. Hatano and K. Nakamura, in the Proceedings of the 7th International Symposium on Superconductivity (ISS '94) Kita-Kyushu 1994.

130 Processing and Development of Isotopically Controlled Materials (ICM)

April 1992 to March 1996

T. Noda, 2nd Research Group

Keywords: isotopically controlled materials, ICM processing facility, isotope separation, chemical vapor infiltration

Materials composed of isotopically selected elements realize the essential solution of subjects such as induced activity, He embrittlement, and compositional change cause by reactions with energetic particles.

The objectives of the program are (1) R&D of *in situ* ICM processing facility (ICMPF) utilizing infrared multi-photon decomposition reaction, (2) search of working materials for isotope separation, (3) development of *in situ* synthesis of isotopically controlled SiC, Si_3N_4, BN etc. and (4) development of ceramics and their composites with advanced properties.

The isotope separation experiment using Si_2F_6 was conducted under the irradiation of pulse infrared laser at 930–985 cm^{-1}. SiF_4 with condensed ^{29}Si and ^{30}Si was produced at 944–967 cm^{-1} while ^{28}Si was concentrated in the residual Si_2F_6. The natural Si is composed of 92.23% of ^{28}Si, 4.67% of ^{29}Si and 3.10% of ^{30}Si. The optimum separation of each isotope mainly depends on the wavenumber of CO_2 laser. At present, $^{30}SiF_4$ of 43.3% and $^{29}SiF_4$ of 12% at maximum were continuously obtained with a yield of 4% at 951.20 cm^{-1} and 10% at 956.20 cm^{-1}, respectively. On the other hand, ^{28}Si concentration occurred in the residual Si_2F_6 and increased with increasing both wavenumber and laser power. The concentration of ^{28}Si was increased up to 99.65% at 952.923 cm^{-1} at 2.81 J. These results indicate massive silicon isotope can be easily obtained by the present process.

In order to conduct Si isotope separation with a high selectivity, it is necessary to prepare high purity Si_2F_6. The use of oxybenzene as a solvent for fluorination of Si_2Cl_6 was found to provide Si_2F_6 with a purity better than 99.9% with a conversion efficiency of 80%.

The simulation code, IRAC, calculating transmutation was improved by combining with a neutron transport calculation code to predict more precisely the transmutation of materials including ICM. Chemical vapor infiltration process to obtain SiC composite with a high purity and improved mechanical properties is being developed. It was required to use low oxygen SiC fiber to perform thermal stability of SiC/Sic composites above 1573 K.

Related Papers

Isotope Separation of Si by Infrared Multi-Photon Decomposition, H. Suzuki, H. Araki and T. Noda, Proc. 2nd Japan/China Sym. on Materials for Advanced Energy Systems and Fission and Fusion Engineering, (1994): 297–301.

Effect of Wavelength of Infrared Laser on the Isotope Selective Decomposition of Si_2F_6, H. Suzuki, H. Araki, and T. Noda, J. Japan Inst. Metals, 58 (1994): 1101–02.

131 Development of Shape Memory Thin Films Formed by PVD Method

April 1993 to March 1998

A. Ishida, 3rd Research Group

Keywords: micromachine, shape memory, Ti-Ni, sputtering

Micromachines such as micromanipulators and fluid microvalves are expected to be used in the near future in various fields such as biotechnology, medicine and the semiconductor industry. In order to produce such a micromachine, the development of an effective microactuator is essential.

We demonstrated that perfect shape memory effect and superelasticity effect can be achieved even in thin films of Ti-Ni formed by sputtering. Furthermore, we found that the shape memory effect was stable against thermal cycling. Even after 100 thermal cycles, the thin films of Ti-Ni still exhibited good shape memory effect. The good shape memory effect seems to come from the fine-grain structure of the sputter-deposited films. The grain size of the films was from 1 to 3 μm, which was smaller than that of bulk specimens, several ten microns. In addition to the grain size, the precipitates distribution in the thin films was also differ-

ent from that in bulk specimens for Ti-rich Ti-Ni composition. In the films, the second phase of Ti_2Ni precipitated inside the TiNi grain, while, in bulk specimens, it distributes on the TiNi gain boundary. Such differences in microstructure make the shape memory behavior of thin films different from that of bulk specimens and hence very interesting. We will continue to investigate the effect of heat treatment and sputtering conditions on the microstructure of Ti-Ni films to improve the shape memory behavior of the films.

Related Papers

Shape Memory Thin Film of Ti-Ni Formed by Sputtering, A. Ishida, A. Takei and S. Miyazaki, Thin Solid Films 228 (1993): 210–14.

Shape Memory Behavior of Ti-Ni Thin Films Annealed at Various Temperatures, A. Ishida, A. Takei, M. Sato, and S. Miyazaki, Proc. of 1994 Material Research Societies Fall meeting (1994) to be published.

132 Precise Composition Control of Ordered Alloys by Chemical Transportation Techniques

April 1992 to March 1995

H. Sasano, Physical Properties Division

Keywords: ordered alloy, chemical transportation

Ordered alloys are expected to have attractive properties. However, the properties are very sensitive to the composition of the alloy. It is hard to control the composition precisely by conventional methods. We tried to control aluminum concentration in Cu-Al, Ni-Al and Ti-Al by a chemical transportation technique. Mixture of aluminum chips and ammonium chloride and metal plates of starting material were separately placed in a sealed alumina tube. The tube was heated in a temperature gradient furnace. It was expected that aluminum chloride gas formed by the reaction of aluminum with ammonium chloride would decompose on the metal plate and then aluminum would diffuse into the metal plate. Aluminum concentration on the metal plate laid on the single phase regions in the binary phase diagram and kept constant values even when the heating duration changed. From these results, it was found that aluminum concentration in any single phase regions could be precisely controlled by this method.

Liquid state process

133 Solidification in the Strong Magnetic Field

April 1995 to March 1998

A. Fukuzawa, Chemical Processing Division

Keywords: dendrite growth, strong magnet, Seebeck effect, Lorentz force

In the dendritic crystal growth, there exists Seebeck current between top and base of dendrites caused by the temperature difference. The current is very weak, however, in the strong magnetic field it would be possible to induce Lorentz force in the solidification front, and make the flow in the liquid metal trapped in the dendrite region. With this effect, it can be expected to make a homogeneous composition ingot from surface to center of the ingot with finer grain size. With above mentioned idea, the research work will be carried out by using an 11.47 Tesla superconducting magnet. In this fiscal year, a furnace to melt and solidify low melting point alloy is going to be built and preliminary tests will be conducted. For the designing of the furnace to use non magnetic materials and to keep the outer shell at room temperature are most important. The outer diameter of the furnace is 57 mm.

134 Basic Study on Refining of Molten Metal and Controlling of Solidification by Electromagnetic Force

April 1994 to March 1997

A. Fukuzawa, Chemical Processing Division

Keywords: cold crucible, levitation melting, electromagnetic force

Cold crucible type levitation melting method using high frequency electric power is known as non-contacting melting method. Therefore, this melting method is advantageous for melting of high purity metals, chemically reactive metals and refractory metals.

In these several years, we have made various kinds of trials on the cold crucible type non-contacting induction furnace and many fundamental results concerning with the cold crucible have been obtained.

One of other advantages of this melting method is to have the separating ability of inclusions from the molten metal, because magnitude of electromagnetic force working toward the molted metal is different from that of inclusions by the physical properties of metal and inclusions. So the shape of the cold crucible, high frequency coil and the electric output power are to be examined to obtain the optimum levitating conditions for separating inclusions from molten metal considering physical properties of materials for melting. Separating mechanism and separating rate of inclusions from levitated molten metal are to be also examined.

135 Investigation on Nucleation and Crystal Growth Mechanism under Heterogeneous Ambient Phase

April 1994 to March 1996

T. Fujii, Chemical Processing Division

Keywords: nucleation, crystal growth, peritectic

reaction, secondary recrystallization, exaggerated grain growth

The purpose of the present study is to obtain the fundamental knowledge for controlling the following crystal growth processes, which occur in the circumstances containing other solid phases of foreign particles.

1) Nucleation and crystal growth with peritectic reaction. 2) Nucleation in solid state reaction and exaggerated grain growth.

Recently, high J_c values have been obtained in the bulk specimens of high T_c oxide superconductors fabricated by means of peritectic solidification process. However, the growth mechanism of these crystals and the role of peritectic reaction in the growth process have not been revealed. In the first subject, we intend to clarify such a growth mechanism on $YBa_2Cu_3O_x$ crystals which melt incongruently at 1000 °C through the metallographic observation and the measurement of growth parameters on the quenched specimens grown at various temperatures.

Investigation will be also made on salicylic acid-acetamid system, in which a peritectic compound at the composition of 1:1 ratio forms at 65 °C. It is possible to observe *in situ* the crystal growth process by means of optical microscopy in the experiment.

In the second subject, we aim to develop the theory of the normal and abnormal grain growth process so as to apply it to the growth of single crystals of intermetallic and ceramic materials as well as metallic materials.

136 Solidification Processing For Particle Dispersed Unidirectionally Grown Composites

April 1994 to March 1996

A. Sato, Advanced Materials Processing Division

Keywords: solidification, unidirectional solidification, composite, particle dispersion

Many kinds of composite materials combined various matrix alloys with numerous reinforcing materials are being produced by multitudinous processings. Therefore, the cost performance of the processing and the properties of the composite materials are the most important factors for the production of composite materials. The properties of particle dispersed composite can be improved by controlling the structure of the matrix alloy. The purpose of this study is expected to obtain basic knowledge and fundamental techniques on the followings; (1) The optimum conditions of the mechanical alloying to make particle uniformly dispersed powder samples: Matrix alloys; composition, size, configuration. Reinforcing particle; composition, size, configuration and volume fraction. Mechanical alloying; strength of stirring, duration of stirring, size and number of balls. (2) The optimum conditions of sintering to produce samples to be used in the following solidification experiment: porosity, temperature and duration of sintering. (3) The optimum conditions of solidification of powder and sintered samples in unit gravity environment on the earth: solidification velocity, temperature gradient, volume fraction of dispersed particle and size and configuration of particle. (4) The optimum conditions of unidirectional solidification: solidification velocity, temperature gradient, volume fraction of dispersed particle and size and configuration of particle. (5) Effect of wettability of the particle added on the engulfment/pushing particle at the unidirectional solidification interface as a function of solidification conditions. (6) Effect of gravity on the engulfment/pushing particle at the unidirectional solidification interface as a function of solidification conditions.

In 1994, the attempt to find out the optimum conditions of mechanical mixing/alloying to make particles uniformly dispersed powder samples was carried out using gas atomized Al powder having an irregular configuration and mean diameter of 30 μm and ceramic powders with various sizes and configurations. When the stirring is not so vigorous and small size balls were used, the size of ceramic powder is not changed while the ceramic powder is mixed uniformly with the metallic power.

137 Metastable Phase Solidification from Undercooled Liquid by Inducing External Nucleation Seed

April 1993 to March 1996

S. Tsukamoto, Advanced Materials Processing Division

Keywords: solidification, undercooling, metastable phase, electromagnetic levitation

Metastable metallic materials produced from deeply undercooled melts can provide some interesting properties. In the previous work, we demonstrated that the metastable phase solidification could be induced with relative ease if the barrier to the nucleation could be avoided in electron beam surface melting. The aim of the investigation is to elucidate the role of nucleation during the solidification of undercooled melts and to develop a new technique for producing metastable bulk materials using an electromagnetic levitation melting and an external seeding.

The correlation between undercooling and competitive phase selection of equilibrium and metastable phases was examined using the electromagnetic levitation melting. Two kinds of stainless steels with different solidification modes of primary ferritic (type 316) and austenitic (type 310S) were used. The microstructure of type 316 showed

an abrupt change at critical undercooling of 180 K from dendritic to fine spherical with increasing undercooling. The chemical segregation behavior of dendritic structure showed a sign of primary ferritic solidification. The fine spherical structure was a product of ferritic solidification which transformed to austenite via a massive transformation. In the electron beam surface melting, on the other hand, the solidification mode of type 316 changed from primary ferritic to austenitic with increasing cooling rate or undercooling. The distinct difference between the levitation and the electron beam processes is the presence of the solid substrates which may allow epitaxial growth or heterogeneous nucleation in the latter case. Then, in the electron beam process, the phase selection is mainly determined by the kinetics of growth which is favored for austenite. In the levitation process, on the other hand, it may be determined by the kinetics of nucleation which is favored for ferrite. Nucleation process control should be effective in producing metastable bulk materials using the external seed during levitation melting.

This research was performed in collaboration with Research Development Corporation of Japan and University of Cambridge.

Related Papers

Metastable Phase Solidification in Electron Beam Welding of Dissimilar Stainless Steels, S. Tsukamoto, H. Harada and H.K.D.H. Bhadeshia (Unv. of Cambridge), Mater. Sci. Eng., A178 (1994): 189–94.

Metastable Alloy Phase Formation from Undercooled Steel and Ti-Al Melts, S. Tsukamoto and O. Umezawa, submitted to Mater. Sci. Eng.

138 Basic Technology Development of Materials Procession in a Short-Duration Microgravity Environment

April 1992 to March 1995

A. Sato, Advanced Materials Processing Division

Keywords: microgravity, solidification, combustion synthesis, superconductor

A Study on Double Combustion Synthesis Apparatus

The main purpose of the study is synthesizing high performance intermetallic compounds using short time micro-gravity environment. The combustion synthesis is a process to produce chemical compounds from elemental powders in a short time using the heat of formation of component elements. The micro-gravity environment is achieved by dropping the experimental apparatus. We developed the "Short time double combustion synthesis apparatus" in order to conduct the combustion synthesis in micro-gravity environment. The experiments were carried out using the combustion synthesis apparatus in order to compare the 1G results with μG results precisely. The velocities of propagation of combustion synthesis were measured by two sets of the W-Re thermocouple.

Observation of Harbingering Phenomena of Solidification/Crystallization

The density change exists between upper and lower part in liquid column of supersaturated aqueous solution of citric acid. This is due to the formation of cluster of citric acid. Thus we tried to prove the existence of the cluster formation.

Aqueous solution of citric acid saturated at 307 K was prepared. The solution was 8 K undercooled. Then observation was carried out using dark-field microscope. But we did not find the cluster. Instead, we saw some precipitates which did not show crystal-like growth. The growing speed and dissolving speed of them are extremely slow.

The reasons why we did not find the cluster are that the distance between clusters is less than the resolving power of microscope and that the reflectivity at cluster surface is too small.

Study on the Synthesis of High Temperature Superconductors

Wettability of molten $Bi_2Sr_2CaCu_2Ox$(Bi-2212) superconductor to a silver substrate was studied in order to obtain basic information concerning crystal nucleation and growth at a molten-oxide/metal interface. Microgravity experiment was carried out by utilizing a parabolic flight of the aircraft (Mitsubishi, MU-300) and by using the wettability measurement system with high accuracy for Bi-2212/Ag samples. Sample preparation technique and operation procedure for the measurement system were established. In the flight experiment, microgravity environment of about 20 seconds was obtained. Wettability of molten Bi-2212 to the silver substrate changes steeply with increasing substrate temperature.

Solid state process

139 Metallurgical Analysis of Micro-Machining Region

April 1993 to March 1996

S. Yamamoto, Advanced Materials Processing Division

Keywords: micro machining, micro-machinability, metallurgical factor, tool dynamometer

The object of this study is to analyze the metallurgical factors which affect micro-machining and to accumulate the data about micro-machinability of materials with a view to microfying mechanical systems. This year a tool dynamometer was made to measure the cutting force during micro-machining (micro-turning, micro-drilling, micro-endmilling).

The micro-shaping device and the micro-turning apparatus are used to investigate finishing surface roughness and cutting force. The crystal anisotropy is a cause of deformation anisotropy of the cutting force, chip shear region and finishing surface. In addition, the relationship between cutting speed (strain rate) and crystal orientation is examined.

In order to measure torque and thrust forces during micro-drilling precisely, it is necessary to minimize friction and vibration of the support axis of sample holder for the tool dynamometer. A thrust ball bearing and a roll bearing are used for the apparatus. It is considered that the hole made by micro-drilling is bent according to the crystal orientation. We are now accurately measuring the difference in position between inlet and outlet using samples whose thickness is by five times larger than that of diameter of drill.

The tool dynamometer of micro-endmilling equips with strain gages symmetrically with respect to the cutting position to measure stress in three directions. We can measure the cutting force corresponding to the microstructure of material by this apparatus.

[140] Cooperative Phenomena of the Transformation Variants

April 1992 to March 1995

H. Miyaji, Advanced Materials Processing Division

Keywords: variant selection, martensitic transformation, Fe-30Ni alloy, internal stress

To clarify the variant selection rules in the martensitic transformation of ferrous alloys, we studied the effect of internal stress on the variant selection, which was induced during the processing of thin sheets. The results were analyzed with the Bain strain model.

The transformation textures of Fe-30Ni alloy sheets rolled at the temperature just above Md and subjected to a sub-zero treatment were determined by a x-ray pole figure method.

It was found that the martensite phase had the pole distribution of the shape of the numeral "8." On the other hand the transformation texture of the martensite phase, which was formed from austenite phase annealed for a stress relieving, had this different pole distribution from the above one.

According to the computer simulation of the transformation texture with the Bain strain model, it was considered that these differences arose from the change of the internal stress in the parent phase: that is in the as-roll specimen the three-axial residual stress affects martensitic transformation, but in the stress relieving treatment specimen the constraint stress from the surrounding parent phase against the lattice deformation affects the martensitic transformation, and the anisotrophy of it based on the specimen size causes the variant selection.

Related Paper

Effect of Specimen Size on the Variant Selection in Martensitic Transformation, H. Miyaji and E. Furubayashi, Textures Microstruct. 12 (1990): 189–97.

Powder processing

141 Study on Solid State Chemical Reaction, its Propagation and Materials Synthesis

April 1993 to March 1996

Y. Kaieda, Chemical Processing Division

Keywords: combustion synthesis, TiNi

The fundamental study to reveal the reactions between solids, solid and liquid, and solid and gas is carried out. The propagation of the reaction and the synthesis process of the materials synthesized through the reaction are also studied. The field of the study covers not only the grasp of the phenomena but the comprehensive understanding of the chemical reaction, the heat transfer, the mass transfer and the other aspects of the synthesis of materials in the solid phase system.

The selection of the combinations of elements, which is focused in the present study, will be investigated. The system of the combination that might exhibit the effect of convection and pressure during the reaction and synthesis process is selected considering the system that performs the effect of liquid and gaseous phase. The system of elements, in which the safety during the experiment is assured, is selected.

Investigation by the thermal analysis with rising temperature in constant speed and/or in alternating speed is carried out to reveal the conditions for the initiation of the reaction, the propagation and the synthesis. The influence of pressure and convection on the phenomena in the reaction process of the system containing gaseous phase or liquid phase is studied using a high gaseous pressure apparatus.

Combustion syntheses of mixture of Ni and Ti powder are carried out in a 100 kg batch scale. The synthesized materials were worked to be wires. The wire samples were examined by a measurement of thermal analysis.

142 Sintering of TiAl Intermetallic Compounds

April 1993 to March 1996

Y. Muramatsu, Chemical Processing Division

Keywords: TiAl intermetallic compound, Nb addition, sintering, HIPing

TiAl intermetallic compounds containing 5-15at% Nb were prepared by sintering mixed

powder compacts of TiH_2, $TiAl_3$ and $NbAl_3$. The sintered compounds were further densified by HIPing at 1470 K and 202 MPa for 3.6 ks without canning. Densifications by sintering and HIPing were examined as functions of Nb content and sintered density. The microstructure of sintered and HIPed compounds was also examined.

The densification by sintering was diminished with increasing Nb content. This was mainly due to the delay of alloying in the mixed powder during sintering with increased addition of $NbAl_3$ powder. The densification by HIPing was also diminished with the increase of Nb content. However, full densification was achieved when Nb contents were less than 10at% for 45at%Al compounds. In the sintered compound with Nb contents more than 10at%, full densification was obtained by HIPing in higher temperatures, for example, 1570 K. HIPed density increased with increasing sintered density, and became saturated when the relative sintered density exceeded 92% for 45at%Al compound containing 10at%Nb. The saturated density was nearly equivalent to theoretical density. The microstructure varied with sintering temperature, and the lamellar structure increased with the rise of the sintering temperature. B2-phase was recognized together with α_2 and γ phases by x-ray analyses on HIPed 45at%Al compounds containing 10at%Nb and over.

Related Papers

Effect of Cr Addition on the Sintering and Sintered Microstructure of TiH_2 + $TiAl_3$ Mixed Powder of TiAl Composition, Y. Muramatsu, T. Ohkoshi, and H. Suga, J. Jpn Soc. of Powder and Powder Metallurgy 41 (1994): 518–22 (in Japanese).

Densification of Sintered TiAl Containing Cr by HIPing and Their HIPed Microstructures, Y. Muramatsu, T. Ohkoshi, and H. Suga, J. Jpn Soc. of Powder and Powder Metallurgy 41(1994): 1437–43 (in Japanese).

Sintering of TiAl Containing Nb and their Densification by HIPing after Sintering, Y. Muramatsu, T. Ohkoshi and H. Suga, to be published in May 1995 (in Japanese).

143 Synthesis and Characterization of advanced Materials Utilizing Colloidal Dispersed Systems

April 1993 to March 1996

Y. Sakka, Chemical Processing Division

Keywords: colloid, fine powder, sintering, gas desorption, nanocomposite

Key developments in processing of fine powders are (1) synthesis of fine powders with controlled sizes, shapes and chemistries, (2) consolidation techniques to control pore volume and pore size distribution, and (3) the role of powders and compacts on the evolution of microstructures during sintering. Although many kinds of techniques in preparing fine powders have been reported, little efforts have been paid on the consolidation of fine powders. In this study, the emphasis will be on the second and third development.

Colloidal processing of nano-sized powders (Al_2O_3, ZrO_2, Ni, etc.) is conducted to obtain porous materials with controlled pore sizes. The most important factor is how to disperse the powders. The porous materials will be used further as starting materials for fabricating nanocomposites, heterogeneous phases, biomimetic materials, etc. Electro-discharge sintering is applied to obtain the advanced materials. In this procedure, the powders are heated by instaneous high electric pulsed power application under uniaxial pressure. Characterization of the synthesized materials is another subject. The gas (especially H_2, H_2O, CO and CO_2) sorption-desorption experiments of metal-ceramics nanocomposite particles are conducted for characterizing the catalytic properties.

Related Papers

Processing of Silicon Carbide-Mullite-Alumina Nanocomposite, Y. Sakka, D.D. Bidinger and I.A. Aksay, J. Am. Ceram. Soc. 78 (1995): 479–86.

Electro-discharge Sintering of (Fe, Co)-B and Ni-B Amorphous Ultrafine Powders Prepared by Chemical Reduction, S. Hong, K. Ozawa and Y. Sakka, J. Jpn. Soc. Powder Powder Metall. 42 (1995): 323–29.

Characterization of (Fe, Ni, Co)-TiN Nanocomposite Particles Synthesized by Reactive Plasma-Metal Reaction Method, Y. Sakka, S. Ohno, T. Uchikoshi, H. Okuyama, and M. Ozawa, Trans. Mat. Res. Soc. Jpn. 14A (1994): 57–60.

144 Characterization of Composite Ultrafine Particles

April 1993 to March 1996

S. Ohno, Chemical Processing Division

Keywords: ultrafine particle, composite UFP, RF-plasma, Me-Ti-O UFP, photocatalytic property, photodecomposition

It is well known that the ultrafine particles (UFP) have many excellent physical and chemical properties. Further, the composite UFP formed by combining between foreign particles in the region of a UFP's size would be expected to improve the properties of UFP and to create a new function.

In this study, we synthesized the composite ultrafine particles (UFP) of Me-Ti-O systems (Me = Ba, Sr, Fe and Ni), which were well-known as an oxide photocatalyzer, using an RF-plasma CVD technique and then characterized the photocatalytic properties of the UFP by the photodecomposition of water.

The UFP of Ba-Ti-O, Sr-Ti-O and Fe-Ti-O systems made from the RF-plasma CVD technique were found to be only a single phase of their respective complex oxides such as $BaTiO_3$, $SrTiO_3$ and $FeTiO_3$, but in the case of Ni-Ti-O system, a small amount of TiO_2, NiO and Ni phases besides $NiTiO_3$ phase because the NiO phase has a low decomposition temperature, alternatively, Ni vapor formed in the plasma is less apt to react with oxygen and/or Ti-O species during the condensation process. It was found that those UFP have a good photocatalytic activity for the decomposition of water and the order of activities is $NiTiO_3$ > TiO_2 > $SrTiO_3$, $FeTiO_3$ > $BaTiO_3$.

145 Development of Particles Assembly Technology for Integration of Functions

April 1992 to March 1996
N. Shinya, 5th Research Group
Keywords: intelligent materials, multiple functions, particle assembly

For creation of intelligent materials, technologies for systematization and integration of multiple material functions should be developed in advance. Systematically coordinated multiple functions will lead to manifestation of intelligent functions, such as self-repair, self-diagnosis, feedback and so on, which can respond to environmental conditions.

In order to provide materials with the systematically coordinated multiple functions, a new approach is made through a development of particles assembly technology in this work. Each particle has a primitive function such as sensor, processor and actuator. Therefore coordinations and systematizations of these primitive functions may be realized through three dimensional particles arrangement. For the arrangement it is necessary to develop the technology which make it possible to assemble several kinds of particles according to structural designs for the manifestation of the coordination and systematization.

As key technologies for the three dimensional particles assembly, a particle manipulation using a micro-probe and a particle arrangement using an electron beam are being studied. For the particle manipulation, a new type probe with dipole electrodes has been developed, and it was confirmed that particles can be easily manipulated by controlling the voltage between the dipole electrodes. The particle arrangement using an electron beam was carried out as follows: (1) electrified patterns were drawn on a substrate by electron beam scanning, (2) the substrate was dipped into a non-polar solvent in which particles were dispersed and (3) the particles adhered to the electrified pattern. By this process, clear particle patterns were obtained.

146 Preparation and Characterization of Ultrafine Powders Used for Making Oxide Superconductors

April 1988 to March 1995
S. Ohno, Chemical Processing Division
Keywords: ultrafine powder, superconducting oxide, Bi-Sr-Ca-Cu-O ceramics, high T_c phase, Ag doping

Improvement of homogeneity, sinterability, and preferable orientation is expected using finer powders as raw materials for superconducting oxide. One objective of this study is to synthesize the ultrafine powders suitable for making superconducting oxide. Various preparation methods are conducted such as reactive plasma-metal reaction, Rf-plasma, CVD, oxalate coprecipitation and citrate sol-gel methods. Then, the factor affecting the superconductivity properties is examined, especially on the appropriate composition, particle size, and sintering conditions.

Recently, we found that the formation of high-T_c (110 K) phase in Bi-Sr-Ca-Cu-O ceramics was enhanced significantly by Ag-doping into the sintered ceramics from a Ag substrate. In order to clarify the doping mechanism of Ag into the ceramics, we have been examined the reaction between various oxide ceramics for superconductor and the Ag substate under a sintering process. From EPMA analysis of sintered ceramics, it is presumed that the trapping site of Ag is a Bi-rich zone which is melting under the sintering process.

147 Study on Properties of Raw Powder of Superconductor using High Pressure Forming

April 1988 to March 1995
Y. Kaieda, Chemical Processing Division
Keywords: combustion synthesis, superconductor, Y-Ba-Cu-O system

The combustion synthesis for making Y-Ba-Cu-O system superconductor is developed. The elemental powders should be used to get a heat of formation in the reaction between the starting metallic powders and an oxygen gas in order to ignite and propagate the combustion synthesis. However the pure metallic yttrium powder is unstable and easily oxidized in the air at room temperature and reactive to water. Pure metallic barium is also unstable and oxidized in the air at room temperature and reactive to water and toxic to human body. To the contrary, pure copper is relatively stable in the air and not reactive to water. It may be instinctive to use pure copper powder as a key material for performing combustion synthesis of Y-Ba-Cu-O system superconductor. The values of the heat of formation of copper oxides are 155.3 kJ/mol for CuO.

The combustion synthesis of Y-Ba-Cu-O system superconductor was performed, using the heat of

formation of copper oxide, under the absolute pressure range of pure oxygen gas at 1.3 kPa to 12.6 MPa to examine whether the heat of formation of copper oxides is enough for sustaining the propagation of the combustion synthesis and synthesizing the Y-Ba-Cu-O system superconductor. The process of combustion synthesis of Y-Ba-Cu-O system superconductor using pure copper powder and pure oxygen gas was revealed and the samples made by combustion synthesis were characterized.

Related Paper

Combustion Synthesis of an Oxide-Superconductor, Y. Kaieda, M. Otaguchi and N. Oguro, Intern. J. Self-Propagating High-Temperature Synthesis 1 (1992): 246–56.

[148] Study on Rapidly Solidified Powders for Superconductive Materials

October 1988 to March 1995

K. Halada, 4th Research Team

Keywords: superconductive materials, rapid solidification, powder, sintering

Sintering of rapidly solidified Bi-Sr-Ca-Cu-O glassy ceramics powder was investigated. Rapidly solidified powder was produced by both method gas atomization and centrifugal atomization from molten oxide. Gas atomized powder composed of fine spherical powder less than 20 mm in diameter and thin fiber with round heads at the end, while ligaments and spherodized glassy powder 0.1 to 1 mm in diameter were obtained by the centrifugal atomization. All of them were amorphous, which had the crystallization temperatures around 500 °C.

The atomized powder once shrank above 500 °C, followed by the second shrinkage around 700 °C, and characteristically expanded from 820 °C before rapid shrinkage above 860 °C, while mixed powder showed a simple shrinkage behavior above 700 °C. $Bi_2Sr_2CuO_6$ crystallized above 500 °C from the atomized powder. $Bi_2Sr_2CaCu_2O_8$ (superconductive phase) appeared above 800 °C, and the partial melting took place around 860 °C. An extraordinary growth of Ca_2CuO_3 phase was observed below the temperature of the remarkable partial melting. The phase-separation generated into Bi-rich part as the counter result of the growing of Ca_2CuO_3 phase, confirmed by newly developed EPMA composition analysis. The Bi-rich part prevented from producing the stable high-T_c phase, because liquid phase broke out from the Bi-rich part below the temperature to make the high-T_c phase stable. Uniformity and fineness of the microstructure of the rapidly solidified powder accelerate formation of stable phase in each temperature, consequently, path of the reaction of rapidly solidified powder was different from mixed powder.

Related Papers

EPMA Composition-coordinate Mapping Analysis of the Phase Change of Atomized Bi-Sr-Ca-Cu Oxide, K. Halada, K. Honma, K. Minagawa, and H. Okuyama, Funtai oyobi Funmatsuyakin 39 (1992): 390–96 (in Japanese).

Sintering of Bi-Sr-Ca-Cu-O Superconductive Material Atomized from Molten Oxide, K. Halada, K. Minagawa, H. Suga, H. Okuyama, S. Ohno and Y. Muramatsu, Advances in Powder Metallurgy & Particulate Materials 8 (1992): 281–92.

Joining

(149) Influence of Surface Composition on Joining of Materials

April 1995 to March 1998

O. Ohashi, Advanced Materials Processing Division

Keywords: surface composition, joining, copper, silicon

Ion bombardment has a cleaning effect on a joining surface. But it causes various damages such as ion implantation and surface roughening. Therefore, it is desired that the influence of surface composition on joining is investigated using metals without damages.

On the other hand, hydroxyl radical and thermal oxide on the surface accelerate the joining process of silicon. The bonding mechanism is not clear yet.

The aim of this study is to investigate; i) the effect of surface composition on joining under the condition without the surface damage, ii) the difference in bonding mechanism of metals and silicon.

Joining of Metals

In this study, we use a surface cleaning method without damages; i) hydrogen radical beam radiation, ii) repetition of ion bombardment and heat treatment. We investigate the effect of surface damage layers and adsorbed gases on properties of copper joint.

Joining of Silicon

In this study, we carry out diffusion joining with various surface treatments; hydroxyl adsorption, thermal oxidization, and bare surface. We investigate effects of adsorptive at bonded interface using following evaluating methods; bending strength, electric resistance, SEM, Auger electron analysis and FT - IR. It is expected that oxygen in material affects disappearance of surface adsorptive, so we also investigate behavior of surface adsorptive in different oxygen concentration using FZ and CZ silicon.

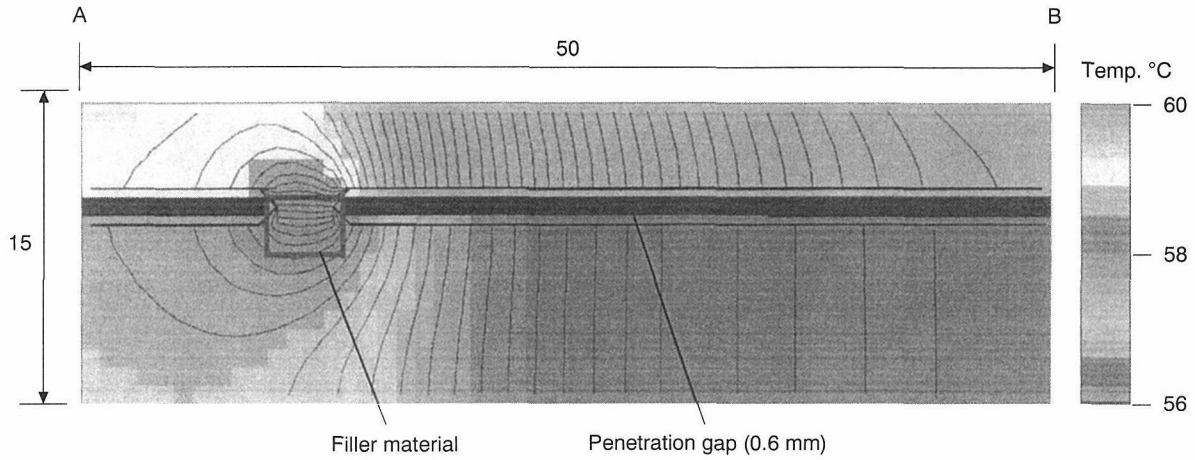

Fig. 5 An example of calculated temperature distribution just before the beginning of capillary penetration. A penetration gap was composed of carbon steel plates. Filler materials was paraffin whose melting temperature was 331K. The side A-B was heated up at 358K.

150 Corrosion of Dissimilar Metals Joints in Reactor Fuel Reprocessing Plants

April 1991 to March 1996

H. Irie, Advanced Materials Processing Division

Keywords: diffusion welding, titanium, zirconium, stainless steel, laser speckle method, corrosion

Dissimilar metal joints are to be used in a new reactor fuel reprocessing plant in Japan. The joints composed of stainless steel and valve metals are made by solid state joining. It is necessary for the safety of plant to assure sufficient mechanical strength and corrosion resistance.

Sufficient diffusion welding of zirconium to 304L type stainless steel could be accomplished using annealed tantalum foil inserted into the joining interface at 1123K. At lower temperature, the joint did not have sufficient tensile strength because of incomplete contact between joining surfaces. At more than 1123K, the complete contact was accomplished, but intermetallic compounds were formed. Precise observations of the intermetallic compounds were carried out. Near the interface of Zr / Ta, tantalum solid-soluted into zirconium and at the interface of Ta / 304L, (Fe, Cr, N)Ta and (Fe, Cr, Ni)$_2$Ta layers were formed in stainless steel. Corrosion by 3N nitric acid at 60 °C occurred at the former layer.

In order to depress the formation of intermetallic compounds, the surface cleaning by Ar ion sputtering is effective. A high accelerating voltage of Ar ion, however, hardened the thin surface layer and suppress the close contact of the interface of both metals.

Laser speckle method for measuring local strain distribution was applied to the joints of Ti / 304L and successful results were obtained when the laser spot diameter was 1.5mm. After increasing detective elements and laser radiation, smaller laser spot will be applied and more precise strain distributions in radial and angular direction will be measured at Zr / Ta / SUS304L tube joints.

151 Fundamental Research on Brazing and EB Welding in Space Environment

April 1994 to March 1996

K. Sasabe, Advanced Materials Processing Division

Keywords: Brazing, EB Welding, Microgravity, Simulation

The characteristic phenomena of molten metal flow during brazing and EB welding have been studied as fundamental research for the establishment of a joining technique in space.

Research on Brazing

A high speed calculating system for the prediction of temperature distributions during brazing using a personal computer has been developed. Using this system, we can calculate about 1000 times faster than using the former system developed in the last year, and the simulation for model experiments can be realized in real time.

Figure 5 shows an example of a temperature distribution calculated by this system. The results of simulation showed good agreement with model experiments.

EB Welding

A high speed video and analysis equipment was selected on the base of experimental results with high speed movie. Its maximum frame speed is 2000 frames / sec (fps). Using this video, photographs were taken during electron beam welding through the window. The number of memory elements of the camera, however, decreases with increase of the speed. At more than 1000fps, a picture of molten metal became obscure and was difficult to be analyzed.

In order to overcome this difficulty, the welding position has to be closer to the window and the picture has to be taken at as right above position as possible. Then the improvement of electron beam equipment, in which the electron gun locates near the window and a mirror is set above the welding position, is undergoing.

152 Low Energy Joining with Controlled Surface Composition

April 1994 to March 1995

O. Ohashi, Advanced Materials Processing Division

Keywords: Joining, surface composition, argon ion bombardment, direct bonding of silicon, hydrogen permeability

The research aims to develop low energy joining techniques based on the control of surface composition. Furthermore, the work is being carried out to develop materials for a special function, i.e., hydrogen purification and silicon devices. The characteristics of the prepared surfaces are examined using ultra high vacuum equipment that enables surface control and analysis. In addition, the surface modification technique by vapor deposition has been examined to improve the hydrogen permeability of some developed membranes. We have obtained the following results:

1. Single crystal silicon can be bonded without a recrystallized zone at the bond-line. The joints of p-type silicon to n-type silicon made under the suitable bonding conditions show the diode characteristics. The properties depends on the bonding temperature.
2. Bonding is often carried out using argon ion bombardment. However, the recent work has shown that the accelerating voltage of ion bombardment significantly affects the bondability of metals. When the ion bombardment is carried out at accelerating voltage of 5 kV, it is difficult to make the joints in spite of no contaminants on bonding surface. When energetic ions strike surface of the material, they give some damages such as roughening, ion implantation and hardening at the surface. The decrease of bondability is attributable to forming hard layer at the bonding surface.
3. Hydrogen permeation characteristics of magnesium were investigated. The hydrogen diffusivity of magnesium was found to be high: it was comparable to that of palladium. On the other hand, hydrogen permeability of magnesium was extremely low. These results suggest that hydrogen solubility of magnesium was very low. Yttrium deposition was effective in modifying the surface of magnesium, and raised the hydrogen permeability of the membrane by several times.

Related Papers

Hydrogen solution and diffusion in L12-ordered (Co, FOe)3V alloy, C. Nishimura, M. Komaki, M. Amano, Proc. 5th Int. Conf. Hydrogen Effects on Materials Behavior (1994).

Hydrogen permeation characteristics of vanadium-molybdenum alloys, C. Nishimura, M. Komaki, M. Amano, Trans. Mat. Res. Soc. Jpn., Vol. 18b (1994): 1273.

Effect of surface composition on diffusion welding in stainless steel, O. Ohashi, Trans. Mat. Res. Soc. Jpn., Vol. 16b (1994): 1245.

Composite process

153 Coatings Formation by Powder Deposition Processes

April 1995 to March 1998

S. Kuroda, Advanced Materials Processing Division

Keywords: thick coatings, spray deposition, electrification

Coatings with thickness over 50 μm are highly demanded in various industries. The most successful process in this category has been a family of thermal spray processes. Thermally sprayed coatings have been used mostly for surface protection but recent applications include more functional areas such as biomedical implant, electric heaters and radiators, and catalytic cleaners. Our group has worked on plasma spray in the past 10 years to clarify the mechanism of coating formation.

This research has two objectives. The first is to extend the study on thermal spray. Special emphasis will be placed to clarify the bonding between sprayed splats, which plays a key role in the development of the microstructure of sprayed deposits. Effects of the substrate temperature, spraying environment, the velocity and temperature of particles before impact on the inter-lamellar bonding will be studied systematically.

The other is to develop a new process to deposit thick coatings with improved properties, such as less porosity. Finer powders than those usually used for thermal spray are electrified and deposited onto a substrate. A possibility to consolidate the deposit by a CO_2 laser is under investigation.

Related Papers

The Quenching Stress in Thermally Sprayed Coatings, S. Kuroda and T. W. Clyne, Thin Solid Films, 200 (1991): 49–66.

Quenching stress in plasma sprayed coatings and its correlation with the deposit microstructure, S. Kuroda, T. Dendo and S. Kitahara, J. Thermal Spray Technol. 4 (1995): 75–84.

154 Forced infiltration process for making composite structures

April 1992 to March 1996

T. Dendo, Advanced Materials Processing Division

Keywords: forced-infiltration, joining, semi-molten state, intermetallic compound

Forced infiltration technique is applied to two different processing purposes in this theme. The first is to manufacture a sort of metal-ceramic composite by infiltration under semi-molten state. Through this process, two types of composite can be obtained; one is of a porous ceramic compact having a metal-ceramic-composite layer near its surface; another is of a ceramic compact joining with a metal layer which is the solid component in semi-molten state. The infiltrating metals employed are Pb-Sn alloys which have a wide region of semi-molten state. The porous compacts used are made of alumina powder. Infiltrating behavior, morphology of the composite structure and bonding quality are investigated in relation to the process parameters such as volume fraction of solid, porosity of ceramic compact, infiltration pressure and so on.

The second is to synthesize intermetallic compounds by forced infiltration into a porous metallic preform. Through the present process, three kinds of Ti-Al compounds are synthesized i.e., Ti_3Al, TiAl and $TiAl_3$. Fraction and distribution of them are mainly affected by the thermal conditions such as pre-heating temperature and pouring temperature. At lower processing temperature, $TiAl_3$ and unreacted Ti are seen, whereas TiAl and Ti_3Al are observed at higher temperature. Morphology of the structural distribution is minutely examined.

Related Papers

Synthesis of Ti-Al Intermetallic Compounds by Reaction during Pressure Infiltration, T. Shirota, K. Hashimoto, M. Nakamura, H. Doi, T. Kimura and T. Dendo, Proc. 43th Join. Conf. Tech. Plast. (1992): 483–86 (in Japanese).

Pressure Infiltration under Semi-molten State for Making Composite Layer Structure, T. Dendo, T. Shirota and M. Kiuchi, Proc. 4th Int. Conf. Tech. Plast. (1993): 194–99.

Infiltrating and Joining Processes under Semi-molten State for Making Metal-Ceramic Composite, T. Shirota, T. Dendo and M. Kiuchi, Proc. 3rd Int. Conf. Proces. Semi-soli. Alloy. Comp. (1994): 407–15.

155 Coating Formation by Molten and Electrified Powders

April 1991 to March 1995

S. Kuroda, Advanced Materials Processing Division

Keywords: plasma spray, surface coating, porosity, high-pressure infiltration

Deposition of molten particles onto solid surface has been investigated with a special interest in surface coating processes such as plasma spray in mind. Recent progress has been made in the evaluation of the pore structure in plasma sprayed coatings and its correlation with the spray conditions. Porosity is more important in sprayed deposits as compared to conventional bulk materials formed by casting or powder metallurgy. This is due to the lamellar structure of sprayed deposits and the existence of pores with a high aspect ratio such as the interlamellar gaps and microcracks. The effects of these pores on the property are far greater than globular pores and therefore accurate understanding of the porosity network in sprayed deposits is essential.

Ni-20Cr alloy and alumina powders were plasma sprayed in air with various spray conditions. Then we have applied a high-pressure infiltration process to fill the porosity in the sprayed deposits with a Bi alloy. After such treatment, cross sections of the specimens were polished and observed under SEM in the back scattered electron mode. Three types of pores such as the interlamellar gaps, globular pores, and microcracks could be easily identified with a high spatial resolution down to 0.1 μm. By comparing the visualized pores with the pore size distributions measured by mercury porosimetry, important information about the pore network could be obtained. For example, even though there are many pores greater than 10 μm within the sprayed deposits, the routes to reach them from outside are narrower than 1 μm. By increasing the substrate temperature during deposition, the number and the size of interlamellar gaps significantly decrease; especially for Ni-20Cr, the deposits become almost impenetrable from outside at a substrate temperature over 600 °C.

Better understanding of the mechanisms of the porosity formation is expected to enable us to tailor the structure and properties of sprayed deposits more effectively in the future.

Related Papers

The Quenching Stress in Thermally Sprayed Coatings, S. Kuroda andT. W. Clyne: Thin Solid Films, 200 (1991): 49–66.

Significance of the quenching stress in the cohesion and adhesion of thermally sprayed coatings, S. Kuroda, T. Fukushima and S. Kitahara, J. Thermal Spray Technol. 1 (1993): 325–32.

Quenching stress in plasma sprayed coatings and its correlation with the deposit microstructure, S. Kuroda, T. Dendo and S. Kitahara: J. Thermal Spray Technol. 4 (1995): 75–84.

Process with aid of beam technology

⑮⑥ Study on the Efficiency of Resonance Photoionization Process

April 1995 to March 1998

Y. Ogawa, Chemical Processing Division

Keywords: resonance photoionization, photoionization induced plasma, auto-ionizing level, Rydberg level, plasma characteristics

Laser resonance photoionization continues to be popular in many research fields and the process may find a wide variety of applications. In this process, atoms are selectively pumped from their ground state to an intermediate excited state and subsequently the excited atoms are ionized by direct photoionization. The ions generated are then extracted from a photoionization induced plasma by an externally applied electric field. One of the important factors in evaluating the process performance is the overall ion yields, which is restricted by two conditions: the small bound-free transition cross-section in the ionization scheme and the space charge limitation in the plasma.

The objective of this study is to improve the overall efficiency of the resonance photoionization process. The research is composed of the following two subjects.

1. Investigation for autoionizing levels or highly excited Rydberg levels to achieve the efficient photoionization of atoms via bound-bound transitions.

2. Measurement of plasma characteristics to elucidate the ion extraction behavior from the plasma.

Related Paper

Laser Material Purification of Neodymium, Y. Ogawa et al., J. Jpn. Inst. Met. 55 (1991): 545–52.

⑮⑦ Analysis/Evaluation of Atomic Scale Compositional Change in Materials Due to The Radiation Damage

April 1995 to March 1998

K. Furuya, Materials Characterization Division

Keywords: radiation damage, SUBNANOTRON, analytical TEM

Radiation damage in materials is characterized by the atomic displacements associated with the destruction of crystalline structure, transmutation by the nuclear reaction and the radiation induced solute segregation by the irradiation of energetic particles such as neutrons and ions. Many types of defects and rearrangement of a chemical composition are supposed to be produced by this atomic process and the resultant microstructure generally becomes complicated with the formations of dislocation loops, voids, precipitates and so on. For the basic understanding of radiation damage, it has been strongly desired to clarify the atomic process. *In situ* observation and analysis in the transmission electron microscope (TEM) is one of the fascinating method to investigate the structural evolution induced by particles bombardments and implantation.

The facility so-called "SUBNANOTRON" as analytical TEM consisting of 1 MeV electrons with two ion accelerators is used in this research to clarify the microstructural aspects of materials under irradiation conditions. In addition, the analytical tools such as EDS and EELS are incorporated to characterize the complicated structural changes of irradiated materials. The dynamic resolution of the SUBNANOTRON has been confirmed to be less than 0.13 nm and the *in situ* atomic scale observation of the formation of defects and defect clusters in FCC metals induced by the 1 MeV electron irradiation has been performed.

For understanding the irradiation induced compositional change of materials, it is necessary to develop proper experimental procedures under the irradiation and / or at post irradiation condition. The improvement of the thin foil preparation, the optimization of heat treatment conditions will be done prior to the irradiation and the optical and conductivity measurements will be done on the irradiated specimens. Comprehensive evaluation of these results as well as TEM observation and analysis is strongly expected to develop new materials for radiation conditions.

⑮⑧ Characterization and control of the optoelectric properties of small crystalline materials with electron probe analysis

April 1995 to March 2000

K. Furuya, Materials Characterization Division

Keywords: small crystalline materials, surface terminated or buried particles, MBE, HRTEM, EDS, EELS, CL

It is possible to characterize and control the specific optoelectric properties of very small crystalline materials, by enclosing the crystals with a different kind of materials, or by terminating the conducting electrons inside particles. This type of small structures are feasible by burying nanometer-sized crystals into materials, covering the surface of one material with other material. In this study, we are trying to create those small "hetero structures" and to characterize their structures.

Surface terminated or buried particles with typical size of several or several tens of nanometer of metals such as Au and Pt would be obtained by electron beam deposition, molecular beam epitaxy (MBE) subsequent heat treatment of surfaces at proper conditions. Another way to achieve the hetero structure is to use electrolysis to make porous structure of semiconductors such as Si and

Ge, whose structure is controlled by the composites of the solvent, applied voltage, temperature and dopants. The characteristics of electronic states of such nano-structure is believed due to the localization of electrons in particular volume which is smaller than the coherent length of conducting electrons.

Structural analysis and evaluation will be carried out to clarify the relation between the atomic structure and the electron state dependent characteristics such as photoluminescence and electron conducting or transport property. High resolution transmission electron microscopy (HRTEM) will be used to observe the atomic structure and energy dispersive x-ray spectroscopy (EDS) for local composite analysis. Optical or electric property evaluation will be achieved using cathode luminescence (CL) to measure the luminescence property, electron energy loss spectroscopy (EELS) for chemical binding energy spectroscopy or electron state spectroscopy.

159 Synthesis of Superconducting and Supermagnetic Ultrathin Films by Use of Ion Implantation

April 1994 to March 1996

K. Saito, Surface and Interface Division

Keywords: superconductivity, giant magnetization, ultrathin films, BiSrCaCuO, $Fe_{16}N_2$, ion implantation

High-quality superconducting BiSrCaCuO ultrathin films have been synthesized by using modified single-target magnetron sputtering and optimizing the heat- treatment conditions. The obtained values of zero-resistance superconducting transition temperature, $T_{c,0}$ were 106 K, 88 K and 58 K for 7 nm, 4nm and 2 nm thick films, respectively. The surface of 7 nm thick films was terraced with very fine steps and became smooth with decreasing the film thickness down to 2 nm. Correspondingly, transport properties of these ultrathin films became isotropic in the film plane. Irradiation with 100 keV range Ar ions was found to improve the $T_{c,0}$ of initially low-quality films and increase the critical current density, J_c, by one or two orders of magnitude.

We have also synthesized magnetic $Fe_{16}N_2$ thin films with giant magnetization by means of N ion implantation into highly (001) oriented Fe films. For 250 nm thick films, $Fe_{16}N_2$ nitrides were formed directly during ion implantation, and increased their volume fraction by multiple implantation, when N ions were implanted from deep to shallow depth regions by decreasing the ion energy. The saturation magnetization of $Fe_{16}N_2$ in the implanted film was estimated to 2.48 μ_B. For 50 nm thick films, more than 90% volume fraction of α'-martensite was formed just after N ion implantation, but hardly transformed into $Fe_{16}N_2$ upon annealing at 150°C. It was found that coating of Cu films on the implanted surface reduced nitrogen escape from the specimen surface and that additional implantation through the Cu films was effective in compensating for nitrogen loss near the surface region.

Related Papers

Preparation and Thickness Dependence of BiSrCaCuO Superconducting Ultra Thin Films, M. Kaise and K. Saito, Proc. 10th Symposium on Surface Layer Modification by Ion Implantation (1994): 41–45.

Synthesis of $Fe_{16}N_2$ by means of Nitrogen Ion Implantation into Fe Thin Films, H. Shinno, K. Saito and M. Uehara, ibid. 17–23.

160 Study on Evaporation Processes by High Energy Density Beams

April 1992 to March 1996

H. Irie, Advanced Materials Processing Division

Keywords: electron beam, laser, evaporation, plasma heating

The electron beam evaporation process has been widely used in coating industry, but it is used at very low evaporation rate in order to prevent the occurrence of sputter. This coating process has been done on the basis of experiences due to the shortage of knowledge of evaporation mechanism. On the other hand, a laser has been considered as a good heating source to produce material vapors in controlled environment. But the laser itself is the same kind of heating source as the electron beam and it will face the same problem as the electron beam does.

In the laser, especially a CO_2 laser, melting and evaporation process of materials, the laser interacts with a plasma which is produced by high temperature metal vapor from the laser irradiation point and the environment gas. The laser is scattered and absorbed by free electrons in plasma and heats up the plasma. This laser induced plasma has a high temperature and ionized gas atoms which have a high ionization potential. It was very difficult, however, that an analysis or a measurement of plasma structure produced over the laser irradiation point because the plasma was very small and metal vapor did not distribute uniformly in the plasma.

In order to produce a large and stable laser induced plasma, and arc (GTA) plasma was used as a seeding plasma. The arc was formed in the horizontal position and the laser was focused and irradiated into the arc plasma center in the transverse direction from the upper side. The plasma was absorbed by the arc and heated it locally. The laser was floated up toward the laser nozzle. This plasma was floating stably under the balance be-

tween the buoyancy and the gas pressure of laser shielding gas from the laser nozzle. This laser induced plasma was very stable even if the arc disappeared. Using this method, the interaction between the laser and the plasma is being investigated. The metallic vapor will be produced by introduction of a metal into this plasma.

161 Diagnostics of Laser Photoionization Induced Plasma

April 1992 to March 1995

Y. Ogawa, Chemical Processing Division

Keywords: laser photoionization, laser induced plasma, drift velocity, ion and electron temperatures, plasma density

Resonance stepwise photoionization method has acquired a wide variety of applications. Novel applications of laser photoionization include it emergence as a feasible method for the processing of high-purity materials and the separation of commercially valuable isotopes, when using as the detection of trace elements, and ion sources for ion implantation, etc. Furthermore, the extraordinary sensitivity and versatility of resonance photoionization spectroscopy have already applied to the identification of high-lying atomic levels, the measurement of transition cross sections, and the studies of chemical reaction, etc.

These applications are mainly based on laser stepwise excitation of atoms and on extraction of ions from weakly ionized plasma produced by the photoionization. The method of laser stepwise resonant photoionization of atoms was suggested more than ten years ago and the basic features and characteristics of this method have been fundamentally realized. However, little is known about the microscopic and macroscopic properties of the laser induced plasma (such as drift velocity, ion and electron temperatures, plasma density and so on) or about the extraction behavior of ions under the applied electric field. We have planned this research work to establish the diagnostic techniques for the weakly ionized plasma, which will contribute in full understanding of ion extraction behavior.

Related Paper

Laser Material Purification Of Neodymium, Y. Ogawa et al., J. Jpn. Inst. Met. 55 (1991): 545–552.

162 *In Situ* Analysis/Evaluation of Radiation Damage in Materials

April 1988 to March 1995

K. Furuya, Materials Characterization Division

Keywords: radiation damage, in situ analysis, dual-beam ion irradiation, SUBNANOTRON, 1 MeV TEM, 200 keV ion implanter, 30 keV ion sputter source

Radiation damage of metallic materials is characterized by the atomic displacements associated with the destruction of crystalline structure by the irradiation of energetic particles such as neutrons and ions. Many types of defects and defect clusters are supposed to produced by this atomic process and the resultant microstructure generally becomes complicated with the formation of dislocation loops, voids, precipitates and so on. For the basic understanding of radiation damage, it has been strongly desired to clarify the process of the atomic displacement. *In situ* observation in the transmission electron microscope (TEM) is a fascinating method to investigate the structural evolution induced by particles bombardments and implantation.

The purpose of this research is to develop a new facility for in *situ* analysis of the microstructural aspects of materials under the dual beam ion irradiation. The facility so-called "SUBNANOTRON" consists of 1 MeV TEM with two ion accelerators. The voltage of 1 MeV for electron was chosen for the resolution better than 0.15 nm, enough thickness of the specimen and enough volume at the specimen position where stressing, heating and cooling will be conducted. Resolution tests were carried out with an amorphous Ge specimen and indicated the value of 0.13 nm calculated at Scherzer defocus condition under dynamic observation with a TV camera. The two analytical tools, UTW-EDS and energy filtered imaging systems are essential to characterize the complicated structural changes of irradiated materials. The performance of these tools were already confirmed with NiSi epitaxial film on Si (100) substrate. Dual ion accelerator systems which consist of 200 keV and 30 keV implanters with a hollow cathode heavy ion source and RF discharge light ion source, respectively are now being installed and the ion irradiation will be performed in the year of 1995.

The preliminary experiments of the electron irradiation was carried out on aluminum TEM specimens at room temperature. The specimens were irradiated with the relatively strong 1000 keV electrons of 1.0×10^{23} electrons/m^2s and, the atomic displacements and the dynamic changes in the morphology of secondary defects were recorded with VTR tapes. The images grabbed from the tape showed aluminum atoms with the interatomic distance of 0.2 nm. Especially pointed out is the line shape atomic displacement associated with the large distortion of lattice fringes in one of two series of apparent (111) planes, while no alteration in the number of lattice planes happens on both sides of the lattice distortion. The present results surely demonstrate the usefulness of the *in situ* irradiation of materials in TEM followed by or with HRTEM observation for disclosing the mechanism of radiation damage in sub-nanometer scales.

Whole system will be completed and ready for operation in the middle of this year, and will be opened for the research collaborations between Japanese and overseas materials scientists.

[163] Control of Surface Reaction and Synthetic Processes Using "State-Controlled" Molecular Beams

April 1994 to March 1995
M. Yata, 1st Research Group
Keywords: State-control, supersonic molecular beam, surface reaction

Our experimental program is aimed to understand the chemical reactivity of molecules on solid surface and the elementary processes of the surface reaction using the "state-controlled" molecular beams. Here, the "state" means the energy distribution of the reactant molecule. We have constructed a supersonic molecular beam system for "state-controlled" molecular beams. Supersonic molecular beam technique is one of the useful techniques to control the "state" of the isolated molecules. Supersonic molecular beam is a neutral beam extracted from an underexpanded, supersonic, continuum jet expansion from a high-pressure gas source into a low-pressure ambient background and has the following virtue: (1) the distribution of translational energy is narrow and, (2) the rotational and vibrational temperatures are very low. This technique is also advantageous for producing molecular beams of widely different translational energies. Using the supersonic molecular beam technique, we start to study "Cu-O" surface reaction dynamics by the following research projects: (1) characterization of supersonic O_2, N_2O or O_3 molecular beam: translational energy distribution and rotational energy relaxation in the supersonic molecular beams, (2) control of the translational energy of O_2, N_2O or O_3 molecular beams, (3) adsorption-desorption dynamics of O_2, N_2O or O_3 on Cu(001) surface, (4) chemical reactivity and reaction processes of Cu atoms and "state-controlled" O_2, N_2O or O_3 molecules on MgO(001) surface.

Our final goal is to get the answer of the following questions: (1) how will the initial states of reactants affect the elementary processes of the reaction?, (2) how can we control the energy disposal of the reactant?, (3) how can we control the branch ratio of the product yield by the way in which the reactants are excited?

[164] R & D of Advanced Heat-Resistant Structural Materials for Very High Temperature Gas-Cooled Reactors

April 1990 to March 1995
T. Tanabe, 3rd Research Group
Keywords: High Temperature Gas-Cooled Reactor (HTGR), Materials-Design, Testing-and-Evaluation

In order to fulfill the national demand for advanced structural materials for high temperature gas-cooled reactors, we have carried out the R & D of new heat-resistant materials for very high temperature use up to 1373 K by combining the materials-design and the testing-and-evaluation technologies. The present status of the R & D is as follows.

1. Development of Advanced Materials Testing-and-Evaluation Technologies: The investigations on the creep damage of Inconel MA754 at 1273 K in an HTGR He environment were performed by using the usual creep specimens with the stress axis parallel (L direction) and perpendicular (LT direction) to the elongated grains of the alloy. Statistical evaluation of the creep damage was made on ruptured specimens by adopting the A-parameter, the ratio of the number of damaged grains to that of the total grains observed. The A-parameter followed the Weibull distributions in all the case investigated. Even in virgin specimens, the A-parameter reached as high as 0.2. Creep damage was increased with the applied stress level in the L direction specimens, whereas the reverse tendency was obtained in the LT direction. This result may be attributed to the rapid growth of voids along the grain boundaries in the LT direction specimens.
2. Development of Advanced Heat-Resistant Materials: Trials to manufacture ODS Ni-Cr-W alloys were carried out by mechanical alloying of powders of the constituent elements in Ni-26%Cr-17%W and those of Y_2O_3. An improvement of their creep rupture lives at 1373 K in the HTGR He environment was recognized through the combination of solution treatment, additional cold work and final heat treatment of the alloy, whereby the grains elongated along the rolling direction. Although the grain aspect ratio reached more than 20, their creep lives did not exceed those of Inconel MA754 probably due to the smaller grain width perpendicular to the rolling direction. Further efforts to improve their lives are now being made.

Related Papers

Effect of Carbon Content and Helium Gas Environment on Creep Crack Growth Properties of Ni-26% Cr-17%W-0.5%Mo Alloy at 1273K, M. Tabuchi, Y. Nakasone, T. Ohba, K. Yagi and T. Tanabe, Metall. Trans., 26A (1995): 383.

Creep Damage in an Oxide Dispersion Strengthened Superalloy in He Gas at Very High Temperature, Y.

Nakasone, I. Mutoh and T. Tanabe, Trans. JSME, to be published.

Creep Damages of Ni-base Superalloys in Helium Gas at Very High Temperatures, Y. Nakasone, I. Mutoh and T. Tanabe, Proc. 1995 ASME/JSME PVP Conf., to be published.

Processing in special environment

(165) Study on Effects of Aging in Magnetic Field on Properties of Thin Films

April 1995 to March 1997

H. Shinno, Surface and Interface Division

Keywords: aging, magnetic field, $Fe_{16}N_2$, ion implantation

Objective of this research is to investigate the basic mechanism of effects of magnetic field on aging behavior of thin films and their application to synthesis of thin films which are difficult to fabricate by other methods. For example, we synthesize $Fe_{16}N_2$ films by aging in magnetic field. $Fe_{16}N_2$ has high saturation magnetization, and has been attracting attention from both theoretical and practical points of view. However, synthesis of single phase $Fe_{16}N_2$ or samples with large volume fraction of $Fe_{16}N_2$ is difficult because $Fe_{16}N_2$ is a metastable state and easily decomposes at temperatures higher than 473 K.

In this study, $Fe_{16}N_2$ is synthesized from α'-martensite by low temperature aging to avoid decomposition. The α'-martensite is fabricated by nitrogen ion implantation into Fe films or sputtering of Fe target in atmosphere of nitrogen and argon.

In α'-martensite, nitrogen atoms occupy interstitial sites at random. $Fe_{16}N_2$ is an ordered state of α'-martensite in which nitrogen atoms occupy regular sites. During the aging, nitrogen atoms diffuse to the regular sites and α'-martensite transforms to $Fe_{16}N_2$. Usually, long time aging is necessary to get a sample with high volume fraction of $Fe_{16}N_2$ since diffusion rate is low at low temperature. In order to increase nitrogen diffusion rate without increasing aging temperature, magnetic field is applied during aging. Magnetostriction may increase diffusion rate of nitrogen by lowering potential barriers for diffusion and accelerate transformation rate from α'-martensite to $Fe_{16}N_2$.

Effects of aging in magnetic field on textures of thin films are also examined. During aging in magnetic field, preferential orientation of nuclei of precipitates may be influenced by magnetic field. This will affect textures and properties of thin films.

Related Paper

Synthesis of $Fe_{16}N_2$ by means of nitrogen ion implantation into Fe thin films, H. Shinno, K. Saito, M. Uehara, Proceedings of the tenth symposium on surface layer modification by ion implantation (1994): 17–23.

(166) Study of regenerator for ultra-low temperatures

April 1995 to March 1996

A. Saito, T. Numazawa, F. Matsumoto, H. Nagai, Strong Magnetic Field Research Station

Keywords: low temperature, regenerator, helium

New facilities for high magnetic field at High Magnet Field Research Station will offer various potentials for developments of new measurement technics on materials sciences. At the cryogenic research group, a new refrigeration system which is adapted for the hybrid magnet has been considered. The refrigeration system will be able to provide enough refrigeration capacity below 1 K under the extreme high magnetic field more than 35 Tesla. A new regenerative refrigeration cycle will be studied here instead of the dilution refrigerator system, because higher refrigeration capacity, stability and special installation design are required in the special condition. First, this study will be focused on regenerator materials. The materials require high heat capacity in the temperature range below 4 K. Several magnetic materials which is possible to make use of magnetic phase transitions and the Shottoky anomalies will be characterized by the measurements on specific heats and magnetocaloric effects. Then, regenerative refrigeration cycles will be studied with computer aided simulations based on the thermodynamic properties of the regenerator materials and the heat exchange gas which is composed by ^3He and ^4He. Finally, experimental regenerator will be assembled and tested. From the experimental data, actual regenerative refrigerator will be designed.

[167] Development of Quantum Microstructure un Ultra Clean Vacuum

April 1990 to March 1995

K. Yoshihara, 4th Research Group

Keywords: ultra clean vacuum, magnetic levitation specimen transfer system

It is that materials with quantum microstructures will possess new and useful properties. However, to create these materials, it is necessary to handle the materials in extremely clean and high vacuum environment. Otherwise, impurities from the environment will deteriorate the material properties. This project is divided into two phases. In the first phase (Apr. 1990–Mar. 1993), we have introduced the sample transfer system by a magnetic levitation system. By using this system, we transfer specimens from one station to the other station without any exposure to contaminating en-

vironment. In the second phase (Apr. 1993–Mar. 1995), we have create materials with quantum microstructures by using this ultra clean vacuum system.

By using new vacuum pumps and special gate valves, we have constructed the extremely high vacuum system (10^{-10} Pa) for two types of magnetic levitation transport system. One is a linear motor system composed of four stators and a carrier which is transferred over stators with three samples. The other system uses couples of the magnets made of super conductive material and permanent magnets. Super conductive magnets moved in a large cryostat at a temperature lower than 100 K. With these magnetic levitation transport system, specimens can be transferred in the vacuum of less than 10^{-8} Pa, and the out gassing rate of these system is lower than that of the traditional transport systems using a feedthrough manipulator or an all-metal magnet coupling.

In the ultra clean vacuum system, we could produce a microstructure on Ti film by Cu segregation. The segregation behavior is significantly affected by the vacuum pressure. The effectiveness of the ultra clean vacuum system has been demonstrated.

Related Papers

Extremely High Vacuum System for Long-distance Transport, M. Tosa, A. Itakura and K. Yoshihara, Vacuum 44 (1993): 549–51.

Magnetic Levitation Transport for XHV Continuous Process, M. Tosa, A. Itakura, M. Harada and K. Yoshihara, J. Vacuum Society of Japan 37 (1994): 789.

Publications

❒ Papers Published in 1994

Characterization/Properties

Electronic and nuclear properties

1. *The In-plane Resistive Transition for Magnetic Fields Paralled to the C-axis in Single Crystalline (La1-xSrx)$_2$CuO$_4$,* S. L. Yuan (Univ. of Tokyo), K. Kadowaki, K. Kishio, Z. J. Yang, K. Kitazawa (Univ. of Tokyo), Advances in Superconductivity, (1994): 135.
2. *The Lorentz Force Free C-axis Magnetoresistivity in HllCll in Single Crystalline (La1-xSrx)$_2$ CuO$_4$,* S. L. Yuan (Univ. of Tokyo), K. Kadowaki, K. Kishio, Z. J. Yang, K. Kitazawa (Univ. of Tokyo), Advances in Superconductivity, (1994): 139.
3. *Critical Analyses of the Resistivity in High Tc-Superconductors: For the Case of Single Crystalline Bi$_2$Sr$_2$CaCu$_2$O$_{8+\delta}$,* K. Kadowaki, T. Mochiku, H. Takeya, S. L. Yuan (Univ. of Tokyo), Y. Saitou (Univ. of Tsukuba), Advances in Superconductivity, (1994): 545.
4. *Redox Potentials of Bromo and Chloro(phthalocyaninato) bismuth(III) Complexes,* H. Isago, Y. Kagaya, Bulletin of the Chemical Society of Japan, 67 (1994): 3212.
5. *Facile Reduction of Dichloro (phthalocyanianto) antimony(V) Cation,* Y. Kagaya, H. Isago, Chemistry Letters, (1994): 1957.
6. *Anomalous Field Dependent Heat Capacity in UPt3 below 1K,* K. Kadowaki, N. Wada (Univ. of Tokyo), J. Alloys and Compounds, 207–08 (1994): 337.
7. *Quantum Tunneling of Flux in the High Tc Superconductor YBa2Cu307-δ,* S. Uji, J. Jpn. Inst. Met., 33 (1994): 395.
8. *Magnetic Properties of Iron Fine Particles in Fe-MgF2 Composite Films,* T. Furubayashi, J. Mag. Mag. Mater, 140–44 (1994): 393.
9. *Anisotropic Electrical Conductivity of α-HxV2O5(x = 0. 00 ~ 0. 27),* M. Shimoda, K. Yagisawa, M. Yoshikawa, J. Mater. Sci., 29 (1994): 478.
10. *Crystal Structure and Hydrogen Occupation in HxV2O5(x = 0. 0 ~ 3. 9),* M. Yoshikawa, K. Yagisawa, M. Shimoda, J. Mater. Sci., 29 (1994): 1319.
11. *Fermi Surface Reconstruction in the Organic Conductor (BEDT-TTF)2TlHg (SCN)4,* S. Uji, H. Aoki, T. Terashima, J.S. Brooks (Boston Univ.), M. Tokumoto, N. Kinoshita, T. Kinoshita, Y. Tanaka (Electrotechnical Laboratory), H. Anzai (Himeji Institute of Technology), J. Phys. Condens. Matter, 6 (1994): 539.
12. *Analysis of de Haas-van Alphen Oscillations and Band Structure of an Organic Superconductor, θ—(BEDT-TTF)213,* M. Tamura, H. Kuroda (Univ. of Tokyo), S. Uji, H. Aoki, M. Tokumoto (Electrotechnical Laboratory), J. Phys. Soc. Jpn., 63 (1994): 615.
13. *Temperature Dependence of Gient Magnetoresistance in Co/Cu Superlattices,* S. Uji, T. Terashima, H. Aoki, Y. Saitou, K. Inomata (TOSHIBA Advanced Research Laboratory), J. Phys. Soc. Jpn., 64 (1994): 1263.
14. *Mixed State of High temperature Superconductors -its Peculiarifies-,* K. Kadowaki, Oyo Buturi, 63 (1994): 354.
15. *Fermi Surface Nesting in the Organic Conductor (BEDT-TTF)2TlHg(SCN)4,* S. Uji, H. Aoki, M. Tokumoto, N. Kinoshita, T. Kinoshita, Y. Tanaka, H. Anzai (Electrotechnical Laboratory), Phys. Rev. B, 49 (1994): 732.
16. *Coexistence of One-and-Three-Dimensional Fermi Surfaces and Heavy Cyclotron Mass in the Molecular Conductor (DMe-DCNQI)2Cu,* S. Uji, T. Terashima, H. Aoki, J. S. Brooks (Boston Univ.), R. Katou, M. Tamura, H. Sawa, M. Kinoshita, H. Aonuma (The Institute fo Solid State Physics The Univ. of Tokyo), Phys. Rev. B, 50 (1994): 15597.
17. *First Observation of 3D Fermi Surface,* S. Uji, Phys. Sci. Magazine, 9 (1994): 40.
18. *Vortex Dynamics above the Irreversibility Line in High-Tc Oxide Single Crystals,* K. Kadowaki, T. Mochiku, H. Takeya, S. L. Yuan (Univ. of Tokyo), Y. Saito (Univ. of Tsukuba), Physica B, (1994): 253.
19. *Vortex Dynamics Above the Irreversibility Line in LSCO,* K. Kadowaki, S. L. Yuan (Univ. of Tokyo), T. Mochiku, K. Kishio, K. Kitazawa (Univ. of Tokyo), Physica B, 194–96 (1994): 2045.
20. *Effect of Pressure on Magnetic Susceptibility in α-and γ-Ce,* T. Naka, T. Matsumoto, N. Mouri (The Institute for Solid State Physics The

Univ. of Tokyo), Physica B, 194–96 (1994): 331.

21. *Fermi Surface and Magnetoresistance in β″-(BEDT-TTF)2AuBr2*, S. Uji, H. Aoki, M. Ukawa, H. Yakushi, M. Tokumoto (Electrotechnical Laboratory), Physica B, 194–96 (1994): 1307.
22. *Interlayer-Josephson Effect and Critical Currents in Single Crystalline $Bi_2Sr_2CaCu_2O_{8+\delta}$*, K. Kadowaki, T. Mochiku, Physica B, 194–96 (1994): 2239.
23. *Effect of Pressure on Crystal Field Splitting in CeP*, T. Naka, T. Matsumoto, Y. Okayama, N. Mouri (The Institute for Solid State Physics The Univ. of Tokyo), Y. Yoshiga, T. Suzuki (Tohoku Univ.), Physica B, 199 (1994): 551.
24. *Decay of Metastable States of High Tc and Conventional "low Tc" Superconductors*, M. Uehara, T. Numazawa, T. Hirano, Physica C, 235 (1994): 2905.
25. *Non-linear Transport Phenomena Along the C-axis in Single Crystalline $Bi_2Sr_2CaCu_2O_{8+\delta}$*, K. Kadowaki, T. Mochiku, H. Takeya, K. Hirata, Y. Saitou, Physica C, 235 (1994): 3275.
26. *Transport Phenomena and C-axis Critical Current Denities in Single Crystalline $Bi_2Sr_2Ca Cu_2O_{8+\delta}$*, K. Kadowaki, T. Mochiku, Proc. of 1994 International Workshop on Superconductivity, (1994): 155.
27. *Magnetic Breakdown and Fermi Surface Nesting in the Organic Conductor (BEDT-TTF)2TlHg (SCN)4*, S. Uji, T. Terashima, H. Aoki, M. Tokumoto, N. Kinoshita, T. Kinoshita, Y. Tanoka, H. Anzai, Proc. of ISSP Symposium, 201 (1994): 482.
28. *Fermi Surface and Magnetoresistance in an Organic Metals β″—(BEDT-TTF)2AuBr2*, S. Uji, H. Aoki, M. Tokumoto (Electrotechnical Laboratory), M. Ukawa, H. Yakushi (Institute for Molecular Science), Proc. of Mater. Res. Soc. Sympo., 328 (1994): 337.
29. *Three-Dimensional Fermi Surface in θ—(BEDT-TTF)213*, T. Terashima, S. Uji, H. Aoki, M. Tamura, H. Kinoshita (The Institute for Solid state physics The Univ. of Tokyo), M. Tokumoto (Electrotechnical Laboratory), Solid State Communication, 91 (1994): 595.
30. *Lorentz Force Independent Dissipation in High Temperature Superconductors*, K. Kadowaki, S. L. Yuan, K. Kitazawa (Univ. of Tokyo), Superconductor Science and Technology, 7 (1994): 519.

Atomistic arrangement

31. *Non-Stoichiometry and Superconducting Transition Temperature in Artificially Layered BSCCO Films*, T. Hatano, A. Ishii, K. Nakamura, Proc. of Advanced Materials '93 VI, A Superconductors Surfaces and Superlattices, (1994): 575.
32. *The Location of Atoms in Re- and V-Containing Multilcomponent Nickel-base Single-Crystal Superalloys*, H. Murakami, H. Harada, H. K. D. H. Bhadeshia (Univ. of Cambridge), Appl. Surf. Sci., 76–77 (1994): 177.
33. *HRTEM Studies on a Superconductor $YPd_2B_2C_x$ Compound*, S. Ikeda, H. Fujii, T. Kimura, H. Kumakura, K. Kadowaki, T. Togano, J. Appl. Phys., 33 (1994): 3896.
34. *Uniformly Layered Mixtures of the Bi_2Sr_2Can—$1CunO_{4+2n}$ Phases Formed in Artificially Layered Films—Structural Analysis and Superconducting Properties*, T. Hatano, K. Nakamura, A. Ishii, S. Ikeda, H. Narita (Yasukawa Electric Corp.), J. Satou (Hitachi Cable, Ltd.), J. Appl. Phys., 75 (1994): 2241.
35. *Nitrogen Effect in Mechanical Alloying of Immiscible Cu-V: Extended X-ray Absorption Fine Structure Study*, K. Sakurai, T. Ri, N. Kuroda, T. Fukunaga, U. Mizutani (Nagoya Univ.), J. Appl. Phys., 75 (1994): 7752.
36. *Resonant Irradiation Creep of 316 Stainless Steel Under Pulsed Duteron Bombardment*, N. Kishimoto, H. Amekura, J. Nuc. Mater, 212–215 (1994): 535.
37. *Infrared and Raman Spectra of Solid Solutions Ti1 - xZrxO2 ($x \leqq 0.1$)*, T. Hirata, M. Kitajima, K. Nakamura, E. Asari (Univ. of Tsukuba), J. Phys. Chem. Sol., 55 (1994): 349.
38. *Structural and Magnetic Studies of Metal-Insulator Transition in Thiospinel CuIr2S4*, T. Furubayashi, T. Matsumoto, T. Hagimoku, S. Nagata (Muroran Institute of Technology), J. Phys. Soc. Jpn., 63 (1994): 3333.
39. *Infrared and Raman Spectroscopic Studies of ZrO_2 Polymorphs Doped with Y_2O_3 or CeO_2*, T. Hirata, E. Asari (Univ. of Tsukuba), M. Kitajima, J. Solid State Chemistry, 110 (1994): 201.
40. *Artificial Bi_2Sr_2Can—$1CunO_{2n+4}$ Films by Sequential Sputter Deposition*, T. Hatano, K. Nakamura, J. Superconductivity, 7 (1994): 239.
41. *Structural Certification and Superconducting Properties in 2234/2223 Superlattice*, T. Hatano, K. Nakamura. K. Kadowaki, Physica B, B194–96 (1994): 2307.
42. *Pressure Effects on the Electrical Resistivities of $(Y_{1-x}Pr_x)_2Ba_4Cu_7O_{15-\delta}$ with X = 0, 0. 1, 0. 4 and 0. 6*, A. Matsusita, T. Yananishi (Shibaura Institute of Technology), H. Yamada (Nagoya Univ.), S. Yamada (Electro-Communication Univ.), S. Takashima, Physica C, 227 (1994): 254.

43. *Structural Disorder and Relaxation in $YBa_2Cu_3O_{7-\delta}$ Thin Films and their Influences on Tc*, K. You, K. Nakamura, Physica C, 235–40 (1994): 581.

44. *Infrared Reflectivity Study of ZrO_2 – H + O_2 Solid Solutions*, T. Hirata, Phys. Rev. B, 50 (1994): 2874.

45. *A Systematic Study on the Growth Temperature Dependence of Structural Disorder and Superconductivity in $YBa_2Cu_3O_{7-\delta}$ Thin Films*, K. You, K. Nakamura, Phys. Rev. B, 50 (1994): 7099.

46. *Volume-Expansion-Induced Lattice Instability and Solid-State Amorphization*, K. Kusunoki, Phys. Rev. Letters, (1994): 295.

47. *Complete Fermi Surface Mapping of $Bi_2Sr_2CaCu_2O_8$ + X(001): Coexistence of Short Range Antiferromagnetic Correlations and Metallicity in the Same Phase*, M. Shimoda, T. Mochiku, K. Kadowaki, P. Aebi, J. Osterwalder (Institute de Physique Universite de Fribourg), P. Schaller, L. S. Chlapbach (Institute de Physique Universite de Fribourg), Phys. Rev. Letters, 72 (1994): 2757.

48. *Electron Diffraction and HRTEM Studies on a New Superconductor YPd_2B_2-C*, S. Ikeda, H. Fujii, T. Kimura, H. Kumakura, K. Kadowaki, K. Togano, Proc. of Int. Cong. Electron Microscopy (1994), 2B (1994): 931.

49. *Bi2223/2234 Superlattice. It's Structural Analysis and Tc*, T. Hatano, K. Kadowaki, K. Nakamura, Proc. of Superconducting Superlattices and Multilayers, 2157 (1994): 207.

50. *Overturning of Molecules in Alternating LB Films of Amphiphilic Diacetylene and Fatty Acid*, S. Arisawa, S. Hara, T. Arise, R. Yamamoto (Univ. of Tokyo), Thin Solid Films, 242 (1994): 295.

Phase transformation and micro structures

51. *Phase Transformations and Interfaces in a MaO Partially Stabilized Zirconia*, F. Abe, S. Ikeda, S. Muneki, K. Yagi, PROC '94, (1994): 216.

52. *Synthesis and Control of Stoichiometry for Intermetallic Compound Films by Molecular Beam Epitaxy* , M. Yata, K. Nakamura, IONICS, 20 (1994): 113.

53. *Tetragonal to Monoclinic Transformation in ZrO2-9. 7mol%MgO during Cyclic Anneling*, F. Abe, S. Muneki, Proc. of International Conference on Solid Phase Transformations in Organic Materials, (1994): 823.

54. *Control of Stoichiometry of Pd Te Intermetallic Compound Films by Molecular Beam Epitaxy*, M. Yata, K. Nakamura, K. Ogawa (Yokohama City Univ.), Proc. of "Processing and Fabrication of Advanced Materials for High Temperature Applications III"), (1994): 451.

55. *Thermal- and Stress-responsibilities of Tetragonal Phase in Partially-stabilized ZrO_2*, S. Muneki, F. Abe, Proc. of the 3rd Sympo. Intelligent Mater., (1994): 22.

Surface and interface properties

56. *Water Adsorption-Characteristics of Two Types of Proton Conducting Antimonic Acids*, Y. Sakka, T. Uchikoshi, K. Ozawa, M. Amano, PROC '94, (1994): 239.

57. *Multi-Layered Segregation of Titanium from Substrate at the Surface of Niobium Film by Rapid Difffusion*, M. Yoshitake, K. Yoshihara, J. Jpn. Inst. Mater, 58 (1994): 768.

58. *Surface Precipitation Process of Epitaxially Growth Graphite(0001) Layers on Carbon-Doped Nickel(111) Surfaces*, D. Fujita, K. Yoshihara, J. Vac. Sci. & Tech., 12 (1994): 2134.

59. *Preparation of Metal Segregated Surface and the Potential of Work Function Control by Surface Segregation*, M. Yoshitake, K. Yoshihara, J. Vac. Soc. Jpn., 37 (1994): 128.

60. *Characterization of (Fe, Ni, Co)-TiN Nanocomposite Particles Synthesized by "Reactive Plasma-Metal" Reaction Method*, Y. Sakka, S. Oono, T. Uchikoshi, H. Okuyama, Proc. of 3rd IUMRS International Conference on Advanced Materials, (1994): 57.

61. *High-Temperature Reactions of an Nb-19at%Al Alloy*, M. Okamoto, I. Tomizuka, A. Miyazaki, Proc. of 3rd IUMRS International Conference on Advanced Materials, (1994): 321.

62. *High-Temperature Reaction of Nb-19at%Al Alloy in Oxygen During a Constant Rate of Heating up to 1000 °C*, M. Okamoto, I. Tomizuka, A. Miyazaki, Zairyo-to-Kankyo, 43 (1994): 364.

63. *A Handy Time-of-Wetness Meter Using Hg Coulometer*, K. Kurosawa, M. T. Torre (ITDI Philippines), T. Kodama, T. Fukushima (Univ. of Ryukyu), Zairyo-to-Kankyo, 43 (1994): 695.

Mechanical properties

64. *Cyclic Fatigue in Silicon Nitride Ceramics*, Guenchoi, S. Horibe (Waseda Univ.), Y. Kawabe, Acta Metall. Mater, 42 (1994): 1407.

65. *Cyclic Fatigue Crack Growth from Indentation Flaw in Silicon Nitride: Influence of Effective Stress Ration*, Guenchoi, S. Horibe (Waseda Univ.), Y. Kawabe, Acta Metall. Mater, 42 (1994): 3837.

66. *Fatigue Crack Propagation Mechanism near Fatigue Thresho lb for SiC Whisher or SiC Paricle Reinforced Aluminum alloy Matrix Composites*, C. Masuda, Y. Tanaka, M. Yamamoto, M. Fukazawa (Tokai Carbon Co., Ltd.), Advanced Composite Materials, 3 (1994): 319.

67. *Review of High Cycle Fatigue Properties of Structural Materials at Cryogenic Temperatures*, O. Umezawa, T. Ogata, T. Yuri, K. Nagai, K. Ishikawa (Toyo Univ.), Advances in Cryogenic Engineering Materials, 40 (1994): 1231.

68. *Effect of Stress on Precipitaton Morphology of γ'—Phase and Creep Strength Propeties of Inconel 713C*, H. Nagai, K. Kimura, F. Abe, K. Yagi, Current Advances in Materials and Processes, 7 (1994): 1796.

69. *Relationship between Deviations from Slip Plane and Slip Systems of Layered Dislocation Structures in Copper Single Crystals*, Y. Kawasaki, Dikawqed "Strength of Metals", (1994): 187.

70. *Effect of Relative Slip Amplitude on Fretting Fatigue of High Strength Steel*, K. Nakazawa, M. Sumita, N. Maruyama, Fatigue & Fracture of Engineering Materials and Structures, 17 (1994): 751.

71. *Cu-Ag Wire Pulsed Magnets With and Without Internal Reinforcement* , T. Asano, Y. Sakai, M. Oshikiri, K. Inoue, H. Maed, IEEE Transactions on Magnetics, 30 (1994): 2106.

72. *Measurements of Elastic Moduli of JIS Steels for Machine Structural Use*, T. Abe, K. Kanazawa, H. Nishijima, J. Mater. Testing. Res. Asso., 39 (1994): 53.

73. *Fracture Properties of Neutron-Irradiated Martensitic 9Cr-WVTa Steels Below Room Temperature*, F. Abe, M. Narui, H. Kayano (Tohoku Univ.), J. Nuc. Mater., 212 (1994): 746.

74. *Effect of Carbon on Irradiation Hardening of Reduced-Activation 10Cr-30Mn Austennitic Steels*, F. Abe, F. A. Garner (Pacific Northwest National Laboratory), H. Kayano (Tohoku Univ.), J. Nuc. Mater, 212 (1994): 760.

75. *Extension of Creep Rupture Life by Sintering of Grain Boundary Cavities in 316 Stainless Steel* , M. Murata, H. Tanaka, N. Shinya, J. Soc. Mater. Sci. Jpn., 43 (1994): 652.

76. *VAMAS Test of Structural Materials at Liquid Helium Temperature*, T. Ogata, K. Nagai, K. Ishikawa (Toyo Univ.), Proc. of Advances in Cryogenic Engineering Materials, 40 (1994): 1191.

77. *Phenomenological Aspects of Fatigue Life and Fatigue Crack Initiation in High Strength Alloys at Cryogenic Temperatures*, O. Umezawa, K. Ishikawa (Toyo Univ.), Mater. Sci. Eng. A, (1994): 397.

78. *Estimation of Long-term Creep Rupture Life for Carbon and Low Alloy Steels by Iso-stress Method*, O. Kanemal, M. Simizu, H. Miyazaki, K. Yagi, Pressure Engineering, 32 (1994): 2.

79. *Abnormal Creep Deformation Behaviour and Inhavant Creep Strength of Carbon Steel*, K. Kimura, H. Kushima, K. Yagi, Proc. of ICSMA 10, (1994): 645.

80. *High Temperature Tensile Properties of a Series of Nickel-base Superalloys on a γ/γ' Tie-Line*, Y. Ro, H. Koizumi, H. Harada, Proc. of Materials for Advanced Power Engineering 1994, (1994): 883.

81. *Strength and Toughness of Tungsten-Stabilized Ferritic/Martensitic Steels for Fusion Reactor*, F. Abe, Proc. of the 2nd Japan/China Symposium on Materials for Advanced Energy System and Fusion Engineering, (1994): 319.

82. *Phase Stability and Creep Behavior of 10Cr-30Mn Austenitic Steels*, F. Abe, Proc. of 10th Int. Conf. Strength of Mater, (1994): 627.

83. *Characterization of Long-term Creep Strength for 12Cr Steel*, H. Kushima, K. Kimura, K. Yagi, K. Maruyama (Tohoku Univ.), Proc. of 10th International Conference on the Strength of Materials, (1994): 653.

84. *Cavity Growth in a Fine-Grained Yttria-Stabilized Tetragonal Zirconia during Superplatic Deformation*, K. Hiraga, H. Takakura, Proc. of 10th Int. Conf. Strength of Mater, (1994): 843.

85. *Means for Producing High Strength Weldments against Fatigue Loading*, A. Oota, N. Suzuki, Y. Maeda, Q. J. Jpn. Weld. Soc., 12 (1994): 440.

86. *High Temperature Strength and Environmetal Performance*, N. Shinya, Q. J. Jpn. Weld. Soc., 63 (1994): 375.

87. *Effect of γ' Phase on Long-Time Creep Rupture Properties of Nickel-base Superalloy, Inconel 713C*, H. Nagai, K. Yokokawa, H. Yoshizu, K. Kimura, K. Yagi, C. Tanaka, Report of the 123rd Committee on Heat-Resisting Metals and Alloys Japan Society for the Promotion of Science, 35 (1994): 137.

88. *Long-term Creep Rupture Properties and Microstructural Change for Udimet 500*, K. Yokokawa, K. Yagi, C. Tanaka, Report of the 123rd Committee on Heat-Resisting Metals and Alloys Japan Society for the Promotion of Science, 35 (1994): 153.

89. *Assessment of Creep Strength Properties of 2. 25Cr-1Mo Steel Based on Creep Deformation Behaviour*, H. Kushima, K. Kimura, F. Abe, K. Yagi, K. Maruyama (Tohoku Univ.), Report of the 123rd Committee on Heat-Resisting Metals and Alloys Japan Society for the Promotion of Science, 35 (1994): 261.

90. *Smart Skins and New Type Snsors*, M. Egashira, Science of Machine, 46 (1994): 1283.

91. *Evaluation of 100,000h Creep Properties on Heat Resistant Steels and Alloys and Farther Develop-*

ment of Research on High Temperature Creep, C. Tanaka, K. Yagi, Tetsu-to-Hagane, 80 (1994): 255.

92. *Dynamic Fracture Tougness and Evaluation of a Thick-Walled Ferritic Spheroidal Graphite Iron*, K. Nakano, T. Yasunaka, Tetsu-to-Hagane, 80 (1994): 330.
93. *Relationship between Fatigue Crack Propagation Properties and Film Thickness*, E. Takeuchi, S. Matsuoka, H. Nishijima, Trans. Jpn. Soc. Mech. Eng., 60 (1994): 344.
94. *Arrest Function on Elevated Fatigue Crack Propagation*, E. Takeuchi, S. Matsuoka, K. Miyahara, H. Hirukawa, Y. Ikeda, Trans. Jpn. Soc. Mech. Eng., 60 (1994): 1487.
95. *Effects of Non-Metallic inclusions on Uniaxial and Reversed Torsion Fatigue Properties of Spring Steels*, T. Abe, K. Kanazawa, Trans. Jpn. Soc. Spring. Res., (1994): 17.
96. *Shaped up Materials—A New Design Concept of Environmental Conscious Heat Resistant Steels*, K. Kimura, H. Kushima, K. Yagi, C. Tanaka, Trans. Mater. Res. Soc. Jpn., 18A (1994): 147.

Measurement and evaluation

97. *Present Status of the High-Field Research Center at the National Research Institute for Metals, Japan*, K. Inoue, T. Kiyoshi, T. Asano, Y. Sakai, Advances in Cryogenic Engineering Materials, 39 (1994): 419.
98. *Determination of Trace Amounts of Zinc in Nickel-Based Heat-Resisting Alloys by Graphite Furnace Atomic Absorption Spectrometry*, K. Ide, M. Kudou (The Metropolitan Police Board), T. Kobayashi, S. Hasegawa, H. Ookouchi, Bunseki Kagaku, 43 (1994): 215.
99. *Determination of Trace Silicon in High Purity Nickel using a Masking Reagent for the Matrix Element* , M. Kiyokawa, H. Yamaguchi, R. Hasegawa, Bunseki Kagaku, 43 (1994): 289.
100. *The Solid Phase Extraction of Organotin Compounds in Sea Water*, M. Gun, Y. Inoue (Yokogawa Analyticals Systems Inc.), K. Ide, K. Satou, H. Ookouchi, Bunseki Kagaku, 43 (1994): 933.
101. *X-ray Photoelectron Spectroscopy Recent Development in Data Treatment*, M. Yoshitake, Bunseki, (1994): 1013.
102. *Improvement of Creep Rupture Properties by Control of Creep Damage at Grain Boundary in Austenite Stainless Steel*, J. Kyouno, H. Tanaka, M. Murata, N. Shinya, Current Advances in Materials and Processes, 7 (1994): 1787.
103. *The Solid Phase Extraction of Organotin Compounds*, M. Gun, Y. Inoue (Yokogawa Analyticals Systems Inc.), K. Ide, K. Satou, H. Ookouchi, Proc. of Environmental Chemistry, 4 (1994): 481.
104. *Evaluation of an Axially and Radially Viewed Inductively Coupled Plasma Using an Echelle Spectrometer With Wavelength Modulation and Second-derivative Detection*, K. Nakamura, C. W. McLeod (Sheffield City Polytechnic), K. Takahashi, O. Kujirai, H. Ookouchi, Metallurgical Transactions A, 9 (1994): 751.
105. *Simultaneous Determination of Seven Trace Impurities (Al, As, Cr, Fe, Ti, V and Zr) High-Purity Nickel Metal and Nickel Oxide by Co precipitation*, O. Kujirai, K. Yamada, J. Analytical Chemistry, 348 (1994): 719.
106. *Development of Three-Dimensional Ultrasonic Simulation and Its Application*, H. Yamawaki, T. Saitou, C. Masuda, H. Fukuhara, J. Appl. Phys., 33 (1994): 3126.
107. *Technologies for Detection of Materials Degradations*, T. Saitou, J. Atomic Energy Soc. Jpn., 36 (1994): 380.
108. *Diffusion of Molten Au-Ag System under Microgravity Conditions*, T. Dan, Y. Muramatsu, T. Yamagota, K. Hoshimoto, T. Kimura, J. Japanese Asso. Crystal Growth, 21 (1994): 385.
109. *Graphite Furnace Atomic Absorption Spectrometry*, T. Kobayashi, J. Jpn. Inst. Mater, 33 (1994): 313.
110. *Analysis of Ultra-trace Elements by GDMS using Ar/H_2 Gas Mixture*, M. Saitou, J. Jpn. Inst. Met., 33 (1994): 346.
111. *Development of Quantitative Auger Electron Spectroscopy with High Accuracy and High Performance*, D. Fujii, J. Jpn. Inst. Mater, 33 (1994): 610.
112. *Determination of Trace Amounts of Pb, Mn and Co in Acidic Solutions of Zirconium and Molybdenum by GF-AAS*, S. Hasegawa, T. Kobayashi, K. Ide, H. Ookouchi, R. Hasegawa, J. Jpn. Inst. Mater, 58 (1994): 23.
113. *Determination of Trace Amounts of Impurities in Molybdenum by Spark Source and Glow Discharge Mass Spectrometry*, M. Saitou, J. Jpn. Inst. Mater, 58 (1994): 188.
114. *Relative Sensitivity Factors for the Analysis of Steel by Glow Discharge Mass Spectrometry*, S. Itou, F. Hirose, R. Hasegawa, J. Jpn. Inst. Mater, 58 (1994): 526.
115. *Fatigue Crack Propagation Mechanism Near Fatigue Threshold for SiC Whiosker of Particle Reinforced Aluminum alloy Matrix Composition*, T. Masuda, Y. Tanaka, M. Yamamoto (Tokai Carbon Co., Ltd.), M. Fukazawa (Tokai Carbon Co., Ltd.), J. Jpn. Soc. Compo. Mater., 20 (1994): 116.

116. *Optimization of Measuring Condition for the Analysis of Trace Elements in Iron and Steels by GF-AAS*, T. Kobayashi, S. Hasegawa, T. Yoshioka, T. Hasegawa, J. Jpn. Inst. Mater, 58 (1994): 789.

117. *Observation of High-Temperature Oxidation of Laser Microscope*, A. Miyazaki, M. Okamoto, O. Tomizuka, J. Mater. Sci. Soc. Jpn., 31 (1994): 29.

118. *Quantitative Examination of Radiation-Induced Disorder in γ' (Ni_3Al) Precipitates with Cooled CCD Camera Attached to TEM*, T. Kimoto, T. Saitou, J. Nuc. Mater, 212–15 (1994): 275.

119. *Development of VAMAS Type Standard Channel Electron Multiplier for Quantitative Auger Electron Spectroscopy*, D. Fujita, K. Yoshihara, Y. Shiokawa (Anelva Corp.), J. Surf. Sci. Soc. Jpn., 15 (1994): 2.

120. *Development of High Resolution Angle Resolved Electron Spectrometer (HR-ARES) for Measurements of Angular Distribution of Elastically or Inelastic*, D. Fujita, T. Yakabe, K. Yoshihara, J. Surf. Sci. Soc. Jpn., 15 (1994): 43.

121. *Round Robin on the Energy Dependence of Sensitivity in Auger Electron Spectroscopy*, M. Yoshitake, K. Yoshihara, J. Surf. Sci. Soc. Jpn., 15 (1994): 376.

122. *New Thickness Evaluation Method for Hydrocarbon Overlayer on the Surface of the Kilogram Prototype with Angle Resolved X-ray Photoelectron Spectrometry*, D. Fujita, K. Yoshihara, J. Vac. Soc. Jpn., 37 (1994): 248.

123. *Microtomagrphy using Conventional X-ray Sources*, Y. Yamauchi, N. Kishimoto, T. Ikuta (Osaka Electro-Communication Univ.), Nondestructive Characterization of Materials, (1994): 129.

124. *40 Tesla Class Hybrid Magnet System*, K. Inoue, T. Takeuchi, T. Kiyoshi, K. Itou, K. Takehana, H. Wada, H. Maeda, Physica B, 201 (1994): 517.

125. *21. 1 Tesla Superconducting Magnet with 50 mm Clear Bore*, M. Oshikiri, K. Inoue, T. Kiyoshi, T. Takeuchi, K. Itou, M. Kosuge, Y. Iijima, M. Yuyama, H. Maeda, Physica B, 201 (1994): 521.

126. *Overview on SiC-Carbon Materials*, T. Noda, Proc. of Carbon Materials, (1994): 61.

127. *Test Operation of Superconductive Part in 40 Tesla Class Hybrid Magnet*, K. Inoue, T. Takeuchi, K. Takehana, K. Itou, T. Kiyoshi, H. Maeda, T. Fujioka (Toshiba Corp.), Proc. of ICEC 15 Cryogenics, 34 (1994): 717.

128. *In Situ TEM Observation of Structural Changes of Ni Silicide Thin Films by FIB Lithography*, M. Tanaka, K. Furuya, Proc. of Beams 1994, (1994): 85.

129. *Anode Behaviour in GTA Welding and Its Effect on Melting Thin Plate—Study on Anode Behaviour on Molten Poll in GTA Wellding (Report 4)*, A. Okada, H. Nakamura, Q. J. Jpn. Weld. Soc., 12 (1994): 94.

130. *Comment on "High Intensity Low Tube-voltage X-ray Source for Laboratory Extended X-ray Absorption Fine Structure measurements"*, K. Sakurai, H. Sakurai (Rigaku Denki Co.), Rev. Sci. Instruments, 65 (1994): 2417.

131. *Practical Energy Scale Calibration Procedure for Auger Electron Spectrometers Using a Spectrometer Offset Function*, D. Fujita, K. Yoshihara, Surf. and Int. Anal., 21 (1994): 226.

132. *Nanoscopic Hardness Measurement by Atomic Force Microscope*, N. Nagashima, S. Matsuoka, K. Miyahara, Trans. Jpn. Soc. Mech. Eng., 61 (1994): 416.

133. *Application of Laser Speckle Strain Measurement to Weld Monitoring*, Y. Muramatsu, S. Kuroda, Welding Journal, 73 (1994): 101S.

134. *In Situ Measurement of Oxidation Ability of Thiobacillus Ferrooxidans by QCM*, N. Washizu, H. Masuda, S. Matsuoka, Zairyo-to-Kankyo, 43 (1994): 316.

Simulation and theory

135. *Modeling of α/α_2 Phase Equilibrium in the Ti-Al System by the Cluster Vaniation Method*, H. Onodera, T. Abe, T. Yokokawa, Acta Metall. Mater., 42 (1994): 887.

136. *Dependence of Diffraction Patterns on X-Ray Optics-Comparison Between Parafocusing Optics and Paralled Beam Optics*, T. Yokokawa, K. Oono, Advanced in X-Ray Chem. Anal. Jpn., 25 (1994): 61.

137. *Crystallization of Sputter Deposited Amorphous Ti-52at%Al Alloy*, T. Abe, S. Akiyama (Kougakuin Univ.), H. Onodera, ISIJ International, 34 (1994): 429 .

138. *Status of Radiation Embrittlement Study for the Pressure Vessel Steels Based on the Irradiation Correlation*, K. Ishino, N. Sekimura (Univ. of Tokyo), J. Nagakawa, K. Shibahara (PNC), M. Suzuki (JAERI), K. Asano (Univ. of Tokyo), J. Atomic Energy Soc. Jpn., 36 (1994): 36.

139. *Basic Irradiation Properties and Evaluation Technique-Long Term Properties*, J. Nagakawa, Proc. of J. Jpn. Inst. Mater. Sympo., (1994): 10.

140. *Outline on Data-Free-Way*, M. Fujita, F. Ueno (PNC), U. Nakajima (JAERI), S. Iwata (Univ. of Tokyo), J. Jpn. Inst. Mater., 33 (1994): 1254.

141. *Distributed Database for Materials (Data-Free-Way)*, M. Fujita, Y. Kurihara, U. Nakajima, N. Yokoyama (JAERI), F. Ueno, S. Kanou (PNC),

S. Iwata (Univ. of Tokyo), Proc. of J. Jpn. Soc. Info. Knowledge, (1994): 39.

142. *Attempt of Environmental Life Cycle Assessment for P/M Parts*, K. Harada, K. Minagawa, K. Yagki, J. Jpn. Soc. Powder Powder Metall., 41 (1994): 1383.

143. *Calculation of Radiation Induced Stress Relaxation*, J. Nagakawa, J. Nuc. Mater., 212–15 (1994): 541.

144. *Development of "Data-Free-Way" Distributed Database System for Advanced Nuclear Materials*, M. Fujita, Y. Kurihara, F. Ueno (PNC), S. Kanou (PNC), U. Nakajima (JAERI), N. Yokoyama (JAERI), J. Nucl. Sci. Technol., 31 (1994): 1314.

145. *Data System of Transmutation and Radioactivation for Nuclear Material Design*, M. Fujii, T. Noda, H. Shiraishi, Proc. of Materials for Advanced Energy Systems '94, (1994): 454.

146. *Metastable Phase Solidification in Electron Beam Welding of Dissimilar Stainless Steels*, S. Tsukamoto, H. Harada, H.K.D.H. Bhadeshia (Univ. of Cambridge), Mater. Sci. Eng, A178 (1994): 189.

147. *Development of Knowledge Base System for Computer Assisted Alloy Design*, K. Hoshimoto, Proc. of 3rd IUMRS International Conference on Advanced Materials, III/A (1994): 173.

148. *Parameter Analysis for Time-dependent Low-cycle Fatigue*, K. Yamaguchi, K. Kobayashi, K. Iijima, S. Nishijima, Trans. ASME, 116 (1994): 479.

149. *Prediction of Fatigue Strength Properties Using Material Strength Database (3rd Report)*, M. Nihei, T. Konno, Trans. Jpn. Soc. Mech. Eng., 60 (1994): 56.

Materials

Non-ferrous materials

150. *Effect of Heat Treatment on the Microstructure and the Mechanical behavior of TZM Alloy*, F. Moritou, J. Nuc. Mater, (1994): 1608.

151. *Characterization of Fracture Surfaces in TZM Alloys*, F. Moritou, Proc. of Klaus Schal Sympo. on Proc and Applications of High Purity Refrectory Metals and Alloys, (1994): 197.

Intermetallic compounds

152. *Modification of BiSrCaCuo System Superconducting Films by Ar Ion Implantation*, K. Saito, Advances in Superconductivity VI, (1994): 875.

153. *Electrical Conductivity of Solid IIa, IIIa Metal Sulfide*, H. Nakamura, Y. Ogawa, A. Kasahara., J. Jpn. Inst. Mater, 58 (1994): 519.

154. *Elastic Constants of some Transition-Metal-Dislicide Single Crystals*, M. Nakamura, Mater. Trans. JIM, 25A (1994): 312.

155. *Environmental Effect on Room Temperature Ductility of Isothermally Forged Tial Base Alloys*, M. Nakamura, N. Itou (Univ. of Kogakuin), K. Hashimoto, T. Tsujimoto (Univ. of Ibaraki), T. Suzuki (Univ. of Kogakuin), Mater. Trans. JIM, 25A (1994): 331.

Composites

156. *Evaluation Method of Fiber Distribution in Short Fiber Reinforced Metals*, Y. Imai, K. Shiota, Y. Shinohara, S. Ikeno, Advanced Composite Materials, 3 (1994): 239.

Materials for mechanical application

157. *Recyclable Materials Design*, K. Nagai, J. Jpn. Inst. Mater, 33 (1994): 524.

158. *High Cycle Fatigue Batiguo Properties of Beta Titanium Alloys*, S. Muneki, F. Moritou, J. Takahashi, N. Kainuma, Y. Kawabe, Metallurgy and Technology of Practical Titanium Alloys, (1994): 191.

159. *A Design Concept for Recyclable Materials with High Quality.* , K. Nagai, Trans. Mater. Res. Soc. Jpn., 18A (1994): 139.

Materials for electronics application

160. *Effect of Ag on Microstructure and Superconducting Properties of* $Bi_2Sr_2CaCu_2O_x$, H. Kumakura, H. Kitaguchi, K. Togano, T. Hasegawa, K. Kobayashi (Showa Electric Wire & Cable Co., Ltd.), Proc. of Advances in Cryogenic Engineering Materials, 40 (1994): 1.

161. *V_3Si Multifilamentary Superconductor with High Overall Jc.* , T. Takeuchi, K. Inoue, M. Kosuge, Y. Iijima, K. Watanabe (Univ. of Tohoku), Proc. of Advances in Cryogenic Engineering Materials, 40 (1994): 891.

162. *Nb_3Al Multifilamentary Wires Continuously Fabricated by Rapid-Quenching*, Y. Iijima, M. Kosuge, T. Takeuchi, K. Inoue, Proc. of Advances in Cryogenic Engineering Materials, 40 (1994): 899.

163. *Phase Changes and Solidification Mechanism of Bi-2212 from Partially Molten State* , H. Kumakura, K. Togano, T. Hasegawa, K. Kobayashi (Showa Electric Wire & Cable Co., Ltd), Advances in Superconductivity VI, 6 (1994): 707.

164. *Observation of Sulfur-terminated GaAs(001)-(2x6) Reconstruction by Scanning Tunneling Microscopy*, S. Tsukamoto, N. Koguchi, Appl. Phys Letters, 64 (1994): 2199.

165. *Synthesis of YNi_2B_2C Thin Films by Magnetron Sputtering*, S. Arisawa, T. Hatano, K. Hirata, T. Mochiku, H. Kitaguchi, H. Fujii, H. Kumakura, K. Nakamura, K. Togano, Appl. Phys. Letters, 65 (1994): 1299.

166. *Superconducting Properties of Bi2223 Tapes Prepared by AGCU Alloy Sheath Doped with Titanion*, B. Matsumoto, H. Maeda, Y. Tanaka, M. Ishizuka, Cryogenic Engineering, (1994): 69.

167. *Development of Bronze-Processed V_3Si Multifilamentary Superconductors for AC Applications*, T. Takeuchi, K. Itou, K. Inoue, Cryogenic Engineering, 29 (1994): 386.

168. *High-Strength and High-Conductivity Cu-Ag Alloy Sheets: New Promising Conductor for High-Field Bitter Coils*, Y. Sakai, K. Inoue, H. Maeda, IEEE Transactions on Magnetics, 30 (1994): AAA.

169. *Structure and Superconducting Properties of the Y-Pd-B-C System*, H. Fujii, S. Ikeda, T. Kimura, S. Arisawa, K. Hirata, J. Alloys and Compounds, 33 (1994): L590.

170. *2x6 Surface Reconstruction of Sulfur-terminated GaAs(001) Observed by Scanning Tunneling Microscopy*, S. Tsukamoto, N. Koguchi, J. Appl. Phys, 33 (1994): 1185.

171. *Internal Oxidation of Ag-$Y_1Ba_2Cu_3$, -$Bi_2Sr_2Ca_1Cu_2$ and -Bi1. 8Pbo. $3Sr_2Ca_2Cu_3$ Alloys, and their Resulting Superconducting Properties*, M. Satou, T. Numazawa, H. Kimura, M. Fukamachi, J. Jpn. Inst. Mater, 58 (1994): 235.

172. *Effects of Impurity Contents of Starting Materials of $YBa_2Cu_3O_x$ on Superconducting Characteristics*, K. Maiwa, K. Honda, K. Kamihira, K. Gotou, T. Fujii, J. Jpn Soc. Powder Metal, 41 (1994): 436.

173. *Effect of Rhenium Oxide Addition on the Superconducting Characteristics in the$YBa_2Cu_3O_x$ Ceramics*, K. Gotou, K. Honda, K. Kamihira, K. Maiwa, T. Fujii, J. Jpn Soc. Powder Metal, 41 (1994): 441.

174. *High-Tc Superconducting Wires -Development of HTSC Swall Coil Magnets*, H. Kitaguchi, New Materials, 5 (1994): 77.

175. *Critical Current Densities and Irreversibility Lines of New Oxycarbonate Superconductors (CuO. 5CO. 5) Ba_2Can-102n + 3(n = 3, 4)*, H. Kumakura, K. Togano, T. Kawashima, E. Muromachi (NIRIM), Physica C, 226 (1994): 222.

176. *Bi-2212 films and tapes irradiated by 120MeV oxygen ions*, K. Kazumata (JAERI), S. Okayasu (JAERI), H. Kumakura, K. Togano, Physica C, 235 (1994): 282.

177. *Superconducting Properties of Ag-l Intercalated $Bi_2Sr_2CaCu_20_y$*, H. Kumakura, H. Kitaguchi, K. Togano (Asahi Glass Co., Ltd), Physica C, 235 (1994): 939.

178. *The Origin of Dissipation in High Tc Superconductors*, K. Kadowaki, S. L. Yuan (Univ. of Tokyo), Phys Rev. Letters, 50 (1994): 7230.

179. *Semiconducting Properties and Thermal Shock Resistance of Boron Doped Iron Disilicide*, Y. Isoda, M. Okamoto, T. Oogoshi, I. Nishida, Proc. of 12th International Conference on Thermoelectrics, (1994): 192.

180. *Formation and Growth Mechanisms of $Bi_2Sr_2CaCu_20_y$ on a Silver Substrate in Partial Melting Method*, T. Hasegawa (Showa Electric Wire & Cable Co. Ltd.), K. Kobayashi (Showa Electric Wire & Cable Co. Ltd.), H. Kumakura, K. Togano, Superconductor Science and Technology, 7 (1994): 579.

Magnetic materials

181. *Role of Rare-Earth Elements for Magnetothermal Perovskite*, H. Kimura, T. Numazawa, M. Satou, T. Iketani (Tohoku Univ.), S. Fukuda (Institute for Material Research Tohoku Univ.), PROC '94, (1994): 262.

Materials for energy applications

182. *Resonance Enhanced Multiphoton Ionization Detection of SiO Desorbing From a Si(111) Surface in Reaction With O_2*, K. Nakamura, M. Kitajima, Appl. Phys. Letters, 65 (1994): 2445.

183. *Multiphoton Louization Detection of SiO Molecule Formed by O_2 Oxidation of Silicon Surface*, K. Nakamura, M. Kitajima, H. Kuroki (Univ. of Tsukuba), J. Appl. Phys, 75 (1994): 4261.

184. *For the Challenging New Stage in Reactor Materials Research*, M. Okada, K. Yagi, J. Nagakawa, J. Atomic Energy Soc. Jpn.

185. *Effects of DC bias on Plasma Oxidation Rate of Solid Surface*, M. Kitajima, K. Nakamura, I. Kamioka, T. Kawabe (Univ. of Tsukuba), Proc. of '94 ICPP, (1994): 309.

186. *Real time Raman Measurements of GaAs under Low Energy He^+ Irradiation*, K. Nakamura, M. Kitajima, E. Asari(Univ. of Tsukuba), J. Maters. Sci. Letters, 13 (1994): 1768.

187. *Development of Reduced-activation Martensitic 9Cr Steels for Fusions Reactor*, F. Abe, T. Noda, H. Araki, M. Okada, J. Nuc. Sci and Tech., 31 (1994): 279.

188. *Low Activation Materials* , T. Noda, J. Plasma and Fusion Res., 70 (1994): 628.

189. *Thermal Relaxation of Graphite Irradiated With Deuteron*, E. Asari (Univ. of Tsukuba), M. Kitajima, K. Nakamura, T. Kawabe (Univ. of Tsukuba), J. Surf. Sci. Soc. Jpn, 15 (1994): 660.

190. *Real-Time Observation of Ultra Thin Silicon Oxide Film Growth by Rapid Elllipsometry*, M. Kitajima, K. Nakamura, H. Kuroki, T. Kawabe (Univ. of Tsukuba), J. Vac Sci. & Tech., A12 (1994): 1431.

191. *Ellipsometric Study on Plasma oxidation of Silicon*, M. Kitajima, J. Vac. Soc. Jpn, 37 (1994): 815.

192. *Ion-Mass Effect on Lattice Disordering Rate of Graphic under Low Energy Ion Irraddiation* , E. Asari (Univ. of Tsukuba), M. Kitajima, K. Nakamura, T. Kawabe (Univ. of Tsukuba), Nuclear Inst. Methods in Phys. Research, B91 (1994): 545.

193. *Lattice Disordering in Graphite under Rare Gas Ion Irradiation Studied by Raman Spectroscopy*, E. Eiri, I. Kamioka (Univ. of Tsukuba), K. Nakamura, T. Kawabe (Univ. of Tsukuba), Phys. Rev. B, 49 (1994): 1011.

194. *Hydrogen Permeation Characteristics of Vandium-Molybdenum Alloys*, C. Nishimura, M. Komaki, M. Amano, Proc. of 3rd IUMRS International Conference on Advanced Materials, 18 (1994): 1273.

195. *Effects of DC Bias On Plasma Oxidation Rate of Solid Surface*, M. Kitajima, K. Nakamura, I. Kamioka, T. Kawabe (Univ. of Tsukuba), Proc. of. '94 ICPP, (1994): 309.

Processing

Separation and synthesis

196. *Synthesis and Characterization of Bromo and Chloro (phthalocyaninato)bismuth (III) Complexes*, H. Isago, Y. Kagaya, Bulletin of the Chemical Society of Japan (Bull. Chem. Soc. Jpn), 67 (1994): 383.

Gaseous process

197. *Processing and Properties of CVI SiC-Carbon Materials*, T. Noda, PROC '94, (1994): 15.

198. *Microstructure of SiC Thin Films Produced on Graphite by Excimer-laser Chemical Vapor Deposition*, H. Suzuki, H. Araki, T. Noda, J. Mater. Sci. Letters, 13 (1994): 49.

199. *Processing of High Purity SiC Composites by Chemical Vapor Infiltration (CVI)*, T. Noda, H. Araki, H. Suzuki, J. Nucl. Mater, 212–15 (1994): 823.

200. *Impurities and Evaluation of Induced Activity of SiC Composites Prepared with Chemical Vapor Infiltration*, T. Noda, H. Araki, H. Suzuki, F. Abe, M. Okada, J. Nucl. Sci. Technol., 31 (1994): 1059.

201. *Effect of Thermal Cycling on Transformation Temperatures of Ti-Ni Thin Films*, M. Satou, A. Ishida, A. Takei, S. Miyazaki (Univ. of Tsukuba), J. Surf. Finishing Soc. Jpn, 45 (1994): 138.

202. *Preparation of In-Plane Textured Y_2O_3-Doped ZrO_2 Thin Film on Polycrystalline Metallic Tape by Modified Bias Sputtering*, S. Aoki (Mitsuba Electric MFG. Co. Ltd.), M. Fukutomi, K. Komori, H. Maeda, J. Vac. Sci. & Tech., 12 (1994): 501.

203. *Preparation of C fiber/SiC and SiC fiber/SiC Composites by CVI for Low Activation*, H. Suzuki, H. Araki, T. Noda, Proc. of Materials for Advanced Energy Systems '94, (1994): 291.

204. *Shape Memory Characteristics of Sputter-deposited Ti-Ni Thin Films*, S. Miyazaki (Univ. of Tsukuba), A. Ishida, Mater. Trans. JIM, 1 (1994): 14.

205. *Laser Deposition of YBCO Thin Films on Metallic Substrate with Biaxally-Textured YSZ Buffer Layers Propared by Modified Bias Sputtering*, M. Fukutomi, S. Aoki (Mitsuba Electric MFG. Co. Ltd.), K. Komori, R. Chatterjee, H. Maeda, Physica C, 219 (1994): 333.

206. *Control of Y_2O_3-Stabilized ZrO_2 Thin Film Orientation by Modified Bias Sputtering*, M. Fukutomi, S. Aoki (Mitsuba Electric Mfg. Co. Ltd), K. Komori, Y. Tanaka, T. Asano, H. Maeda, Thin Solid Films, 239 (1994): 123.

207. *Grain Orientation of the $YBa_2Cu_3O_y$ Superconducting Thin Films Prepared by Low Pressure Plasma Flash Evaporation Technique and its De-*

pendence On, K. Komori, M. Fukutomi, S. Aoki, (Mitsuba Electric Mfg. Co., Ltd.), H. Maekawa, Thin Solid Films, 251 (1994): 63.

Liquid state process

208. *Preparation of Bi_2Sr_2 (Ca, Y)$Cu_2O_{8+\delta}$ Single Crystal by TSFZ Method*, T. Mochiku, K. Kadowaki, Proc. of Advanced Materials '93, (1994): 349.
209. *Growth of Dysprosium Garnet Single Crystals with Spiral Shape using Czochralski Technique*, H. Kimura, T. Numazawa, M. Satou, H. Maeda, Crystal Research and Technology, 29 (1994): 317.
210. *Phase Transformation of BaB_2O_4 during Annealing Process*, H. Kimura, T. Numazawa, M. Satou, PROC '94, (1994): 266.
211. *Melting in Floating—Challenge to the Non Contact Melting of Refractory Metals*, M. Yamazaki (Chubu Electric Power Company Inc.) A. Fukuzawa, K. Morita (Fuji Electric Corp.), J. Inst. Elec. Eng. Jpn, 114 (1994): 156.
212. *Structure of Hyper-eutectic Al-Si Alloys Obtained by a Rapid Solidification Process with Vigoross Agitation*, G. Aragane, Y. Oosawa, S. Takamori, A. Satou, J. Jpn. Inst. Mater, (1994): 160.
213. *Rare-earth Distribution Behaviour and Lattice Parameter Change on Rare-earth Substituted Garnet Single Crystals*, H. Kimura, T. Numazawa, M. Satou, J. Mater. Sci. Letters, 13 (1994): 1164.
214. *Twisting from the Viewpoint of Crystals*, H. Kimura, J. Japanese Asso. Crystal Growth, 21 (1994): 204.
215. *Growth and Properties of $Bi_2Sr_2(Ca,Y)Cu_2O_{8+\delta}$*, T. Mochiku, K. Kadowaki, Physica C, 235–40 (1994): 523.
216. *Effect of Cold Crucible Shape on Levitation Force toward Solid Metal Ball*, K. Sakuraya, T. Watanabe, T. Iwasaki (Chubu Electric Power Company, Inc.), T. Tatsuo, M. Fujita (Fuji Electric Corp.), Tetsu-to-Hagane, 80 (1994): 693.

Solid state process

217. *Cutting Force of Low Alloy Steels in the Cutting Speed Range in Which a Built-up Edge Forms*, S. Yamamoto, H. Nakajima (Hosei Univ.), H. Miyaji, Tetsu-to-Hagane, 80 (1994): 469.

Powder processing

218. *Characterization of the Surface Oxide Layer of Fine Iron Particles*, T. Uchikoshi, Y. Sakka, M. Yoshitake, T. Furubayashi, K. Yoshihara, Advanced Materials '93 I, 14A (1994): 68.
219. *Synthesis and Application of Intermetallic Compounds Produced by Combustion Synthesis Process*, Y. Kaieda, Ceramics Japan, 29 (1994): 203.
220. *Processing and Some Properties of Nanocomposites*, Y. Sakka, PROC '94, (1994): 73.
221. *Functionally Gradient Materials for Use in Thermal Barrier Coating Applications*, S. E. Niedzialek, G.C. Stangle (Alfred Univ.), Y. Kaieda, J. Self-propagating High-Temperature Synthesis, 2 (1994): 269.
222. *Effect of Cr Addition on Sintering and Sintered Microstructure of Ti + $TiAl_3$ Mixed Powders of TiAl Composition*, Y. Muramatsu, T. Oogoshi, H. Suga, J. Jpn. Soc. Powder Powder Metall., 41 (1994): 518.
223. *Fe-Fe Composite as an Attempt for Ecomaterialization by Micro-structure Control*, K. Harada, K. Minagawa, R. Yamamoto, T. Itubo (The Institute for Solid State Physics The Univ. of Tokyo), J. Jpn. Soc. Powder Powder Metall., 41 (1994): 1361.
224. *Densification of Sintered TiAl Containing Cr by HIPing and Their HIPed Microstructures*, Y. Muramatu, T. Oogoshi, H. Suga, J. Jpn. Soc. Powder Powder Metall., 41 (1994): 1437.
225. *Processing of Silicon Nitride-Mullite-Alumina Nanocomposites*, Y. Sakka, I. A. Aksay (Department of Chemical Engineering and Princeton Materials Institute Princeton Univ.), Nanostructured Materials, 4 (1994): 169.
226. *A Study of the Passivating Oxide Layer on Fine Nickel Particles* , T. Uchikoshi, Y. Sakka, M. Yoshitake, K. Yoshihara, Nanostructured Materials, 4 (1994): 199.

Joining

227. *Diffusion Joining of Single Crystal Ni-Based Super Alloy*, O. Oohashi, S. Meguro, and T. Yamagata, J. Jpn. Inst. Mater, 59 (1994): 319.
228. *Effect of Surface Composition on Diffusion Welding in Stainless Steel*, O. Oohashi, Proc. of 3rd IUMRS Int. Conf. on Advanced Materials, (1994): 1245.

Process with aid of beam technology

229. *Effect of Wavelength of Infrared Laser on the Isotopeselective Decomposition of Si_2F_6*, H. Suzuki, H. Araki, T. Noda, J. Jpn. Inst. Mater, 58 (1994): 1101.
230. *Isotope Separation of Si by Infrared Multi-Photon Decomposition* , H. Suzuki, H. Araki, T. Noda, Proc. of Materials for Advanced Energy Systems '94, (1994): 297.

231. *Basic Parameters in Heat Transport in Argon-Helium Mixed Gas Arcs*, J.P. Zijp, K. Hiraoka, Q. J. Jpn. Weld. Soc., 12 (1994): 21.

Processing in special environment

232. *Pulsed Magnet System*, T. Asano, K. Inoue, EMC, 7 (1994): 22.

233. *Operations of a 20-T Superconducting Magnet with a Large Bore*, T. Kiyoshi, K. Inoue, K. Itou, T. Takeuchi, M. Oshikiri, M. Kosuge, Y. Iijima, H. Maeda, IEEE Transaction on Magnetics, 30 (1994): 2110.

234. *Casting of Superconducting Composite Materials*, H. Fujii, H. Kitaguchi, H. Kumakura, K. Togano, M. Mouri (NASDA), J. Japanese Asso. Crystal Growth, 21 (1994): 16.

235. *Sharing of AES and XPS Spectral Data with the COMMON DATA PROCESSING SYSTEM*, K. Yoshihara, M. Yoshitake, J. Vac. Sci. and Tech., A12 (1994): 2342.

236. *Evacuation Properties of a Large Mu-metal Chamber for High Resolution Angle Resolved Electron Spectrometer*, T. Yakabe, D. Fujita, K. Yoshihara, J. Vac. Soc. Jpn., 37 (1994): 177.

237. *Copper-Silver Wire Coils for Pulsed Magnet*, T. Asano, Y. Sakai, M. Oshikiri, K. Inoue, H. Maeda, Physica B, 201 (1994): 556.

❒ NRIM Publications (Apr. 1994 to Mar. 1995)

1. Bulletin of National Research Institute for Metals, in Japanese.
2. Annual Report of National Research Institute for Metals, in Japanese.
   For fiscal year of 1993 (Feb. 1994)
3. Kinzaigiken News, in Japanese.
   Nos. 4 to 12 (1994) and Nos. 1 to 3 (1995)
4. NRIM Research Activities, in English.
   (Dec. 1994)
5. NRIM Special Report, in English.
   Nos. SR-95-1 and 2 (Mar. 1995)
6. Material Strength Data Sheet, in English.
   NRIM Creep Data Sheet,
   Nos. 21B and 25B (Sep. 1995)
   Nos. 32A (Mar. 1995)
   NRIM Fatigue Data Sheet,
   Nos. 79 to 84 (Dec. 1994)

International Exchange Apr. 1994 to Mar. 1995

❐ International Collaboration Research

Australia

1. Study on Surface Modification of Metals with Ultra-High Temperature Heat Sources. (CSIRO)
2. Studies on Conductor Fabrication Process of High-Tc BiSrCaCuO Superconductors. (University of Wollongong)

Brazil

1. Study on Ni-Base Superalloys. (Fundacao de Technologia Industrial)

Canada

1. Damage Evaluation and Remaining Life Prediction of Structural Materials. (Canadian Center for Mineral and Energy Technology)

China

1. Investigation of High Temperature Titanium Alloy for Application over 600 °C. (Northwest Institute for Non-Ferrous Metal Research)
2. Studies on Structural Control and Superconducting Properties of High Temperature Superconductors. (Institute of Metal Research Academia Sinica)
3. Study on the Combustion Synthesis of Intermetallic Compounds. (Northwest Institute for Non-Ferrous Metal Research)
4. Fundamental Study on the Improvement of Superconductivity for High-T_c Oxide. (Northwest Institute for Non-Ferrous Metal Research)
5. Study of Localized Corrosion Damage of Corrosion Resistance Alloys in High Temperature Aqueous Solution. (Shanghai Jiao Tong University)

Finland

1. Development of Superconductive Thin Oxide Coatings. (Tampere University of Technology)

France

1. Superconducting and Cryogenic Magnetic Materials. (Service National des Champs Intenses, Centre National de la Recherche Scientifique Grenoble and Others)

Germany

1. Development of Superconducting Materials. (Kernforschungszentrum Kerlsruhe)
2. Exchange of Creep and Fatigue Data Sheet. (5 Institutes)

Italy

1. Superconducting Properties of Advanced Superconductors in Time-Varying Magnetic Fields. (CISE Spa, Technologia Innovative Thermophysics & Cryogenics Sec.)
2. Intercomparison of Methods and Materials for Strain Measurements at Cryogenic Temperatures. (Instituto di Metrogia "G. Colonettie"-C.N.R.)
3. Study on the Mechanism of Deformation, Fracture and Corrosion in Ni-Based Superalloys. (Instituto per la Tecnologia dei Materiali Metallicinon Tradizionali)

Korea

1. Development of the Aluminaid-Base Intermetallic Compounds for Structural. (Korea Institute of Machinery and Metals)
2. Performance Characterization of Materials at High-Temperature. (Korea Standards Research Institute)
3. Development of Metallic Superconducting Materials. (Korea Research Institute of Standard Science)
4. Thermoelectric Research for Advanced Intermetallic Compounds. (Rapidly Solidified Materials Research Center)

Russia

1. Research Cooperation on Materials Property Data Modelling. (Institute Inorganic Chemistry, Academy of Science, Siberia)
2. Water Purification through Adsorptive Electrochemical Dispersed Systems. (Frumukin Institute of Electrochemistry)

Sweden

1. Application of Advanced Electromagnetic Technology to the Metallurgical Processing. (Royal Institute of Technology)
2. Fabrication and Characterization of Semiconductor Quantum Dots. (University of Lund)

U.K.

1. Evaluation of Life and Remaining Life Prediction of Huge Structures under Service Operation. (Welding Institute)

U.S.A.

1. Combustion Synthesis for Production of Ceramic, Intermetallic and Composite Materials. (Alfred University)
2. Research and Development on Systems and Materials for Magnetic Refrigerators. (Francis Bitter National Magnet Laboratory)
3. Database of Properties for High-Temperature Superconducting Materials. (National Institute of Standards and Technology)
4. Studies of High-Strength/High Conductive Materials and Their Application to High-Field Magnets. (Francis Bitter National Magnet Laboratory)
5. Fundamental Studies on the Conductor Fabrication of High Temperature Oxide Superconducting Materials. (University of Illinois)
6. Evaluation Methods for Superconductors. (National Institute of Standards and Technology)

❐ List of Guest Researchers

*STA Fellowship

Nationality and Name	Affiliation	Term	Research Subject
Australia			
Shi Xue Dou	University of Wollongong, Center for Superconducting and Electronic Materials	H7.2.19 to H7.2.25	Critical Current Density and Flux Pimming in Ag-Sheathed BSCCO Tapes
Canada			
Denis P. Masson	University of California, San Diego	H7.3.10 to H3.21	Internal State-selective Detection for the Surface Reaction using Laser Spectroscopic Techniques
China			
Jinhua Ye	Osaka University	H3.10.1 to H6.9.30	Pressure Effects on Physical Properties of Magnetic Materials
Piao Min	University of Tsukuba	H6.1.1 to H8.12.31	Research on Effects of Lattice Defects on Phase Transformations and Precipitations of Alloys by NRTEM
Liu Jian Hong	Harbin Institute of Technology	H6.1.12 to H7.4.30	Microstructure and Mechanical Properties of Ti_2AlNb Intermetallic Compounds Produced by the Powder Metallurgy Process
Huang Ying Kai*	University of Amsterdam	H6.4.14 to H7.4.13	Fundamental Study of Electromagnetic Materials with Strong Electron Correlations
Feng Yi	University of Wisconsin, Applied Superconductivity Center	H6.10.27 to H6.11.11	High Resolution Transmission Electron Microscopy Observation of Bismuth Oxide Superconductors
Wei Sun	Tohoku University, Institute for Materials Research	H6.11.1 to H9.10.31	In situ Observation and Structural Analysis of High Tc Superconductors for Fusion Research at Low Temperature
Zeng Quanpu	Northwest Institute for Nonferrous Metal Research	H7.3.2 to H7.3.31	Fracture Mechanisms of Ceramic Particulates-reinforced Ti-based Metal Matrix Composites
Yan Jin*	University of Manitoba, Dept. Mechanical and Industrial	H7.3.22 to H8.1.21	Development of High Strength Metal Base Composites with Excellent Physical Properties by the Advanced Bronze Method

Nationality and Name	Affiliation	Term	Research Subject
France			
Herve Rouch*	S2MC (Laboratories de Science des Surfaces et Materiaux Carbone)	H6.11.1 to H8.7.31	Control of Surface Reaction and Synthetic Processes by "State-controlled" Molecular Beams
Jean Louis Bobet*	University of Bordeaux I	H6.3.1 to H7.8.31	Thermostructural Composites Laboratory Effect of Residual Stress on Mechanical Properties for SiC/Ti-15-3 Metal Matrix Composite
Germany			
Arman Nyilas	Kernforschungszentrum Karlsruhe	H6.10.30 to H6.11.13	International Cooperative Research on Modeling and Characterization of Advanced Materials
Christian Roth*	Technische Universitat Clausthal	H7.3.28 to H9.3.27	Designing of Continuous Refining Process
Hungary			
Jozsef Toth*	Institute of Nuclear Research of the Hungarian Academy of Science	H6.3.22 to H6.9.21	Control of Surface Atomic Layer and Technological Development of Surface Electron Spectroscopic Tomography
Tian Bo Yuan	Shanghai Nuclear Engineering Research and Design Institute	1993.11.30 to 1993.12.9	Studies of Local Corrosion Damage of Corrosion Resistant Alloys in High Temperature Water
India			
R. Sethumadhavan*	Bishop-Heber College	H6.2.1 to H7.1.31	Fundamental Study on Biocompatibility of Materials
Balvinder Gogia*	Panjab University, Physics Department	H7.2.5 to H8.8.4	Study on the Single Crystal Growth of High Temperature Oxide Superconductors
Indonesia			
Salim Mustofa	BATAN	H7.3.13 to H7.3.24	Japan-Indonesia Cooperation Program on Cooperative Education Program
Korea			
Hong Seong-Hyeon	Ssangyong Research Center	H5.12.13 to H6.11.30	Preparation and Characterization of Nanophase Materials
Sung-Keun Lee	Dong-A University, Department of Metallurgical Engineering	H6.1.5 to H6.8.20	Fretting Fatigue of Biomaterials in Pseudo-Body Fluid
Sae Chae Jeoung	Korea Research Institute of Standards and Science, Spectroscopy Laboratory	H7.3.6 to H7.3.26	Time-Resolved Spectroscopic Analysis of Chemical Reaction Using Ultra Short Pulse Laser Spectroscopic Techniques
Chang-Joo Kim	Korea Institute of Machinery and Metals	H7.2.10 to H7.3.9	Research on Ti-alloys
Ahn Jeong-Ju	Yeung Nam University	H7.1.10 to H7.2.24	Mechanical Engineering Department Tensile Damage Evaluation of SiC Particle Reinforced Aluminium Alloy Matrix Composites
Joo Kwang-Chul	Hanyang University, Department of Metallurgy and Materials Science	H7.1.10 to H7.2.24	Fabrication and Characterization of Bismuth Oxide Superconducting Tapes
Jonghun You*	University of Texas at Dallas, Center of Quantum Electronics	H7.2.1 to H8.1.31	The Synthesis of Superconducting Ultrathin Films by the Combined Use of Magnetron Sputtering and Ion Implantation Techniques
Kim Dong Yup	Ssang Yong Research Center, Dept. of Elec. and Magnetic Materials	H6.11.9 to H7.11.8	Preparation and Magnetic Properties of Chemically Stabilized Iron-nitride Magnetic Fluids
Han-Cheol Choe	Chonnam National University, Engineering Research Institute	H6.11.9 to H7.3.7	Environmental Degradation of Structural Materials for Light Water Reactors
Kim Suk Won	Korea Institute of Nuclear Safety, Nuclear Regulatory Inspection Division	H6.12.1 to H7.3.31	Same as above
Sung-Joon Kim	Korea Institute of Machinery and Metals	H6.4.2 to H7.4.1	Structure Analysis and Fatigue Properties Evaluation of Ti-based Metal Matrix Composites

Nationality and Name	Affiliation	Term	Research Subject
Kim Yoon-Bae	Korea Research Institute of Standards and Science	H6.5.24 to H6.8.11	Training on the Construction of High Magnetic Field Facilities and the Measurement of Magnetic Properties under the High Field
Kim Eui Sub	University of Tsukuba	H6.6.1 to H6.9.16	Study on Radiation Damage of Metallic Materials
Kim Young-Joo	Korea Research Institute of Standards and Science	H6.8.23 to H6.11.18	Training on the Fabrication of a U-focus X-ray CT and Development of Computer Softwares for Image Processing
Jaeln Jeong	Research Institute for Science and Technology	H6.9.1 to H7.2.28	Control of Surface Atomic Layer and Technological Development of Surface Electron Spectroscopic Tomography
Netherlands			
Anne de Visser*	University of Amsterdam	H7.2.16 to H7.3.3	Fundamental Study of Electromagnetic Materials with Strong Electron Correlations
Philippines			
Barbara Dar Juan T10	Industrial Technology Development Institute, Department of Science and Technology	H7.2.6 to H7.7.27	Japan-ASEAN Cooperation Program on Materials Science and Technology, Philippine Project on Atmospheric Corrosion (Metallic Coating)
Switzerland			
James K. Gimzewski	Zurich Research Laboratory, IBM Research Division	H7.2.22 to H7.3.23	Collaboration on Nanoscopic Observation of the Surface
Walter Paul Joss	Grenoble High Field Magnet Laboratory	H7.2.16 to H7.3.8	de Haas-van Alphen Effect of Heavy Fermion Compounds
Thailand			
Pakdi Thongcharoen	Department of Mineral Resources Ministry of Industry Metallurgy Division	H7.3.20 to H7.6.8	Japan-ASEAN Cooperation Program on Materials Science and Technology, Thai Project on Atomspheric Corrosion (Organic Coating)
U.K.			
Paul J. Warren*	University of Oxford	H6.4.11 to H7.4.10	APFIM Study on Microstructure on NiTi-base Precipitation Hardening Intermetallic Alloys
Timothy Martin King*	CEC, Joint Research Center, Institute for Advanced Materials	H6.9.30 to H8.9.29	Enabling and Encouraging the Global Sharing of Materials Information for Use in Advanced Complex Analysis Procedures
Archie Macrobert Campbell	University of Cambridge, IRC in Superconductivity	H7.2.2 to H7.3.1	Study on the Application of Pinning Theory on the Critical Current Measurement of Superconductors
John Singleton	University of Oxford	H7.2.10 to H7.3.10	Magnetic Properties of Kondo Insulator Compounds
Richard A. Doyle	IRC in Superconductivity, University of Cambridge	H7.3.13 to H7.4.10	Study of Electronic Transport Properties in Superconducting Vortex State on High Tc Superconductor Bi2212 Single Crystal
U.S.A			
James S. Brooks	Florida State University, National High Field Magnet Laboratory	H6.8.1 to H6.9.15	Quantum Oscillations of Organic Conductors
Ferdinand Bartels	University of California, Berkeley	H6.10.28 tlo H6.11.13	Study on Evaluation of Magneto-mechanical Instability for Metastable Austenitic Steels
James S. Schilling	Washington University, Department of Physics	H7.1.5 to H7.1.14	Study of Pressure Effects on Material Physics and Development of Magnetization-measurement System under Low Temperature and High Pressure
Eric Ernst Hellstrom	University of Wisconsin, Applied Superconductivity Center	H7.2.19 to H7.3.5	Study on the Formation of Superconducting Phase in Bismuth Oxide Superconducting Tapes

❒ Brief Introduction of STA Fellowship

The Science and Technology Agency (STA), an administrative organ of the Government of Japan, offers opportunities for promising young foreign researchers in the fields of science and technology to conduct research at Japan's national laboratories and public research corporations (excluding universities and university-affiliated institutes). The program is managed by the Research Development Corporation of Japan (JRDC), a statutory organization under the supervision of STA in cooperation with the Japan International Science and Technology Exchange Center (JISTEC).

Fellowship qualifications are as follows:

1. Possession of doctor's degree.
2. Less than 35 years of age, in principle.
3. Sufficient good health for research work and life in Japan.
4. Sufficient language ability in Japanese or English.

The tenure will be 6 months to 2 years. JRDC provides expenses for round-trip, monthly living with family, initial setting-in and travel in Japan. Research expenses willl be paid for the host institute. Further information can be obtained at:

Japan International Science and Technology Exchange Center (JISTEC)
2-20-5, Takezono
Tsukuba City, Ibaraki Pref. 305, Japan
Phone +81-298-53-8250
Fax +81-298-53-8260

Organization of NRIM

❒ Organization

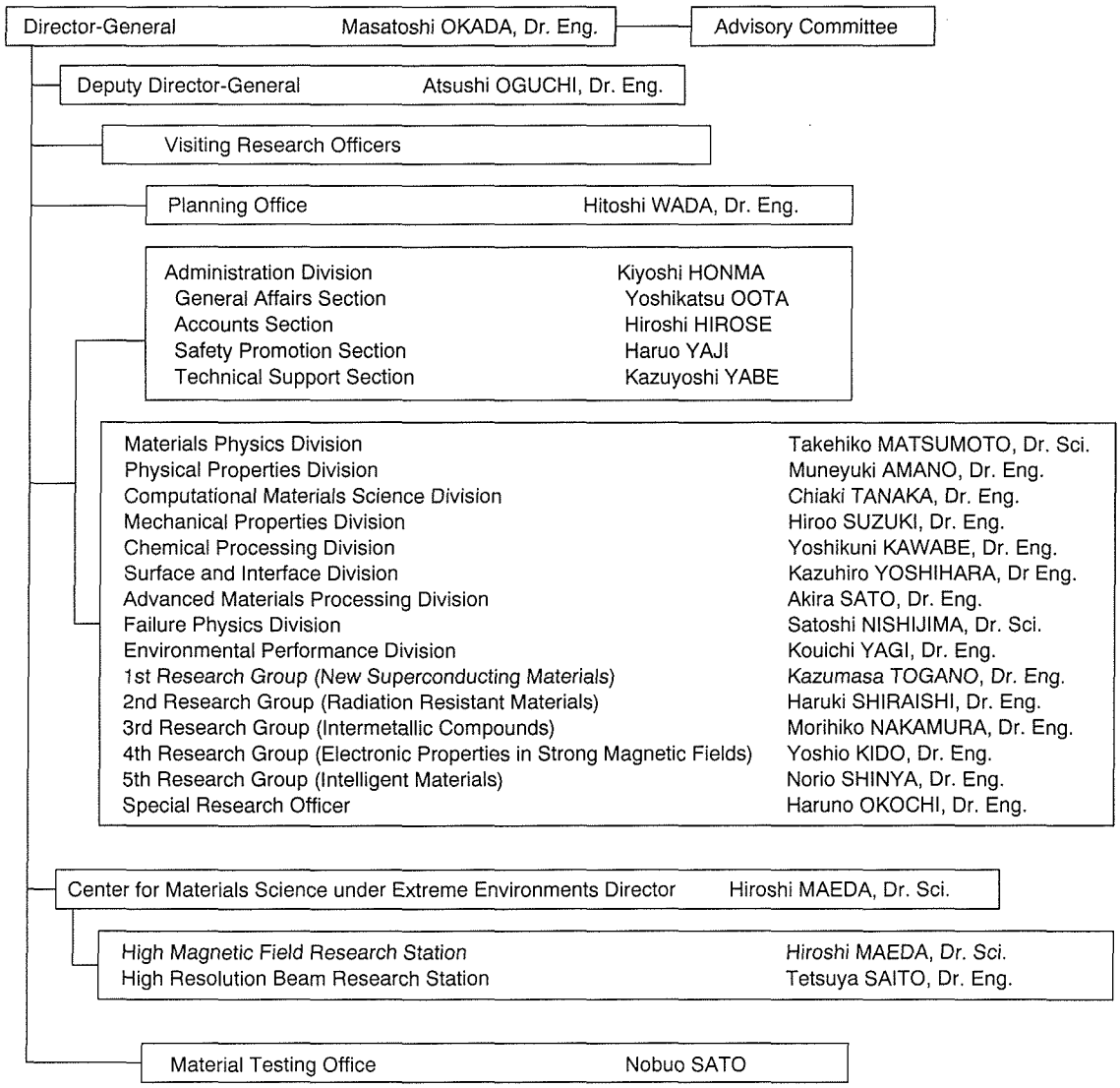

❒ Budget and Personnel in Fiscal Year of 1994

Budget	
Research and facilities	5,805
Personnel expenses	3,737
Total	9,542

unit: million yen

Personnel	
Administrative staffs	90 (9)
Researchers	330 (6)
Total	420 (15)

Number in parenthesis: Material Testing Office

How to get to NRIM

To NRIM Tsukuba Site
1-2-1 Sengen, Tsukuba-shi, Ibaraki 305
Phone +81-298-53-1000, Fax +81-298-53-1005

Narita Airport
↓ by JR Narita Express train approxmately 60 minutes
Tokyo Station
Yaesu-Minami Exit
↓ by Joban Highway Bus for Tsukuba Center approximately 70 minutes
Tsukuba Center
Bus Terminal
↓ by taxi approximately 5 minutes, or on foot approximately 15 minutes
NRIM

To NRIM Meguro Site
2-2-54 Nakameguro, Meguro-ku, Tokyo 153
Phone +81-3-3719-2271, Fax +81-3-3719-2177

Narita Airport
↓ by JR Narita Express train approxmately 60 minutes
Tokyo Station
↓ by JR Yamanote Line train approximately 25 minutes
Ebisu Station
↓ by taxi approximately 5 minutes, or on foot approximately 15 minutes
NRIM

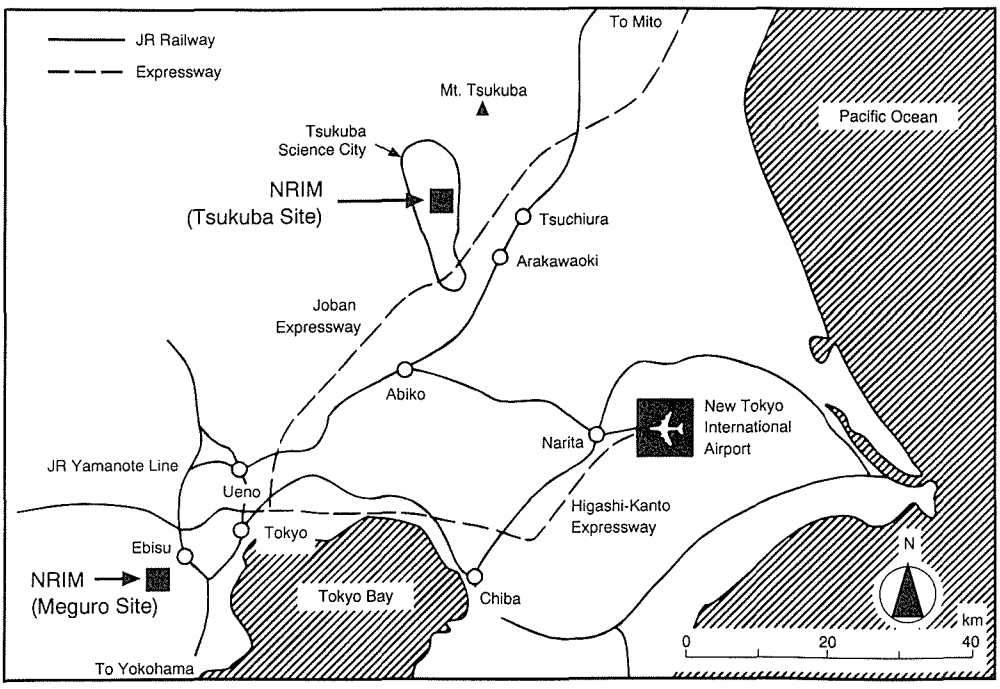

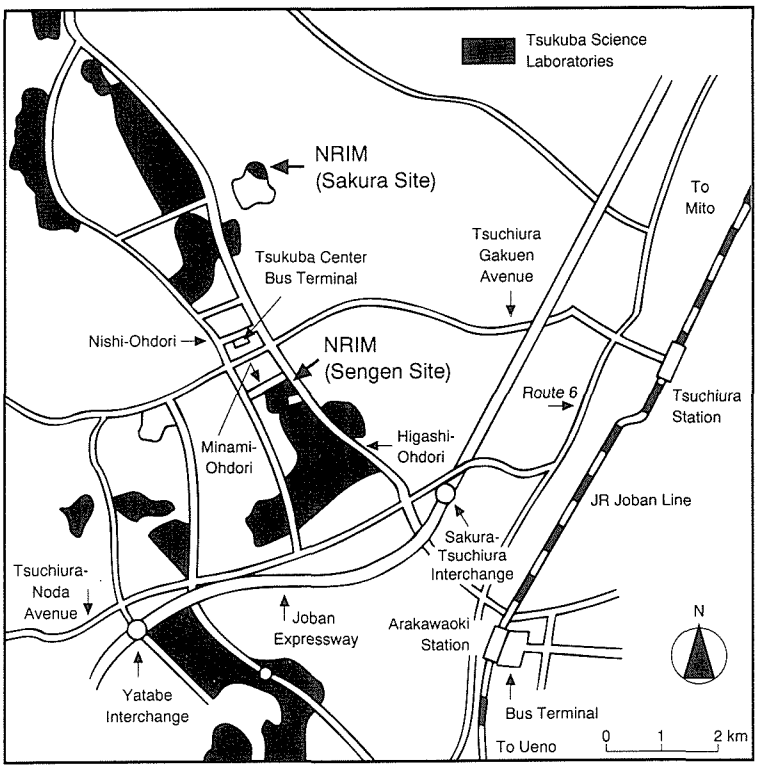

Tsukuba Site

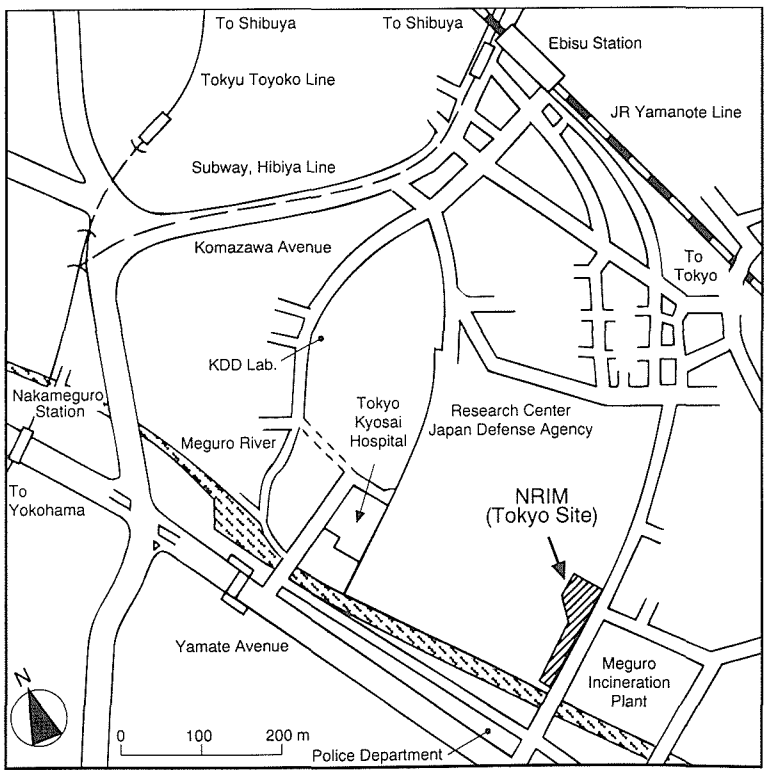

Tokyo Site

List of Keywords

A

ac loss 86
adsorption 1
advanced materials 69
advanced nuclear materials 92, 94
AES 71
AFM 58, 69
Ag doping 104
AgCu alloy sheath 83
AgCu sheath-tape 50
aging 113
alloy design 92
aluminum alloys 59, 64
analytical TEM 109
angle resolved photoelectron spectroscopy 42
anisotropic microstructure 68
anode 66
antimonic acid 46
antimony 95
argon ion bombardment 107
atmospheric corrosion 56
atomic configuration 48
atomic layer epitaxy 82
atomic scale characterization 97
atomistic models 52
atoms manipulation 53
auto-ionizing level 109

B

B fiber 80
Bacteria 56
band gap 42
Bi(Pb)SrCaCuO 83
Bi-based oxide superconductor 27
Bi-based oxide superconductors 91
Bi-Sr-Ca-Cu-O ceramics 104
$Bi_{2-x}Sb_xTe_{3-y}Se_y$ 84
$Bi_2Sr_2CaCu_2O_{8+x}$ 49
binding nature 49
bio-simulator 96
biocompatibility evaluation *in vitro* 35
biomaterials 35, 96
BiSrCaCuO 50, 110
Bitter magnet material 31
BN 80
Boro-carbide superconductor 82
borocarbide superconductor 25
Brazing 106
bronze method 80
bubble morphology 93

C

carbonaceous material 54
cast iron 5
cation disorder 50
cavitation 58, 63
cavity nucleation and growth 21
CCD camera 49
cell adhesion force 96
ceramics 60
charge carrier 77, 80
chemical transportation 76, 99
chemical vapor infiltration 98
chemisorption 54
chlorine 1
CL 109
cold crucible 99
colloid 103
combustion synthesis 101, 102, 104
composite 80, 100
composite materials 68
composite UFP 103
composites 81
computer aided metallography 77
computer modelling 48, 91
computer simulation 68, 75, 93
computer-image analysis 72
conductor materials for high-field magnets 83
cooled CCD camera 70
copper 56, 105
corrosion 56, 106
crack 52
creep 58, 75
creep behavior 78
creep crack growth 61
creep deformation 61, 63
creep strength 91
creep-damaged microstructure 77
crevice 92
critical current 86, 90
critical current density 27, 82, 85, 91
cross sectional TEM method 48
cryogenic temperature 60
crystal growth 99
CT 72
Cu alloy 80
Cu-Ag alloy 31
Cu-Ag microcomposite alloy 83
CVD 74
cyclic deformation 62
cyclic fatigue 60
cytotoxicity 96

D

damage accumulation 21
data share 92, 94
data transfer 71
Data-Free-Way 92, 94
database 47, 71, 73, 75, 92
deep sea sediments 70
deformation 62

dendrite growth 99
deposition 50, 90
dictionary 65
diffusion 76
diffusion welding 106
direct bonding of silicon 107
direct current glow discharge 65
distributed database 92, 94
distribution of chemical elements in sub-micron region 64
distribution of chemical elements on metallurgical structures 72
drift velocity 111
dual-beam ion irradiation 111
dynamic strain 65

E

EB Welding 106
ecomaterial 95
ecomaterials data base 85
EDS 109
EELS 109
electrical conductivity 77, 80
electrification 19, 107
electrode reaction 54
electromagnetic devices 42
electromagnetic force 99
electromagnetic levitation 100
electromagnetic method 67
electron beam 110
electron holography 49
electron irradiation 7
electron microscopy 72
electron Moiré method 63
electron spectroscopy 73
electron spin resonance 45
electron-probe microscopy 64
electronic structure 45, 74, 95
elevated temperatures 60
elevated-temperature 9
elongation 78, 79
energy conversion 84
EPMA 66
evaluation 83
evaluation of environment load 85
evaporation 110
exaggerated grain growth 99
extreme high vacuum 23
extreme particle field 48

F

f electron 17
fast breeder reactor 59
fatigue 11, 59
fatigue crack 62
fatigue crack growth 9
fatigue hardening 76
fatigue of metals 64
fatigue properties 62
fatigue softening 76
Fe-30Ni alloy 102
Fe-Fe composite 95
$Fe_{16}N_2$ 110, 113
FEM 75
Fermi surface 15, 17
Fermi surface map 49
FeS 56
field emitter 53
film 85
fine magnetic particles 91
fine particles 97
fine powder 103
fine structures 5
finite element method 93
first-order phase transition 44
first-principles theory 1
flame spraying 88
floating zone method 77
fluctuation of order parameter 70
fluidized bed 74
flux pinning 86
flux quantum 85
forced-infiltration 108
fracture 52, 62
frequency response 68
fretting fatigue 96
function of human beings 74
functionally graded materials (FGM) 84
fuzzy logic 72

G

GaAs 55
GaAs(001) surface 1
garnet solid solution 91
gas analysis 67
gas desorption 103
GD-MS 67
GF-AAS 67, 70
giant magnetization 110
grain alignment 82
grain boundary 51, 70, 82
grain morphology control 78
grain orientation 87
graphic data 47
growth process of surface defect 93

H

heat input 66
heavy fermion 17
heavy fermions 44
helium 113
helium embrittlement 93
helium-free magnet 91
hexa-fluoro-disilane 29
high current 48
high intensity electron gun 49
high magnetic field 43, 45
high pressure 43, 46

high pressure infiltration 3
high resolution electron microscopy 52
high resolution magnet 33, 89
high resolution superconducting magnet 84
high strength 80
high T_c phase 104
High T_c superconductors 72
high T_c superconductors 49
high temperature 65
High Temperature Gas-Cooled Reactor (HTGR) 112
high temperature plasma 82
high temperature strength 13, 79
high temperature superconductors 85
high temperature x-ray diffraction 88
high-field magnet 33, 89
high-field material 31
high-field superconducting magnet 33, 84, 89
high-pressure 44
high-pressure infiltration 108
high-strength/high-conductive material 83
high-T_c oxide superconductors 50
high-T_c superconductor 88
high-temperature superconductor 45
highly correlated electron system 43
HIPing 102
HRTEM 48, 66, 109
human senses 74
hybrid magnets 33, 89
hydrogen 51
hydrogen permeability 107
hysteresis 58

I

ICM processing facility 98
ICP-AES 67
image analysis 86
image convolve 57
improvement of resolution with computer-image analysis 64
in situ analysis 111
in situ analysis 7
in situ measurement 48
in situ strain measurement 65
in vivo tests 96
information-base 65
infrared multi-photon decomposition 29
infrared/Raman spectroscopy 47
infrared-reflectance spectra 49
inherent creep strength 61
inhibitor 56
insert coil 27
insertion/extraction reaction 46
integrated process 23
intelligent materials 9, 63, 81, 104
interface 44, 51
interlaboratory testing 69
interlamellar contact 3
intermetallic compound 78, 108
Intermetallic Compound 79
intermetallic compound 25
intermetallics 51
internal oxidation 88
internal stress 102
intrinsic Josephson Junctions 42
ion and electron temperatures 111
ion implantation 110, 113
ion intensity 73
ionic conductor 46, 77, 80
iron base alloy 80
irradiation 62, 93
irreversibility field 87
isotope separation 98
isotopically controlled materials 29, 98

J

joining 105, 108
Joining 107
Josephson devices 42

K

kelvin probe 56
kinetics 51
knowledge converter 65
knowledgebase 73
Kondo effect 43, 44

L

laser 73, 110
laser induced plasma 111
laser photoionization 111
laser speckle method 65, 106
laser-ultrasonic 68
lattice image 52
lattice misfit 92
LCA 95
leakage testing 67
levitation melting 99
life extension 63
linear motor drive 23
long length 83
long-pulsed magnet 33, 89
long-term creep 62
Lorentz force 99
low cycle fatigue 59, 92
low density 92
low dimensional 45
low pressure plasma jet 97
low temperature 43, 46, 91, 113

M

magnetic chromatography 97
magnetic field 52, 113
magnetic flux 67
magnetic levitation 23
magnetic levitation specimen transfer system 113
magnetic properties 43
magnetic relaxation 44

magnetic separation 97
magnetic shielding 88
magnetization 46
manipulation 19
martensitic steels 61
martensitic transformation 52, 102
mass spectrometry 65, 73
material design 47
material element 66
material strength 75
materials characterization 71
materials damage 69, 81
materials design 65
materials evaluation 67
materials properties 74
Materials-Design 112
MBE 50, 109
MCP 49
Me-Ti-O UFP 103
measurement technique 83
mechanical alloying 57
mechanical properties 77, 81
mechanism of superconductivity 74
melt-growth method 87
melt-solidification 87
mercury intrusion porosimeter 3
metal complex 95
metal salts 35
metallic ion 54
metallurgical factor 101
metamagnetic transition 17
metastable phase 74, 100
metastable state 44
$Mg_2Sn_{1-x}Ge_x$ 84
micro machining 101
micro-machinability 101
microcomposite 31
microcracking 3
microgravity 101
Microgravity 106
micromachine 98
microstructural evolution 61, 62
Microstructure 79
microtomography 72
microwave cavity 82
mirror finishing 65
mixed gas 66
MLC/ICP-MS 70
MMC's 81
modeling 69
modelling 75
moire interference 58
molecular beam epitaxy 55
molecular dynamics 52, 69
multi-slice method 70
multifilamentary superconductor 90
multifilamentary wires 83
multiphase structure 85
multiple functions 104
multivariate statistical analysis 74

N

nano-scale 53
nanocomposite 103
nanometer structure 55
nanotechnology 81
Nb addition 102
Nb-matrix Nb_3Sn wires 86
Nb_3Al 90
Nb_3Al+Nb two phase structure 77
negative ion source 48
network 47, 73
Ni-base superalloy 48
Ni_2TiAl precipitate 48
Ni_3Al 77
NiTi-base alloy 48
non-destructive evaluation 67
nondestructive evaluation 68
NRIM Fatigue Data Sheets 59
nucleation 99

O

oil quenching 88
order parameter 70
ordered alloy 76, 99
organic conductor 15
organotin 70
oxidation 57, 79
oxidation resistance 91
oxide ceramics 63
oxide superconducting magnet 84
oxide superconductor 82, 83
oxide superconductors 47, 73

P

particle assembly 19, 104
particle dispersion 100
particle reinforcement 13
particulate 81
particulate-reinforced 81
$Pb_{1-x}Sn_xTe$ 84
peritectic reaction 99
phase equilibrium 48
phase identification 64
phase transformation 61
phase transition 47
phase-transformation 65
Phonons 47
photocatalytic property 103
photodecomposition 103
photoionization induced plasma 109
phythalocyanine 95
piezo actuator 58
pinning center 42, 90
plasma characteristics 109
plasma density 111
plasma heating 110
plasma spray 108
plasma spraying 88
porosity 108

potential distribution 56
powder 95, 105
powder metallurgy 81
powder-in-tube technique 50
pressure dependence 43
property evaluation 69
protection layer 80
proton conduction 46
pulsed magnet material 31
pure titanium 76

Q

quantum oscillation 15
quantum tunneling 44
quantum well boxes 55

R

radiation 66
radiation damage 7, 62, 109, 111
rapid solidification 3, 105
rapid-quench 90
rare gas 65
reaction 54
real-time observation 93
recyclable materials design 85
Redox potential 56
refractory superalloy 91
regenerator 113
relation matrix 74
residual stress 11
resolution limit of TEM at low temperature 49
resonance photoionization 109
rf glow discharge 73
RF-plasma 103
room-temperature ductility 77
Rydberg level 109

S

S segregation 57
saturated surface compositon 53
SC-alloy 92
scanning tunneling microscopy 55
SCC 94
sea water 70
secondary recrystallization 99
Seebeck effect 99
self controlling 9
self-compositon control 53
self-organizing 65
self-recovering of creep cavity 63
self-restoring 81
self-sensing 81
SEM 66
semi-molten state 108
shape memory 98
shape memory alloy 76, 94
shape memory effect 52
shape recovery 94
short-time TEM imaging 49
sialon 5
silicides 44
silicon 105
silicon isotope separation 29
silicon tetra-fluoride 29
Simulation 106
single crystal 44
sintering 102, 103, 105
sintering method 87
slow scan CCD camera 48
small crystalline materials 109
solid electrolyte 77, 80
solid phase extraction 70
solid solutions 47
solid surface 54
solid-solution hardening 13
solidification 100, 101
spectrum 71
spin Peierls 45
SPM image 57
spray deposition 107
sputtering 98
stacking fault 52
stacking faults 7
stage I fatigue 60
stage II fatigue 60
stainless steel 75, 106
stainless steels 77
standard reference data 64
State-control 112
static fatigue 60
steel 11
steels and alloys 59, 64
STM 53, 69
stress corrosion cracking 92
stress relaxation 62
stress/strain sensitivities 86
strong magnet 99
structural design of solid solution alloys 85
structural stability 54
structure control 95
structure image 52
STS 53
sub-millimeter 45
SUBNANOTRON 109, 111
subsurface fatigue crack initiation 60
super conducting transport 23
super-lattice 50
superconducting oxide 104
superconductive materials 105
superconductivity 110
superconductor 48, 101, 104
superlattice 82
superplasticity 21, 63
supersonic molecular beam 112
surface 73
surface and interface analysis 71
surface coating 108
surface composition 105, 107

surface flaw 67
surface reaction 112
surface reaction dynamics 93
surface segragation 53
surface terminated or buried particles 109
synchroton radiation 71

T

tape 85
TEM structure 76
tensile stress 52
Testing-and-Evaluation 112
textured buffer layer 82
theory 45
thermal conductivity 84
thermal plasma 97
thermal shock 78
thermal spray coating 57
thermodynamics 51
thermoelectric materials 84
thermoelectric property 84
thermomechanical processing 79
thick coatings 107
thick film 88
thin film 25, 50
thin films 97
thin water layer 56
three-dimension 72
Ti-3-8-6-4-4 76
Ti-6Al-4V 76
Ti-Ni 98
$Ti_{48}Al_{52}$ amorphous alloy 74
TiAl 78, 79, 80
TiAl intermetallic compound 102
TiAl-base alloy 54
TiB_2 78, 80
TiNi 102
tip effect 57
titanium 81, 106
titanium alloy 60
titanium-aluminides 13
tomography 72, 73
tool dynamometer 101
toughening microstructure 58
toughness 61
transformation mechanism 51
transition metal oxides 47, 49
transition temperature 87
transmutation 92
trapping 51
triazinedithiole 56

U

ultra clean vacuum 113
ultrafine particle 103
ultrafine powder 104
ultrasonic vibration 5
ultrathin films 110
unconventional superconductivity 44
undercooling 100
unidirectional solidification 77, 100

V

V_5Si_3 86
VAMAS project 69
vapor deposition 85
vaporization 66, 97
variant selection 102
vortex dynamics 42

W

W fiber 80
water absorption 46
welded joint 75
welded joints 59
weldment 11
work function 53
work hardening ability 93

X

x-ray 72
x-ray fluorescence 71
x-ray total reflection 97
XPS 71
XRD 66

Y

Y-Ba-Cu-O system 104
Y_2O_3 dispersion 57
$YBa_2Cu_3O_x$ 87
YBaCuO film 50
yttrium-based superconductor 90

Z

zirconia 21
zirconia ceramics 61
zirconium 106
$Zr_{1-x}Hf_xO_2$ 49

γ-Mo_4O_{11} 49
1 GHz NMR system 84
1 MeV TEM 7, 111
200 keV ion implanter 111
30 keV ion sputter source 111
316 FR stainless steel 59

NRIM Research Activities
1995
Date of Issue: 29 March, 1996

Publisher:
Eiichi MUTOU
Planning Office
National Research Institute for Metals
1-2-1, Sengen, Tsukuba-shi, Ibaraki 305 Japan
Phone: +81-298-53-1000, Fax: +81-298-53-1005

Typeset using SGML by Uniscope Inc., Tokyo

NRIM Research Activities

1995